

**On aspects of plasma surface interactions studied by  
spectroscopic techniques**

**INAUGURALDISSERTATION**

zur

Erlangung des akademischen Grades eines  
Doktors der Naturwissenschaften (Dr. rer. nat.)  
an der Mathematisch-Naturwissenschaftlichen Fakultät  
der

Ernst-Moritz-Arndt-Universität Greifswald

vorgelegt von

Dmitry Lopatik

geboren am 23. November 1986

in Minsk (Weißrussland)

Greifswald, 21. März 2013



Dekan:	Prof. Dr. Klaus Fesser
1. Gutachter:	Prof. Dr. Jürgen Röpcke
2. Gutachter:	Prof. Dr. Achim von Keudell
Tag der Promotion:	26. Juni 2013



*Dedicated to my family and  
to everyone who has believed in me!*



# Contents

<b>Abstract</b>	<b>11</b>
<b>Kurzfassung</b>	<b>15</b>
<b>Аннотация</b>	<b>19</b>
<b>1 General introduction</b>	<b>25</b>
1.1 Non-equilibrium plasmas .....	25
1.2 Plasma diagnostic methods .....	27
1.3 Interaction with surfaces .....	30
1.4 Scope of the thesis .....	31
<b>2 Infrared laser absorption spectroscopy for plasma diagnostics</b>	<b>33</b>
2.1 Low pressure discharges .....	33
2.1.1 Glow discharge plasma .....	34
2.1.2 Capacitively coupled plasma .....	35
2.1.3 Microwave discharges .....	36
2.2 Radiation sources in the mid infrared spectral range .....	37
2.3 Basic principles of absorption spectroscopy .....	40
<b>Bibliography for Chapters 1 and 2</b>	<b>46</b>
<b>3 Spectroscopic study of pulsed DC plasmas used for nitriding processes</b>	<b>53</b>
3.1 Introduction .....	53
3.2 Experimental .....	55
3.3 Results and discussion .....	58
3.3.1 Measurement of $\text{NH}_3$ concentrations by TDLAS .....	58
3.3.2 QMS analysis of the $\text{N}_2\text{--H}_2$ plasma .....	59
3.3.3 Plasma nitriding experiments .....	63
3.4 Summary and conclusions .....	65

<b>4</b>	<b>On kinetic and chemical phenomena in dust producing RF plasmas</b>	<b>67</b>
4.1	Introduction .....	68
4.2	Experimental.....	70
4.3	Results and discussion.....	74
4.3.1	General features of species concentrations and particle growth at Ar and He plasma conditions.....	74
4.3.2	Dynamic of the species concentrations .....	77
4.3.3	Fragmentation and conversion efficiencies.....	81
4.4	Summary and conclusions .....	83
	<b>Bibliography for Chapters 3 and 4</b>	<b>84</b>
<b>5</b>	<b>On surface relaxation of vibrationally excited nitrogen</b>	<b>89</b>
5.1	Introduction .....	90
5.2	Experimental.....	91
5.2.1	Discharge setup .....	91
5.2.2	Quantum cascade laser diagnostics .....	92
5.2.3	Calibration of absorption measurements .....	93
5.3	Results: validation of the diagnostics method.....	95
5.3.1	Relaxation measurements in $CO_2-N_2$ .....	95
5.3.2	Relevant processes.....	95
5.4	Modelling of vibrational kinetics in $N_2-CO_2$ mixtures: determination of $\gamma$ .....	97
5.4.1	Relaxation processes in $CO_2-N_2$ .....	97
5.4.2	Model description .....	99
5.4.3	Modelling results .....	101
5.5	Application of $CO_2$ titration as a diagnostic tool.....	106
5.5.1	Relaxation of $N_2(v)$ on catalytic surfaces .....	106
5.5.2	Kinetics of vibrational excitation of $N_2$ in a pulsed DC discharge.....	107
5.6	Summary and conclusions .....	109
<b>6</b>	<b>Influence of plasma treated catalytic surfaces on molecular oxidation</b>	<b>111</b>
6.1	Introduction .....	112
6.2	Experimental.....	114
6.2.1	Discharge tube configuration .....	114
6.2.2	Time-resolved quantum cascade laser diagnostics .....	115
6.2.3	Experimental procedure .....	117
6.3	Results and discussion.....	118
6.3.1	Kinetics of $C_2H_2$ destruction on a pre-treated $TiO_2$ surface .....	118
6.3.2	Oxidation of adsorbed reaction intermediates .....	121
6.3.3	Photo-catalytic oxidation of $C_2H_2$ and $CO$ .....	122
6.4	Summary and conclusions .....	125
	<b>Bibliography for Chapters 5 and 6</b>	<b>126</b>

<b>7</b>	<b>Application potential of EC-QCLs for plasma diagnostics</b>	<b>131</b>
7.1	Introduction.....	132
7.2	Experimental .....	133
7.2.1	EC-QCL test setup .....	133
7.2.2	Three channel EC-QCL spectrometer and MW plasma reactor .....	136
7.3.	Results and discussions.....	139
7.3.1	Laser line width determination .....	139
7.3.2	Evolution of molecular concentrations and of the gas temperature in Ar/N <sub>2</sub> /CH <sub>4</sub> MW plasmas .....	141
7.3.3	Laser power variation for validation of concentration measurements ..	143
7.3.4	Wavelength modulation spectroscopy in He/Ar plasmas .....	145
7.4	Summary and conclusions.....	146
<b>8</b>	<b>Plasma chemistry in RF plasmas containing ATI</b>	<b>147</b>
8.1	Introduction.....	147
8.2	Experimental .....	150
8.3	Results and discussion .....	153
8.4	Summary and conclusions.....	156
	Bibliography for Chapters 7 and 8	158
<b>9</b>	<b>Conclusions and outlook</b>	<b>163</b>
<b>10</b>	<b>Appendix</b>	<b>169</b>
10.1	Abbreviations .....	169
10.2	List of symbols.....	172
	Acknowledgment	175
	Curriculum Vitae	177
	Scholarly contributions	179
	Declaration	185



# Abstract

In this work, various aspects of fundamental physics and chemistry of molecular gas discharges are presented with emphasis on the interaction between species, activated by low-pressure plasmas, and surfaces. As already known, synergistic effects of multiple plasma-generated species are responsible for surface modification. However, due to the large number of internal parameters of a discharge and the complex plasma processes the identification of correlations between plasma characteristics and their effects on surfaces are complicated.

Therefore, the aim of this thesis is to improve the understanding of several phenomena associated with plasma–surface interactions by measuring or calculating fundamental kinetic, transport or spectroscopic data needed to interpret measurements and hereby, to support some future applications of plasmas.

On the basis of these issues, *in-situ* observation of chemical processes occurring at active screen plasma nitriding (ASPN) has been performed. For the monitoring of excited species and stable plasma products a quadruple mass spectrometer (QMS) was applied combined with tunable diode laser absorption spectroscopy (TDLAS) diagnostics. The temporal dependencies of concentrations of several molecular species were monitored and found to be in the range of  $10^{13}$  to  $10^{15}$  molecules  $\text{cm}^{-3}$ . Moreover, profound knowledge of related process conditions such as gas ratio, process temperature, and bias activation power has been achieved. The results of the performed measurements showed a qualitatively good agreement with the kinetics reported in the literature and thus, prove the applicability of the implemented approach for monitoring of nitriding mechanisms at certain process conditions in the ASPN.

The following chapter thematizes dusty plasmas which exhibit interesting aspects, not only from the view of astrophysics but also for its application in the laboratory. Even relatively low concentrations of dust particles in plasmas can initiate novel dynamics due to

their collective interactions. For a better understanding of these effects, chemical phenomena in hydrocarbon-containing Ar/He dusty plasmas have been studied combining TDLAS and Fourier transform infrared (FTIR) spectroscopy techniques. The experiments were done in a RF capacitively coupled (cc) parallel plate reactor,  $f = 13.56$  MHz. Using TDLAS, the temporal evolution of  $C_2H_2$ ,  $C_2H_4$ ,  $CH_3$ ,  $CH_4$ ,  $CO$ , and  $CO_2$  concentrations were measured whereas the formation of dust particles was simultaneously monitored by FTIR. The concentrations of all hydrocarbon species were found to be strongly correlated with the dynamic of the dust formation. The values of the calculated fragmentation of the precursor molecules and of the conversion rates of the produced hydrocarbons were in a comparable order of magnitude as those in surface wave discharges and in planar microwave (MW) plasmas.

The investigation of surface processes cannot be done without knowledge of the surrounding gas phase and plasma chemistry. Even in the first milliseconds after ignition, plasma can have an impact on the chemistry of the volume and therefore, influence the species interacting with the surface. Since quantum cascade lasers (QCL) are commercially available, the application of infrared laser absorption spectroscopy (IR-LAS) for measurements with the time resolution down to about 100 ns has become feasible and can open up new possibilities for highly sensitive and selective *in-situ* diagnostic of several molecular species.

Owing to the performance of this technique, a new method for the determination of the wall de-excitation probability  $\gamma_{N_2}$  of vibrationally excited  $N_2$  has been proposed. Based on the idea of titrating vibrationally excited  $N_2$  by a small admixture of infrared (IR) active molecules – gas mixtures containing small amount of titrating gas ( $CO_2$ ) in  $N_2$  at low pressure were excited by a few millisecond long DC discharge pulse. Using a 3-channel QCL spectrometer, TRIPLE Q, dedicated to time resolved *in-situ* gas sensing, the relaxation kinetics of titrating molecules was followed in the afterglow phase. Afterwards, a vibrational kinetics model of the  $N_2$ - $CO_2$  system was developed. The agreement between the model and the experiment allowed the calculation of the value of the  $N_2(v=1)$  relaxation probability, which was found to be  $1.1 \times 10^{-3}$  for silica and Pyrex,  $9 \times 10^{-3}$  for smooth  $TiO_2$  surfaces, and  $4 \times 10^{-2}$  for sol-gel films impregnated with  $TiO_2$  particles. It was established that for catalytic materials the relaxation probability of the first vibrational level of nitrogen  $\gamma_1$  depends on the pre-treatment of the surface and on the applied titrating gas. Consequently, the probability of  $N_2(v)$  surface losses can be directly assumed from the measured relaxation curves.

Apart from traditional technical plasma applications, the use of electric discharges is a promising technique for toxic gas removal, especially when these gases are present at low concentrations. In spite of increasing number of investigations, the selectivity of the reaction products and energy efficiency are remaining a challenge. On the example of  $C_2H_2$  and CO the reactivity of plasma treated photo-catalytic  $TiO_2$  surfaces for their oxidation was studied.

A  $TiO_2$ -coated Pyrex discharge tube was exposed to low pressure RF plasmas using  $O_2$ , Ar or  $N_2$  ( $f=13.56$  MHz,  $p=0.53$  mbar,  $P=17$  W) and additionally has been stimulated by heating and UV radiation treatment. The temporal development of the concentrations of the precursor gases  $C_2H_2$  or CO and of possible higher molecular reaction products has been monitored using QCLAS and MS techniques. It has been shown, that under RF oxygen plasma treatment, reactive oxygen species could be grafted onto the surface of  $TiO_2$  and further, that their reactivity depends on the reacting molecules. The reactive adsorption of  $C_2H_2$  molecules on the inner surface of the tube reactor has showed a density of about  $7.5 \times 10^{12}$   $C_2H_2$  molecules  $cm^{-2}$ , however no adsorption phenomena for CO could be monitored. Studying the  $C_2H_2$  oxidation in a post-treatment phase stimulation by heating or UV radiation confirms that the reaction  $(O_{ads} + C_2H_2)_{TiO_2}$  produces some adsorbed intermediates. Therefore, the analysis of performed measurements provides information about plasma surface stimulation, molecular adsorption processes, and surface chemistry phenomena.

Nowadays industrial used plasmas are consisting of complex gas mixtures. Their investigation often requires the simultaneous information about a variety of reaction products. Using external cavity quantum cascade lasers (EC-QCLs), the tunability over much broader spectral ranges than with a typical lead salt lasers or distributed feedback QCLs can be achieved. Based on their internal properties, high output power, intrinsic narrow line width and wide spectral tunability, EC-QCLs have a high potential for applications for plasma diagnostic purposes. In the framework of this thesis several EC-QCLs operating between  $1300$  and  $2250\text{ cm}^{-1}$  ( $4.42 - 7.66\text{ }\mu\text{m}$ ) have been used for the analysis of physical and chemical phenomena in Ar/ $N_2$ /CH<sub>4</sub> MW plasma. Furthermore, in a pure He/Ar MW discharge the wavelength modulation spectroscopy (WMS) technique has been applied for high sensitivity detection of transient plasma species. Finally, using IR-LAS based on a cw EC-QCL arrangement the evolution of the six stable molecules, CH<sub>4</sub>,  $C_2H_2$ ,  $C_2H_4$ , H<sub>2</sub>O, HCN, and HNO<sub>3</sub>, has been simultaneously monitored in Ar and Ar/ $N_2$  RF discharges containing aluminium tri-isopropoxide (ATI).



# Kurzfassung

Im Rahmen der vorliegenden Arbeit wurden sowohl physikalische als auch chemische Aspekte von molekularen Entladungen untersucht. Sie konzentriert sich auf Umwandlungsprozessen von verschiedenen Spezies, die durch Niederdruckplasmen aktiviert und von der Oberfläche katalysiert werden. Es ist allgemein bekannt, dass synergistische Effekte von mehreren, im Plasma entstandenen Spezies für die Oberflächenmodifikation zuständig sind. Allerdings ist die Anzahl von internen Parametern einer Entladung so hoch und die Effekte sind generell so kompliziert, dass sogar die Identifizierung der Verbindung zwischen Eigenschaften des Plasmas und deren Auswirkungen auf die Oberflächen sehr aufwendig ist.

In diesem Zusammenhang das Verständnis von verschiedenen, durch Plasma-Oberflächen-Wechselwirkungen auftretenden Phänomenen zu verbessern, war das Hauptziel dieser Dissertation. Um eine bessere Einsicht zu ermöglichen werden grundlegende kinetische-, spektroskopische- oder Transportdaten interpretiert. Dadurch können auch mehrere verschiedene Anwendungsmöglichkeiten von Plasmen unterstützt werden.

Auf Grund dieser Problemstellung wurden die chemischen Prozesse, die beim Plasmanitrieren mit einem Aktivgitter (ASPN) stattfinden, *in-situ* beobachtet. Die Kombination eines Quadrupel-Massenspektrometers (QMS) zusammen mit einer, auf Absorptionsspektroskopie mittels durchstimmbarer Laserdioden basierender Diagnostik (TDLAS), ist für das Monitoring der angeregten Spezies und stabilen Plasmaproducte angewendet worden. Die Konzentrationen verschiedener, molekularer Spezies wurden verfolgt und im Bereich von  $10^{13}$  bis  $10^{15}$  Moleküle  $\text{cm}^{-3}$  gemessen. Außerdem wurde der Einfluss von Prozessparametern, wie z.B. Mischungsverhältnisse, Temperatur und Bias-Leistung, untersucht. Die Ergebnisse der durchgeführten Messungen stimmten mit der in der Literatur aufgeführten Kinetik gut überein und beweisen hiermit die Anwendbarkeit des

implementierten Ansatzes des Monitorings von Nitrier-Mechanismen im ASPN bei veränderten Prozessbedingungen.

Der nächste Aspekt der vorliegenden Studie umfasst staubige Plasmen, die interessantes Gebiet nicht nur aus Sicht der Astrophysik sondern auch für die Anwendung im Labor darstellen. Dank ihrer kollektiven Wechselwirkung können selbst relativ geringe Konzentrationen von Staubpartikeln in Plasmen zu einer neuen Dynamik führen. Zum besseren Verständnis dieser Effekte wurden die chemischen Phänomene in staubigen Kohlenwasserstoff enthaltenden Ar/He Plasmen mit Methoden der TDLAS und der Fourier-Transformations-Infrarotspektroskopie (FTIR) untersucht. Die Experimenten wurden in einem RF-cc gekoppeltem Parallelplattenreaktor ( $f = 13.56$  MHz) durchgeführt. Die zeitliche Entwicklung der  $C_2H_2$ ,  $C_2H_4$ ,  $CH_3$ ,  $CH_4$ ,  $CO$  und  $CO_2$ -Konzentrationen wurde mittels TDLAS gemessen und die Staubpartikelbildung wurde mit FTIR überwacht. Die Konzentrationen aller Kohlenwasserstoffspezies sind stark mit der Dynamik der Staubbildung korreliert. Die berechnete Fragmentierungsrate des Prekursors und die Bildungsraten der erzeugten Kohlenwasserstoffe bewegen sich in vergleichbarer Größenordnung, wie in den Oberflächenwellenentladungen und planaren Mikrowellenplasmen (MW).

Das Verständnis der Oberflächeneffekte kann nicht ohne Kenntnis der angrenzenden Gasphase und der plasmachemischen Prozesse erfolgen. Schon in den ersten Millisekunden nach dem Zünden können Plasmen Auswirkungen auf die Reaktionschemie des Volumens haben und damit auch die Wechselwirkung zwischen molekularen Spezies mit der Oberfläche beeinflussen. Da seit 10-15 Jahren Quantenkaskadenlaser (QCL) im Handel erhältlich sind, ist die Anwendung der Infrarotlaser Absorptionsspektroskopie (IR-LAS) für Messungen mit einer zeitlichen Auflösung von bis zu 100 ns möglich geworden. Dies eröffnet neue Möglichkeiten für hochempfindliche und selektive *in-situ* Diagnostik mehrerer molekularer Spezies.

Aufgrund der Leistungsfähigkeit dieser Technik ist diese neue Methode für die Bestimmung der Wand-Abregung-Wahrscheinlichkeit schwingungsangeregten  $N_2$  vorgeschlagen worden. Bezogen auf die Idee, schwingungsangeregten  $N_2$  durch eine kleine Beimischung von infrarotaktiven Molekülen zu titrieren – Gasgemische enthaltende geringe Menge  $CO_2$  in  $N_2$  bei niedrigem Druck wurden bei einer kurze gepulste DC-Entladung angeregt. Ein dreikanaliges QCL-Spektrometer, TRIPLE Q, wurde für die zeitaufgelöste *in-situ* Diagnostik der Relaxationskinetik der Titrations-Moleküle im Afterglow zum Einsatz gebracht. Danach wurde die Schwingungskinetik des  $N_2$ - $CO_2$ -Systems modelliert.

Die  $N_2(v=1)$  Relaxationswahrscheinlichkeit konnte mit  $1.1 \times 10^{-3}$  für Siliciumdioxid und Pyrex,  $9 \times 10^{-3}$  für glatte  $TiO_2$  Oberflächen und  $4 \times 10^{-2}$  für mit  $TiO_2$ -Partikeln imprägnierte Sol-Gel-Filme bestimmt werden. Die Berechnung obengenannter Werte war durch den Vergleich von experimentellen und modellierten Ergebnissen möglich. Wie weiterhin festgestellt wurde, ist die Relaxationswahrscheinlichkeit des ersten Vibrationsniveaus von Stickstoff  $\gamma_1$  für katalytische Materialien von der Vorbehandlung der Oberfläche und vom Titriergas abhängig, wobei die Wahrscheinlichkeit von  $N_2(v)$ -Verlusten an der Oberfläche direkt aus den gemessenen Relaxationskurven bestimmt werden kann.

Neben einer Vielzahl von klassisch technischen Plasmaanwendungen ist der Einsatz elektrischer Entladungen für die Beseitigung von toxischen Gasen eine vielversprechende Technik, insbesondere, wenn diese Gase in niedrigen Konzentrationen vorliegen. Obwohl die Anzahl an Untersuchungen der Stoffwandlung in der letzten Zeit stetig zugenommen hat, stellt deren Energieeffizienz und Selektivität der Reaktionsprodukte eine bedeutsame Herausforderung dar. Motiviert durch diese Herausforderungen wurde die Reaktivität von plasmabehandelten photokatalytischen  $TiO_2$ -Oberflächen für  $C_2H_2$ - und CO-Oxidation untersucht.

Die Innenseite eines mit  $TiO_2$  beschichteten Entladungsrohres aus Pyrex war einem RF Niederdruckplasma in  $O_2$ , Ar und  $N_2$  ( $f=13.56$  MHz) ausgesetzt und wurde zusätzlich durch Erwärmen oder UV-Strahlung stimuliert. Die zeitliche Entwicklung der Konzentration der Prekursorgase  $C_2H_2$  oder CO und möglicher höherer molekularer Reaktionsprodukte, wurde mittels QCLAS und MS-Techniken untersucht. Es wurde festgestellt, dass unter Einfluss einer RF-Sauerstoffplasmabehandlung, reaktive Sauerstoffspezies auf der Oberfläche der  $TiO_2$  gepropft werden können und ihre Reaktivität vom Reaktionsmolekül abhängt. Während reaktive Adsorption von  $C_2H_2$ -Molekülen auf der inneren Oberfläche des Rohrreaktors eine Dichte von etwa  $7.5 \times 10^{12}$  Molekülen  $cm^{-2}$  aufwies, konnte keine Adsorption von CO nachgewiesen werden. Der Stimulationseffekt der  $C_2H_2$  Oxidation durch Erwärmen oder UV-Strahlung hat bestätigt, dass die Reaktion  $(O_{ads} + C_2H_2)_{TiO_2}$  zur Produktion einiger auf der Oberfläche adsorbierten Zwischenprodukte führt. Die Analyse der durchgeführten Messungen gibt Auskunft über die Stimulation von Oberflächen durch Plasmen, molekulare Adsorptionsprozesse sowie chemische Phänomene an den Oberflächen.

Die heutzutage von der Industrie verwendeten Plasmen bestehen aus komplexen Gasgemischen, deren Untersuchung meist eine gleichzeitige Kenntnis einer Vielzahl von Reaktionsprodukten erfordert. Dies kann durch Verwendung von Quantenkaskadenlasern mit

externer Kavität (EC-QCL) realisiert werden, die über einen weitaus breiteren Spektralbereich durchgestimmt werden können, als dies bei typischen Bleisalzlasern oder QCLs möglich ist. Basierend auf den Merkmalen – hohe Ausgangsleistung, inhärent schmales Geräteprofil und breite spektrale Durchstimmbarkeit, haben EC-QCLs ein enormes Potenzial für Anwendungen zum Zwecke der Plasmadiagnostik. Im Rahmen dieser Arbeit werden verschiedene EC-QCLs, die zwischen  $1300$  und  $2250\text{ cm}^{-1}$  ( $4.42 - 7.66\text{ }\mu\text{m}$ ) emittieren, für die Analyse von physikalischen oder chemischen Phänomenen in  $\text{Ar}/\text{N}_2/\text{CH}_4$  MW Plasmen verwendet. Weiterhin wird eine spektroskopische Technik basierend auf Wellenlängenmodulation (WMS) in einer reinen  $\text{He}/\text{Ar}$  MW Entladung für hochempfindliche Detektion transienter Plasmaspezies angewendet. Neben der Untersuchung der bereits erwähnten Plasmen, wird ein EC-QCL für ein gleichzeitiges Monitoring von sechs stabilen Molekülen ( $\text{CH}_4$ ,  $\text{C}_2\text{H}_2$ ,  $\text{C}_2\text{H}_4$ ,  $\text{H}_2\text{O}$ ,  $\text{HCN}$  und  $\text{HNO}_3$ ) in  $\text{Ar}$  sowie  $\text{Ar}/\text{N}_2$  RF Entladungen, mit enthaltenden Aluminium-tri-isopropoxiden (ATI) eingesetzt.

# Аннотация

В данном диссертационном исследовании представлено детальное рассмотрение некоторых аспектов фундаментальной физики и химии молекулярных газовых разрядов. Особое внимание в работе было уделено изучению взаимодействий между поверхностями и частицами (электронами, ионами, атомами, молекулами, радикалами и др.), образуемыми в плазме при низком давлении. Синергетические эффекты, вызываемые комбинацией реагирующих в плазме частиц, и их влияние на модификацию поверхности, рассмотрены в научной литературе. Однако, в связи с тем, что количество внутренних параметров газового разряда высоко, а происходящие в нем процессы, как правило, достаточно сложны, определение связи между характеристическими параметрами разряда и его влиянием на поверхность часто бывает затруднительным.

Целью представленной работы является исследование явлений, связанных с плазмо-поверхностными взаимодействиями путем измерений и вычислений фундаментальных кинетических, транспортных и спектроскопических данных, необходимых для интерпретации экспериментов и способствующих последующим применениям газовых разрядов.

В ходе работы было проведено *in-situ* наблюдение химических явлений, возникающих в процессе плазменного азотирования стальных деталей с применением активного сетчатого экрана (ASPN). Использование квадрупольного масс-спектрометра (QMS) в сочетании с методом абсорбционной спектроскопии на основе перестраиваемых лазерных диодов (TDLAS) дало возможность осуществить мониторинг как возбужденных частиц, так и стабильных продуктов плазмы, чьи концентрации были найдены в диапазоне от  $10^{13}$  до  $10^{15}$  см<sup>-3</sup>. Кроме того, были получены детальные сведения о происходящих процессах при изменении таких

параметров, как соотношение концентраций используемых газов, температура разряда или напряжение смещения (BIAS). Результаты проведенных исследований согласуются с опубликованной ранее кинетикой происходящих процессов и тем самым доказывают применимость реализованного подхода к мониторингу механизмов плазменного азотирования с применением активного сетчатого экрана.

Повышенный интерес к пылевой плазме обусловлен ее распространенностью в сфере астрофизических исследований, а также использованием в качестве предмета изучения в лабораториях. Актуальность данного вопроса определяется способностью пылевых частицы в плазме, даже при сравнительно низких концентрациях, благодаря их коллективным взаимодействиям, инициировать образование новых динамических процессов. Для более углубленного понимания происходящих эффектов химические явления плазмы в Ar или He с добавлением углеводородов изучались методами абсорбционной- (TDLAS) и ИК-Фурье-спектроскопии (FTIR). Для проведения экспериментов использовался реактор с параллельно расположенными металлическими электродами, генерировавшими высокочастотный емкостной разряд ( $f = 13.56$  МГц). Изменение концентрации молекул  $C_2H_2$ ,  $C_2H_4$ ,  $CH_3$ ,  $CH_4$ , CO,  $CO_2$  с течением времени были измерено с помощью метода абсорбционной спектроскопии, в то время как образование частиц пыли в разряде контролировалось Фурье-спектрометром. Использование данных методик позволило определить существенную корреляцию концентрации всех углеводородных частиц с динамикой образования пыли. Рассчитанные скорости фрагментации молекулы-прекурсора, а также скорость формирования других углеводородов сопоставимы с аналогичными величинами в поверхностных СВЧ разрядах (MW) на поверхности диэлектрика или на плоской пластине.

Исследование поверхностных эффектов невозможно без понимания влияния на них окружающей газовой фазы совместно с плазмохимическими процессами. Начиная с первых миллисекунд после генерации, плазма в состоянии оказывать влияние на химический состав реагирующей смеси и, следовательно, на виды частиц взаимодействующих с поверхностью. Вследствие увеличившейся в последнее время коммерческой доступности квантово-каскадных лазеров (QCL), применение методов инфракрасной спектроскопии, основанной на поглощении лазерного излучения (IR-LAS), стало возможным для проведения исследований с временным разрешением примерно до 100 нс, что, в свою очередь, открывает новые перспективы для

высококочувствительных и селективных диагностических измерений.

Благодаря высокой производительности данного типа лазеров в ходе работы был предложен новый метод для определения вероятности релаксации на поверхности колебательно-возбужденных молекул  $N_2$ . Основываясь на идее титрования колебательно-возбужденного  $N_2$  с примесью ИК-активных молекул, смесь газов, содержащая небольшое количество  $CO_2$  в  $N_2$  при низком давлении, возбуждалась коротким (несколько миллисекунд) импульсным разрядом постоянного тока (DC). При помощи TRIPLE-Q-спектрометра, базирующегося на применении трех независимых квантово-каскадных лазеров, наблюдалась кинетика релаксации молекул  $CO_2$  в фазе послесвечения. Также в ходе работы была разработана колебательная модель кинетики системы  $N_2$ - $CO_2$ . Согласование между моделью и экспериментом позволило рассчитать значения вероятности релаксации  $N_2(v=1)$ , найденные равными  $1.1 \times 10^{-3}$  для кремниевой и Ругех поверхностей,  $9 \times 10^{-3}$  для гладкой поверхности  $TiO_2$  и  $4 \times 10^{-2}$  для поверхности пропитанной нано-частицами  $TiO_2$ . В дополнение было установлено, что релаксационная вероятность первого колебательного уровня азота  $\gamma_1$  для каталитических материалов зависит от способа предварительной обработки поверхности и применяемого газа титрования. Кроме того, определение вероятности потерь  $N_2(v)$  на поверхности оказалось возможным благодаря прямому анализу измеренных релаксационных кривых.

Помимо традиционных технических применений плазмы, использование электрических разрядов для удаления токсичных газов является перспективным методом, особенно в случаях, когда их концентрация незначительна. Несмотря на растущее в последнее время число исследований, селективность продуктов реакции наряду с энергетической эффективностью остается серьезной проблемой.

В данной работе, на примере процесса окисления  $C_2H_2$  и  $CO$ , исследовалась реакционная способность фото-каталитической поверхности  $TiO_2$ , обработанной в плазме. Для этого в стеклянной трубке (Ругех), внутренняя поверхность которой была покрыта  $TiO_2$ , зажигался высокочастотный разряд (RF) в газовой среде ( $O_2$ ,  $N_2$ ,  $Ar$ ) при низком давлении ( $f=13.56$  МГц). Затем поверхность дополнительно нагревалась, либо подвергалась воздействию УФ-излучения. В дальнейшем, используя TRIPLE-Q- и масс-спектрометр, проводилось наблюдение изменения концентраций молекул-прекурсоров  $C_2H_2$  или  $CO$ , а также последующих продуктов реакций данных молекул с поверхностью. В ходе проведения экспериментов было показано, что разряд в

кислороде может способствовать осаждению активных форм кислорода на поверхности  $\text{TiO}_2$ , а их реакционная способность зависит от вступающих в реакцию веществ. Так, плотность реактивно-адсорбированных молекул  $\text{C}_2\text{H}_2$  на внутренней поверхности трубки была найдена в размере  $7.5 \times 10^{12} \text{ см}^{-2}$ , однако влияние каталитической поверхности на адсорбционную способность  $\text{CO}$  не было экспериментально установлено. Стимулирование процесса окисления  $\text{C}_2\text{H}_2$ , осуществлялось путем нагревания газоразрядной трубки или ее облучения УФ-светом. Данные эксперименты подтвердили, что реакция  $(\text{O}_{\text{ads}} + \text{C}_2\text{H}_2)_{\text{TiO}_2}$  приводит к образованию некоторых промежуточных продуктов, адсорбированных на поверхности. Таким образом, анализ проведенных измерений предоставляет информацию об эффекте активации поверхности путем обработки плазмой, о молекулярных процессах адсорбции, а также происходящих химических реакциях на поверхности.

Используемые в настоящее время в промышленности виды плазменных разрядов часто зажигаются в сложно-компонентных газовых смесях, и для их практического применения необходимо одновременное получение информации о различных продуктах реакции. Альтернативой типичным в спектроскопических исследованиях лазерам на основе солей свинца или квантово-каскадным лазерам с распределенной обратной связью, могут стать квантово-каскадные лазеры с внешним резонатором (EC-QCL), настройка которых возможна в гораздо более широком спектральном диапазоне. Обладание такими характеристическими особенностями как высокая мощность излучения, узкий инструментальный профиль, а также возможность внутренней перенастройки на широком интервале, определяет высокий потенциал данных лазеров для их применения в диагностических целях. В рамках представленной работы несколько квантово-каскадных лазеров с внешним резонатором, перенастраиваемых в диапазоне от  $1300$  до  $2250 \text{ см}^{-1}$  ( $4.42 - 7.66 \text{ мкм}$ ) были использованы для анализа физических или химических явлений в  $\text{Ag}/\text{N}_2/\text{CH}_4$  микроволновой плазме. Кроме того, спектральный метод, использующий в своей основе модуляцию длины волны (WMS-спектроскопия), был применен для высокочувствительного обнаружения частиц с очень коротким периодом жизни в  $\text{He}/\text{Ar}$  СВЧ разряде. В заключение, EC-QCL был использован для одновременного отслеживания эволюции молекул,  $\text{CH}_4$ ,  $\text{C}_2\text{H}_2$ ,  $\text{C}_2\text{H}_4$ ,  $\text{H}_2\text{O}$ ,  $\text{HCN}$ , и  $\text{HNO}_3$ , в ВЧ разряде, зажигаемом в  $\text{Ar}$  и  $\text{Ar}/\text{N}_2$  атмосфере с добавлением триизопроксид алюминия (ATI).





# 1 General Introduction

## 1.1 Non-equilibrium plasmas

*“We shall use the name plasma to describe this region containing balanced charges of ions and electrons.”*

Irving Langmuir

Plasma is often called the “fourth state of matter” or even the “first state of matter” as far the most common phase of ordinary matter in the universe. Plasma is frequently subdivided into in high- or low-temperature plasmas. A further differentiation relates to thermal and non-thermal plasmas, or non-equilibrium plasmas (see table 1.1). Plasma can be understood as a weakly to partially ionized gas, containing a significant number of neutral and electrically charged constituents, which are in strong non-equilibrium in the velocity and energy distributions [1]. While high-temperature plasmas show an equal energy level of all charged particles, non-equilibrium plasmas are characterized by a presence of generally hot electrons (up to tens of eV), whereas the neutral gas temperature is relatively low (few tenths of eV). From collisions with neutral molecules these electrons can efficiently create vibrationally and electronically excited species as well as reactive radical fragments, which in their turn can produce unique structures in the gas phase and on surfaces. Generated by electron impact of excited species photons can have a more or less strong impact on other species or the plasma boundaries. In these boundaries externally generated electromagnetic radiation interacts most sufficient with the plasma. Therefore, due to these strong gradients, plasma properties can change dramatically leading to plasma-surface interactions [2-4].

Nowadays exists a variety of methods for producing non-equilibrium plasmas. Divided into glow, pulsed corona, dielectric barrier, radio frequency and microwave discharges, they can be generated at laboratory or industrial scale [5]. All these discharge plasma sources attempt to produce non-equilibrium plasmas at low- as well as at atmospheric pressure, which has a strong influence on the amount of collisions between the gas species and their free path length. In low pressure plasmas due to a fewer collisions a sufficient difference in temperature between the plasma species can be achieved. Whereas an increasing gas pressure entails an increased efficiency of energy transfer between the interacted gas species, which leads to higher temperature of all species.

Therefore, non-equilibrium plasmas stand under growing interest not only as model systems in basic research, but also in plasma processing and technology. They are useful in the large number of applications important to our live, among them are surface treatment (coating, etching, cutting, welding) and thin film deposition, lightning manufacture and medical applications such as sterilization, blood coagulation and wound healing [6-8]. Moreover, the approach of combining non-equilibrium plasmas with catalyst for toxic gas removal and air pollution control has been a technical as well as a scientific challenge over the past decade [9-11]. In addition such plasmas play a part in supersonic combustion engines for aerospace engineering and are present in fusion reactors [12, 13].

**Table 1.1:** *General categories of plasmas.*

	Low-temperature Plasma (LTP)		High-temperature Plasma (HTP)
	Non-thermal LTP	Thermal LTP	
Related temperature	$T_{\text{ion}} \approx T_{\text{gas}} \approx 300\text{K}$ $T_{\text{ion}} \ll T_e \leq 10^5 \text{ K}$	$T_e \approx T_{\text{ion}} \approx T_{\text{gas}}$ $T_{\text{all}} \leq 2 \times 10^4 \text{ K}$	$T_{\text{ion}} \approx T_e \approx T_{\text{gas}}$ $T_{\text{all}} \geq 10^6 - 10^8 \text{ K}$
Electron density	$n_e \approx 10^{10} \text{ m}^{-3}$	$n_e \geq 10^{20} \text{ m}^{-3}$	$n_e \geq 10^{20} \text{ m}^{-3}$
Degree of ionization		$10^{-8} - < 1$	$\approx 1$
Pressure		$10^{-6} - 1 \text{ bar}$	$\geq 1 \text{ bar}$
State		Homogeneous	Filamentary
Example	Low-pressure glow discharge	Arc plasma at atmospheric pressure	Fusion plasmas

The wide application range motivates fundamental investigations of the plasma chemistry and kinetics, which requires detailed knowledge of the main plasma parameters obtained by appropriate diagnostic techniques. It is well known, that the final goal strongly depends on a variety of interacting internal parameters of the process discharge such as species concentration, neutral gas temperature, electron density, electron temperature, ion fluxes and energies, potential distributions or the electron distribution function. On the other

hand, the internal parameters of the discharge are influenced by externally adjustable parameters like discharge power, the process gases and their pressure, the bias voltages or externally applied magnetic fields. Furthermore, the discharge geometry has a crucial influence on the process as well.

While the desired result is strongly depended on these internal parameters, the final users are often irresponsible or not familiar to these. Nowadays, it is no longer possible to run plasma processes without an understanding of the basic relations between them. In this case, the online monitoring of transient or stable plasma reaction products in chemical reactors, in particular the measurement of their ground state concentrations is the key to an improved knowledge of the plasma chemistry and kinetics in these molecular discharges.

## 1.2 Plasma diagnostic methods

To get better insight in the processes occurring in the plasma many different techniques are being employed. Although most of them are already well established, plasma diagnostics is still a very challenging discipline [14]. Ideally, as much as possible plasma parameters should be diagnosed simultaneously. The best technique needs to be non-invasive, to obviate perturbations of the discharge, and allow the in-situ approach without the additional extracting of samples. Furthermore, it should be selective to the target parameter or species and provide time-resolved measurements by temporal and spatial resolutions smaller than the typical time and length of the instabilities. In addition, it has to be calibration-free. Because these properties are not available in a single device together, often there is a need for multi-channel diagnostics [15-17].

The study in the field of low-temperature plasmas has a long tradition, since in the beginning of last century the method of electric probe measurements was developed by Langmuir *et al* [18]. In general, from the exponential part of current-volt characteristics, basic parameters of the plasma, like the electron density, electron temperature or electron energy distribution function (EEDF) can be deduced [19-21]. However, the technique of probe measurements belongs to invasive methods and is limited to the low pressure discharges.

Mass Spectrometry (MS) as well as Gas Chromatography (GC) are often used for the qualitative and quantitative analysis of the molecular species with sensitivity down to ppm [22-24]. These both methods are hard applicable for detection of transient species like radicals

or ions. Beside, based on an ex-situ sampling approach they are showing rather low, in the range of minutes, temporal resolution. Nevertheless, a mass spectrometer is the most common tool to be found in the field of plasma diagnostics and GC is a standard method in the chemical or pharmaceutical industry.

Optical Emission Spectroscopy (OES), as one of the non-invasive methods, is an important tool for fast and accurate analysis of the chemical elements at the complete range from sub-ppm to percentage levels [15, 25-28]. All relevant elements can directly be analyzed simultaneously. Modern OES spectrometer feature high spectral and time resolution with a sensitivity near the single photon detection limit. Hence, the calculation of population densities requires additional knowledge of the EEDF, appropriate cross-sections and transition probabilities with additional instrumental calibration.

The investigation of plasma physics and chemistry by methods based on traditional optical absorption spectroscopy (OAS) has become now of increasing interest. Owing to increasing availability of powerful, tuneable and narrow line width laser, this *in-situ* diagnostic can be applicable at a wide spectral range. OAS in the infrared (IR), visible, vacuum ultraviolet (VUV) and extreme ultraviolet (XUV) spectral regions can provide wealthy information of the discharge processes. Measurements of line intensities, broadening and shifts can yield valuable information on atom, molecule and ion densities in excited and ground states, as well as about gas, vibrational and rotational temperatures.

With Laser Induced Fluorescence (LIF) transitions are induced between excited states of certain ion species. This method yields the information of ground state number densities with high spatial, up to mm, and good temporal, in the range of ns, resolution [25, 29, 30]. An advantage over other OAS techniques is that it is possible to get two- and three-dimensional images since fluorescence taking place in all directions. However, only relative concentrations can be measured by means of LIF. Thereby, to gain the absolute concentrations of the species reliable calibration procedures are required. Comparing to OES, LIF is technically more complicated, but offers rather better spatial resolution.

In case of Coherent Anti-Stokes Raman Scattering (CARS) a multiple photon sheaf induces molecular vibrations and produces a signal in which the emitted waves are coherent with one another. This signal can be used to determine molecular properties like concentrations, rovibrational population distributions or temperatures. CARS is applicable for measurements requiring the time resolution in the nanosecond range and can be used to determine the species concentration down to  $10^{12} \text{ cm}^{-3}$  [31-34].

For a long period of time infrared spectroscopy has been a main technique for plasma and materials analysis in the laboratory. The absorption peak distribution in an infrared spectrum is given in a unique way for each different material because they correspond to the frequencies of vibrations between the bonds of the atoms. It means, there are no two compounds that produce exact the same infrared spectrum. Species identification is deduced from the spectral line positions while line profiles are often connected with gas temperature and relative intensities provide the knowledge about species concentration. Therefore, infrared spectroscopy is an excellent tool for qualitative as well for quantitative analysis.

In order to overcome the limitations encountered with dispersive instruments Fourier transform infrared spectroscopy (FTIR) can be used for quantitative *in-situ* plasma investigations [35, 36]. The combination of continuous broadband light source with a Michelson interferometer offers wide spectral range sensitivity with a relatively sensitive detection limit, which is in the order of ppm. However, the measurement speed is limited by the mirror speed and the wavelength range.

Cavity Ring-Down Spectroscopy (CRDS) is one more high-sensitive method of laser absorption spectroscopy [37, 38]. It has numerous applications and enables measurement of absolute densities by samples, which scatter and absorb the light. The absorption path lengths in the kilometers range, which can be achieved by appropriate instruments, provide the determination of absorptions as low as  $10^{-9}$  by the temporal resolution in the order of microseconds. Limited availability of tunable laser light at the appropriate wavelength and of high reflectance mirrors at those wavelengths is probably the main disadvantage of this method.

Owing to recent development and commercial availability of different electromagnetic radiation sources mid infrared laser absorption spectroscopy (MIR-LAS) has been offered as an attractive new option for plasma diagnostic purposes. Based on Tunable Diode Lasers and applied in this work (see chapters 3 and 4) MIR-TDLAS has been intensively used also by many other authors for determination of neutral gas temperatures [39], study of dissociation processes or detection of free radicals [40-43], or temporally resolved measurements of hydro- or fluorocarbon plasmas [39, 44-48]. On the other hand (chapters 5 and 6), the development of Quantum Cascade Lasers (QCL) [49] operating at room temperature has enabled them to become a good alternative to TDL in application for the IR-LAS measurements [50, 51]. Furthermore, the tunability over much broader spectral ranges than with a typical lead salt laser or QCL has been achieved using external cavity (EC)

configurations [52]. At present EC-QCLs are used for increasing number of applications including studies of plasma chemistry and reaction kinetics in non-equilibrium plasmas (chapters 7 and 8).

Therefore the method of IR-LAS was chosen as the main diagnostic technique of this thesis, since a wide variety of species in the plasma can be detected and absolute number densities of different stable molecules or radicals can be determined.

### 1.3 Interaction with surfaces

The effects of non-equilibrium plasmas may not be considered separately from the understanding of processes that take place between the plasma and surfaces inside the reactor. Different parts of a vacuum chamber, e.g. walls or electrodes as well as substrates can alter a plasma process by collecting or releasing material or by becoming electrically charged, which can lead to chemical functionalizing of the surface [4]. Therefore, influence of the reactive plasma discharges over a surface is widely used in materials processing, e.g. plasma-enhanced chemical vapour deposition (PECVD) or polymerization.

In the 1970s, when the potential of plasmas for material modification was realized, a synergetic effect between  $\text{Ar}^+$  ions and reactive  $\text{XeF}_2$  molecules for poly-Si etching has been discovered by J. W. Coburn *et al* in beam experiments [53]. Measuring the difference between the etch rate with both beams simultaneously and the sum of the rates observed with the two beams separately, they were successful to demonstrate the synergism between the ion beam and the reactive neutral species. At the same time J. A. Thornton using an argon glow discharge has deposited thick metal films (25  $\mu\text{m}$ ) onto glass and metallic substrates under various conditions of substrate temperature, gas pressure, and plasma bombardment [54]. Besides, there exist a large number of studies referring to this period and pursuing the same aim where different discharges were used. [55-58]. Therefore, synergetic effects between charged and neutral species were observed in the process of film growth in low temperature plasmas. The following studies have further convinced that plasma-created species with a variety of energies and momenta, chemical activity, and transport characteristics, are responsible for the unique surface modification [4, 59-62].

Nowadays, plasma-surface processes are an interesting topic gaining their importance finding the applications in medicine, chemistry and physics, biology and bioengineering,

material science, as well as in electrical and chemical engineering, and in many others fields [63]. However, the operational parameter spaces are so large and the effects are sometimes so fine and complex that quantification, characterization and prediction of the interactions between reactive plasmas with complex surfaces are still an important scientific challenge [4].

## 1.4 Scope of the thesis

This thesis aims on the investigation of surface processes including knowledge of the kinetics of the surrounding gas phase and reactive plasma chemistry. High performance spectroscopy such MIR-LAS and precise knowledge of spectroscopic properties open up possibilities of accurate plasma parameter measurements, the basis of any plasma diagnostic method.

The thesis begins with two theoretical chapters. These chapters give a brief overview of the reactive gas discharges, discuss investigation techniques for plasma-chemical processes and provide the information about the basic principles of the absorption spectroscopy in the MIR spectral range.

In the first experimental chapter, chapter 3, the chemical phenomena in  $N_2-H_2$  plasmas studied by the combination of two spectroscopic techniques TDLAS and MS are shown. The valuable knowledge of active nitrogen species playing a decisive role in the nitriding process can contribute to the further development of this technique [64].

Chapter 4 includes further investigations of the hydrocarbon chemistry in relation to dust particle formation in Ar and He RF plasmas of a capacitively coupled parallel plate reactor with admixtures of  $C_2H_2$  and  $CH_4$ . The time dependence of molecular concentrations obtained by TDLAS and the determination of fragmentation/conversion efficiencies are presented. Besides, the outcome of FTIR measurements – analyzing of the dust formation dynamic in reactive low temperature molecular plasmas, is also discussed there [65].

The development of a new method for the wall de-excitation probability determination of vibrationally excited  $N_2$  ( $\gamma_{N_2}$ ) at different surfaces exposed to low pressure plasmas is demonstrated in chapter 5. A short dc discharge pulse is used to excite a mixture containing a small amount of  $CO_2$  in  $N_2$ . Due to a nearly resonant and very efficient vibrational energy transfer between  $N_2$  and the asymmetric  $\nu_3$  mode of  $CO_2$ , its vibrational excitation is an image

of the vibrational excitation of  $N_2$ . Thereby, the vibrational relaxation of the titrating molecules is monitored *in-situ* using QCLAS in the afterglow phase and has become interpreted in terms of a numerical model of non-equilibrium vibrational kinetics in  $CO_2$ - $N_2$  mixtures [66].

As next, chapter 6 concerns the problem of pollution abatement from gas exhausts, which is an important contribution for environmental and health protection. Methods of QCLAS applied to catalytic surfaces exposed to low pressure  $Ar/O_2$  plasmas, demonstrates the ability of such surfaces to adsorb reactive atomic species. The stimulation of catalytic surfaces via plasma treatment is an innovative approach but far from being fully understood [67].

Focusing on the analysis of physical and chemical phenomena in molecular plasmas, chapter 7 presents potential application of EC-QCLs as a promising radiation source for IR-LAS, manifesting new aspects of this spectroscopic approach [68].

In addition, in chapter 8, the attractive properties of EC-QCLs, such as wide spectral tunability, intrinsic narrow line width, and high output power is applied for investigations of  $Ar$  and  $Ar/N_2$  RF plasmas with admixtures of metal organic precursor (ATI), playing an important role for the deposition of  $Al_xO_y$  layers in CVD processes. Thereby, a high potential of EC-QCL as an IR light source to be applied for multi-species gas or plasma medium diagnostics is proposed [69].

Finally, in the chapter 9, the results of the study are summarized and a brief outlook on further research efforts is given.

Some parts of this work have been, fully or partly, published already.

## **2 Infrared laser absorption spectroscopy for plasma diagnostics**

Different types of low pressure discharges have been investigated in this work. Methods of absorption spectroscopy in the mid infrared range based on semiconductor laser sources have been employed as diagnostic tools. The following chapter briefly describes basic principles of the used plasma discharges as well as provides a link between diagnostic methods based on infrared laser absorption spectroscopy and plasma parameters.

### **2.1 Low pressure discharges**

Non-equilibrium plasmas, depending on the pressure they operate at, can be divided into low- or atmospheric pressure discharges (see figure 2.1). Low pressure discharges are characterized by the insufficiency of molecules, which are available for the electrons to collide with and to generate a new free electron. The degree of ionization in such discharges is rather small. Due to a fewer collisions the sufficient difference in temperature between the plasma species in low pressure plasmas can be achieved. On the other hand, if the pressure is higher, the probability of collision is higher, because an increase in pressure leads to an increase of the density of species. In this way, the free path of the electrons before colliding decrease and they gain less energy. Furthermore, with increased pressure the rate of reaction increases involving reacting gases. Finally, the efficiency of the energy transfer between the interacted gas species is influenced. Therefore, the higher temperature of all species is inevitable.

This subchapter is focused on physics of low pressure plasmas and discharge types used in the thesis. Basic principles are briefly discussed here.

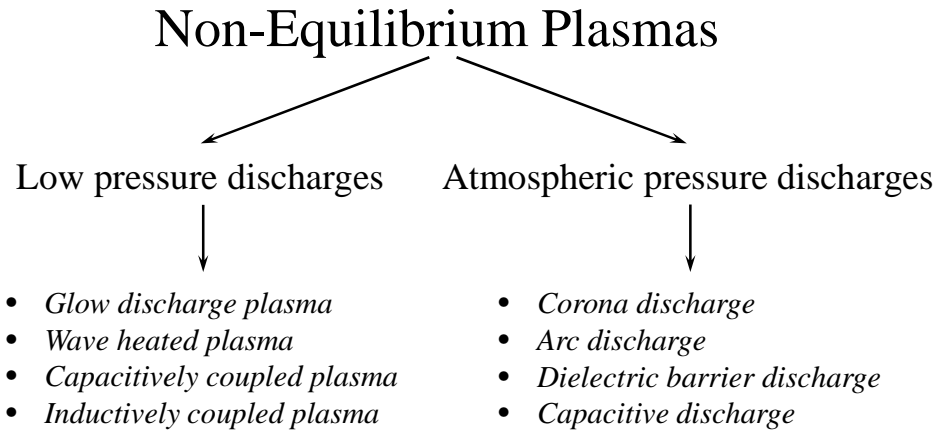


**Figure 2.1:** Classification of non-thermal plasmas depending on the operating pressure.

### 2.1.1 *Glow discharge plasma*

Glow discharge plasmas are generated by applying of DC or low frequency ( $<100$  kHz) RF electric fields to the gap between two metal electrodes, that are inserted in a cell filled with gas at low pressure (typically up to  $p=15$  mbar). They are characterized by thermodynamic equilibrium and quasineutrality. The effective electron temperature in glow discharges is significantly higher than the temperature of gas or electrode.

Physically a glow discharge can be explained as follows: there is always a certain amount of charged particles in any volume filled by some gas, usually argon or another noble gas, and isolated from the external atmosphere. Under influence of an electric field in the tube they started to move to the corresponding poles, the positively charged ions are driven towards the cathode by the electric potential, and the electrons are driven towards the anode by the same potential. This chaotic relocation of ions and electrons leads to the collisions with the gas atoms or molecules, inducing the excitation and ionization processes. Due to ionization collisions the formation of positive charged ions is happened, providing the electron emission from the cathode. These new released electrons are responsible to new ionization collisions, which bring a new portion of ions and electrons into the discharge. Electron excitation of gas atoms with followed de-excitation leads to the emission of radiation, giving rise to a gas discharge [70, 71]. Furthermore, at sufficiently high voltages, collisions within the cathode caused by the ions and electrons bombardment are able to eject a portion of cathode material due to the energy redistribution. This process is called as cathode sputtering [71, 72] and is typical for operating at low pressure.

A special form of a continuous DC discharge is a pulsed DC plasma, used in many industrial applications owing to (i) higher operation power, (ii) variable duty cycle of on-off plasma stages, better performance control, and (iii) prevention or minimization of some undesirable effects [71].

Therefore, this type of discharge finds application in lightning and laser manufactory as well as in the microelectronics industry for surface modification, like sputtering, deposition, chemical etching, etc. In addition, glow discharge plays an important role in plasma physics and analytical chemistry, because the investigation of light produced by the discharge can give a better understanding of the atomic interactions in the gas [71, 73].

### 2.1.2 *Capacitively coupled plasma*

One of the most common types of industrial plasma sources, capacitively coupled plasma (CCP), is generated with high frequency RF electric fields (typically  $f = 13.56$  MHz) applied to a pair of flat metal electrodes. Typically, one of two electrodes is connected to the RF power supply, whereas the second is grounded. The gas pressure in the reactor can be varied from tenth of mbar up to tens of mbar, but the operation at atmospheric pressure is also possible.

The mechanism is similar to what happens in a glow discharge. While the frequencies are low, the ions accelerated in the electric field move to the electrodes and produce secondary electrons. Later, when the frequency increases, and the electric field is strong enough, it can lead to electron avalanche. A large number of free electrons facilitate the gas to become electrically conductive, which accompanies light emission from excited atoms or molecules [74].

For CCP the presence of sheath regions covering the RF electrodes is typical, as it happens in a DC glow discharge. These sheaths at the plasma boundaries act as some kind of dielectric or a capacitor and have impact on the discharge current and plasma density. Since the RF discharge is presented in two forms, so-called  $\alpha$  and  $\gamma$  mode [75], internal properties of sheath regions can be different. In case of lower currents and a positive V-I characteristics, typical for the  $\alpha$  mode, these zones own very small electrical conductivity and low concentration of charge carriers. The intensity of the emitted radiation has the maximum at the electrodes and is decreasing towards the center of the gap between the electrodes. In

contrast, in the  $\gamma$  mode, determined by higher currents and partially negative V-I characteristics, the emitted light is sufficiently more intense [71, 76].

One of the disadvantages of this type of plasma, generated at a low gas temperature, is a low plasma density by uncontrollable ion fluxes and ion energies independently of each other. Moreover, the CCPs are characterized by losses of the input power, which are wasted for ion acceleration instead of plasma generation. Nevertheless, it is worthwhile to mention, that capacitively coupled discharges are often applied to dry etching and film deposition (e.g. sputtering, PECVD), since they have good uniformity properties by simple reactor construction [73].

### 2.1.3 *Microwave discharges*

Microwave (MW) plasmas are electrodeless excited discharges in a gas by rapidly varying electric field in the GHz frequency range. According to the excitation conditions MW plasmas are distinguished into electron cyclotron resonance (ECR), surface wave and resonator discharges [71]. Detailed information of the different discharge types can be found elsewhere [70, 71, 77, 78].

A basic MW plasma reactor consists of a microwave power supply as well as of the plasma load. The power transport is provided by rectangular waveguides or coaxial cables. The optimization of the energy transfer and the minimization of power reflections are realized by applicator. Moreover, there is one more element in this system – circulator, which should protect the power supply from reflected power. Typical for MW plasmas inhomogeneities due to the limited skin depth, can be minimized, when the plasma is generated by coupling the microwaves from the MW generator to the plasma volume without any magnetic field [71]. Thus, the homogeneous MW discharges can be realized by the construction of planar MW plasma reactor, used in this work and described in detail in reference [79]. A typical property of such arrangement is the high chemical reactivity of plasma produced species.

The MW plasmas generated at low pressure are intensively used in many industrial applications such as semiconductor production, plasma etching or deposition and surface cleaning [73]. The advantages of MW discharges in plasma chemistry are primarily related to the possibility of building reactors for the production of very pure and highly chemical reactive mediums.

## 2.2 Radiation sources in the mid infrared spectral range

Recently, one of the most urgent scientific challenges was the establishment and further development of effective monitoring systems for impurities detection in plasma, trace-gas or ambient air, present in small concentrations. The implementation of analytical solutions in the IR spectral range often requires the application of optical radiation sources, which output power exceed the corresponding parameters of non-selective thermal radiation sources. Moreover, a variety of practical tasks demand these devices to be broad tunable, meaning generate an optical radiation over a wide spectral range furthermore providing simple technical control of radiation parameters.

The attractiveness of the MIR spectral range ( $3 - 20 \mu\text{m}$ ) is based on a number of circumstances. First of all, characteristic transparency window of the ambient air ( $3 - 5 \mu\text{m}$ ,  $8 - 12 \mu\text{m}$  and other) can be found in this region. From the spectroscopic point of view this spectral range looks perspective for the detection of the most common gases and molecules, which vibrational-rotational characteristic absorption spectra are placed here. In addition, the emitted radiation in the MIR spectral range is less susceptible to scattering, than the near-infrared radiation, visible or UV regions.

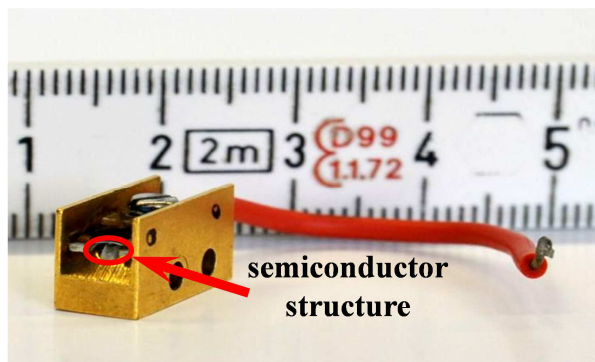


**Figure 2.2:** Photograph of a lead salt diode laser.

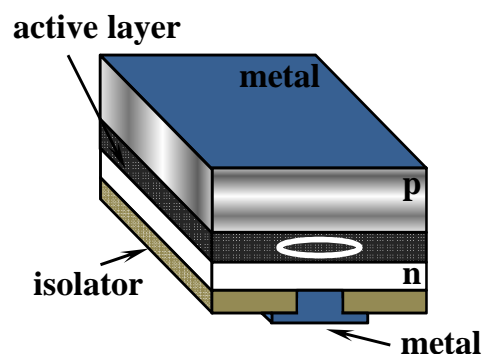


**Figure 2.3:** Schematic diagram of the structure of laser diode.

Tunable diode laser absorption spectroscopy (TDLAS) in the mid infrared spectral range using lead salt lasers (see figures 2.2 and 2.3) as radiation sources has been proven to be a versatile diagnostic technique of molecular plasmas. In particular TDLAS is well suited for the monitoring of absolute ground state concentrations of a wide variety of molecular species including radicals and molecular ions thereby providing a link with chemical modeling of the plasma (see [80] and references therein). Until now, the main applications of TDLAS have been for investigating molecules and radicals in fluorocarbon etching plasmas and in plasma

containing hydrocarbons [80]. For the simultaneous monitoring of multiple molecular plasma species TDLAS systems, which make use of several lead salt lasers, have been developed in the past [81, 82].

The recent development and commercial availability of pulsed and continuous wave (cw) quantum cascade lasers (QCLs) for wavelengths longer than  $3.4\ \mu\text{m}$  and inter-band cascade lasers (ICLs) for shorter wavelength offer an attractive new option for MIR-LAS for plasma diagnostic purposes. A typical QCL chip as well as three generations of the quantum cascade laser measuring and control system (Q-MACS) laser heads are illustrated in figures 2.5 and 2.6. Compared to lead salt lasers distributed feedback (DFB) QCLs provide (i) continuous mode-hop free wavelength tuning, (ii) increasingly high output powers, (iii) near room temperature operation and (iv) narrow line width radiation. In conjunction with integrated DFB gratings, the emission wavelength of this new class of thermoelectrically cooled semiconductor lasers can be custom tailored over a wide range throughout the infrared molecular fingerprint region. Their total emission range is typically limited to less than  $7\ \text{cm}^{-1}$ . Therefore a multi-component detection to study infrared active compounds in reactive plasmas requires, as in the TDLAS case, the combination of several QCLs in a spectrometer [83]. Meanwhile the variety of QCLs and ICLs operating at room temperature are considered as substitutes for cryogenic cooled lead salt lasers, which has led to a rapid development of MIR-LAS from a niche position to a standard diagnostic technique [50].

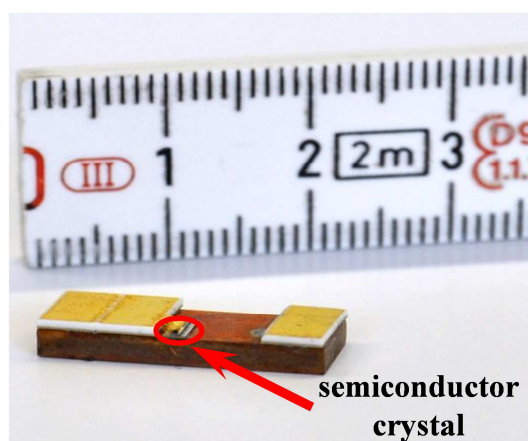


**Figure 2.5:** Photo of a QCL chip. The semiconductor crystal (small black spot) is placed on the copper cooling body and bonded to the electrical contacts by gold wires.



**Figure 2.6:** Photo of three different generations of Q-MACS laser heads, presenting their time development from the year 2006 to 2013. From left to right, uncapsuled QCL chip in a laser head, which can be pumped out, TO-3 and TO-8 packaging of QCLs.

Recently, tunability over much broader spectral ranges than with a typical lead salt laser or DFB-QCL has been achieved using external cavity (EC) configurations. Nowadays, EC-QCLs (figure 2.7), which are available in pulsed or continuous wave (cw) working mode, can be tuned over more than  $100\text{ cm}^{-1}$ . Modern cw EC-QCL provide mode-hop free (MHF) tuning ranges in the order of up to  $80\text{ cm}^{-1}$ , at small line width of typically 20 to 60 MHz ( $6 - 18 \times 10^{-4}\text{ cm}^{-1}$ ) at power values of up to 350 mW [84]. In selected examples even much higher tuning ranges and power values have been achieved [85].



**Figure 2.7:** Photo of a commercially available EC-QCL (Daylight Solutions), which was used in this study.

At present EC-QCLs are used for an increasing number of applications including high resolution isotope analysis, explosive detection and trace gas monitoring [85-91]. The acquisition of MIR photoacoustic spectra of solids and surface adsorbed species using EC-QCLs has become feasible [92-94]. Nano-scale spatial resolution has been achieved by combining EC-QCLs with an atomic force microscope to detect the thermal expansion of polymer samples [95]. Pulse radiolysis of condensed-phase samples demonstrated a nano-second time resolution based on EC-QCL spectroscopy [96]. Liu and co-workers used a DFB-QCL and an EC-QCL as radiation sources for multiple pass absorption (MPA) and cavity enhanced absorption (CEA) to measure high resolution jet-cooled infrared spectra of methyl lactate and of the Ar-H<sub>2</sub>O complex [97]. They found a considerable worse detection limit with the EC-QCL compared to the DFB-QCL caused by the slow scan rate ( $<100\text{ Hz}$ ) of the piezoelectric transducer (PZT) which is used for fine tuning of the grating of the EC system. In contrast, the EC-QCL was well suited for high resolution spectroscopic studies of jet-cooled samples [97]. In low pressure gases, as N<sub>2</sub>O and CH<sub>4</sub>, fast chirped EC-QCLs have been used to study non-linear phenomena, like the rapid passage effect [98-101]. The advantageous properties of a cw EC-QCL for direct and wavelength modulation spectroscopy

at the example of nitric oxide detection have been demonstrated by Hancock and co-workers [102]. Recently the same team used EC-QCLs for sub-Doppler Lamb-dip measurements on a low-pressure sample of NO [100].

Therefore, the summarized information of characteristic features of used laser absorption spectroscopy methods is presented in table 2.1. Although that FTIR technique is based on continuous light source, this method is included here for comparison as a spectroscopic method providing broadband investigation of a gas phase composition.

**Table 2.1:** Comparison of infrared spectroscopy techniques used for plasma diagnostic.

	FTIR	TDLAS	QCLAS	EC-QCLAS
<b>Tunability</b>	whole MIR	10-100 cm <sup>-1</sup>	1-10 cm <sup>-1</sup>	over 100 cm <sup>-1</sup>
<b>Time resolution</b>	s ... min	ms ... $\mu$ s	ns ... ms	down to ns
<b>Output power</b>	0.1...10 mW	0.1...1 mW	1...10 mW	up to 350 mW
<b>Sensitivity</b>	10 <sup>-2</sup> ...10 <sup>-3</sup>	10 <sup>-3</sup> ...10 <sup>-5</sup>	10 <sup>-3</sup> ...10 <sup>-5</sup>	10 <sup>-3</sup> ...10 <sup>-5</sup>
<b>Selectivity</b>	10 <sup>-1</sup> cm <sup>-1</sup>	10 <sup>-4</sup> ...10 <sup>-3</sup> cm <sup>-1</sup>	10 <sup>-3</sup> ...10 <sup>-2</sup> cm <sup>-1</sup>	10 <sup>-4</sup> cm <sup>-1</sup>
<b>Operation</b>	room T	20...130 K	near room T	room T
<b>Detection</b>	LN <sub>2</sub> detectors	LN <sub>2</sub> detectors	TE detectors	TE detectors

## 2.3 Basic principles of absorption spectroscopy

Absorption spectroscopy (AS) as one of the methods of qualitative and quantitative analysis is based on the interaction of electromagnetic radiation with the investigated substance and measuring its absorption as a function of wavelength or frequency. Possible applications of this method in the visible and ultraviolet (UV) regions are rather limited due to the property of absorption bands to hide their fine structure owing to the broadening. Whereas in the IR region they are narrow and their number is large. In addition, absorption bands in IR spectra are characteristic, meaning they provide immediately information about the molecule structure. Thus the IR spectra are characterized by an individuality, which determines the value of AS in this spectral range for identification and investigation of organic compounds structure [103, 104].

An incident beam of monochromatic light with intensity  $I_0$ , passing the absorbing layer of thickness  $L$  through, owing to absorption and scattering processes comes out with reduced intensity  $I(l)$ . The variation of the intensity  $dI$  absorbed by the small region  $dl$  can be defined by the expression (see figures 2.8 and 2.9):

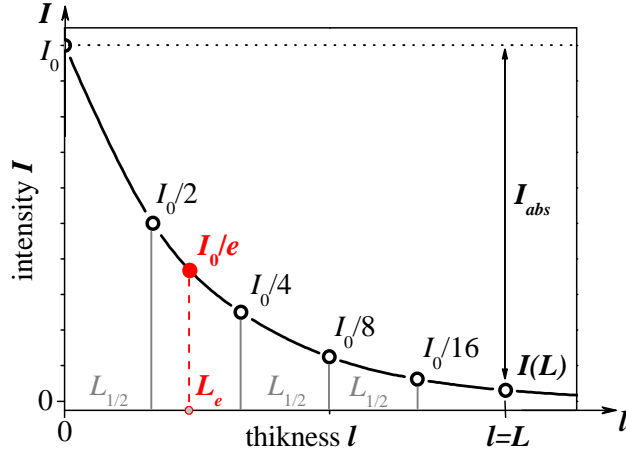


**Figure 2.8:** Schematic illustration of the variation of monochromatic light intensity passing the absorbing material, where  $L_{1/2}$  – absorbing layer, which varies the intensity by factor of two.

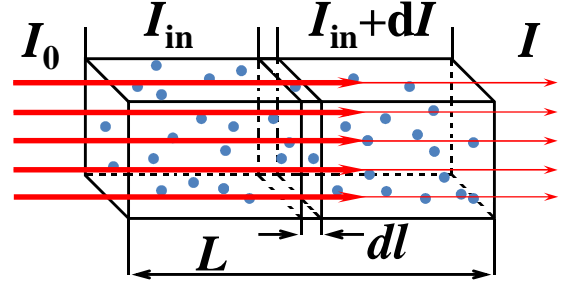


**Figure 2.9:** The variation of intensity of external radiation from  $I_0$  to  $I$  due to absorption in a gas or plasma sample of thickness  $L$ .

$$dI(\nu) = (j(\nu) - k(\nu)) \cdot I_0(\nu) dl \quad (2.1)$$

where  $j(\nu)$  is the emission coefficient and  $k(\nu)$  is the absorption coefficient. In case of several absorption species  $k(\nu)$  is expressed as their sum with corresponding concentration  $n$  per unit and absorption cross-section  $\sigma(\nu)$  [103, 105]:

$$k(\nu) = \sum_i k_i(\nu) = \sum_i n_i \cdot \sigma_i(\nu) \quad (2.2)$$

Compared to the visible spectral range the scattering cross-section for molecules in the infrared is much smaller than the absorption one, because the typically investigated molecules are much smaller than the wavelengths [106]. When the absorbing medium is homogeneous, scattering and emission effects can be neglected and equation (2.1) simplifies to:

$$dI(\nu) = -k(\nu) \cdot I_0(\nu) dl \quad (2.3)$$

If the absorption coefficient  $k(\nu)$  is constant, formula (2.3) can be integrated over an effective absorption length  $L$ :

$$\ln \left( \frac{I_0(\nu)}{I(\nu)} \right) = k(\nu) \cdot L \quad (2.4)$$

Thus, the basic principle of the linear absorption spectroscopy is expressed by formula (2.4), which is well known as the Beer-Lambert law. The integration of  $k(\nu)$  over frequency of a single absorption line provides the calculation of absolute concentration  $n$  of the absorbing species:

$$K = \int_{\nu} k(\nu) \cdot d\nu = \frac{1}{L} \int_{\nu} \ln \left( \frac{I_0(\nu)}{I(\nu)} \right) d\nu = n \cdot S \quad (2.5)$$

where  $S$  is the line strength in  $\text{cm molecule}^{-1}$ . It can be found in different databases like GEISA [107] or HITRAN [108] or is listed in books [109, 110]. Using this proportionality factor the profile function of a single absorption line can be expressed as follows:

$$\sigma(\nu - \nu_0) = S \cdot f(\nu - \nu_0) \quad (2.6)$$

where  $\nu_0$  is the resonance frequency of the transition and  $f(\nu - \nu_0)$  is the normalized line profile function

$$\int_{\text{line}} f(\nu - \nu_0) d\nu = 1 \quad (2.7)$$

Single absorption lines in the discrete absorption spectra are not strictly monochromatic and are additionally broadened in almost all cases [79]. Several broadening mechanisms lead to spectral intensity distribution near the resonance frequency  $\nu_0$ . The natural line shape has the form of Lorentz-profile with the “half width at half maximum” (HWHM)  $\nu_L$  due to finite lifetime of excited state and is defined by:

$$f_L(\nu - \nu_0) = \frac{\nu_L}{\pi \cdot (\nu - \nu_0)^2 + \nu_L^2} \quad (2.8)$$

From the well-known Heisenberg uncertainty principle:

$$\nu_L = \frac{\Delta E}{\hbar} = \frac{1}{\pi \cdot \tau_l} \quad (2.9)$$

The time constant  $\tau_l$  is the time required for the excited system loses its energy  $\Delta E$  and is determined by the rates of spontaneous emission and non-radiative relaxation transitions. Additionally, the line width depends on the number of collisions per second. In this case, the number density of the molecules and the relative speed of the molecules have much stronger influence on the line shape and the natural broadening is negligible. Then, the line width  $\nu_p$  at pressure  $p$  and temperature  $T$  is expressed as follows:

$$\nu_p = \nu_{L,STP} \left( \frac{p}{p_0} \right) \left( \frac{T_0}{T} \right)^{\frac{1}{2}} \quad (2.10)$$

where  $\nu_{L,STP}$  is the line width at standard conditions ( $p_0 = 10^3$  mbar and  $T_0 = 273$  K). For pressure broadened spectral lines the HWHM can be found in the range of  $10^{-4} \text{ cm}^{-1}$  at pressures lower than 5 mbar, whereas at atmospheric pressures it can reach values up to  $10^{-2} \text{ cm}^{-1}$ .

The next source determining the width of the spectral lines is Doppler broadening, which is caused by the random thermal motion of the atoms or molecules in different directions and at different speeds. In this case, instead of a broadened line with the resonance frequency  $\nu_0$  a set of narrow spaced lines is observed. Enveloping of this set gives a contour of the broadened by Doppler effect line, which form is determined by the distribution of the velocity of the gas particles. In case of Maxwell velocity distribution the spectral line has a form described by a Gaussian function

$$f_D(\nu - \nu_0) = \frac{1}{\nu_D \sqrt{\pi}} \cdot \exp \left[ -\frac{(\nu - \nu_0)^2}{\nu_D^2} \right] \quad (2.11)$$

with  $\nu_D$  – Doppler HWHM:

$$\nu_D = \frac{\nu_0}{c} \sqrt{2 \cdot k_B N_A \ln 2 \frac{T}{M}} = 3.58 \cdot 10^{-7} \sqrt{\frac{T}{M}} \cdot \nu_0 \quad (2.12)$$

where the Boltzmann constant  $k_B = 1.3806503 \times 10^{-23} \text{ J} \cdot \text{K}^{-1}$ , the Avogadro constant  $N_A = 6.02214129 \times 10^{23} \text{ mol}^{-1}$ ,  $M$  is the gram molecular weight in  $\text{g} \cdot \text{mol}^{-1}$  and  $c$  – the light velocity.

In general, the overall broadening is a convolution of thermal- with the natural- or pressure broadening. Mathematically convoluted Gaussian and Lorentz profiles in so called Voigt profile can describe the line shape more accurately. Under condition that  $\nu_0 = 0$ , the convolution of (2.8) and (2.11) can be simplified and presented as:

$$f_V(\nu, \nu_D, \nu_L) = \int_{-\infty}^{+\infty} f_D(\nu_1, \nu_D) \cdot f_L(\nu - \nu_1, \nu_L) d\nu_1 \quad (2.12)$$

Nevertheless, the role of Doppler broadening is particularly significant in the optical range at room or even higher temperatures and instead of Voigt only Gaussian profile can be used.

Finally, the observed profile of a spectral line is often influenced by the resolution of the spectral instrument (called instrumental profile). In this case, the natural line shape, can be significantly changed by the finite line width of the laser beam due to impact of the optical elements of the experimental setup. However, the contribution  $\nu_{Instr.}$  can be excluded from the observed line profile  $\nu_{obs}$  by calibration over a selected line of a reference gas at known pressure. The relation to the Gaussian line profile is expressed as:

$$\nu_{Instr.} = \sqrt{\nu_{obs}^2 - \nu_D^2} \quad (2.13)$$

Therefore, under low pressure conditions taking into account (2.5), (2.6) and (2.13) the absolute number density of molecules is substantiated by

$$n = \frac{\nu_{obs}}{S \cdot L} \sqrt{\frac{\pi}{\ln 2}} \ln \left( \frac{I_0}{I} \right) \quad (2.14)$$

The determination of molecular concentration using AS is an efficient approach for quantitative analysis, when several aspects leading to some limitations are considered. At the present stage, most of industrial applications as well the laboratory research often require the detection of very low mixing ratios of gases with absorbance sensitivities in the lower than  $10^{-5}$  range.

For such small absorptions the sensitivity of direct absorption measurements can be improved by using wavelength modulation spectroscopy (WMS). One of the most valuable aspects of this technique is the signal ability to be detected at a frequency at which the noise sources are less likely to interfere with the signal. Moreover, this method produces a difference signal, which is directly proportional to the species concentration.

The general approach to WMS comprises additionally modulation of the laser wavelength with a rapid sinusoid at frequency  $\nu_{laser}$  much smaller than the width of the absorption line [111, 112]:

$$\nu_{laser}(t) = \nu_0 + \alpha \cdot \sin(\nu_m t) \quad (2.15)$$

where  $\nu_m$  is the modulation frequency with the amplitude  $\alpha$ . The interaction between the rapidly modulating wavelength and a nonlinear absorption feature gives rise to harmonic components in the detector signal, so that the excess external noise is reduced and the signal-to-noise ratio is enhanced. In modulation spectroscopy most of measurements are performed at the second harmonic ( $2f$ ), because like in direct absorption, the  $2f$  signal is strongly

dependent on spectral parameters and gas properties and can therefore be compared with spectral simulations to infer gas properties.

It is obvious from the above, that the sensitivity of an experiment is typically influenced on the signal-to-noise ratio (SNR), which compares the power of a desired signal to the power of background noise:

$$SNR = \frac{I_{abs}}{\Delta I} = \frac{1-I}{\Delta I} \approx \frac{I_0}{\Delta I} k(\nu) \cdot L \quad (2.16)$$

Certainly the measurements may be performed if the ratio  $\frac{I_{abs}}{\Delta I} > 1$ , which indicates more signal than noise. Defined that a minimum  $SNR=1$  and taking into account (2.2), following equation can be expressed [103]:

$$n_{min} \sigma \approx \frac{\Delta I}{I_0 \cdot L} \quad (2.17)$$

To sum it up, in order to get higher sensitivity the noise of the detection system  $\Delta I$  must be minimized. Since the molecular density is in connection to effective length, another way for enhancement in the signal level can be achieved by employing of optical multi-pass arrangements based on spherical optics, e.g. White- (figures 2.10 and 2.11), Herriott- and Chernin-cell, or astigmatic mirrors (McManus) [113-116]. On the principle of multiplied reflection up to several hundred times the absorption path length of up to hundreds of meters can be realized in these different designed cells.

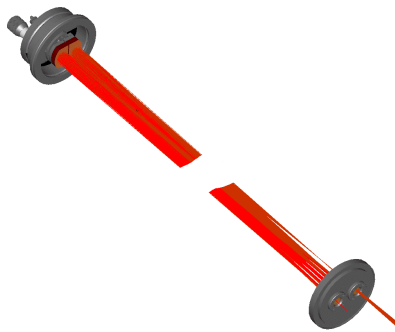


**Figure 2.10:** Schematic diagram of the beam configuration in the multipass optics of White-type.



**Figure 2.11:** Field mirror of the White cell showing the images of He-Ne laser reflection. In this case, a cell with 36 passes is presented.

## Bibliography for Chapters 1 and 2

- [1] R. Balescu, *Aspects of Anomalous Transport in Plasmas*, Inst. of Physics Pub, (2005).
- [2] R.A. Cairns, *Plasma Physics*, UK, (1985).
- [3] R. Hazeltine, F. Waelbroeck, *The Framework of Plasma Physics*, Westview, Boulder CO, (2004).
- [4] M.J. Kushner, D.B. Graves, et al, *Report of the Department of Energy Office of Fusion Energy Sciences Workshop on Low Temperature Plasmas*, (2008).
- [5] G. Bonizzoni, E. Vassallo, *Vacuum* **64**, 327 (2002).
- [6] F. Chen, *Phys. Plasmas* **2**, 6 (1995).
- [7] M. Kuchenbecker, N. Bibinov, A. Kaemling, D. Wandke, P. Awakowicz, W. Vioel, *J. Phys. D: Appl. Phys.* **42**, 045212 (2009).
- [8] K.-D. Weltmann, T. von Woedtke, *Eur. Phys. J. Appl. Phys.* **55**, 13807 (2011).
- [9] B. Penetrante, *Non-Thermal Plasma Techniques for Pollution Control*, ed S. Schultheis, NATO ASI Series G34 parts A and B (Berlin: Springer), (1993).
- [10] A. Rousseau, L.V. Gatilova, O. Guaitella, C. Guillard, F. Thevenet, J. Röpcke, G. Stancu, *Appl. Phys. Lett.* **87**, 221501 (2005).
- [11] O. Guaitella, F. Thevenet, E. Puzenat, C. Guillard, A. Rousseau, *Applied Cata. B.* **80**, 296 (2008).
- [12] M.A. Peretich, W.F. O'Brien, J.A. Schetz, *Plasma torch power control for scramjet application*, Virginia Space Grant Consortium, (2007).
- [13] F.L. Tabares, V. Rohde, *Plasma Phys. Control. Fusion* **46**, B381 (2004).
- [14] A.J.H. Donne, *Transactions of Fusion Science and Technology* **45**, 383 (2004).
- [15] R. Hippler, S. Pfau, M. Schmidt, K.H. Schoenbach, *Low Temperature Plasma Physics*, Wiley-Vch Verlag, Berlin, (2001).
- [16] I.H. Hutchinson, *Principles of Plasma Diagnostics*, Cambridge University Press, Cambridge, (1987).
- [17] R.H. Huddleston, S.L. Leonard, *Plasma diagnostic techniques*, Academic Press, London (1965).

- [18] I. Langmuir, H.M. Mott-Smith, *Gen. Elec. Rev.* **26**, 731 (1923).
- [19] A. Rousseau, E. Teboul, N. Lang, M. Hannemann, J. Röpcke, *J. Appl. Phys.* **92**, 3463 (2002).
- [20] M. Hannemann, *Contrib. Plasma Phys.* **9**, 50 (2010).
- [21] H. Maurer, M. Hannemann, R. Basner, H. Kersten, *Phys. Plasmas* **17**, 113707 (2010).
- [22] M. Schmidt, R. Foest, R. Basner, *Mass spectrometric diagnostics in Low Temperature Plasma Physics*, ed. R. Hippler, S. Pfau, M. Schmidt, K.H. Schoenbach, Wiley-Vch Verlag Berlin, (2001).
- [23] J.L. Jauberteau, L. Thomas, J. Aubreton, I. Jauberteau, A. Catherinot, *Plasma Chem. Plasma Process.* **18**, 137 (1998).
- [24] L.G. Nielsen, K.O. Ash, E. Thor, *Clin. Chem.* **2**, 24 (1978).
- [25] P. Fendel, A. Francis, U. Czarnetzki, *Plasma Sources Sci. Technol.* **14**, 2005.
- [26] J. Röpcke, A. Ohl, *Contrib. Plasma Phys.* **31**, 669 (1991).
- [27] J. Röpcke, A. Ohl, *Contrib. Plasma Phys.* **34**, 575 (1994).
- [28] G. Hancock, J.P. Sucksmith, M.J. Toogood, *J. Phys. Chem.* **94**, 3269 (1990).
- [29] R. De Avillez Pereira, D.L. Baulch, M.J. Pilling, S.H. Robertson, G. Zeng G, *J. Phys. Chem. A* **101**, 9681 (1997).
- [30] T. Doerk, M. Hertl, P. Pfelzer, S. Hädrich, P. Jauernik, J. Uhlenbusch, *Appl. Phys.* **B64**, 11 (1997).
- [31] M. Lefebvre, M. Pealat, J.P. Taran, *Pure & Appl. Chem.* **64**, 685 (1992).
- [32] S.M. Gladkov, A.M. Zheltikov, N.I. Koroteev, M.V. Rychev, A.B. Fedotov, *Sov. J. Quantum Electron.* **19**, 7 (1989).
- [33] M. Baeva, H. Gier, A. Pott, J. Uhlenbusch, J. Höschele, J. Steinwandel, *Plasma Chem. Plasma Proc.* **21**, 225 (2001).
- [34] S. Hädrich, B. Pfelzer, J. Uhlenbusch, *Plasma Chem. Plasma Process.* **19**, 91 (1999).
- [35] B.A. Cruden, M.V.V.S. Rao, S.P. Sharma, M. Meyyappan, *Plasma Sources Sci. Technol.* **11**, 77 (2002).
- [36] N. Hershkowitz, R.A. Breun, *Rev. Sci. Instrum.* **68**, 880 (1997).

- [37] J.P. Booth, G. Cunge, L. Biennier, D. Romanini, A. Kachanov, *Chem. Phys. Lett.* **317**, 631 (2000).
- [38] R. Engeln, K.G.Y. Letourneur, M.G.H. Boogaarts, M.C.M. van de Sanden, D.C. Schram, *Chem. Phys. Lett.* **310**, 405 (1999).
- [39] M. Haverlag, E. Stoffels, W.W. Stoffels, G.M.W. Kroesen, F.J. De Hoog, *J. Vac. Sci. Technol. A* **14**, 380 (1996).
- [40] J. Röpcke, L. Mechold, M. Käning, W.Y. Fan, P.B. Davies, *Plasma Chem. Plasma Process.* **19**, 395 (1999).
- [41] S. Naito, N. Ito, T. Hattori, T. Goto, *Jpn. J. Appl. Phys.* **34**, 302 (1995).
- [42] N.T. Hunt, J. Röpcke, P.B. Davies, *J. Mol. Spectr.* **204**, 120 (2000).
- [43] M. Osiac, J. Röpcke, P.B. Davies, *Chem. Phys. Lett.* **344**, 92 (2001).
- [44] G. Lombardi, G.D. Stancu, F. Hempel, A. Gicquel, J. Röpcke, *Plasma Sources Sci. Technol.* **13**, 27 (2004).
- [45] F. Hempel, P.B. Davies, D. Loffhagen, L. Mechold, J. Röpcke, *Plasma Sources Sci. Technol.* **12**, 98 (2003).
- [46] F. Hempel, J. Röpcke, A. Pipa, P.B. Davies, *Mol. Phys.* **101**, 589 (2003).
- [47] G. Lombardi, K. Hassouni, G.D. Stancu, L. Mechold, J. Röpcke, A. Gicquel, *Plasma Sources Sci. Technol.*, **14**, 440 (2005).
- [48] M. Magane, N. Itabashi, N. Nishiwaki, T. Goto, C. Yamada, E. Hirota, *Jpn. J. Appl. Phys.* **29**, L829 (1990).
- [49] M. Beck, D. Hofstetter, T. Aellen, J. Faist, U. Oesterle, M. Illegems, E. Gini, H. Melchior, *Science* **295**, 301 (2002).
- [50] S. Welzel, F. Hempel, M. Hübner, N. Lang, P. B. Davies, J. Röpcke, *Sensors* **10**, 6861 (2010).
- [51] G. Wysocki, M. McCurdy, S. So. D. Weidmann, C. Roller, R.F. Curl, F.K. Tittel, *Appl. Opt.* **43**, 6040 (2004).
- [52] G. Wysocki, R. Lewicki, R.F. Curl, F.K. Tittel, L. Diehl, F. Capasso, M. Troccoli, G. Hofler, D. Bour, S. Corzine, R. Maulini, M. Giovanni, J. Faist, *Appl. Phys. B: Lasers and Optics* **92**, 305 (2008).

- [53] J.W. Coburn, H. F. Winters, *J. Appl. Phys.* **50**, 3189 (1979).
- [54] J.A. Thornton, *J. Vac. Sci. Technol.* **11**, 666 (1974).
- [55] J.L. Vossen, *J. Vac. Sci. Technol.* **8**, S12 (1971).
- [56] M. Fukutomi, M. Kitajima, M. Okada, R. Watanabe, *J. Electrochem. Soc.* **124**, 1420 (1977).
- [57] J.J. Hanak, J.P. Pellicane, *J. Vac. Sci. Technol.* **13**, 406 (1976).
- [58] D.J. Ball, *J. Appl. Phys.* **43**, 3047 (1972).
- [59] S. Maniv, W. D. Westwood, *J. Appl. Phys.* **51**, 718 (1980).
- [60] J.A. Thornton, *J. Vac. Sci. Technol.* **4**, 3059 (1986).
- [61] D.J. Oostra, A. Haring, A.E. de Vries , F.H.M. Sanders, G.N.A. van Veen, *Nucl. Instrum. Meth. B* **13**, 556 (1986).
- [62] J.R. Conrad, J.L. Radke, R.A. Dodd, F.J. Worzala, N.C. Tran, *J. Appl. Phys.* **62**, 4591 (1987).
- [63] R. d'Agostino, P. Favia, C. Oehr, M.R. Wertheimer, *Plasma Process. Polym.* **2**, 7 (2005).
- [64] I. Burlacov, K. Börner, H.-J. Spies, H. Biermann, D. Lopatik, H. Zimmermann, J. Röpcke, *Surf. Coat. Technol.* **206**, 3955 (2012).
- [65] F. Hempel, D. Lopatik, B. Sikimic, I. Stefanovic, J. Winter, J. Röpcke, *Plasma Sources Sci. Technol.* **21**, 055001 (2001).
- [66] D. Marinov, D. Lopatik, O. Guaitella, M. Hübner, Y. Ionikh, J. Röpcke, A. Rousseau, *J. Phys. D: Appl. Phys.* **45**, 175201 (2012).
- [67] D. Lopatik, M. Hübner, D. Marinov, O. Guaitella, A. Rousseau, J. Röpcke, "On the reactivity of plasma treated photo-catalytic TiO<sub>2</sub> surfaces for oxidation of C<sub>2</sub>H<sub>2</sub> and CO", *submitted to J. Phys. D: Appl. Phys.*, (2013).
- [68] D. Lopatik, N. Lang, U. Macherius, H. Zimmermann, J. Röpcke, *Meas. Sci. Technol.* **23**, 115501 (2012).
- [69] D. Lopatik, S. Niemietz, M. Fröhlich, J. Röpcke, H. Kersten, *Contrib. Plasma Phys.* **1**, 201200044 (2012).
- [70] A. Bogaerts, R. Gijbels, *Spectrochimica Acta Part B*, **53**, 1 (1998).

- [71] H. Conrads, M. Schmidt, *Plasma Sources Sci. Technol.* **9**, 441 (2000).
- [72] J. Inczedy, T. Lengyel, A.M. Ure, *Compendium of Analytical Nomenclature*, Blackwell Science, (1998).
- [73] A. Bogaerts, E. Neyts, R. Gijbels, J. van der Mullen, *Spectrochimica Acta Part B* **57**, 609 (2002).
- [74] P. Verdonck, *Dry Etching for Integrated Circuit Fabrication*, in *Processos de Microeletrônica*, ed. Baranauskas, (1990).
- [75] Yu.P. Raizer, *Gas Discharge Physics*, Berlin: Springer, (1991).
- [75] M. Lieberman, A. Lichtenberg, *Principles of Plasma Discharges and Materials Processing*, New York: Wiley, (1994).
- [77] J. Marec, P. Leprince, *J. Phys. IV* (France) **8**, Pr7-1, (1998).
- [78] Yu.A. Lebedev, *Journal of Physics: Conference Series* **257**, 012016 (2010).
- [79] F. Hempel, *Absorption Spectroscopy Studies In Low Pressure Non Equilibrium Molecular Plasmas Using Tunable Infrared Diode Lasers*, Logos Berlin, (2003).
- [80] J. Röpcke, G. Lombardi, A. Rousseau, P.B. Davies, *Plasma Sources Sci. Technol.* **5**, S148 (2006).
- [81] J. Röpcke, L. Mechold, M. Käning, J. Anders, F.G. Wienhold, D. Nelson, M. Zahniser, *Rev. Sci. Instr.* **71**, 3706 (2000).
- [82] J.B. McManus, D. Nelson, M. Zahniser, L. Mechold, M. Osiac, J. Röpcke, A. Rousseau, *Rev. Sci. Instr.* **74**, 2709 (2003).
- [83] M. Hübner, S. Welzel, D. Marinov, O. Guaitella, S. Glitsch, A. Rousseau, J. Röpcke, *Rev. Sci. Instr.* **82**, 093102 (2011).
- [84] R.F. Curl, F. Capasso, C. Gmachl, A.A. Kostorev, B. McManus, R. Lewicki, M. Pusharsky, G. Wysocki, F.K. Tittel, *Chem. Phys. Lett.* **487**, 1 (2010).
- [85] I. Sydoryk, A. Lim, W. Jäger, J. Tulip, M.T. Parsons, *Appl. Optics* **49**, 945 (2010).
- [86] R.J. Walker, R.J. Van Helden, G.A.D. Ritchie, *Chem. Phys. Lett.* **501**, 20 (2010).
- [87] A. Karpf, G.N. Rao, *Appl. Optics* **49**, 1406 (2010).
- [88] R. Furstenberg, C.A. Kendziora, J. Stepnowski, S.V. Stepnowski, M. Rake, M.R. Papantonakis, V. Nguyen, G.K. Hubler, R.A. McGill, *Appl. Phys. Lett.* **93**,

- 224103 (2008).
- [89] A. Karpf, G.N. Rao, *Appl. Optics* **48**, 5061 (2009).
- [90] R. Lewicki, J.H. Doty III, R.F. Curl, F.K. Tittel, G. Wysocki, *Proc. Natl. Acad. Sci. America, PNAS* **106**, 12587 (2009).
- [91] A. Hugi, R. Maulini, J. Faist, *Semicond. Sci. Technol.* **25**, 083001 (2010).
- [92] Q. Wen, K.H. Michaelian, *Optics Lett.* **16**, 1875 (2008).
- [93] E.L. Holthoff, D.A. Heaps, P.M. Pellegrino, *Sensors J.* **10**, 572 (2010).
- [94] C.W. Van Neste, L.R. Senesac, T. Thundat, *Appl. Phys. Lett.* **92**, 234102 (2008).
- [95] F. Lu, M.A. Belkin, *Optics Expr.* **19**, 19942 (2011).
- [96] D.C. Grills, A.R. Cook, E. Fujita, M.W. George, J.M. Preses, J.F. Wishart, *Appl. Spectroscopy* **64**, 563 (2010).
- [97] X. Liu, Y. Xu, Z. Zu, W.S. Tam, I. Leonov, *Appl. Phys. B: Lasers and Optics* **102**, 629 (2011).
- [98] J.H. Van Helden, R. Peverall, G.A.D. Ritchie, R.J. Walker, *Appl. Phys. Lett.* **94**, 051116 (2009).
- [99] J.H. Northern, G.A.D. Ritchie, E.P. Smakman, J.H. Van Helden, R.J. Walker, G. Duxbury, *Appl. Phys. B : Laser and Optics*, **102**, 37 (2011).
- [100] G. Hancock, G.A.D. Ritchie, J.H. Van Helden, R. Walker, D. Weidman, *Optical Eng.* **49**, 111121 (2010).
- [101] R.J. Walker, J.H. Van Helden, J. Kirkbride, E.A. McCormack, M.T. Bell, D. Weidman, G.A.D. Ritchie, *Optics Lett.* **36**, 4725 (2011).
- [102] G. Hancock, J.H. Van Helden, R. Peverall, G.A.D. Ritchie, R.J. Walker, *Appl. Phys. Lett.* **94**, 201110 (2009).
- [103] S. Welzel, *New Enhanced Sensitivity Infrared Laser Spectroscopy Techniques Applied to Reactive Plasmas and Trace Gas Detection*, Logos Berlin, (2009).
- [104] W. Schmidt, *Optische Spektroskopie*, Wiley-VCH, Weinheim, (2000).
- [105] S. S. Penner, *Quantitative Molecular Spectroscopy and gas Emissivities*, Pergamon Press, London-Paris, (1959).

- [106] <http://people.csail.mit.edu/jaffer/SimRoof/ThermalOptics>
- [107] N. Jacquinet-Husson, E. Ariés, J. Ballard, A. Barbe, G. Bjoraker, B. Bonnet, L.R. Brown, C. Camy-Peyret, J.P. Champion, A. Chédin, A. Chursin, C. Clerbaux, G. Duxbury, J.M. Flaud, N. Fourrié, A. Fayt, G. Graner, R. Gamache, A. Goldman, V. Golovko, G. Guelachvili, J.M. Hartmann, J.C. Hilico, J. Hillman, G. Lefèvre, E. Lellouch, S.N. Mikhailenko, O.V. Naumenko, V. Nemtchinov, D.A. Newnham, A. Nikitin, J. Orphal, A. Perrin, D.C. Reuter, C.P. Rinsland, L. Rosenmann, L.S. Rothman, N.A. Scott, J. Selby, L.N. Sinita, J.M. Sirota, A.M. Smith, K.M. Smith, V.G. Tyuterev, R.H. Tipping, S. Urban, P. Varanasi, M. Weber, *J. Quant. Spectrosc. & Radiat. Transfer* **62**, 205 (1999).
- [108] L.S. Rothman, D. Jacquemart, A. Barbe, D.C. Benner, M. Birk, L.R. Brown, M.R. Carleer, C. Chackerian, K. Chance, L.H. Coudert, V. Dana, V.M. Devi, J.M. Flaud, R.R. Gamache, A. Goldman, J.M. Hartmann, K.W. Jucks, A.G. Maki, J.Y. Mandin, S.T. Massie, J. Orphal, A. Perrin, C.P. Rinsland, M.A.H. Smith, J. Tennyson, R.N. Tolchenov, R.A. Toth, J.V. Auwera, P. Varanasi, G. Wagner, *J. Quant. Spectrosc. Radiat.* **96**, 139 (2005).
- [109] G. Guelachvili, K.N. Rao, *Handbook of Infrared Standards*, Academic Press, Orlando, (1986).
- [110] A.G. Maki, J.S. Wells, *Wavenumber Calibration Tables From Heterodyne Frequency Measurements*, NIST Special Publication 821, (1991).
- [111] W. Demtröder, *Laser Spectroscopy*, Springer-Verlag Berlin Heidelberg, (1998).
- [112] H. Wei, G. Xiaoming, L. Xiaoyun, L. Weizheng, H. Teng, P. Shixin, S. Jie, Y. Yong, Q. Jun, Z. Weijun, *Optica Applicata* **XXXV**, 1 (2005).
- [113] J.U. White, *J. Opt. Soc. Am.* **32**, 285 (1942).
- [114] S.M. Chernin, E.G. Barskaya, *Appl. Opt.* **30**, 51 (1991).
- [115] D. Herriott, H. Kogelnik, R. Kompfner, *Appl. Opt.* **3**, 523 (1964).
- [116] J.B. McManus, P.L. Kebabian, M.S. Zahniser, *Appl. Opt.* **34**, 3336 (1995).

### **3 Spectroscopic study of pulsed DC plasmas used for nitriding processes**

The active screen (AS) nitriding is an advanced technology for the plasma nitriding of steel components providing a number of advantages over conventional plasma nitriding. Developed in the last decade, the AS technology has found its industrial application, however the understanding of the fundamental mechanisms and their relationship is not complete. For the first time the mid infrared tunable diode laser absorption technique in combination with the quadruple mass spectrometry has been applied in this work. *In-situ* diagnostics of chemical phenomena in the  $N_2-H_2$  plasmas under variation of the process conditions such as  $H_2$  to  $N_2$  gas ratio, process temperature and bias activation power provided valuable information about the concentration of active nitrogen species in the vicinity of the samples surfaces. The thickness of the compound layer representing the nitriding efficiency was used as a response to nitriding conditions for the evaluation of selected process parameters derived from the plasma diagnostic studies. A 1:1 gas mixture of the  $N_2-H_2$  process gases seems to be most effective to get thick compound layers [1].

#### **3.1 Introduction**

The active screen plasma nitriding (ASPN) is a novel plasma assisted nitriding technique for a surface-engineering treatment with a high application potential [2]. The main advantages of the ASPN over a conventional plasma process are caused by the replacement of the glow discharge from the components to a separate metal screen (active screen, AS) surrounding the entire workload. This approach has significantly reduced or even completely eliminated any possible damage caused by edge effects, hollow cathode discharges and

arcing. During the nitriding process the active screen plays a twofold role – it generates a mixture of active species required for the nitriding process and it radiates the heat, produced by the plasma discharge, resulting in a uniform temperature distribution over the workload parts even with highly different geometry. The worktable and the parts are placed in a floating potential or a weak cathodic potential is applied.

Although the ASPN technology developed in the last decade has been proven its industrial applicability, the understanding of the fundamental mechanisms and their relationship required to effective use of its potential is not complete and still in the focus of investigation of many research groups worldwide [3-12]. According to the fundamental differences of the ASPN technology compared to conventional plasma processes an improved knowledge of nitriding mechanisms is necessary to be developed. During the plasma nitriding with an active screen the mechanism of the nitrogen mass transfer to the surfaces of the metallic parts cannot be described with a single mechanism. George [3] suggested that active neutral nitrogen species generated at the active screen play a decisive role. Hubbard *et al* [8-10] stated that “sputtering and deposition” mechanism proposed by Li and Bell [4-6] cannot explain sufficiently the mass transfer in the ASPN process. They proposed that energetic nitrogen ions or neutrals originating from the active screen and a sufficient bias applied to the worktable ensures the uniform nitriding results in the commercial ASPN setup. Ricard and co-workers [13-16] put a lot of diagnostic effort into the study of discharge and post-discharge phenomena in  $N_2-H_2$  plasmas. Their OES diagnostic results provided unambiguously a major role of the neutral atomic nitrogen in the nitriding process during the post-discharge. A concept of the remote plasma source makes both methods comparable, but not equivalent. An electrostatic confinement effect and intensive radiation produced by the AS are two more factors affecting the kinetics of gas reactions in the vicinity of the probe surface.

Only in few studies non-disturbing *in-situ* plasma diagnostic methods have been applied to study the plasma processes involved in plasma nitriding at the industrial scale ASPN unit [12]. For a better understanding of the chemical phenomena in  $N_2-H_2$  plasmas and their contribution to the nitriding process a combination of two spectroscopic techniques, mid infrared tunable diode laser absorption (TDLAS) and quadruple mass spectrometry (QMS) have been used in this work.

**Figure 3.1:**

*Photo of the ASPN plasma reactor with the applied diagnostics systems for TDLAS- and QMS-measurements. Left side – TDLAS system IRMA with optical table and control unit and right side – quadrupole mass spectrometer [1].*

During the plasma nitriding the growth of compound layers (CL) is primarily determined by the presence of active nitrogen species in the vicinity of the probe surface. The CL thickness was used as a response for the evaluation of selected process conditions derived from the plasma diagnostic studies.

## 3.2 Experimental

The AS plasma nitriding experiments were performed in an industrial-scale 15 kW pulsed DC plasma system ( $f = 1$  kHz and 60% duty cycle). The inner volume of the reactor was about  $1 \text{ m}^3$ . As an active screen a double wall metal mesh with 800 mm in diameter and 750 mm in height was placed in the middle of the reactor surrounding the workload. A separate generator (Magpuls,  $P = 10$  kW) running at  $f = 10$  kHz with a 50% duty cycle supplied a negative Bias-voltage to the worktable. The pressure in the furnace was pumped to a base pressure of 70 Pa.

The process gases were introduced into the discharge chamber through separate mass flow controller (MFC). Using TDLAS, the dependencies of  $\text{NH}_3$  concentration on several plasma parameters were monitored. Additionally, QMS was used to detect stable plasma products in the chamber.

Figure 3.1 shows the ASPN plasma reactor with the applied diagnostic systems for TDLAS- and QMS-measurements. In figure 3.2 a sketch of the construction of the reactor

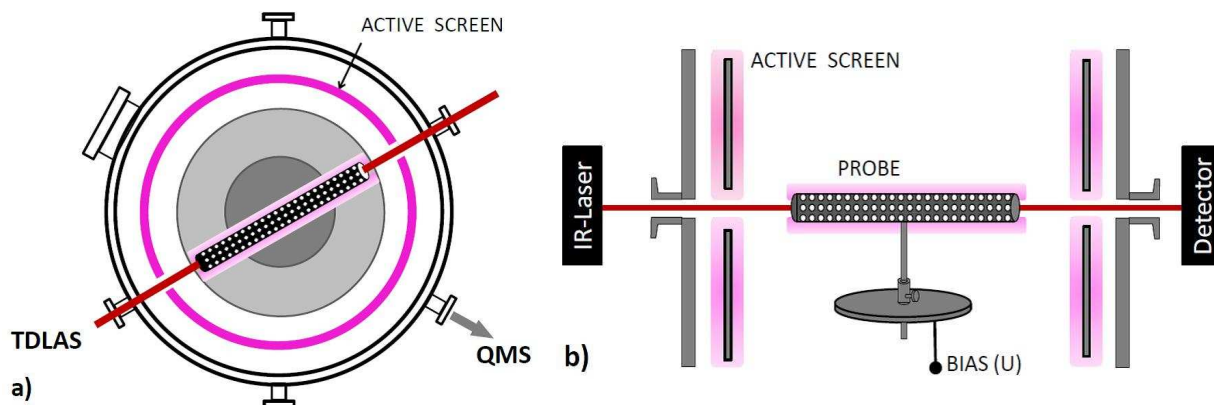


**Figure 3.2:** Sketch of the reactor together with the applied plasma diagnostic techniques: top view (a), side view (b) [1].

together with the applied plasma diagnostic techniques is given. In addition, a special metallic mesh tube with a length of 60 cm, a diameter of 4 cm and a mesh-size of about 1.5 cm, representing a probe, was installed in the middle of the worktable for the simulation and the monitoring of plasma processes near the probe surface. Plasma intensification due to the hollow cathodes in the mesh holes was negligible in the working pressure range. The probing beam of the TDLAS system was guided directly through this probe tube. During the plasma phases two pressure values were used, 200 or 300 Pa, respectively. The flow rate was kept constant at 80 l/h. Two precursor gases were used:  $N_2$  and  $H_2$ . The gas mixture was varied by changing the partial gas flows. The temperature was varied from 400 to 570°C depending on the experimental conditions (table 3.1).

**Table 3.1:** The ASPN process parameters used for plasma diagnostics studies.

Gas mixture	Pressure, Pa	Temperature, °C	Range or composition	Bias power, %
$N_2 + H_2$	200, 300	400, 570	0 – 75% $H_2$	0 – 20
		400, 450, 500	50% $H_2$	

For the TDLAS measurements of  $NH_3$  concentrations a compact and transportable IR multi-component acquisition system (IRMA) was used [17]. The IRMA system contains four independent laser stations. The narrowband infrared emission of four lead salt diode lasers was used to monitor the infrared absorption features of the target species. The four diode lasers are mounted in individual cold stations, which are thermally coupled to the cold finger of a closed cycle cryostat. The temperature of each laser is controlled at milli-Kelvin precision between 30 K and 100 K. Four grating monochromators serve as mode filters. The light of the four lasers is converged into a single beam, which is used for measurement in the plasma of

the ASPN reactor. The data acquisition system for the four-channel tunable diode system consists of two computers combined with two high speed boards and two dual diode laser controllers housed in a single transportable rack (figure 3.1).

Based on rapid scan software using direct absorption with sweep integration, the absolute concentrations of several molecular species can be measured simultaneously within milliseconds. In the present study with the IRMA system several absorption lines of  $\text{NH}_3$  species were observed in the  $\text{N}_2/\text{H}_2$  plasma. Figure 3.3 shows typical absorption spectra of  $\text{NH}_3$  measured with the IRMA system in the plasma of the ASPN reactor. Absorption lines at  $887\text{ cm}^{-1}$  have been used.

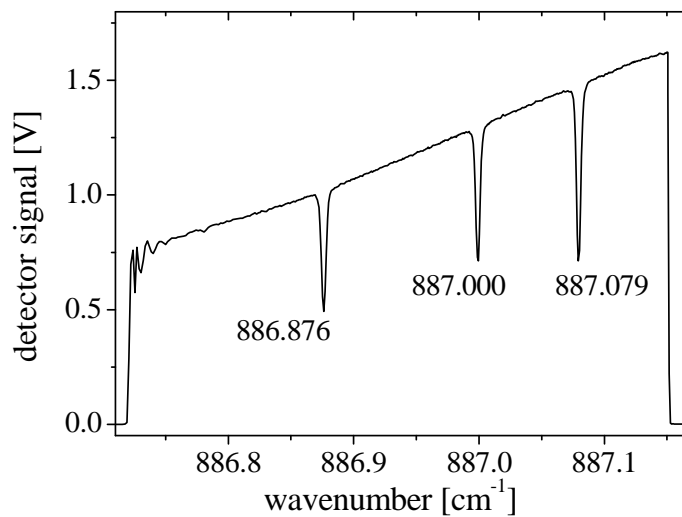


**Figure 3.3:** Typical absorption spectrum of  $\text{NH}_3$  around  $887\text{ cm}^{-1}$  [1].

For the monitoring of the process gases a quadrupole mass spectrometer (QMS 200, Balzers) was applied simultaneously to the TDLAS diagnostics. Some additional experiments have been carried out for the mass spectroscopic analysis of the neutral gas species in the vicinity of the probe tube surface. Inside the cylindrical probe a fused silica pipe of the QMS gas inlet system was placed in the same manner as TDLAS probing beam. The reduction of the process pressure down to the working pressure of the quadrupole analyzer ( $<10^{-5}$  mbar) was achieved by a gas dosing valve (UDV 040, Pfeiffer). For the QMS measurements the working pressure was kept constant at 200 Pa to provide a prompt response on process changes.

Based on plasma diagnostic experiments the role of active nitrogen species was examined experimentally by performing a series of nitriding tests. Three grades of steel commonly used for mechanical components and tools, i.e. 42CrMoV4, 31CrMoV9 and X38CrMoV5-1, were investigated under selected nitriding process conditions. All the samples

were wet ground down with 1000 grit SiC paper, cleaned and dried with hot air before the treatment. The nitriding results were metallographically analyzed. The composition profiles were obtained by means of glow discharge optical emission spectrometry (GDOES).

### 3.3 Results and discussion

#### 3.3.1 Measurement of $\text{NH}_3$ concentrations by TDLAS

A first experiment was performed at a temperature of  $570^\circ\text{C}$  and at a pressure of 2 mbar. During the experiment the ratio of  $\text{H}_2$  to  $\text{N}_2$  in the feed gas of the reactor was gradually changed up to 75% of  $\text{H}_2$ . To maintain the probe temperature constant the AS power was automatically adjusted from the value of 8 kW at 0%  $\text{H}_2$  to almost 10 kW for 75%  $\text{H}_2$ . In addition, at certain  $\text{H}_2$  concentrations the value of the bias power was varied between 0 and 20% of the AS power.

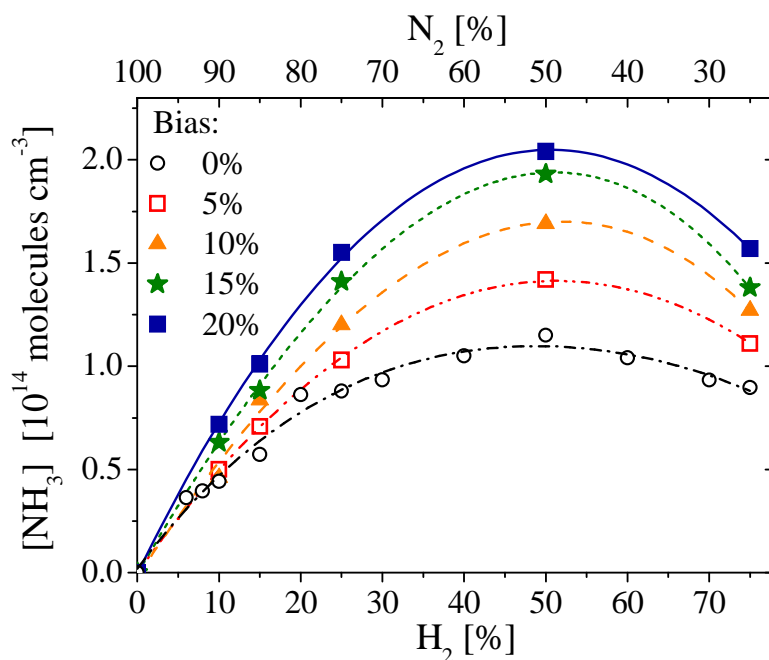


**Figure 3.4:** Influence of the bias power in % of the active screen power on the  $\text{NH}_3$  concentration in the  $\text{N}_2$ - $\text{H}_2$ -plasma ( $P = 200$  Pa and  $T = 570^\circ\text{C}$ ) [1].

An increase of the bias power results in reduction of the AS power. Figure 3.4 shows the dependence of the  $\text{NH}_3$  concentration on the  $\text{N}_2$ - $\text{H}_2$  mixture ratio for different values of the bias power. The concentration of  $\text{NH}_3$  was found to be in the range of 0.2 – 1.2%. The concentration of the produced  $\text{NH}_3$  is growing up with the admixture of bigger amounts of  $\text{H}_2$ ,

up to the ratio  $H_2:N_2=1:1$ . The increase of the bias value leads to an increase of the concentration of  $NH_3$ .

### 3.3.2 QMS analysis of the $N_2$ – $H_2$ plasma

A QMS experiment was designed identically to the TDLAS experiment with introduction of a silica gas inlet system instead of the probing beam in the middle of the probe tube. A temperature of 400°C was alternatively chosen for this experiment to maximize the response signal. The typical QMS spectra of the process gas for pure  $N_2$  (b) and  $N_2 + 75\% H_2$  (c) plasmas are shown in figure 3.5.

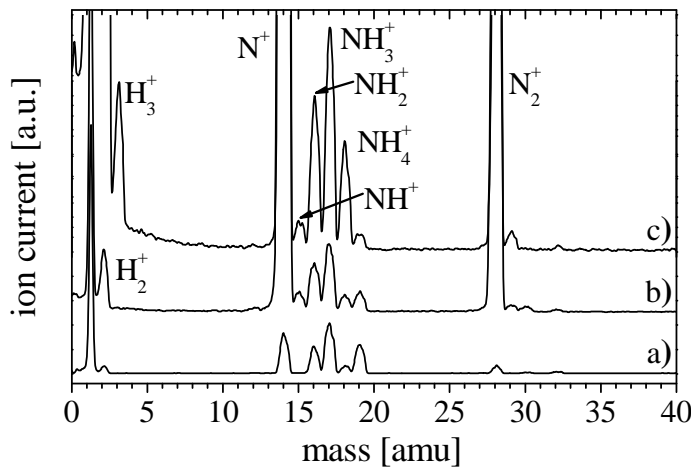


**Figure 3.5:** Typical QMS spectra measured from different gas mixtures: a) the background spectrum in the QMS measured at the pressure of  $10^{-7}$  Pa, b) pure  $N_2$ , c)  $N_2 + 75\% H_2$  [1].

and 18 amu was attributed to the increase of the  $NH_3$  concentration represented in the QMS spectrum by a series of  $NH_x +$  fragments with  $x=1, 2, 3$ , and 4, respectively.

The increase of the feed gas ratio of  $H_2$  to  $N_2$  up to 50% is accompanied by an increase of the  $NH_3$  concentration. A higher admixture of  $H_2$  to the process gas (above 50%) leads to reduction of the  $NH_3$  concentration. Therefore, a clear coincidence of TDLAS and QMS measurements was found. Application of the bias power of up to 20% of the AS power to the probe tube considerably increases the  $NH_3$  concentration as well (see figure 3.6).

An increase of the process temperature from 400 to 500°C reduced significantly the  $NH_3$  concentration. The  $NH_3$  level was slightly growing with the application of the bias power (figure 3.7). It is worth to note that the effect of the bias power is stronger at 400 and 450°C.

The highest admixture of  $H_2$  into the process gas leads to a pronounced increase of the intensity of the  $H_2$  peaks at 2 and 3 amu ( $H_2^+$  and  $H_3^+$ , respectively). The presence of the  $H_3^+$  radical in the QMS spectra at the higher concentration of  $H_2$  is due to ionization processes in the QMS ionization chamber. In addition, an intensification of the QMS peaks at the mass numbers  $m/z=15, 16, 17$

In figure 3.8 (on the left axis) the intensity ratio of two masses ( $N^+/N_2^+$ ) is plotted as a function of the  $H_2$  gas admixture for different values of the bias power. This ratio relates to the degree of dissociation of the  $N_2$  molecules which occurred during the ionization in the mass spectrometer. It is known that the dissociation process of the QMS is highly statistical in the ionization chamber. Only a small part of the electron energy is transferred to break the molecule bond. Exceeding a certain value (the dissociation energy), which is specific for different molecules, the chemical bond will be broken and the parent molecule is dissociated into fragment molecules. The dissociation yield depends strongly on the energetic state of the parent molecule. For energetically excited molecules possessing electrons on higher vibration levels the dissociation probability is higher.

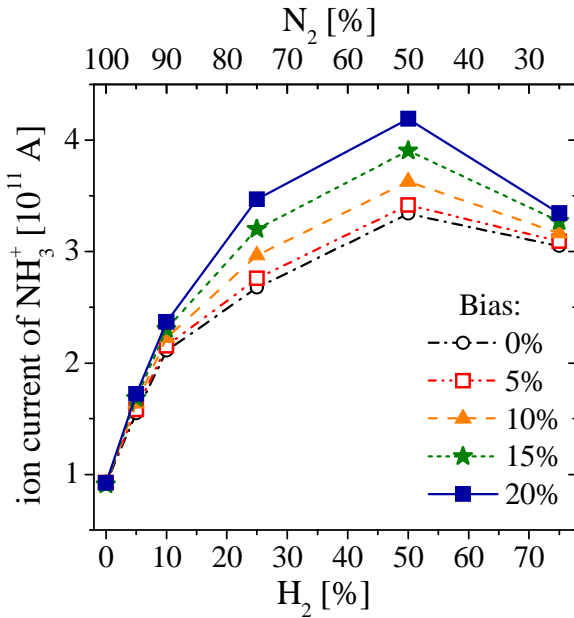


**Figure 3.6:** Dependence of the  $NH_3^+$ -peak intensity (17 amu) on the  $H_2/N_2$  ratio in different values of the bias power (in % of the AS power),  $T= 400^\circ\text{C}$  and  $P= 200$  Pa [1].

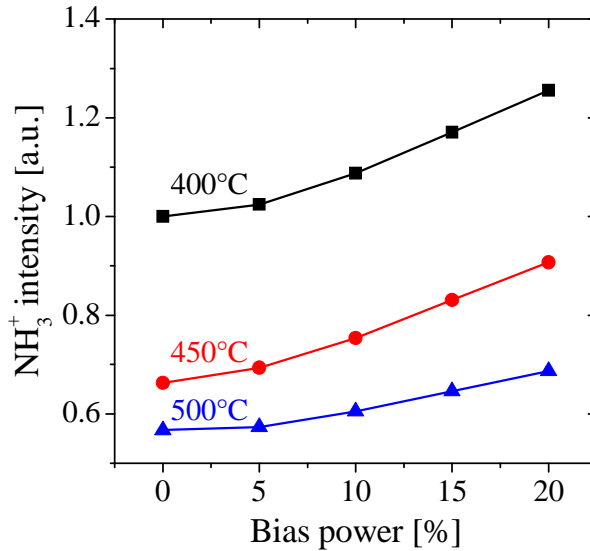


**Figure 3.7:** Dependence of the relative  $NH_3^+$ -peak intensity (17 amu) on the bias power (in % of the AS power) at different process temperatures. The  $N_2/H_2$  ratio is 1:1 and  $p= 200$  Pa. All values are normalized to the ion current intensity at  $400^\circ\text{C}$  and at 0% bias [1].

The quenching reactions of  $H_2$  with highly excited  $N_2$  molecules lead to a reduction of  $N_2$  dissociation yield, i.e. the ratio  $N^+/N_2^+$  is decreased. It is worth noting that the QMS-signal of both nitrogen masses ( $N^+$  and  $N_2^+$ ) dropped significantly for the  $H_2$  admixture

above 20% (see figure 3.8 on the right axis for  $N^+$ -radical). This fact is very essential for nitriding process.

As it was stated by different research groups based on conventional plasma nitriding process [18], it is unlikely that the  $NH_x$ -species produced in the  $N_2$ - $H_2$  plasma are the active nitriding species. In case of ASPN, the role of the  $NH_3$  radicals produced in the  $N_2$ - $H_2$  plasma in the nitriding process is not enough investigated. The  $NH_x$ -species produced by AS could act as precursor providing the atomic N after dissociation near the probe surface. On the other hand, this mechanism will lose its effectiveness significantly either at higher temperature above 500°C or for the  $H_2$  concentration of much higher than 50%. The application of the bias power intensifies both the generation of the  $NH_x$ -species and the increase of the concentration of active nitriding species, e.g. the N atoms in ionized or neutral form, simultaneously near the probe surface. The latter is very essential for the ASPN process. The higher level of the bias power improves significantly the nitriding results. Therefore, one may conclude that the generation rate of  $NH_x$ -species could be an indicator of an effective nitriding process in the  $N_2$ - $H_2$  plasma. A mechanism of energetic exchange between excited  $N_2^*$  species and  $NH_3$  molecules was claimed by Swerts *et al* in their patent [19]. They have invented a new method for remote plasma activated nitridation with a quite similar idea as in the ASPN. The remote plasma excited  $N_2^*$  species were mixed with the flow of  $NH_3$  gas resulting in activation of the  $NH_3$  species, which finally improves significantly the nitridation efficiency.

A discharge power applied to the AS point is a next important parameter which contributes to the generation of excited  $N_2^*$  and ammonia molecules. As mentioned above the AS power was automatically increased with further admixture of the  $H_2$  gas to maintain the process temperature constant (see figure 3.9a). Actually, the concentration of the  $NH_x$ -species in the reactor is a product of probability of the plasma-chemical reactions and their intensification due to applied AS power. The application of bias or change of the reactor temperature at the fixed  $H_2/N_2$  gas ratio leads immediately to a self-adjustment of the AS power (see figure 3.9b) and therefore to a change of the concentration of plasma species.

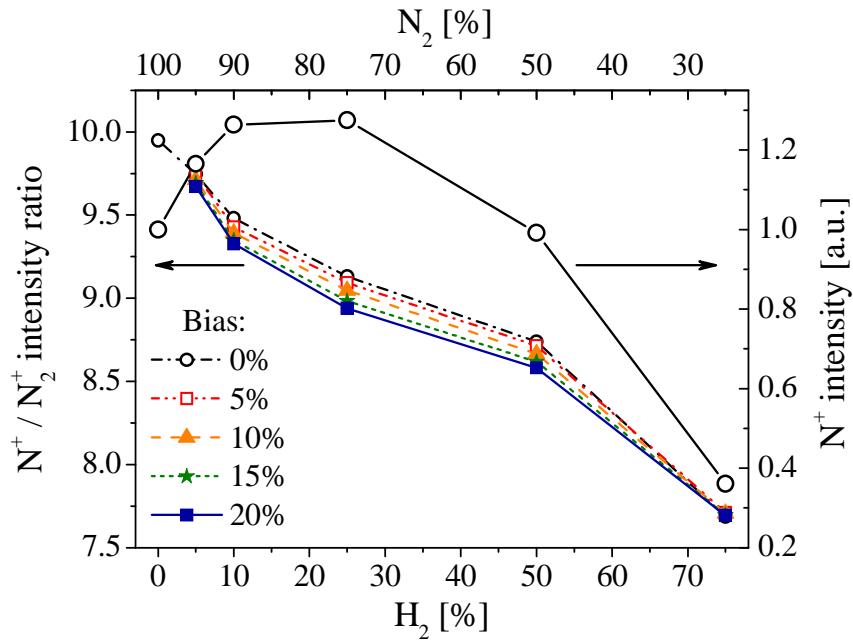


**Figure 3.8:** The  $N^+/N_2^+$  intensity ratio versus the  $H_2/N_2$  ratio for different values of bias power (in % of AS power),  $T = 400^\circ\text{C}$  and  $p = 200\text{ Pa}$  (left axis); dependence of the relative  $N^+$ -peak intensity (14 amu) on the  $H_2/N_2$  ratio without bias (right axis) [1].

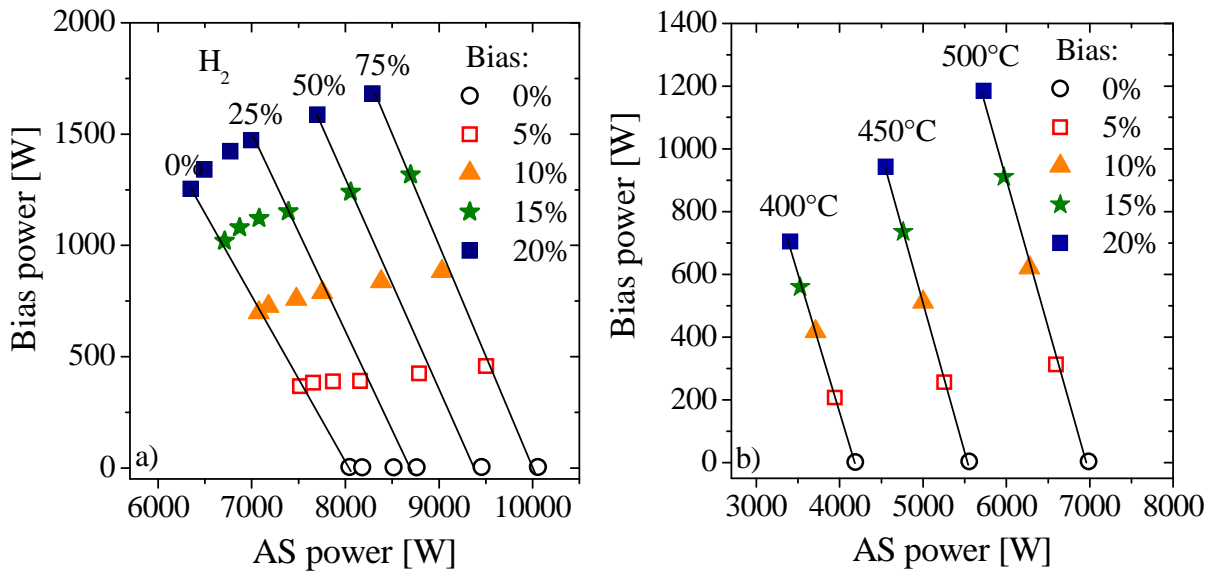


**Figure 3.9:** The relationship between the values of AS and bias power under certain process conditions: a) variation of the  $H_2$  fraction at the fixed process temperature of  $570^\circ\text{C}$ , b) variation of the process temperature at the fixed  $H_2$  fraction at 50% [1].

It is an essential characteristic of the ASPN process compared to conventional plasma nitriding. A twofold function of the AS, i.e. heating and generation of plasma species, determines the decisive mechanism responsible for the nitriding results at certain process conditions. To prove the assumptions made by both diagnostic methods that the generation rate of the  $\text{NH}_x$ -species depends on the ASPN process conditions and is related to the activity of the active nitrogen a short series of nitriding experiments was performed on the ASPN system. The influence of selected process conditions, in particular the  $\text{H}_2$  to  $\text{N}_2$  gas ratio was investigated.

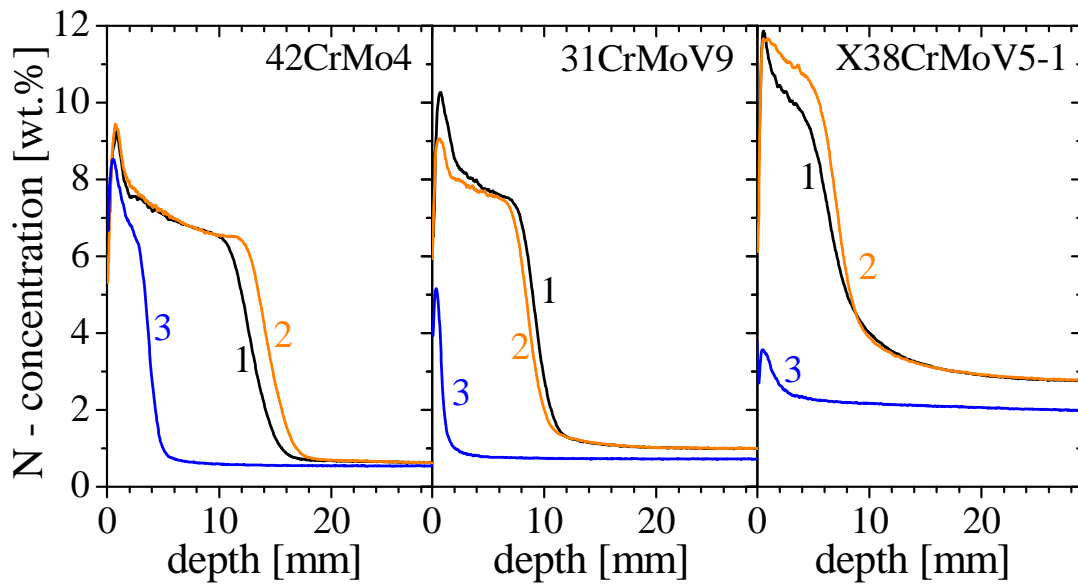
### 3.3.3 Plasma nitriding experiments

The results obtained from both plasma diagnostic methods were implemented in design of the experimental program (see table 3.2 for details). Three mixtures of the process gas with different  $\text{H}_2$  to  $\text{N}_2$  ratios (1:3, 1:1, and 3:1) and the bias power at the level of 15% of the AS power applied to the work table were used. To determine a nonmaterial-specific response of the nitriding conditions three typical nitriding steels (42CrMo4, 31CrMoV9, X38CrMoV5-1) were chosen for the experiments. The GDOES results providing information about the depth profile of nitrogen concentration and about the thickness of compound layer (CL) for each steel grade processed at three gas mixtures are presented in figure 3.10. The CL thickness results obtained from GDOES spectra are summarized in table 3.3. In most cases the  $\text{H}_2:\text{N}_2=1:1$  gas ratio tends to be more favorable to obtain a thick CL, which indicates a higher nitriding activity and therefore a higher concentration of active nitrogen at the probe surface during the nitriding process.

This statement was also supported by diagnostic results. However, despite a similar generation rate of ammonia monitored by diagnostics both for 25% and 75% of  $\text{H}_2$  admixtures, the worse nitriding results obtained in the experiment with the highest  $\text{H}_2$  concentration showed that the generation rate of the  $\text{NH}_x$ -species alone is not sufficient to predict entirely the nitriding results, in particular for the  $\text{H}_2$  admixtures above 50%. Changes of the concentration and the energetic state of  $\text{N}_2$ -species (see figure 3.8), as well as their reactivity with the probe surface should be taken into account. It is most likely that other mechanisms are dominating in this case. To clarify that further investigations are planned.

**Table 3.2:** *The ASPN process parameters.*

Nr.	Treatment cycles	Process medium		Pressure, Pa	Process duration, h	15% of bias power, W
		Gas mixture ratio	Total gas flow rate, l/h			
1	Heating + sputter	Ar/H <sub>2</sub> = 1:1	30	150	1.5	1000
2	Nitriding at T = 570 °C	H <sub>2</sub> /N <sub>2</sub> = 1:3	80	300	4	1120
		1:1				1190
		3:1				1260
3	Purge + cooling	Ar	60	300	0.5	-

**Figure 3.10:** *The N-concentration depth profiles for three steel grades (42CrMo4, 31CrMoV9, X38CrMoV5-1) and three H<sub>2</sub>/N<sub>2</sub> gas ratios: 1) 1:3, 2) 1:1, 3) 3:1. [1]***Table 3.3:** *ASPN nitriding results. (CL thickness in  $\mu\text{m}$ ).*

Nr.	Gas mixture H <sub>2</sub> :N <sub>2</sub>	42CrMo4	31CrMoV9	X38CrMoV5-1
1	1:3	12.6	9.1	6.2
2	1:1	13.9	8.5	7.0
3	3:1	3.8	0	0

### 3.4 Summary and conclusions

Plasma nitriding with an active screen contains a variety of mechanisms contributing to the nitriding process. Depending on process conditions, plasma unit size and design, one or another mechanism dominates. The application of plasma diagnostic methods provided valuable knowledge about the plasma processes and mechanisms during the real nitriding experiments in industrial scale plasma setups. The application of two spectroscopic techniques TDLAS and QMS for monitoring the reactions in the  $H_2-N_2$  plasma provided us the information about the concentration of active nitrogen species playing a decisive role in the nitriding process. The generation rate of the ammonia obtained from the diagnostics seems to correlate well with the nitriding results, however not for the  $H_2/N_2$  gas ratio exceeding 50%. Nevertheless, a combination of two diagnostic methods applied for the first time in the ASPN process has proven their applicability for investigation of nitriding mechanisms at certain process conditions.



## 4 On kinetic and chemical phenomena in dust producing RF plasmas

In Ar and He radio frequency (RF) plasmas with admixtures of  $C_2H_2$  and  $CH_4$  the hydrocarbon chemistry have been studied in relation to dust particle formation by means of infrared tunable diode laser absorption spectroscopy (TDLAS) combined with Fourier transform infrared (FTIR) spectroscopy. The experiments were performed in a RF capacitively coupled parallel plate reactor at a frequency of  $f=13.56$  MHz, a pressure of  $p=0.1$  mbar and a flow rate of  $\Phi=8$  sccm of Ar or He with admixtures of 0.5 sccm  $C_2H_2$  or 1 sccm  $CH_4$ . The power was  $P=15$ W. Using TDLAS, the temporal evolution of the concentrations of the methyl radical and of four stable molecules,  $C_2H_2$ ,  $CH_4$ ,  $C_2H_4$  and CO, have been monitored in the plasma. Simultaneously, the growth process of the dust particles was analysed by FTIR spectroscopy. The degree of dissociation of the acetylene precursor was found to be nearly constant in the range of 96% under stabilized conditions for both the Ar and He plasmas. In contrast, the degree of dissociation of the methane precursor varied between 45% and 90% depending (i) on the appearance of dust particles in the reactor volume and (ii) on the Ar or He plasma conditions. The methyl radical concentration was found to be in the range of  $10^{11}$  molecules  $cm^{-3}$ . The concentrations of all hydrocarbon species were strongly correlated with the dynamic of the dust formation. Fragmentation efficiencies of acetylene ( $R_F(C_2H_2) = 3.2 \times 10^{16}$  molecules  $J^{-1}$ ) and of methane ( $R_F(CH_4) = (0.16 - 2.5) \times 10^{16}$  molecules  $J^{-1}$ ) and conversion efficiencies to the produced hydrocarbons ( $R_C = (0.23 - 8.5) \times 10^{14}$  molecules  $J^{-1}$ ) could be estimated in dependence on the discharge conditions in the RF plasma [20].

## 4.1 Introduction

In reactive low temperature molecular plasmas the formation of dust is a well-known phenomenon [21-23]. Numerous properties of dusty plasmas and dust particles were extensively analysed in the last decades. This included dust formation, particle growth, astrophysical importance of dust, build-up of strongly coupled systems, formation of voids and many other aspects. Different source gas compositions are used in reactive plasma processes to produce nano- and micro-sized particles. Additionally to the thin film deposition, dust particles can be produced by reactive plasma polymerization, depending on the discharge conditions such as gas flow rate, input power and pressure [24, 25]. Dust as the by-product of thin film deposition or plasma etching can seriously deteriorate the quality and reliability of the products in semiconductor industry [26]. On the other hand, dust particles embedded in thin films can significantly improve their properties [27]. The controlling of the dust particle formation to either suppress or to enhance their formation and how to design dust particles with tailored properties is still a challenge [28].

In recent years numerous studies on hydrocarbon plasma chemistry [29] and controlled dust particle formation in hydrocarbon plasmas have been reported [30-35]. Depending on the precursor gases and background or matrix gases, dust with different chemical compositions and different crystalline structures has been produced [28, 33]. Using a capacitively coupled pulsed radio frequency plasma it was possible to suppress or enhance the production of dust in hydrocarbon plasmas by applying different pulse frequencies and duty cycles [35, 36], following the experience for a silicon-based plasma [30]. The physical and chemical properties of both the active phase and the plasma afterglow seem to play an important role in dust formation [35].

Frequently  $C_2H_2$  and  $CH_4$  have been used as main chemical precursor gases for nanoparticle formation in plasmas. The  $C_2H_2$  containing plasma has a much stronger tendency to form dust. To initiate the nucleation of dust precursor in  $CH_4$  plasmas some amount of  $C_2H_2$  is needed [37].

In a number of mass spectroscopy [23, 31, 38] and broadband infrared absorption spectroscopy [23, 32, 33] studies the behaviour of different neutrals, ions and ionic clusters has been analysed in hydrocarbon-based dust forming plasmas. Mass spectroscopy studies usually can reveal the dominant plasma chemistry products but absolute species concentrations are difficult to determine, in particular, in the case if radicals are concerned.

Therefore, the relevant reaction pathways for particle nucleation are difficult to deduce. These pathways can be better understood by coupling plasma and chemistry modelling [39, 40]. However, basic plasma chemical phenomena are still not fully analyzed.

For a better understanding of the plasma chemical phenomena in dust-producing discharges information about the time-dependent absolute ground state concentration of precursor molecules and of transient and stable molecular products in relation to the dust formation would be very helpful. Tunable diode laser absorption spectroscopy (TDLAS) in the mid-infrared spectral range using lead salt lasers as radiation sources has been proven to be a versatile diagnostic technique. In particular, TDLAS is well suited for the measurement of absolute ground state concentrations of a wide variety of molecular species including radicals and molecular ions thereby providing a link with chemical modelling of the plasma (see [41] and references therein). Until now, the main applications of TDLAS have been for investigating molecules and radicals in fluorocarbon etching plasmas and in plasma containing hydrocarbons [41]. Based on the TDLAS method online measurements with temporal resolutions down to the  $\mu\text{s}$ -range can be performed [41]. Such time-resolved observations of concentration changes of molecular species, e.g. after abrupt changes under experimental conditions, can provide valuable information about kinetics in the plasma and can be used to estimate gas phase reaction constants or surface reaction probabilities [42-44].

The recent development and commercial availability of pulsed and continuous wave quantum cascade lasers (QCLs) for wavelengths longer than  $3.4\ \mu\text{m}$  and inter-band cascade lasers (ICLs) for shorter wavelength offer an attractive new option for mid-infrared laser absorption spectroscopy (IR-LAS) for plasma diagnostic purposes. Distributed feedback (DFB) QCLs provide continuous mode-hop free wavelength tuning. Their total emission range is typically limited to less than  $7\ \text{cm}^{-1}$ . Recently tunability over much broader spectral ranges than with a typical DFB-QCL has been achieved using external cavity (EC) configurations. Nowadays, EC-QCL, which are available in pulsed or continuous wave working mode, can be tuned over more than  $100\ \text{cm}^{-1}$  and provide mode-hop free tuning ranges in the order of  $80\ \text{cm}^{-1}$  [45]. Meanwhile the varieties of QCLs and ICLs operating at room temperature are considered as substitutes for cryogenic cooled lead salt lasers, which have led to a rapid development of IR-LAS from a niche position to a standard diagnostic technique [46, 47]. In conjunction with integrated DFB gratings, the emission wavelength of this new class of thermoelectrically cooled semiconductor lasers can be custom tailored over a wide range throughout the infrared molecular fingerprint region. Recently in a study of the

nucleation-growth cycle of carbon nano-particles the acetylene concentration has been monitored using QCL absorption spectroscopy under similar experimental conditions as in the present investigation [48]. Hundt and co-workers reported a relation between of the growth cycle period of particles to the initial acetylene concentration and a strong decrease in the concentration of the acetylene precursor gas with discharge power [48]. An unexpected temperature dependence of the dust particle growth rate in low pressure Ar/C<sub>2</sub>H<sub>2</sub> plasmas was described by Beckers and Kroesen [49].

Unfortunately, for wavelengths longer than 12  $\mu\text{m}$  the number of commercial available QCLs is rather limited. For the detection of the methyl radical the  $\nu_2$  band at 16.5  $\mu\text{m}$  is a promising spectral region, but here no QCLs are available as radiation sources. Therefore, for this study the traditional TDLAS technique has been chosen.

In the present investigation the hydrocarbon chemistry in relation to dust particle formation in Ar and He RF plasmas of a capacitively coupled parallel plate reactor with admixtures of C<sub>2</sub>H<sub>2</sub> and CH<sub>4</sub> has been in the centre of interest. Using TDLAS, the temporal evolution of the concentrations of the methyl radical and of four stable molecules, C<sub>2</sub>H<sub>2</sub>, CH<sub>4</sub>, C<sub>2</sub>H<sub>4</sub> and CO, has been monitored in the plasma. Simultaneously, the growth process of the dust particles was analysed by Fourier transform infrared (FTIR) spectroscopy. One of the objectives was to determine the fragmentation efficiencies of the precursor molecules and the conversion efficiencies to the produced hydrocarbons. Another focus was the analysis of correlations between the dynamic of the dust formation and the time dependence of molecular concentrations and the differences found in Ar- and He-dominated plasmas.

## 4.2 Experimental

The experimental arrangement of the capacitively coupled parallel plate reactor with the TDLAS and FTIR spectroscopy systems is shown in figure 4.1. The electrodes are made of stainless steel, had a diameter of 30 cm and were located inside a 50 cm diameter 30 cm high stainless steel cylinder chamber. The electrode gap, which can be varied externally, was fixed to 8 cm in these experiments and the electrodes are symmetrically driven at a frequency of  $f = 13.56$  MHz. The power applied to the electrodes was  $P = 15$  W measured before the match box and the discharge was driven in continuous wave mode. The match box was adjusted to keep the reflected power to less than a few per cent of the forward power. The specific

advantage of this discharge arrangement is the relatively large electrode diameter, which guarantees a rather homogeneous confinement of the particles and a high sensitivity for line of sight diagnostics as infrared absorption spectroscopy. The experimental setup was described in detail in [23, 34, 36]. During plasma operation the pressure was  $p = 0.1$  mbar for flow rates of  $\Phi = 8$  sccm of Ar or He and admixtures of 0.5 sccm of  $C_2H_2$  or 1 sccm of  $CH_4$ . The pressure was regulated by mass flow controllers and a throttle valve in the exit port to a turbo molecular pump with a maximum nominal pumping speed of about  $150 \text{ l s}^{-1}$ . The gas residence time was approximately 1 min [23, 34].

The experiments were performed in Ar or He dominated plasmas following a standardized procedure.

(i) *The Ar plasma case:* After flushing the chamber with pure Ar first nano-particles are formed in a plasma polymerization process with acetylene as precursor gas [34, 50]. From former studies in the same reactor it is known, that in Ar/ $C_2H_2$  discharges dust particles are formed spontaneously even at the relatively low power of  $P = 15$  W, which has been used in the present experiments. After this first dust initiation period, with a length of about 9 min, the acetylene admixture was stopped and after 2 min of pure Ar plasma substituted by a methane admixture of 1 sccm, while holding the Ar flow constant. The experiment was finished after the dust, which had been produced during the methane admixture, reached a critical particle size and disappeared out of the discharge zone caused by developing of a void, i.e. a particle free region inside the plasma volume [51, 52]. The whole duration of this experiment was of a length of about 41 min.

(ii) *The He plasma case:* In this experiment Ar as main feed gas was substituted by He. Again after flushing the chamber with pure He, a flow of  $\Phi = 0.5$  sccm of  $C_2H_2$  were added to the feed gas and the plasma was switched on to initiate the formation of first nano-particles. After this first dust initiation period, with a length of about 19 min, the acetylene admixture was stopped and after 2 min of pure He plasma substituted by a methane admixture of 1 sccm, while holding the He flow constant. The experiment was finished after further 11 min, while monitoring the molecular concentrations by TDLAS and the dust production via FTIR spectroscopy. The whole duration of this experiment was of a length of about 32 min.

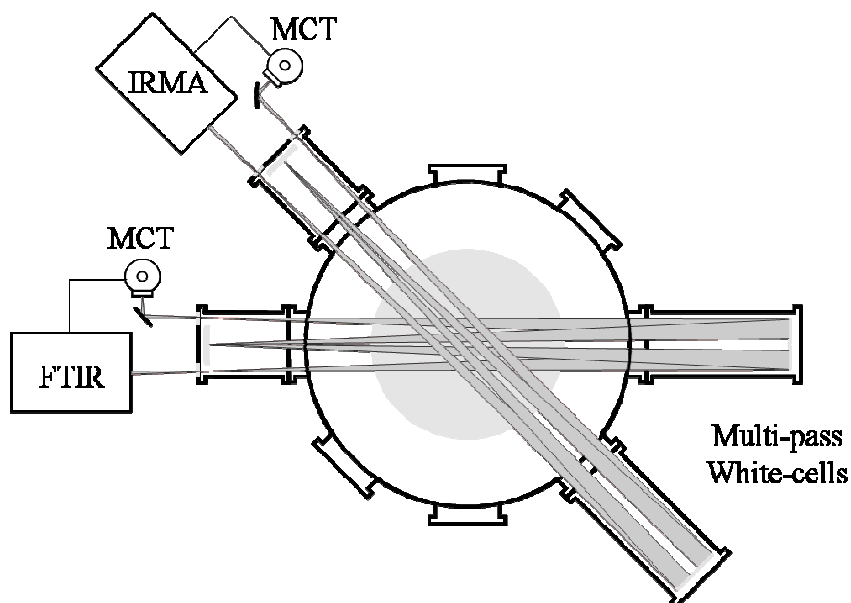


**Figure 4.1:** *Experimental arrangement: top view [20].*

For the time resolved infrared TDLAS measurements presented here a compact and transportable infrared multi-component acquisition system (IRMA) was used. While the optical setup of IRMA allowed the parallel usage of up to four different lasers, for improved signals and sensitivity reasons only two lasers were operated in parallel in the present case, sharing the same beam path through the chamber. In all measurement cycles one of the lasers was used to monitor the concentration developments of  $\text{CH}_4$  and  $\text{C}_2\text{H}_2$ , used as hydrocarbon precursor source gases, while the second laser was selected to monitor one of the molecular products of the plasma chemical processes. Therefore, in the present case the concentrations of  $\text{CH}_3$ ,  $\text{C}_2\text{H}_4$  and  $\text{CO}$  have been determined in separate measurement cycles. A detailed description of the IRMA system and of the rapid scan software used for data analysis can be found elsewhere [17].

**Table 4.1:** *Species, spectral positions and line strengths used for the TDLAS measurements.*

Species	Spectral position [ $\text{cm}^{-1}$ ]	Absorption line strength [ $\text{cm}^{-1}/(\text{molecule cm}^{-2})$ ]	Ref.
$\text{CH}_4$	1302.777	2.357E-20	[34]
$\text{C}_2\text{H}_2$	1302.595	1.199E-19	[34]
	1302.889	4.622E-21	
$\text{CH}_3$	606.1203	4.53E-19	[35, 36]
$\text{C}_2\text{H}_4$	888.3572	6.106E-21	[34]
$\text{CO}$	2169.198	4.440E-19	[34]

The infrared laser beam from the IRMA system had the diameter of about 2 cm and was transferred using gold-coated mirrors via KBr-windows to an optical long path cell (White cell type [53], 36 passes, absorption length: 11.5 m), which was mounted to the plasma chamber for improved sensitivity (figure 4.1). The diode laser beam leaving the cell was focused on a standard HgCdTe infrared detector by an off-axis parabolic mirror. The identification of lines and the determination of their absolute positions were carried out using well-documented reference gas spectra and an etalon of known free spectral range for interpolation [52]. Spectral positions and absorption line strengths of molecular ground state absorption lines used for the measurements are listed in table 4.1.

It should be noted that the absorption line strength of the second, weaker  $C_2H_2$  line at  $1302.889\text{ cm}^{-1}$  is not included in the HITRAN database [54]. Therefore it had to be determined from the ratio of their relative absorption compared to the line at  $1302.595\text{ cm}^{-1}$ .

The absorption line strength of the  $CH_3 - Q(3,3)$  line used here was taken from the work of Stancu *et al* [55, 56]. For the calculations of the concentrations a gas temperature of 300 K was used since this as a good average for the gas temperature over the line of sight, comprising the active zone between the discharge electrodes and the afterglow surrounding them, and over the course of the measurement. This temperature was justified by earlier measurements [57] where  $306 - 333\text{ K} \pm 10\text{ K}$  was found with dust above the electrodes and 293 K with Ar only, at the same pressure and discharge power of  $P = 15\text{ W}$ .

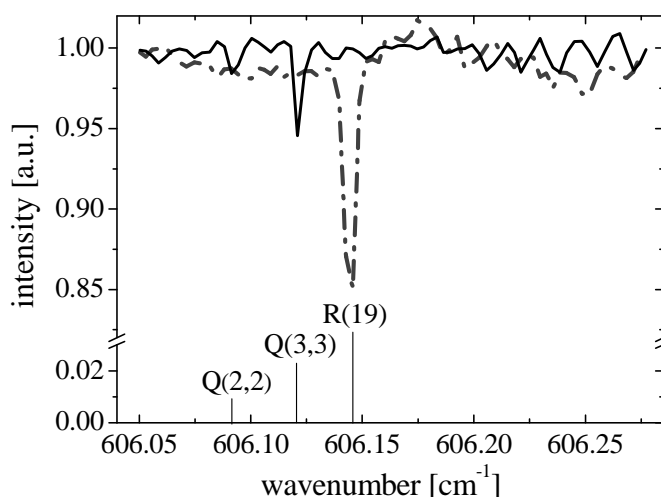


**Figure 4.2:**  
*Example spectrum of the  $CH_3$  free radical in an Ar/ $CH_4$  plasma showing two Q branch lines from the  $\nu_2$  fundamental band. The dashed line is a calibration spectrum from  $N_2O$  [20].*

Figure 4.2 shows an exemplary spectrum of the  $CH_3$  free radical in an Ar/ $CH_4$  plasma with two Q branch lines from the  $\nu_2$  fundamental band. The dashed line is a calibration spectrum from  $N_2O$ .

In the plasma volume the growth process of the particles was monitored by means of FTIR spectroscopy. To monitor the particle growth the temporal evolution of the absorbance at  $5000\text{ cm}^{-1}$  was measured. This approach for *in-situ* detection of the particle growth in the reaction chamber is described in more detail in refs. [23, 33]. Briefly, the IR beam from the FTIR spectrometer (Bruker) was directed through KBr windows in the plasma chamber and was focused with a focal mirror onto an external liquid nitrogen-cooled HgCdTe detector. By means of a multi-pass technique, it was possible to achieve an optical path length in the plasma of up to 7.2 m, i.e. 24 passes. The diameter of the beam was about 2 cm. Due to the reflections of the beam in the multi-pass cell the area monitored by the FTIR spectrometer has the dimensions of about  $2 \times 5\text{ cm}^2$ .

## 4.3 Results and discussion

### 4.3.1 General features of species concentrations and particle growth under Ar and He plasma conditions

The time dependence of concentrations of molecular species measured by TDLAS in Ar and He plasmas with admixtures of  $\text{C}_2\text{H}_2$  or  $\text{CH}_4$ , the degree of dissociation of the precursor gases combined with the *in-situ* absorbance measurement of the FTIR system at  $5000\text{ cm}^{-1}$ , monitoring the formation of dust in the reactor chamber, are shown in figures 4.3 and 4.4. The left columns of figures 4.3 and 4.4 present the experimental data measured in the Ar plasma case, while in both figures the right columns represent the conditions found in the He plasma case. The experiments have been structured in time in different phases, which characterize the change in important plasma and particle parameters, see table 4.2.

In figure 4.3 the time-dependent concentrations of five molecular species,  $\text{CH}_3$ ,  $\text{CH}_4$ ,  $\text{C}_2\text{H}_2$ ,  $\text{C}_2\text{H}_4$  and  $\text{CO}$  for the Ar and He plasmas, are shown. As explained in the former chapter, the concentrations of  $\text{C}_2\text{H}_4$  and  $\text{CO}$  have been determined in separate measurements and are included for completeness here. In the He plasma case the concentration of  $\text{C}_2\text{H}_4$  was below the limit of detection of about  $10^{11}\text{ molecules cm}^{-3}$ .

Figure 4.4(a) gives the absorbance at  $5000\text{ cm}^{-1}$  measured by the FTIR spectrometer showing one period of the periodical particle growth from the initiation of the nucleation up to a critical particle size and the disappearance out of the inner reactor volume, as described in

[51, 52]. In figure 4.4(c), the degree of dissociation of the precursor molecules  $C_2H_2$  in phase Ar 1 and of  $CH_4$  in the phases Ar 3–5 is shown.

The right column of figure 4.4 is structured in a comparable way for the He plasma case. Figure 4.4(b) again gives the absorbance at  $5000\text{ cm}^{-1}$  for monitoring a possible particle nucleation and growth, while figure 4.4(d) depicts the degree of dissociation of the hydrocarbon precursors for phases 1 and 3 of the experiment.

**Table 4.2:** *Experimental phases of the measurements in the Ar and He plasma case.*

Phase	Plasma on/off	Hydrocarbon Precursor Gas	Status of Particle Formation
Ar 0	Off	$C_2H_2$	No growth
Ar 1	On	$C_2H_2$	Initiation of nucleation
Ar 2	On	None	No further growth
Ar 3	On	$CH_4$	Growth of particle diameter up to maximum
Ar 4	On	$CH_4$	Particles start to disappear from reactor volume
Ar 5	On	$CH_4$	Reactor volume free of particles
He 0	Off	$C_2H_2$	No growth
He 1	On	$C_2H_2$	Slight initiation of nucleation
He 2	On	none	Reaching of a distinct maximum of number and size
He 3	On	$CH_4$	Small particle number present

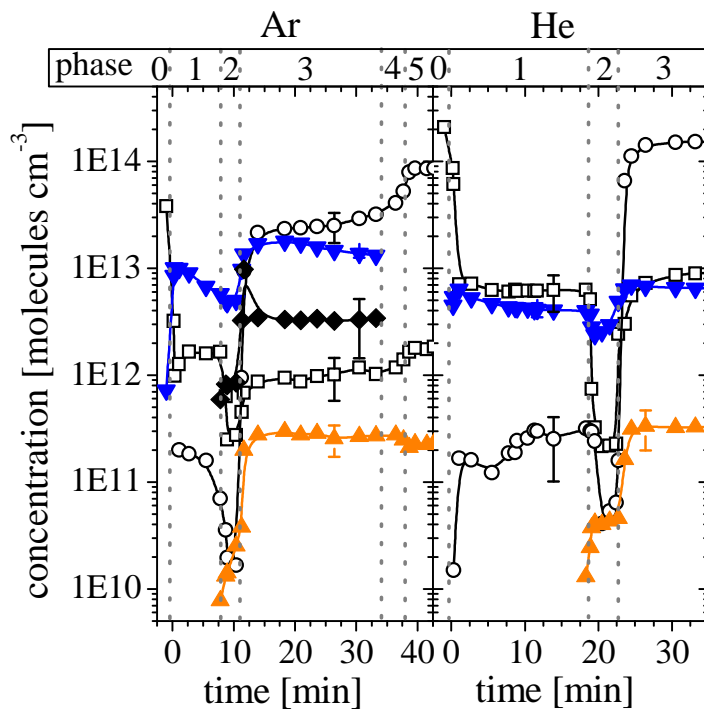
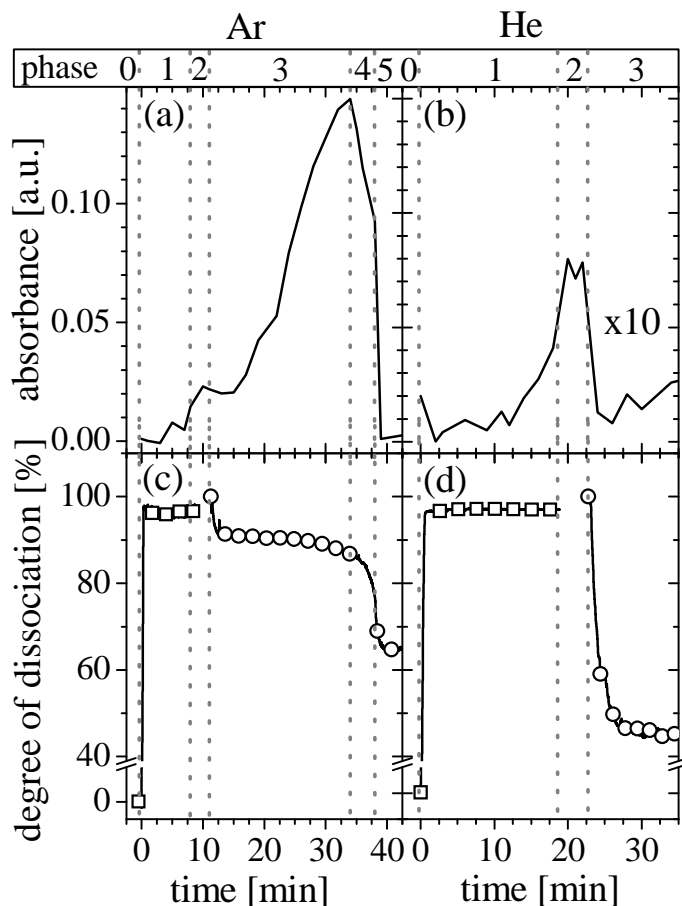


**Figure 4.3:**

*Molecular concentrations in Ar, left panel, and He RF plasmas, right panel, with admixtures of  $C_2H_2$  or  $CH_4$  in different experimental phases, see table 4.2, as a function of the time ( $\square$  -  $C_2H_2$ ,  $\circ$  -  $CH_4$ ,  $\blacklozenge$  -  $C_2H_4$ ,  $\blacktriangle$  -  $CH_3$ ,  $\blacktriangledown$  -  $CO$ ) [20].*

**Figure 4.4:**

Temporal evolution (i) of the absorbance at  $5000\text{ cm}^{-1}$ , measured by FTIR, monitoring the dust production in the reactor (sub-diagrams (a) and (b)) and (ii) of the degree of dissociation of the precursor gases  $\text{C}_2\text{H}_2$  ( $\square$ ) and  $\text{CH}_4$  ( $\circ$ ) (sub-diagrams (c) and (d)) in Ar, left panel, and He RF plasmas, right panel, with admixtures of  $\text{C}_2\text{H}_2$  or  $\text{CH}_4$  in different experimental phases, see table 4.2 [20].



Figures 4.3 and 4.4 give an overview of the degree of dissociation as well as the product concentration which ranges over four orders of magnitude. Some useful generalizations follow from this figure. There are some differences between the species concentration time profiles measured in the Ar and He plasma case. In the He plasma case no  $\text{C}_2\text{H}_4$  could be found in the limit of detection, while in the Ar plasma case the concentration of the  $\text{C}_2\text{H}_4$  product was in the order of about  $4 \times 10^{12}\text{ molecules cm}^{-3}$ . The degree of dissociation of the acetylene precursor was found to be nearly constant in the range of 96% under stabilized conditions for both the Ar and He plasmas. Here it should be noted that in a former study a slightly larger degree of dissociation of up to 99% has been obtained at an essentially higher power value of  $P=80\text{ W}$  in the Ar/ $\text{C}_2\text{H}_2$  plasmas by measuring the decay of Ar metastables in the plasma afterglow [57]. The reasons for the slight deviation between the TDLAS results presented here and the Ar metastable decay time measurements are (i) the higher discharge power, but also (ii) the fact that the Ar metastables are only present in the active space of the plasma, which makes only a part of the TDLAS absorption length. The outer-electrode space where the acetylene is not dissociated contributes effectively to a decrease in the degree of

dissociation measured by TDLAS. Recent measurements using QCL absorption spectroscopy reveal 99.5% as degree of dissociation of  $C_2H_2$  under comparable discharge conditions [58].

In contrast, the degree of dissociation of the methane precursor varied between 45% and 90% depending (i) on the appearance of dust particles in the reactor volume and (ii) on the Ar or He plasma conditions. The methyl radical concentration was found to be in the range of  $10^{11}$  molecules  $cm^{-3}$  for both plasma cases. It is interesting to note, that the concentration of the methyl radical could be stably monitored only in the case when  $CH_4$  was used as the precursor gas. In the initiation phases of the nucleation, Ar 1 and He 1, the methyl concentration was below the detection limit of about  $10^{10}$  molecules  $cm^{-3}$ . The concentrations of all hydrocarbon species were strongly correlated with the dynamic of the dust formation. This is in particular obvious in the behaviour of the degree of dissociation of the methane precursor in the phases Ar 3 and 4. With the disappearance of the dust particles out of the monitored reactor volume, the degree of dissociation decreases from about 90% to nearly 65%. Further details of the concentrations dynamics are discussed in the following section.

#### 4.3.2 *Dynamic of the species concentrations*

In figure 4.5 the time dependence of the relative concentration of the hydrocarbon precursor  $C_2H_2$  at the beginning of the Ar and He plasma experiments, i.e. the transition between the phases Ar 0 and Ar 1 and between He 0 and He 1, is shown. The concentrations of these experiments have been normalized for clearer visibility of the dynamic effects. As expected, in the reactor with the ignition of the plasma the concentration of  $C_2H_2$  decreases relatively fast, in the Ar plasma case even about twice as fast as in the He plasma experiment, i.e. in about 17 s (Ar plasma,  $T_{Ar2}$ ) respectively in about 34 s (He plasma,  $T_{He2}$ ) a stable value of the degree of dissociation of nearly 96% is reached.

For the Ar plasma case this dynamic behaviour had already been observed by Kovačević and co-workers using a mass spectrometer for monitoring the mass 26 (acetylene) [28]. They found exactly the same time of about 17 s for comparable experimental conditions at a power of  $P = 15$  W. In the paper of Kovačević *et al* also a strong change of the slope of the concentration decay is reported a few seconds after the discharge ignition.

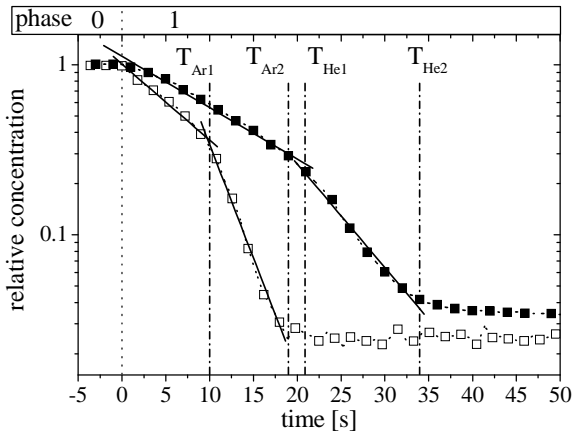


**Figure 4.5:** Relative concentration of the  $C_2H_2$  precursor in Ar (□) and He (■) RF plasmas as a function of time in the transition between the experimental phases Ar 1-2 and He 1-2, see table 4.2 [20].

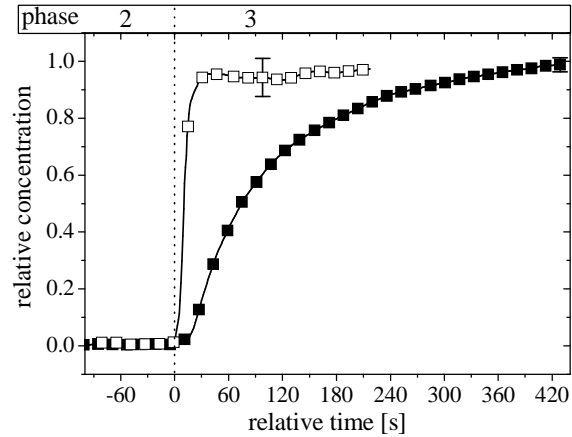


**Figure 4.6:** Relative concentration of  $C_2H_2$  in Ar (□) and He (■) RF plasmas as a function of time in the transition between the experimental phases Ar 2-3 and He 2-3, see table 4.2 [20].

The same effect can be seen in the present TDLAS study, showing two distinct slopes of the decreasing  $C_2H_2$  concentration after igniting the discharge. This phenomenon appears not only with Ar, but also, with different slope characteristics, in the He plasma case. In [28] these two slopes are related to two phases of dust production, nucleation and formation of bigger particles, connected with increasing electron temperature  $T_e$ , being responsible for a faster depletion of the acetylene precursor. Further, Kovačević *et al* found essential differences in the particle growth rate while comparing  $N_2$  and Ar plasmas. In the  $N_2$  case the growth rate was three times higher than in the Ar case [28].

In this study the reactivity rate of the He-dominated plasma in terms of the  $C_2H_2$  depletion seems to be considerably reduced compared with the Ar case. This can be concluded from the time dependencies shown in figure 4.5 but also, even more impressive, from the comparison of the absorbance data at  $5000\text{ cm}^{-1}$  presented in figures 4.4(a) and (b). From figure 4.4(b) combined with figure 4.5 it can be concluded, that a relatively small nucleation of particles is initiated, reaching a distinct maximum in the phase He 2, with absorbance values of about 20 times smaller as in the Ar case. In phase He 3 the particle nucleation and growth processes are obviously again of very low efficiency.

A different reactivity of the He plasma compared with the Ar plasma case can also be found by analyzing the temporal behaviour in the transition phase Ar 2-3 and He 2-3, i.e. as  $CH_4$  has been used as hydrocarbon precursor instead of  $C_2H_2$ . In figure 4.6 the normalized increase in the  $C_2H_2$  concentration produced from the admixed  $CH_4$  precursor over time is

shown. In the Ar plasma case the maximum of the  $C_2H_2$  concentration is reached within less than 60 s, which is in the order of the residence time of the reactor. In contrast, the He-dominated plasma requires about 7 min to reach a stable value of the  $C_2H_2$  concentration. But it is necessary to underline, that the  $C_2H_2$  production in the Ar case leads to concentrations of about  $10^{12}$  molecules  $cm^{-3}$ , while the He plasma achieves nearly a one order of magnitude higher acetylene concentration ( $10^{13}$  molecules  $cm^{-3}$ ) and this even at a much smaller degree of dissociation of  $CH_4$  of less than 50%, see figure 4.4.

A further remarkable difference of both plasma cases can be found near to the end of both experiments. In the He plasma case the concentrations of  $CH_3$ ,  $C_2H_2$ ,  $CH_4$  and even CO are relatively stable in phase He 3, see figure 4.3. In contrast, in the Ar plasma case several interesting features of the temporal behaviour of the molecular concentrations related to the disappearance of the particles have been detected, shown in figures 4.7 and 4.8. With the beginning of phase Ar 4 the particles start to move out of the volume of observation, see figure 4.4(a).

This process changes the plasma conditions, what is reflected (i) in a reduced degree of dissociation of the precursor  $CH_4$ , (ii) in an increasing concentration of the product  $C_2H_2$  and (iii) in a slightly decrease of the methyl concentration. Directly at the transition between the phases Ar 4 and 5 the remaining particles tend to vanish in a very short time scale. The changing plasma conditions, in particular the lower  $T_e$ , can be seen immediately in a steep decrease in the methyl radical concentration, which is reduced of about 25% within a time of  $T_1 = 5.4$  s. After reaching this minimum the methyl concentration increases again within a short period of about  $T_2 = 7.2$  s, and then further shows a relatively constant value. It is worthwhile to compare the temporal behaviour of the methyl radical concentration at the transition of the phases Ar 4-5 with the depletion of acetylene in phase Ar 1, shown in figure 4.5. The specific dynamics of the methyl radical concentration, shown in figure 4.8(b), can be interpreted as a proof for a new start of the nucleation process of the dust production after about 12.6 s, i.e. after  $T_1 + T_2$  from the disappearance of nearly all particles out of the volume of observation in the reactor. Further, it is interesting to note that the  $CH_3$  radical, which has a life time of about 40 ms, is a fast and sensitive probe of changing plasma conditions [55]. The concentration of stable molecules is much less appropriate to study faster processes, because of the residence time of about 1 min in the reactor volume. Nevertheless, the increasing  $CH_4$  concentration shows an interesting temporal behaviour as a proof of a considerable change of the plasma conditions. In particular, there are three obvious inflection

points in the concentration curve, which are in direct time coincidence with the decreasing  $\text{CH}_3$  concentration, see figure 4.8.

Concerning the detected CO it should be mentioned, that the authors assume, that oxygen for the CO production was provided by unspecified layers inside the reactor, which can act as a source of adsorbed oxygen for quite a long time. The CO concentration was found to be in the order of  $10^{13}$  molecules  $\text{cm}^{-3}$  or less, depending on the discharge conditions. Therefore, the monitored CO represents about 1% or less of the carbon atoms available in the plasma reactor.

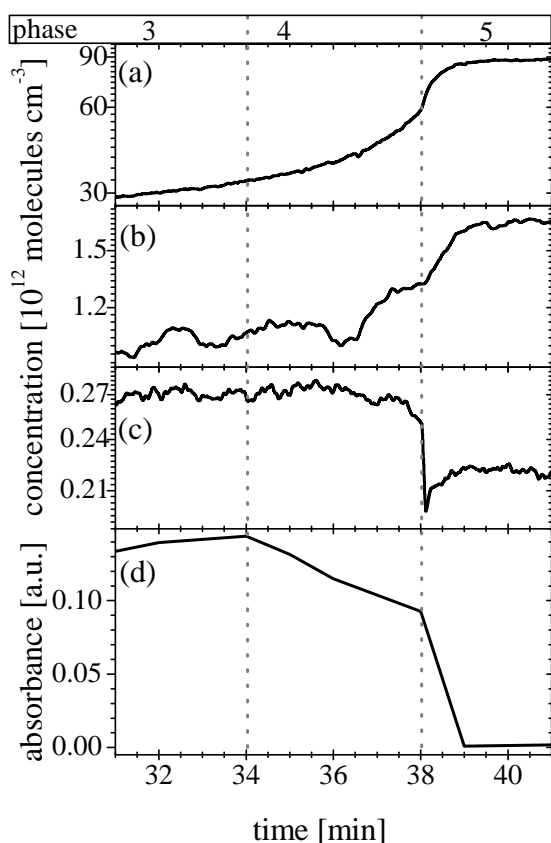


**Figure 4.7:** Molecular concentrations in Ar RF plasmas with admixtures of  $\text{CH}_4$  in the experimental phases Ar 3-5, see table 4.2, as a function of the time ((a)  $\text{CH}_4$ , (b)  $\text{C}_2\text{H}_2$ , (c)  $\text{CH}_3$ ) and (d) the absorbance at  $5000\text{ cm}^{-1}$ , measured by FTIR, monitoring the dust production in the reactor [20].

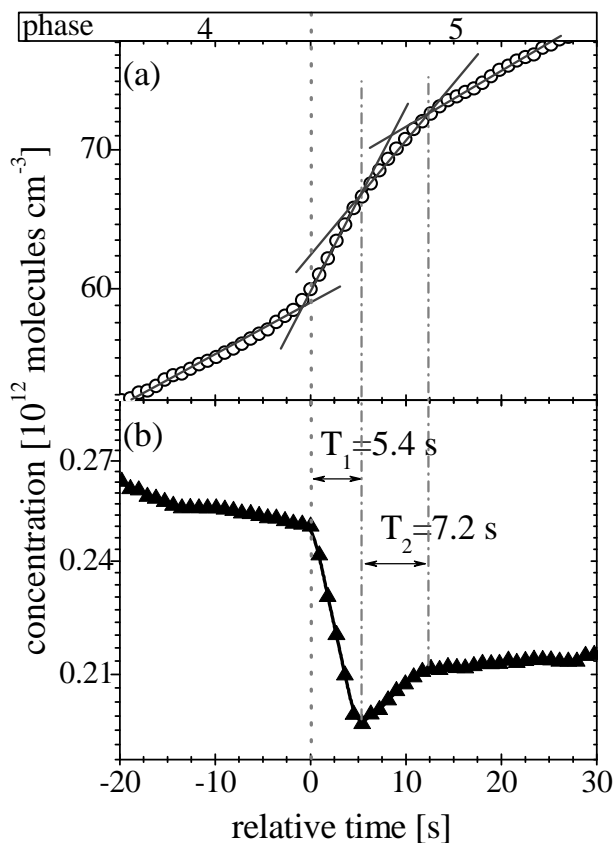


**Figure 4.8:** Detailed view on the temporal behaviour of the concentrations of  $\text{CH}_4$  (a) and  $\text{CH}_3$  (b), in an Ar RF plasma as a function of time in the transition between the experimental phases Ar 4-5, see table 4.2 [20].

### 4.3.3 Fragmentation and conversion efficiencies

For further insight into plasma chemical conversion, the experimental data concerning acetylene and methane dissociation were used to estimate absolute fragmentation efficiencies of  $C_2H_2$  and  $CH_4$  and conversion efficiencies to the observed main products  $CH_4$ ,  $C_2H_2$ ,  $C_2H_4$  and  $CH_3$ . The efficiencies are normalized for the discharge power.

The fragmentation efficiency  $R_F$  of the hydrocarbon precursor molecules, acetylene and methane, is calculated by analogy to ref. [58, 59] as

$$R_F = \Phi_P \frac{1}{60} \frac{D}{100} \frac{N_o}{P} \quad (4.1)$$

where  $R_F$  has units of molecules  $J^{-1}$ ,  $\Phi_P$  is the precursor flow rate (sccm),  $D$  is the percentage degree of dissociation of the precursor molecules,  $N_o$  is the number of molecules per  $cm^3$  at STP ( $2.69 \times 10^{19}$  molecules  $cm^{-3}$ ) and  $P$  is the power in W.

The conversion efficiency,  $R_C$ , to plasma product molecules is expressed analogously as

$$R_C = n_{molecule} \frac{\Phi_{total}}{60} \frac{10^3}{p} \frac{1}{P} \quad (4.2)$$

where  $R_C$  has units of molecules  $J^{-1}$ ,  $n_{molecule}$  is the measured molecular concentration in molecules  $cm^{-3}$ ,  $\Phi_{total}$  is the total gas flow rate in sccm,  $p$  is the pressure in mbar and  $P$  is the power in W.

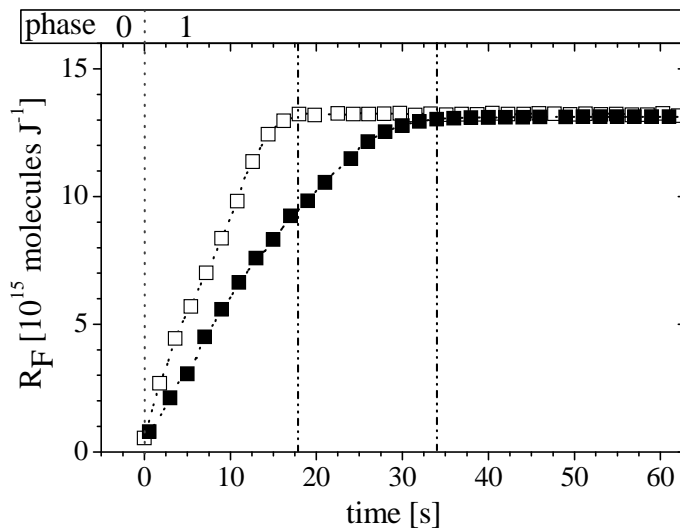


**Figure 4.9:**

The fragmentation efficiency,  $R_F$ , of acetylene in Ar ( $\square$ ) and He ( $\blacksquare$ ) RF plasmas as a function of time in the transition between the experimental phases Ar 0-1 and He 0-1, see table 4.2 [20].

Fragmentation efficiencies of acetylene,  $R_F(\text{C}_2\text{H}_2) = 3.3 \times 10^{16} \text{ molecules J}^{-1}$ , and of methane,  $R_F(\text{CH}_4) = (0.16 - 2.5) \times 10^{16} \text{ molecules J}^{-1}$ , and conversion efficiencies to the produced molecular species in the range  $R_C = (0.23 - 8.5) \times 10^{14} \text{ molecules J}^{-1}$  could be estimated in dependence on the discharge conditions in the RF plasma. The efficiencies of conversion to particular reaction products are based on the measurements of absolute concentration values.

Figure 4.9 shows as an example the respective efficiencies of fragmentation of acetylene depending on time for the Ar and He plasma case. It is interesting to note that after a time of about 30 s the final fragmentation efficiency of  $\text{C}_2\text{H}_2$  is identical in the Ar and He plasma case. Further detailed information about relevant fragmentation and conversion efficiencies representing selected phases of the Ar and He plasma case is given in table 4.3.

It should be mentioned that the values of the calculated fragmentation and conversion efficiencies of the present RF plasma are comparable to values found in surface wave discharges and in planar microwave plasmas [58, 59]. In general, in this study higher conversion efficiencies have been found for the He plasma case.

**Table 4.3:** *Fragmentation efficiencies,  $R_F$ , and conversion efficiencies,  $R_C$ , of different experimental phases in the Ar and He plasma case.*

Phase	Fragmentated molecule	$R_F$ [molecules $\text{J}^{-1}$ ]	Produced Molecule	$R_C$ [molecules $\text{J}^{-1}$ ]
Ar 1	$\text{C}_2\text{H}_2$	$3.2 \times 10^{16}$		
Ar 3	$\text{CH}_4$	$2.5 \times 10^{16}$	$\text{CH}_3$	$2.6 \times 10^{13}$
			$\text{C}_2\text{H}_2$	$9.9 \times 10^{13}$
			$\text{C}_2\text{H}_4$	$3.4 \times 10^{13}$
			$\text{CO}$	$1.7 \times 10^{14}$
Ar 5	$\text{CH}_4$	$1.7 \times 10^{16}$	$\text{CH}_3$	$2.3 \times 10^{13}$
			$\text{C}_2\text{H}_2$	$1.8 \times 10^{14}$
He 1	$\text{C}_2\text{H}_2$	$3.2 \times 10^{16}$		
He 3	$\text{CH}_4$	$1.6 \times 10^{15}$	$\text{CH}_3$	$3.2 \times 10^{13}$
			$\text{C}_2\text{H}_2$	$8.5 \times 10^{14}$
			$\text{CO}$	$6.9 \times 10^{14}$

## 4.4 Summary and conclusions

In this study it has been possible to determine the absolute ground state concentration of the methyl radical and of four stable species under a wide range of experimental conditions by infrared diode laser absorption spectroscopy providing a link with the dynamic behaviour of the dust formation in a capacitively coupled RF discharge, the ultimate objective being a better understanding of chemical and reaction kinetic processes occurring in dust-producing plasmas. Although several molecular species concentrations have been monitored in absolute scale, the mass balance of the whole dust producing process is far from being comprehensively analysed. Future studies should include (i) further stable, in particular higher hydrocarbon molecules as well as other important intermediates, but also (ii) a quantitative analysis of the dust production rate in the discharge. In addition to  $\text{CH}_3$  this includes other free radicals, as for example  $\text{C}_2\text{H}$ ,  $\text{CH}_2$  and  $\text{CH}$  and would lead to an improved modelling potential based on reliable reaction rates, which are essentially required as well as more kinetic data on elementary reactions.

## Bibliography for Chapters 3 and 4

- [1] I. Burlacov, K. Börner, H.-J. Spies, H. Biermann, D. Lopatik, H. Zimmermann, J. Röpcke, *Surf. Coat. Technol.* **206**, 3955 (2012).
- [2] J. Georges, *US Patent* **5**, 989, 363 (1999).
- [3] J. Georges, *Heat Treat. Met.* **28**, 33 (2001).
- [4] C.X. Li, T. Bell, *Heat Treat. Met.* **1**, 1 (2003).
- [5] C. Zhao, C.X. Li, H. Dong, T. Bell, *Surf. Coat. Technol.* **201**, 2320 (2006).
- [6] C.X. Li, *Surf. Eng.* **26**, 135 (2010).
- [7] H.-J. Spies, H. Le Thien, H. Biermann, *HTM Z. Werkst. Wärmebeh. Fertigung* **60**, 240 (2005).
- [8] P. Hubbard, D.G. McCulloch, E.D. Doyle, S.J. Dowey, J.N. Georges, *BHM* **151**, 441 (2006).
- [9] P. Hubbard, S.J. Dowey, J.G. Partridge, E.D. Doyle, D.G. McCulloch, M.B. Taylor, *Surf. Coat. Technol.* **204**, 1145 (2010).
- [10] P. Hubbard, S.J. Dowey, E.D. Doyle, D.G. McCulloch, *Surf. Eng.* **22**, 243 (2006).
- [11] S.C. Gallo, H. Dong, *Surf. Coat. Technol.* **203**, 3669 (2009).
- [12] D. Cleugh, *Surf. Eng.* **18** (2), 133 (2002).
- [13] A. Ricard, *Surf. Coat. Technol.* **59**, 67 (1993).
- [14] A. Ricard, T. Czerwicz, T. Belmonte, S. Bockel, H. Michel, *Thin Solid Films* **341**, 1 (1999).
- [15] B. Gordietsy, C.M. Ferreiray, M.J. Pinheiroy, A. Ricard, *Plasma Sources Sci. Technol.* **7**, 363 (1999).
- [16] S. Bockel, A.M. Diany, A. Ricard, *Surf. Coat. Technol.* **74–75**, 474 (1999).
- [17] J. Röpcke, L. Mechold, M. Käning, J. Anders, F.G. Wienhold, D. Nelson, M. Zahniser, *Rev. Sci. Instrum.* **71**, 3706 (2000).
- [18] J.M. Priest, M.J. Baldwin, M.P. Fewell, *Surf. Coat. Technol.* **145**, 152 (2001).
- [19] J. Swerts *et al.*, *US Patent* **7**, 629, 270 B2 (2009).

- [20] F. Hempel, D. Lopatik, B. Sikimic, I. Stefanovic, J. Winter, J. Röpcke, *Plasma Sources Sci. Technol.* **21**, 055001 (2012).
- [21] J. Perrin, C. Hollenstein, *Dusty Plasmas*, ed A. Bouchoule, New York: Wiley, 1999.
- [22] U. Kortshagen, U. Bhandarkar, *Phys. Rev. E* **60**, 887 (2001).
- [23] E. Kovačević, I. Stefanović, J. Berndt, J. Winter, *J. Appl. Phys.* **93**, 2924 (2001).
- [24] H. Kobayashi, A.T. Bell, M. Shen, *Macromolecules* **7**, 227 (1974).
- [25] J.M. Tibbitt, R. Jensen, A.T. Bell, M. Shen, *Macromolecules* **10**, 647 (1974).
- [26] G.S. Selwyn, J. Singh, R.S. Bennet, *J. Vac. Sci. Technol. A* **7**, 2758 (1974).
- [27] P.R.I. Cabarrocas, S. Hamma, S.N. Sharma, G. Viera, E. Bertran, J. Costa, *J. Non-Cryst. Solids* **227**, 871 (1974).
- [28] E. Kovačević, J. Berndt, I. Stefanović, H-W. Becker, C. Godde, Th. Strunskus, J. Winter, L Boufendi, *J. Appl. Phys.* **105**, 104910 (2009).
- [29] J. Benedikt, *J. Phys. D: Appl. Phys.* **43**, 043001 (2010).
- [30] Ch. Hollenstein, W. Schwarzenbach, A.A. Howling, C. Courteille, J-L. Drier, L. Sansonnens, *J. Vac. Sci. Technol. A* **14**, 535 (1996).
- [31] C. Deschenaux, A. Affolter, D. Magni, C. Hollenstein, P. Fayet, *J. Phys. D: Appl. Phys.* **32**, 1876 (1999).
- [32] S. Stoykov, C. Eggs, U. Kortshagen, *J. Phys. D: Appl. Phys.* **34**, 2160 (2001).
- [33] I. Stefanović, E. Kovačević, J. Berndt, Y. Pendleton, J. Winter, *Plasma Phys. Control. Fusion* **47**, A179 (2005).
- [34] J. Winter, J. Berndt, S.H. Hong, E. Kovačević, I. Stefanović, O. Stepanović, *Plasma Sources Sci. Technol.* **18**, 034010 (2009).
- [35] J. Berndt, E. Kovačević, I. Stefanović, L. Boufendi, *J. Appl. Phys.* **106**, 063309 (2009).
- [36] J. Berndt, E. Kovačević, V. Selenin, I. Stefanović, J. Winter, *Plasma Sources Sci. Technol.* **15**, 18 (2006).
- [37] J. Berndt, S. Hong, E. Kovačević, I. Stefanović, J. Winter, *Vacuum* **71**, 377 (2003).

- 
- [38] J. Benedikt, A. Consoli, M. Schulze, A. von Keudell, *J. Phys. Chem. A* **111**, 10453 (2007).
- [39] K. De Bleecker, A. Bogaerts, W. Goedheer, *Phys. Rev. E* **73**, 026405 (2006).
- [40] K. De Bleecker, A. Bogaerts, W. Goedheer, *Appl. Phys. Lett.* **88**, 151501 (2006).
- [41] J. Röpcke, G. Lombardi, A. Rousseau, P.B. Davies, *Plasma Sources Sci. Technol.* **15**, S148 (2006).
- [42] J. Röpcke, L. Mechold, M. Käning, W.Y. Fan, P.B. Davies, *Plasma Chem. Plasma Process.* **19**, 395 (1999).
- [43] R.A.B. Zijlmans, O. Gabriel, S. Welzel, F. Hempel, J. Röpcke, R. Engeln, D.C. Schram, *Plasma Sources Sci. Technol.* **15**, 564 (2006).
- [44] J.H. van Helden, W. Wagemans, G. Yagci, R.A. Zijlmans, D.C. Schram, R. Engeln, G. Lombardi, G.D. Stancu, J. Röpcke, *J. Appl. Phys.* **101**, 043305 (2007).
- [45] R.F. Curl, F. Capasso, C. Gmachl, A.A. Kostorev, B. McManus, R. Lewicki, M. Pusharsky, G. Wysocki, F.K. Tittel, *Chem. Phys. Lett.* **487**, 1 (2010).
- [46] S. Welzel, F. Hempel, M. Hübner, N. Lang, P.B. Davies, J. Röpcke, *Sensors* **10**, 6861 (2010).
- [47] M. Hübner, S. Welzel, D. Marinov, O. Guaitella, S. Glitsch, A. Rousseau, J. Röpcke, *Rev. Sci. Instrum.* **82**, 093102 (2011).
- [48] M. Hundt, P. Sadler, I. Levchenko, M. Wolter, H. Kersten, K. Ostrikov, *J. Appl. Phys.* **109**, 123305 (2011).
- [49] J. Beckers, G.M.W. Kroesen, *Appl. Phys. Lett.* **99**, 181503 (2011).
- [50] S. Hong, J. Berndt, J. Winter, *Plasma Sources Sci. Technol.* **12**, 46 (2003).
- [51] J. Berndt, E. Kovačević, I. Stefanović, O. Stepanović, S.H. Hong, L. Boufendi, J. Winter, *Contrib. Plasma Phys.* **49**, 107 (2009).
- [52] I. Stefanović, Ch. Scharwitz, E. Kovačević, J. Berndt, J. Winter, *IEEE Trans. Plasma Sci.* **36**, 1018 (2008).
- [53] J.U. White, *J. Opt. Soc. Am.* **32**, 285 (1942).
- [54] L.S. Rothman, D. Jacquemart, A. Barbe, D.C. Benner, M. Birk, L.R. Brown, M.R. Carleer, C. Chackerian, K. Chance, L.H. Coudert, V. Dana, V.M. Devi,

- J.M. Flaud, R.R. Gamache, A. Goldman, J.M. Hartmann, K.W. Jucks, A.G. Maki, J.Y. Mandin, S.T. Massie, J. Orphal, A. Perrin, C.P. Rinsland, M.A.H. Smith, J. Tennyson, R.N. Tolchenov, R.A. Toth, J. Vander Auwera, P. Varanasi, G. Wagner, *J. Quant. Spectrosc. Radiat. Transfer* **96**, 139 (2005).
- [55] G.D. Stancu, J. Röpcke, P.B. Davies, *J. Chem. Phys.* **122**, 014306 (2005).
- [56] G.D. Stancu, A.V. Pipa, G. Lombardi, P.B. Davies, A. Gicquel, B.P. Lavrov, J. Röpcke, *Contrib. Plasma Phys.* **45**, 358 (2005).
- [57] I. Stefanović, N. Sadeghi, J. Winter, *J. Phys. D: Appl. Phys* **43**, 152003 (2010).
- [58] F. Hempel, P.B. Davies, D. Loffhagen, L. Mechold, J. Röpcke, *Plasma Sources Sci. Technol.* **12**, S98 (2003).
- [59] L. Mechold, J. Röpcke, X. Duten, A. Rousseau, *Plasma Sources Sci. Technol.* **10**, 52 (2001).



## 5 On surface relaxation of vibrationally excited nitrogen

A new method for the determination of the wall de-excitation probability  $\gamma_{N_2}$  of vibrationally excited  $N_2$  on different surfaces exposed to low-pressure plasmas has been developed. A short DC discharge pulse of only a few milliseconds was applied to a mixture containing 0.05 – 1% of  $CO_2$  in  $N_2$  at a pressure of 133 Pa. In these low pressure conditions the main quenching process of  $N_2(v)$  is heterogeneous relaxation. Due to a nearly resonant fast vibrational transfer between  $N_2(v)$  and the asymmetric  $v_3$  mode of  $CO_2$  the vibrational excitation of these titrating molecules is an image of the degree of vibrational excitation of  $N_2$ . In the afterglow, the vibrational relaxation of  $CO_2$  was monitored *in-situ* using quantum cascade laser absorption spectroscopy (QCLAS). The experimental results were interpreted in terms of a numerical model of non-equilibrium vibrational kinetics in  $CO_2$ - $N_2$  mixtures. Heterogeneous relaxation was the main quenching process of  $N_2(v)$  under the conditions of this study, which allowed determination of the value of  $\gamma_{N_2}$  from the best agreement between the experiment and the model. The new method is suitable for  $\gamma_{N_2}$  determination in a single plasma pulse with the discharge tube surface pretreated by a low-pressure plasma. The relaxation probability of the first vibrational level of nitrogen  $\gamma_I = (1.1 \pm 0.15) \times 10^{-3}$  found for Pyrex and silica is in reasonable agreement with the literature data. Using the new technique the  $N_2(v=1)$  quenching probability was measured on  $TiO_2$  surface,  $\gamma_I = (9 \pm 1) \times 10^{-3}$ . A linear enhancement of the  $N_2(v)$  wall deactivation probability with an increase in the admixture of  $CO_2$  was observed for all studied materials. In order to explain this effect, a vibrational energy transfer mechanism between  $N_2(v)$  and adsorbed  $CO_2$  is proposed [1].

## 5.1 Introduction

Vibrationally excited  $N_2$  plays an important role in plasma chemistry, gas lasers and atmospheric re-entry [2-12]. In nitrogen containing plasmas, vibrationally excited  $N_2(v)$  acts as an energy reservoir that affects electron kinetics, chemistry and thermodynamic properties of the plasma. In the case of gas discharges in nitrogen-containing mixtures, electron impact excitation of  $N_2$  vibrations often dominates the energy balance of the electrons [2, 7, 8].

The vibrational-translational/rotational (V-T/R) relaxation in  $N_2$  is very slow [4, 13-14]. Therefore, high degrees of vibrational excitation of  $N_2$  may be reached under typical discharge conditions. In bounded laboratory plasmas, relaxation on the reactor walls is the most efficient  $N_2(v)$  loss mechanism for pressures up to few tens of mbars [4]. Therefore, the knowledge of the heterogeneous deactivation probability of  $N_2$  is crucial for plasma modelling.

The number of experimental studies devoted to the determination of  $N_2(v)$  loss probabilities on different surfaces is rather limited [15-19]. The main difficulty in such experiments is the detection of vibrationally excited nitrogen that does not exhibit dipole allowed transitions in emission and has absorption features only in VUV. Therefore, calorimetric methods [15], spontaneous or coherent Raman scattering [16-18] or infrared titration with  $CO_2$  [19] were used in the past. Typically, all the experiments were carried out in a flowing discharge system and the concentration of  $N_2(v)$  was measured as a function of the distance in the post-discharge. The probability of vibrational quanta losses in collisions with the wall ( $\gamma_{N_2}$ ) was determined from the measured decay of  $N_2(v)$ . One of the shortcomings of the described techniques was the uncontrollable surface state under flowing post discharge exposure. Authors [16-18] pointed out drifts in measured values of  $\gamma_{N_2}$  with increasing exposure time.

The list of materials for which the  $N_2(v)$  quenching probability has been determined so far is relatively short. Modelling of  $N_2$ -containing plasmas for new applications such as material processing [9, 20] or plasma-catalyst technology [21] requires the knowledge of  $\gamma_{N_2}$  for a broad range of surfaces. Moreover, the problem of surface state modification by plasma exposure has to be adequately addressed. The development of a simple and reliable technique for *in-situ*  $\gamma_{N_2}$  determination was therefore the main motivation for this study.

In this work we use the idea of titrating vibrationally excited  $N_2$  by a small amount of an

infrared (IR) active molecule, CO<sub>2</sub> in our case, a method already proposed in [19]. Gas mixtures containing 0.05 – 1% of CO<sub>2</sub> in N<sub>2</sub> were excited by a pulsed DC discharge at a pressure of 133 Pa in a cylindrical discharge tube. Time resolved quantum cascade laser absorption spectroscopy (QCLAS) was used to follow the relaxation kinetics of CO<sub>2</sub> *in-situ*. Due to a very efficient vibrational coupling between nitrogen and carbon dioxide, the excitation of titrating molecules reflects the degree of vibrational excitation of N<sub>2</sub>. The experimental results were interpreted using a numerical model of vibrational kinetics in CO<sub>2</sub>–N<sub>2</sub> mixtures. This approach allowed the determination of  $\gamma_{N_2}$  from the best accord between the measurements and the simulations while using  $\gamma_{N_2}$  as the only tuning parameter of the model.

## 5.2 Experimental

### 5.2.1 Discharge setup

The schematic diagram of the experimental setup is shown in figure 5.1. The experiments were performed in a cylindrical reactor of 60 cm full length and of 2 cm inner diameter. The central 40 cm long interchangeable part of the discharge tube was made of fused silica, Pyrex or fused silica coated with a sol-gel TiO<sub>2</sub> film. The vacuum system was pumped using an oil-free scroll pump to a base pressure of 0.1 Pa. The typical gas pressure during the experiments was 133 Pa. The working gas was prepared by mixing of N<sub>2</sub> (99.9999% purity) with a pre-fabricated mixture containing 1% of CO<sub>2</sub> in N<sub>2</sub>. The typical CO<sub>2</sub> admixtures were in the range of 0.05 – 1%. After the filling, the discharge tube was shut off from the vacuum system using two pneumatic valves. Then single plasma pulse experiments were carried out under static conditions. After each discharge pulse the reactor was refilled with a new gas mixture.

A pulsed DC discharge was created by applying a high voltage to a pair of electrodes via a 60 k $\Omega$  ballast resistor ( $R_b$ ). The discharge voltage was measured with a HV probe (LeCroy PPE20kV). The discharge current was deduced from the voltage drop on an 18.4  $\Omega$  series resistor placed between the cathode and the ground. Both current and voltage signals were digitalized using an oscilloscope (LeCroy 44Xi, 400 MHz). A typical rise time of the discharge current was 20  $\mu$ s, the pulse duration was chosen to be in the range of 1 – 5 ms. The discharge current was set by adjusting the amplitude of the applied high voltage, all the

experiments were done with  $I = 50$  mA and  $U_{HV} = 4.6$  kV. The injected energy was about 0.3 J per pulse. Before a series of measurements was started the reactor was cleaned by flowing discharge in argon for 30 min at a pressure of 26 Pa.

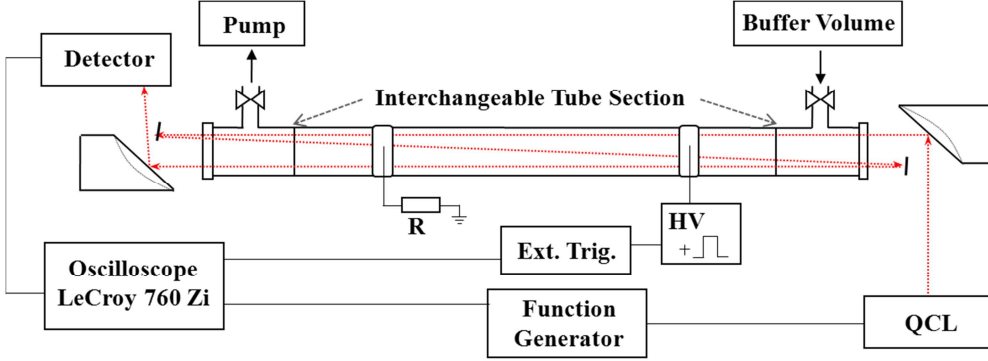


**Figure 5.1:**  
*Experimental setup [1].*

### 5.2.2 Quantum cascade laser diagnostics

The detection of  $\text{CO}_2$  was performed using a three-channel QCLAS spectrometer TRIPLE Q [22] dedicated to time-resolved *in-situ* gas sensing. In this study only one channel of the TRIPLE Q system was used. The QCL was operated in the *intra-pulse mode* with typical pulse lengths of the order of 100 – 200 ns [23-24]. The QCL (Alpes Lasers) was housed in a temperature-stabilized laser head and operated by a pulsed laser driver (Q-MACS Basic, neoplas control). The divergent laser radiation was collimated using an off-axis parabolic mirror. This beam was directed three times through the discharge tube and finally focused onto a fast detector (IRDM-600, neoplas control). The detector module contained a temperature controller, which was specifically adjusted to the detector element (VIGO, PDI-2TE-10/12) and pre-amplifier (bandwidth: 600 MHz, rise time: 2 ns).

A detailed description of the laser setup and spectroscopic data processing can be found elsewhere [22]. The detector signal was recorded by an oscilloscope (LeCroy 760Zi-A, 6 GHz, 40 GS/s) and then analyzed on a computer. In order to eliminate the absorption by atmospheric  $\text{CO}_2$ , the whole optical path was covered and purged by  $\text{N}_2$ . A single absorption spectrum of the species of interest can be acquired in a very short time of the order of 100 ns. The maximum duty cycle of the QCL used in this study was limited to 2% and therefore the maximum pulse repetition rate was 200 kHz, which set the limit of the time resolution. Typically, a train of 7600 successive spectra was recorded in the memory of the oscilloscope that corresponded to 40 – 400 ms of continuous acquisition.

### 5.2.3 Calibration of absorption measurements

An inherent property of the QCL absorption measurements in the intra-pulse mode at low pressures is the so-called rapid passage effect [26]. It consists in the distortion of the absorption features due to the non-linear effects in the interaction of the fast frequency chirped and highly intense laser radiation with the ensemble of absorbing molecules [25]. An example of a typical absorption spectrum of CO<sub>2</sub> is shown in figure 5.2. As pointed out in [27-28], due to the absorption line distortion, the direct application of the Beer-Lambert law for concentration determination is not possible and a calibration is required. The calibration was performed by introducing in the reactor a mixture containing known concentration of CO<sub>2</sub> diluted in N<sub>2</sub> in the reactor. In this study the CO<sub>2</sub> P28 transition of the (00<sup>0</sup>1←00<sup>0</sup>0) band at 2324.976 cm<sup>-1</sup> was used. The detection limit was found to be  $5 \times 10^{12}$  molecules cm<sup>-3</sup>.

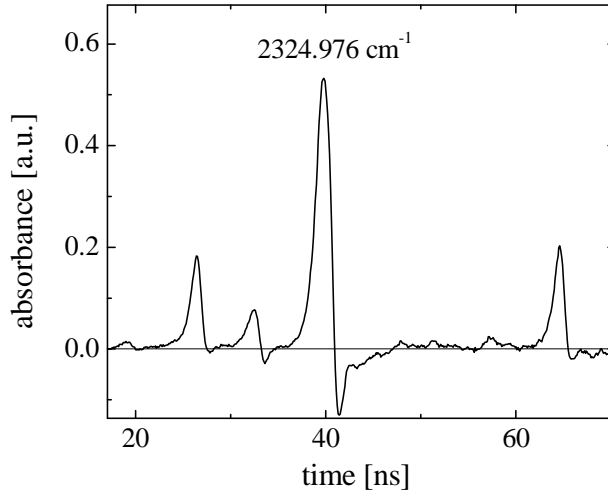


**Figure 5.2:** Absorption spectrum of CO<sub>2</sub>. Negative absorbance peaks are due to the rapid passage effect [1].

The integrated absorption coefficient can be written in the following form:

$$\int \ln \left( \frac{I_0}{I} \right) d\nu = \frac{h\nu_{ik}}{c} B_{ik} \left( n_i - \frac{g_i}{g_k} n_k \right) K \quad (5.1)$$

where integration is performed over a fraction of the distorted absorption line until the point where the logarithm turns zero as described in [22]. In (5.1)  $B_{ik}$  and  $\nu_{ik}$  are the Einstein coefficient and the frequency of the observed transition,  $n_i$  ( $n_k$ ),  $g_i$  ( $g_k$ ) are the population and the statistical weight of the lower or upper level, respectively,  $K$  is the calibration factor accounting for the line distortion. Taking into account the Boltzmann relation between  $n_i$  and  $n_k$  and the total density of molecules on the lower ( $[\text{CO}_2(00^0 0)] \equiv N_0$ ) and the upper ( $[\text{CO}_2(00^0 1)] \equiv N_1$ ) vibrational levels (5.1) can be expressed as follows:

$$\int \ln \left( \frac{I_0}{I} \right) dv = \frac{h\nu_{ik} B_{ik} e^{-\frac{E_i}{kT}}}{c Q_{rot}} \left( N_0 - \frac{g_i}{g_k} e^{\frac{E_i - E_k}{kT}} N_1 \right) K \quad (5.2)$$

where  $E_i$  and  $E_k$  correspond to the rotational energy of the lower and the upper levels respectively,  $Q_{rot}$  is the rotational partition function. Effectively (5.2) may be rewritten as

$$\int \ln \left( \frac{I_0}{I} \right) dv = \alpha (N_0 - \beta N_1) \quad (5.3)$$

where  $\alpha$  is found from the calibration and  $\beta = e^{(E_i - E_k)/kT}$  depends on the chosen transition. The value of  $\beta = 1.145$  at 296 K was found using the values of  $E_i$  and  $E_k$ , taken from the HITRAN database [29].

At room temperature the  $\text{CO}_2$   $v_2$  bending mode has a non-negligible population. This means that the total density of  $\text{CO}_2$  differs from the density of the molecules in the ground vibrational level  $N_0$ . This has been taken into account for the calibration of the integrated absorption coefficient against the value of  $(N_0 - \beta N_1)$ . The calibration curve is shown in figure 5.3.

When working under equilibrium conditions at moderate temperatures the contribution of the stimulated emission may be neglected ( $N_1 \sim 0$ ). However, in non-equilibrium plasmas high vibrational temperatures of  $T_v \sim 2000 - 6000$  K are usually reached [2-9] and the second term in equation (5.3) becomes significant.

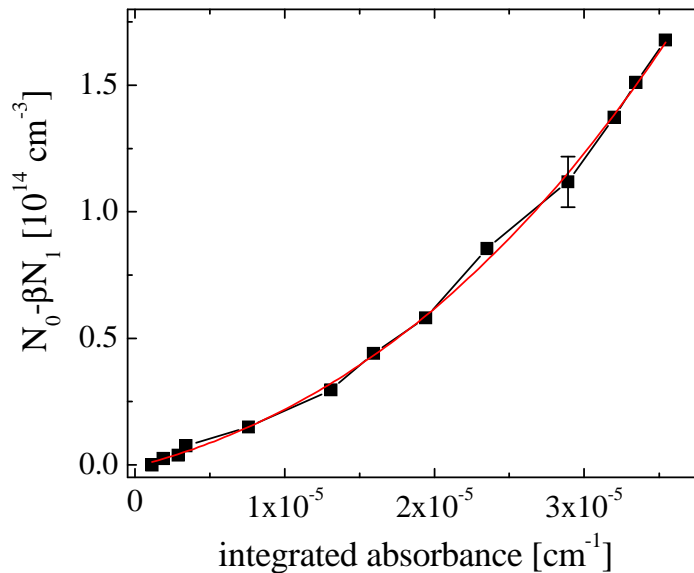


**Figure 5.3:** Calibration curve. Experimental points are fitted with a third-order polynomial [1].

## 5.3 Results: validation of the diagnostics method

### 5.3.1 Relaxation measurements in $\text{CO}_2 - \text{N}_2$

The reactor was filled with mixtures containing 0.066 – 0.5%  $\text{CO}_2$  in  $\text{N}_2$  at  $p = 133$  Pa and a discharge pulse of 5 ms length with a current of  $I = 50$  mA was applied. Figure 5.4 shows the time evolution of the value of  $(N_0 - \beta N_1)$  using the fused silica for the central part of the discharge tube. It should be noted that the acquisition is made in a *single pulse* mode without accumulation.

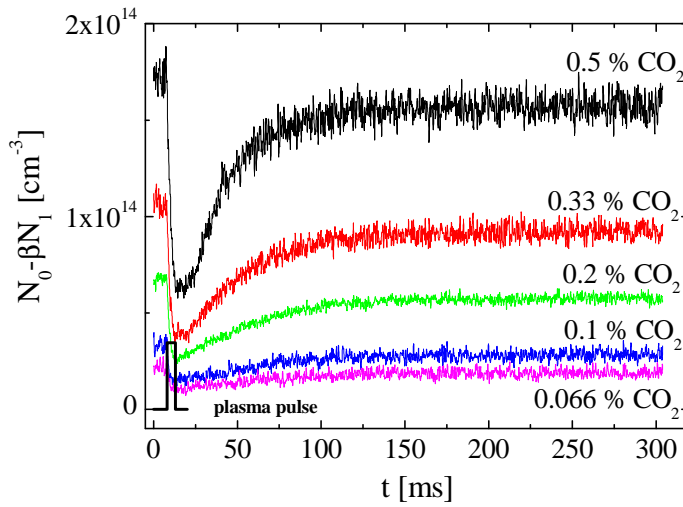


**Figure 5.4:**

*Time evolution of the value of  $(N_0 - \beta N_1)$  after a  $I = 50$  mA,  $\tau = 5$  ms pulse at 133 Pa. The central part of the discharge tube was made of fused silica. Different curves correspond to different initial concentrations of  $\text{CO}_2$  [1].*

The measured population difference undergoes a fast decrease during the discharge pulse followed by a relatively slow relaxation to the stationary level in the afterglow. The stationary level of the value of  $(N_0 - \beta N_1)$  after the pulse is about 15% lower than the initial value which can be explained by the dissociation of  $\text{CO}_2$  in the discharge. In further discussion we will show that the characteristic relaxation time decreases with increasing concentration of  $\text{CO}_2$ .

### 5.3.2 Relevant processes

The fast decrease of the measured value of  $(N_0 - \beta N_1)$  when the discharge pulse is applied may be explained by three principal processes:

1. Variation of the rotational distribution of  $\text{CO}_2$  due to gas heating.
2. Dissociation of  $\text{CO}_2$ .
3. Vibrational excitation of  $\text{CO}_2$ .

As it was shown in [27], an increase in the gas temperature in the discharge may significantly alter the transition line strength. This effect has to be considered for concentration measurements and may also be used for the gas temperature determination in some cases. In [30] we have measured the temporal variation of the gas temperature in the discharge active phase and in the afterglow using optical emission spectroscopy of the  $\text{N}_2^+ 2^+$  band at 337 nm. The plasma-induced fluorescence technique [31] was used in order to obtain emission spectra in the post discharge. The gas temperature was deduced from the fitting of experimental spectra using Specair software [32]. An increase of the gas temperature by  $\Delta T = 150$  K was found at the end of a 5 ms 50 mA pulse in 133 Pa  $\text{N}_2$ . In our case following the procedure described in [27] we have estimated a 30% decrease in the absorption coefficient of  $\text{CO}_2$  for the gas temperature  $T_g = 450$  K in the discharge active phase. This proves that gas heating may have a strong effect. However, in [30] it was shown that the gas temperature reaches the temperature of the wall in the post-discharge within 2-3 ms. The relaxation of the value of  $(N_0 - \beta N_1)$ , shown in figure 5.4, is much slower and hence it cannot be related to the thermal effects. One can note that the curves plotted in figure 5.4 exhibit no fast increase when the discharge is stopped as would be expected if the variation of gas temperature had a strong influence on the absorption measurements. This may be due to the three passage laser beam alignment which mostly probes the cold gas in the vicinity of the wall. Another factor contributing to the reduction of the temperature effect is the radial redistribution of gas density caused by the temperature gradient. At the tube axis the concentration of neutrals decreases and at the same time it increases in the cold zone near the wall. Anyhow, in the discussion below we are interested in the relaxation process that takes place on the timescale of several tens of milliseconds when the gas temperature is already in equilibrium with the reactor walls.

The dissociation of  $\text{CO}_2$  in the discharge with a subsequent recombination of produced CO and O at the reactor walls may also influence the kinetics of  $\text{CO}_2$  in the afterglow. However, surface association of oxygen atoms with carbon monoxide on silica surface,  $\text{O} + \text{CO}|_w$ , is known to be inefficient [33] compared to the recombination of oxygen atoms,  $\text{O} + \text{O}|_w$  [31]. Therefore, it is unlikely that after 60% depletion of the initial carbon dioxide in the discharge the dissociation products recombine back into  $\text{CO}_2$  with only 15% of  $\text{CO}_2$  being eventually lost.

A test experiment was done in order to confirm the low efficiency of the  $\text{O} + \text{CO}|_w$  recombination process under the conditions of this study. A single discharge pulse with a

length of 5 ms at a current of  $I = 50$  mA was applied in a mixture of  $\text{CO}/\text{Ar}/\text{O}_2 = 0.5/49.5/50$  at a pressure of 133 Pa under static conditions. The concentration of  $\text{CO}_2$  measured after the discharge pulse was about  $1 \times 10^{13}$  molecules  $\text{cm}^{-3}$ . A simple estimation shows that the density of atomic oxygen at the end of the pulse was in the order of  $10^{15}$   $\text{cm}^{-3}$ , the density of CO was  $1.5 \times 10^{14}$  molecules  $\text{cm}^{-3}$ . Thus, even with an excess of atomic oxygen recombination into  $\text{CO}_2$  does not exceed 10% of the initial CO concentration. It is evident that under the experimental conditions shown in figure 5.4, the density of CO and O available for recombination are approximately equal and they are always smaller than those in the experiment with the  $\text{CO}/\text{Ar}/\text{O}_2$  mixture. Hence we conclude that the surface re-association of CO and O has only a minor role under the conditions of this study. Therefore, 15% depletion of the  $\text{CO}_2$  concentration measured after the discharge pulse, shown in figure 5.4, is the real value of the degree of dissociation of  $\text{CO}_2$  in the discharge.

It is concluded that the vibrational excitation is the main process responsible for the observed relaxation kinetics of  $\text{CO}_2$  in the afterglow. As follows from the preceding discussion, starting after about 3 ms in the afterglow, the depletion of the value of  $(N_0 - \beta N_1)$  relative to the stationary late post-discharge level is determined exclusively by the redistribution of  $\text{CO}_2$  molecules over different vibrational levels.

## 5.4 Modelling of vibrational kinetics in $\text{N}_2$ - $\text{CO}_2$ mixtures: determination of $\gamma$

### 5.4.1 Relaxation processes in $\text{CO}_2 - \text{N}_2$

Let us consider the processes responsible for the relaxation kinetics shown in figure 5.4. During the 5 ms plasma ON phase vibrations of both  $\text{CO}_2$  and  $\text{N}_2$  are efficiently excited by electron impact [34]. In the afterglow, vibrational relaxation of the mixture takes place due to the exchange of vibrational energy between different modes of  $\text{CO}_2$  and  $\text{N}_2$  as well as the relaxation on the reactor walls.

It is known from a number of works [16, 35] that the deactivation probability of  $\text{CO}_2(01^10)$  and  $\text{CO}_2(00^01)$  on glass surfaces is found to be in the range of  $\gamma_{\text{CO}_2} \sim 0.18 - 0.4$ . To the best of our knowledge there are no data available for the  $\nu_1$  mode, but it would be reasonable to suggest that the deactivation probability of this mode is also relatively high.

Under our conditions for  $\gamma_{\text{CO}_2} \geq 0.1$ , the lifetime of the vibrationally excited  $\text{CO}_2$  is limited by the diffusion towards the wall and does not exceed 2 ms. Experimentally observed characteristic relaxation time was in the range of few tens of milliseconds. This proves that vibrational excitation of  $\text{CO}_2$  persists in the afterglow. As it is shown in [19, 36, 37], the excitation of  $\text{CO}_2$  in the post-discharge takes place in the V-V' exchange process (R1).

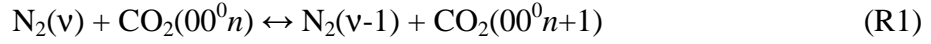
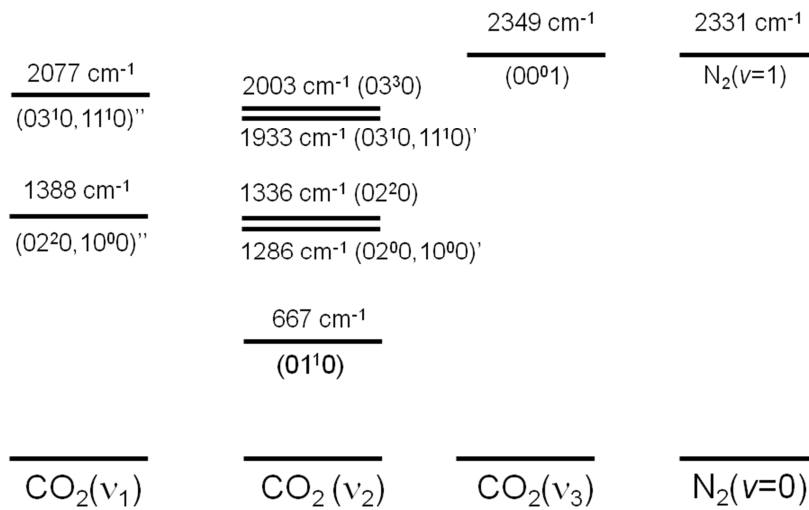


Figure 5.5 shows the diagram of the vibrational levels of  $\text{N}_2$  and  $\text{CO}_2$ , the vibrational state notation is taken from [38-39]. For the first excited levels,  $\text{N}_2(v=1)$  and  $\text{CO}_2(00^01)$ , process (R1) is almost resonant and as a consequence it is rather fast,  $k_{\text{R1}} = 7 \times 10^{-13} \text{ cm}^{-3} \text{ s}^{-1}$  at 300 K [39]. As is shown later, the high efficiency of (R1) leads to the equalization of the vibrational temperatures of  $\text{N}_2$  and the  $\text{CO}_2(00^0v_3)$ . Therefore, the excitation of  $\text{CO}_2$  is an image of the degree of the vibrational excitation of  $\text{N}_2$ .

It is known that in nitrogen the VT relaxation at room temperature is very slow, for  $\text{N}_2(v=1)$   $k_{\text{VT}} = 7 \times 10^{-22} \text{ cm}^{-3} \text{ s}^{-1}$  [13-14]. Thus, the relaxation of the low-lying vibrational levels is controlled by impurities and by quenching on the reactor walls [2-4]. Under the conditions of this study in pure  $\text{N}_2$ , surface relaxation is dominant due to the low level of impurities in the gas used. According to [41] VT quenching by atomic nitrogen may be an important source of  $\text{N}_2(v)$  relaxation. However, under our conditions at room temperature and with the typical degree of dissociation of 1% [2], the VT relaxation by N atoms is negligible. Relaxation caused by  $\text{CO}_2$  becomes increasingly important upon the addition of  $\text{CO}_2$ .



**Figure 5.5.** Diagram of the vibrational levels of  $\text{N}_2$  and  $\text{CO}_2$  [1].

### 5.4.2 Model description

In order to interpret the observed relaxation kinetics and to get an insight into the vibrational deactivation on the surface, a vibrational kinetics model of the N<sub>2</sub>-CO<sub>2</sub> system was developed. The model is zero dimensional and it incorporates excitation of vibrations by electronic impact (e-V), V-V and V-T exchange in the N<sub>2</sub> subsystem as well as the V-V' exchange (reaction (R1)) between N<sub>2</sub> and CO<sub>2</sub> and intramolecular vibrational relaxation in CO<sub>2</sub>. Relaxation in collision between two CO<sub>2</sub> molecules was neglected due to the low concentration of admixed CO<sub>2</sub>. Electron impact excitation of CO<sub>2</sub> was also ignored because we are interested only in the afterglow phase where CO<sub>2</sub> is excited in collisions with N<sub>2</sub>(v). The system of kinetic equations can be written in a symbolic form:

$$\frac{dN_2(i)}{dt} = \left(\frac{dN_2(i)}{dt}\right)_{e-V} + \left(\frac{dN_2(i)}{dt}\right)_{VV}^{N_2-N_2} + \left(\frac{dN_2(i)}{dt}\right)_{VT} + \left(\frac{dN_2(i)}{dt}\right)_{R1}^{N_2-CO_2} + \left(\frac{dN_2(i)}{dt}\right)_W \quad (5.4)$$

$$\frac{dCO_2(k)}{dt} = \left(\frac{dCO_2(k)}{dt}\right)_{R1}^{CO_2-N_2} + \left(\frac{dCO_2(k)}{dt}\right)_{VT} + \left(\frac{dCO_2(k)}{dt}\right)_{intra}^{CO_2-N_2} + \left(\frac{dCO_2(k)}{dt}\right)_W + \left(\frac{dCO_2(k)}{dt}\right)_{RD} \quad (5.5)$$

where W accounts for the wall losses, RD is the spontaneous radiative decay term.

The system of equations was solved for 40 vibrational levels of N<sub>2</sub> and 6 levels of CO<sub>2</sub> ((00<sup>0</sup>0), (00<sup>0</sup>1), (00<sup>0</sup>2), (01<sup>1</sup>0), [(02<sup>0</sup>0,10<sup>0</sup>0)',(02<sup>0</sup>0,10<sup>0</sup>0)",(02<sup>2</sup>0)], [(03<sup>1</sup>0,11<sup>1</sup>0)',(03<sup>1</sup>0,11<sup>1</sup>0)",(03<sup>3</sup>0)]). The groups of three levels in square brackets have close energies and are affected by the Fermi resonance. Therefore, they were treated as a single effective level [37-38] (100)<sub>eff</sub> and (110)<sub>eff</sub> respectively.

The e-V rates were found from the solution of Boltzmann equation using the EEDF solver developed by Dyatko *et al* [42] taking into account superelastic collisions between electrons and vibrationally excited N<sub>2</sub> molecules. The average electron density was calculated based on the discharge current and the electron drift velocity obtained from the Boltzmann equation solution. The electron density was assumed to be constant during the pulse in accordance with the experimentally measured current waveforms. The value of the reduced electric field in pure N<sub>2</sub> was taken from [2, 43]  $E/N= 80$  Td and it was assumed to be constant during the pulse as it was done by Pintassilgo *et al* [44] under similar conditions in N<sub>2</sub>/O<sub>2</sub>

pulsed DC discharge. Upon the addition of CO<sub>2</sub>, the sustaining discharge voltage was gradually increased, 10% rise compared with pure N<sub>2</sub> was measured for 0.5% CO<sub>2</sub> in N<sub>2</sub>. We neglected the influence of CO<sub>2</sub> addition on the cathode fall voltage. The increase of the  $E/N$  proportional to the discharge voltage was assumed taking into account a correction for the literature value 210 V of the cathode fall [45]. It is worth noting that e-V rates are not very sensitive functions of  $E/N$  because of the low-energy threshold of vibrational excitation. Typically, a variation of  $E/N$  from 70 to 90 Td leads to less than 20% increase in the electron excitation rate of the first vibrational level of N<sub>2</sub>.

We used the most recent set of V-V and V-T rates in N<sub>2</sub> calculated in [13-14] using a semiclassical trajectory method. Only single-quantum transitions were taken into account. The rates of the V-V' exchange between N<sub>2</sub> and CO<sub>2</sub> as well as V-T and intramolecular relaxation rates in CO<sub>2</sub> were taken from [36-40]. The exchange reaction (R1) was considered for 40 levels of N<sub>2</sub> and 3 levels of CO<sub>2</sub>(00<sup>0</sup>v<sub>3</sub>). The dependence of the rate of (R1) on the vibrational quantum number of N<sub>2</sub> and CO<sub>2</sub> is not known. In this study it was assumed to follow the analytical expressions of the Schwartz, Slawsky and Hertzfeld (SSH) theory [4]. The Einstein coefficients for spontaneous emission in CO<sub>2</sub> were taken from [37].

Surface relaxation was introduced as an effective volume process with the frequency that can be written as [43]:

$$\nu_w = \left( \frac{\Lambda^2}{D} + \frac{2r}{\gamma v_{th}} \right)^{-1} \quad (5.6)$$

where  $\Lambda = (r/2.4)$  is the characteristic diffusion length,  $r$  is the tube radius,  $D$  is the diffusion coefficient,  $v_{th}$  is the average thermal velocity of the molecules and  $\gamma$  is the probability of surface deactivation.

It was assumed that  $\gamma_{CO_2} = 0.2$  for all the vibrational levels of CO<sub>2</sub> [16, 35] and a complete accommodation of vibrational energy was supposed.

The *only* tuning parameter of the model was therefore the probability of the vibrational deactivation of N<sub>2</sub> on the surface ( $\gamma_{N_2}$ ). At present, there is no clear understanding of the dependence of  $\gamma_{N_2}$  on the vibrational quantum number  $v$ . Usually, a single quantum quenching is assumed with  $\gamma_{N_2}$  being either constant for all the vibrational levels or linearly proportional to  $v$ . As it was discussed in the most recent study, which employed CARS measurements of N<sub>2</sub>( $v$ ) with  $v = 0 - 5$  [17-18], even the direct measurement of individual vibrational levels does

not allow an unambiguous determination of the  $\gamma_{N_2}$  variation with  $v$ . The main reason for this is the fast V-V exchange in the gas phase that establishes a Treanor vibrational distribution function on the lower vibrational levels [4]. As a result, the relaxation of the system as a whole takes place with the individual rates significantly masked. Determination of the  $\gamma_{N_2}$  dependence on  $v$  is beyond the limits of the technique developed in this study. In accordance with [17-18], below we assume that  $\gamma_{N_2}$  is proportional to  $v$ ,  $\gamma_{N_2}(v) = \gamma_I \cdot v$  where  $\gamma_I$  is the quenching probability of  $N_2(v=1)$ . It is worth noting that such a dependence on  $v$  is more physical than the constant  $\gamma$  hypothesis. In the harmonic oscillator approximation, linear increase with the vibrational quantum number describes not only the scaling of the transition dipole momentum but it is also valid for the gas phase V-T and V-V exchange rates.

### 5.4.3 Modelling results

Figures 5.6 and 5.7 show the typical output of the model. In figure 5.6 the vibrational distribution function (VDF) of  $N_2$  in the ground state is shown for different delays after the ignition of the discharge pulse. For times interior to 1 ms the VDF is governed by the electron impact excitation which is efficient for  $v=1-9$  and the VDFs reflect the excitation pattern. With increasing degree of excitation, the V-V exchange tends to establish a Treanor distribution on the lower vibrational levels. The population of the higher vibrational levels takes place due to the ladder-like V-V exchange and it is delayed compared with the evolution of the VDF on the low-lying levels. In the post-discharge (delays longer than 5 ms), the relaxation of the VDF is determined by the losses of vibrational energy on the reactor walls and in collisions with  $CO_2$ . The formation of a plateau-like VDF on the intermediate vibrational levels is well known in  $N_2$  [2, 4, 46] and it originates from the interplay between resonant and non-resonant processes of the V-V exchange.

Figure 5.7 depicts the time evolution of the  $CO_2$  vibrational levels population. During the 5 ms discharge pulse, one can see a depletion of the  $CO_2(00^0 0)$  concentration and appearance of the molecules in the excited states due to the vibrational transfer from  $N_2(v)$ . In the afterglow, the vibrational distribution of  $CO_2$  relaxes to thermal equilibrium following the relaxation of the VDF of  $N_2(v)$ . The analysis of the results of the simulation shows that  $N_2(v)$  and  $CO_2(00^0 v_3)$  are strongly coupled because the V-V' exchange between  $N_2$  and  $CO_2$  in reaction (R1) is much faster than the quenching of  $CO_2(00^0 v_3)$ . It was found that the

vibrational temperatures of  $N_2$  and  $CO_2(00^0v_3)$  are very close and they obey the well-known analytical relation [4]:

$$\frac{E_1^{CO_2}}{T_1^{CO_2}} - \frac{E_1^{N_2}}{T_1^{N_2}} = \frac{E_1^{CO_2} - E_1^{N_2}}{T_{gas}} \quad (5.7)$$

where  $T_1^{CO_2}$  ( $T_1^{N_2}$ ) and  $E_1^{CO_2}$  ( $E_1^{N_2}$ ) correspond to the effective temperature and the energy of the first vibrational level of  $CO_2$  ( $N_2$ ),  $T_{gas}$  is the gas temperature.

Vibrational modes other than  $CO_2(00^0v_3)$  are weakly populated and do not contribute to the depletion of the value of  $(N_0 - \beta N_1)$ . The overpopulation of  $CO_2(kl^m0)$  after the discharge pulse compared with the 296 K level does not exceed 5% of the total  $CO_2$  concentration. The low population of  $CO_2$  modes, which are not directly coupled to  $N_2(v)$ , can be explained by a relatively slow intramolecular exchange in  $CO_2$  compared with the surface losses and spontaneous emission. For example, at a pressure of 133 Pa the total quenching frequency of  $CO_2(00^01) \rightarrow CO_2(kl^m0)$  by  $N_2$  is  $\nu_{intra} \sim 130 \text{ s}^{-1}$  while the contribution of the emission and surface losses is  $\nu_{W+RD} \sim 1030 \text{ s}^{-1}$ .

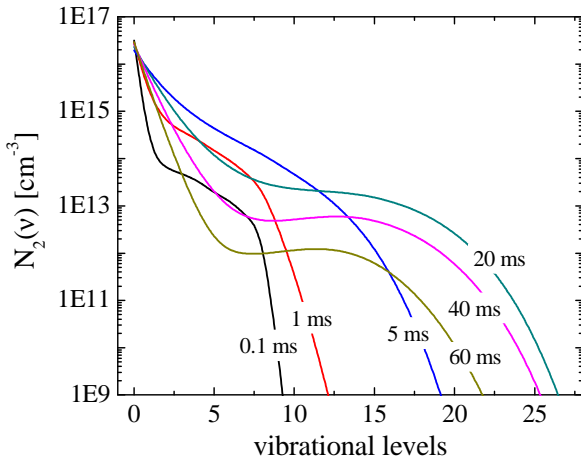


**Figure 5.6:** Calculated time evolution of the  $N_2$  vibrational distribution function in a single discharge pulse with  $\tau = 5 \text{ ms}$ ,  $I = 50 \text{ mA}$  and  $p = 133 \text{ Pa}$  in a 0.2%  $CO_2$ - $N_2$  gas mixture. The beginning of the discharge pulse corresponds to  $t = 0$  [1].

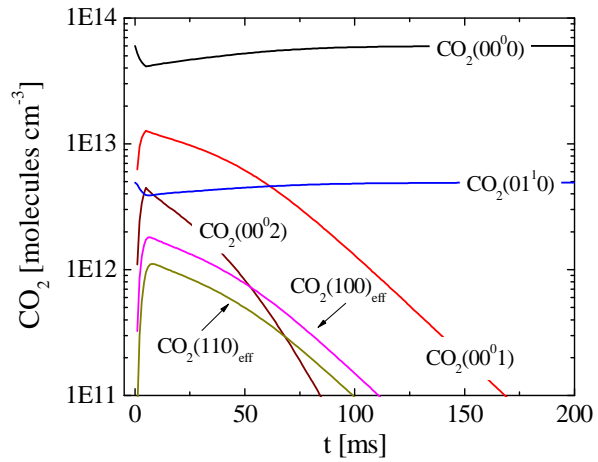


**Figure 5.7:** Time evolution of the population of the vibrational levels of  $CO_2$ . Discharge conditions are the same as in figure 5.6 [1].

To simplify the comparison between measurements and simulation, experimental curves depicted in figure 5.4 as well as the results of calculation were normalized for the final stationary value of  $(N_0 - \beta N_1)$ . The value of  $\gamma_1$  in the simulations was varied until the best fit was achieved. Normalized experimental and simulated curves for 0.2%  $CO_2$  are shown

in figure 5.8. The best agreement between the experiment and the simulations was obtained with  $\gamma_I = 1.6 \times 10^{-3}$ . The calculated curves with  $\gamma_I = 1.4 \times 10^{-3}$  and  $1.8 \times 10^{-3}$  illustrate the sensitivity of the model to the  $\gamma_I$  variation and allow one to estimate the relative error of the determination of  $\gamma_I$  within  $\pm 15\%$ . It is worth noting that the variation of  $\gamma_{N_2}$  affects primarily the relaxation time in the post discharge. The absolute value of  $(N_0 - \beta N_1)$  just after the discharge is independent of  $\gamma_{N_2}$  as long as the pulse duration is much shorter than the characteristic relaxation time.

One can note that the magnitude of the measured relaxation signals is well reproduced in the simulation. Depletion of the value of  $(N_0 - \beta N_1)$  is determined by the degree of vibrational excitation of  $N_2$  after the discharge and therefore we can conclude that the electron impact excitation of  $N_2$  is correctly treated in the model.

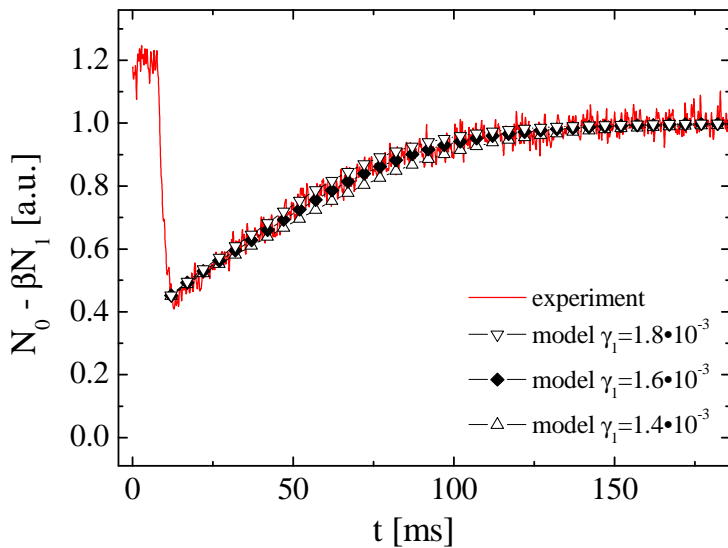


**Figure 5.8:** Normalized experimental relaxation curve with 0.2% of  $CO_2$  (—). Quartz discharge tube. Results of calculations with  $\gamma_I = 1.4 \times 10^{-3}$  (— $\nabla$ —),  $\gamma_I = 1.6 \times 10^{-3}$  (— $\blacklozenge$ —),  $\gamma_I = 1.8 \times 10^{-3}$  (— $\triangle$ —).  $\gamma_{N_2}$  is supposed to increase linearly with the vibrational quantum number  $\gamma_{N_2}(v) = \gamma_I \cdot v$  [1].

Calculations with different concentrations of added  $CO_2$  were performed for the conditions shown in figure 5.4. The agreement between the experimental results and the model was achieved by varying the value of  $\gamma_I$  for every given  $CO_2$  concentration. It was found that the best fit value of  $\gamma_I$  increases systematically with increasing  $CO_2$  concentration. Figure 5.9 shows the obtained dependence; an increase of  $\gamma_I$  by a factor of 2 over the studied range of the  $CO_2$  concentration can be seen.

From the calculation viewpoint the increase in the best fit value of  $\gamma_I$  as a function of the  $CO_2$  concentration signifies that the gas phase processes of  $N_2(v)$  quenching by  $CO_2$  that were taken into account in the model are not sufficient to reproduce experimentally observed relaxation kinetics. In the model we have included all the known gas phase processes of  $N_2(v)$

quenching by  $\text{CO}_2$ . Therefore, we believe that the obtained increase in the surface quenching probability of  $\text{N}_2(v)$  upon the addition of  $\text{CO}_2$  is a real physical effect and it is not related to the incompleteness of the model.

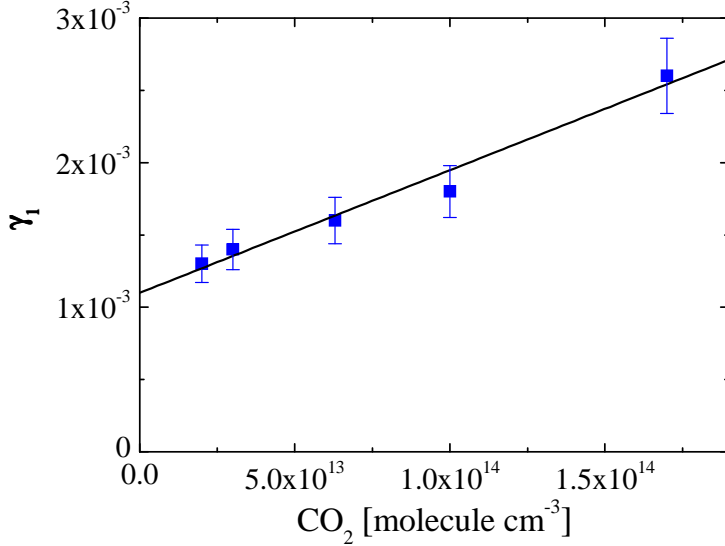


**Figure 5.9:** Wall deactivation probability of  $\text{N}_2(v=1)$  as a function of the added  $\text{CO}_2$  concentration (—■—). Linear fit with (—) –  $\gamma_1 = 0.0011 + 8 \times 10^{-18} \times [\text{CO}_2]$  [1].

To support this statement let us consider the most important mechanisms of  $\text{N}_2(v)$  vibrational relaxation in the presence of  $\text{CO}_2$ . According to [38-39] V-T quenching of  $\text{N}_2(v)$  by  $\text{CO}_2$  is very inefficient ( $k_{VT} = 1 \times 10^{-22} \text{ cm}^3 \text{ s}^{-1}$ ). The effective mechanism of  $\text{N}_2$  vibrational quanta losses in  $\text{N}_2\text{-CO}_2$  mixture proceeds via the fast transfer  $\text{N}_2(v) \leftrightarrow \text{CO}_2(00^0n)$  followed by the quenching of  $\text{CO}_2(00^0n)$ . Therefore, the “leakage” of  $\text{N}_2$  vibrational quanta is proportional to the  $\text{CO}_2$  concentration. Taking into account that  $\text{CO}_2(00^0n)$  is nearly in equilibrium with  $\text{N}_2(v)$  the characteristic frequency of  $\text{N}_2$  quanta losses in such two-step process can be written as follows:

$$\varphi = [\text{CO}_2] \frac{v_{\text{intra+W+RD}}}{[\text{N}_2]} \quad (5.8)$$

where  $v_{\text{intra+W+RD}}$  is the quenching frequency of  $\text{CO}_2(00^0n)$ ,  $[\text{N}_2]$  and  $[\text{CO}_2]$  is the concentration of  $\text{N}_2$  and  $\text{CO}_2$  respectively. Calculation using (5.8) for  $\text{CO}_2$  concentration ranging between  $2 \times 10^{13} - 2 \times 10^{14} \text{ molecules cm}^{-3}$  yields  $\varphi = 0.8 - 8 \text{ s}^{-1}$ . At the same time the characteristic frequency of the surface relaxation of  $\text{N}_2(v=1)$  calculated using (5.6) with the  $\gamma_1$  values from figure 5.9 is found in the range  $25 - 60 \text{ s}^{-1}$ . Therefore, the relaxation induced by the presence of  $\text{CO}_2$  in the gas phase is far too slow to explain the experimental results from figure 5.4. Using model calculations we have found that in order to reproduce experimentally observed time evolution of  $(N_0 - \beta N_1)$  with a fixed value of  $\gamma_1$ , the total quenching frequency of  $\text{CO}_2(00^0n)$  has to be increased by a factor of 10. In the previous

sections it was shown that the quenching of  $\text{CO}_2(00^0n)$  is dominated by the diffusion limited surface vibrational deactivation and spontaneous emission. Therefore, the value of  $v_{\text{intra+W+RD}}$  is known with a sufficient accuracy and its underestimation by a factor of 10 is very unlikely. Hence, we conclude that the strong increase of the  $\text{N}_2(v)$  relaxation frequency with increasing  $\text{CO}_2$  concentration is likely due to a modification of the surface state.

The physical mechanism of the  $\text{CO}_2$  induced enhancement of  $\gamma_l$  may consist in the transfer of the vibrational energy between the gas phase  $\text{N}_2(v)$  and  $\text{CO}_2$  molecules adsorbed on the quartz surface. In [47] similar mechanism was proposed to explain the experimentally measured surface relaxation rates in pure  $\text{CO}_2$ .

In figure 5.9 the data points are approximated by a linear function  $\gamma_l = 0.0011 + 8 \times 10^{-18} \times [\text{CO}_2]$  where  $[\text{CO}_2]$  is the concentration of carbon dioxide in molecules  $\text{cm}^{-3}$ . The intercept value  $\gamma_1^0 = (1.1 \pm 0.15) \times 10^{-3}$  can be considered as the wall deactivation probability of  $\text{N}_2(v=1)$  on fused silica in pure nitrogen. It is worth noting that in contrast to  $\gamma_l$  values shown in figure 5.9, the value of  $\gamma_1^0$  does not depend on the rates of  $\text{CO}_2$  relaxation that were used in the model.

Similar experiments were performed with a Pyrex discharge tube and the deactivation probability was found  $\gamma_1^0 = (1.1 \pm 0.15) \times 10^{-3}$  on Pyrex surface. The published data for Pyrex and fused silica are found in the range  $(0.2 - 1) \times 10^{-3}$  [15-19] depending on the surface pretreatment history. Any comparison between different experimental data is not straightforward due to the differences in the surface preparation; surface roughness may also vary depending on the specific materials' supplier and it is almost never specified. Therefore, we consider the agreement between the results of this work and the available literature data to be generally good.

It is worth mentioning that the obtained value of  $\gamma_l$  depends on the assumption made regarding the vibrational quantum number dependence of  $\gamma_{N_2}$ . As was mentioned above, the  $\gamma_{N_2} = \gamma_l - v$  hypothesis is justified by the similarity with the gas phase quenching processes of harmonic oscillators. Nevertheless, other dependences cannot be excluded. For example, assuming  $\gamma_{N_2}$  to be constant for all the vibrational levels of  $\text{N}_2$ , we obtain the best fit value of  $\gamma_1^0 = (1.5 \pm 0.2) \times 10^{-3}$  for silica and Pyrex. Therefore, the choice of the vibrational level dependence of  $\gamma_{N_2}$  may introduce an additional systematic error of  $\gamma_l$  determination. One should note that the dependence of  $\gamma_{N_2}$  on  $v$  is an unknown input parameter of any vibrational

kinetic model of  $N_2$ . We believe that in the models that use the values of  $\gamma_I$  found in this work, the effect of the systematic error of  $\gamma_I$  determination may be significantly reduced if the same ( $\gamma_{N_2} = \gamma_I - \nu$ ) hypothesis is used.

## 5.5 Application of $CO_2$ titration as a diagnostics tool

### 5.5.1 Relaxation of $N_2(\nu)$ on catalytic surfaces

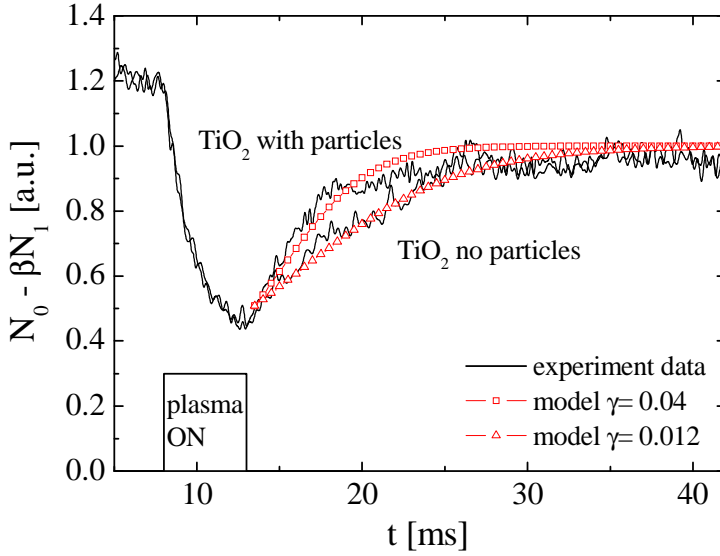
The procedure described in the previous sections can be used to investigate the processes of vibrational excitation and de-excitation of  $N_2$  in pulsed DC discharge. The information on the de-excitation mechanisms is obtained from the time evolution of the relaxation signals similar to those shown in figure 5.4. Using this technique the measurements of the relaxation kinetics at the inner surface of the discharge tube covered with  $TiO_2$  sol-gel film with or without impregnated  $TiO_2$  Degussa P25 particles were performed. Introduction of the particles in the film produced a very rough surface while the film without particles was smooth. Titanium dioxide is a promising material for plasma-catalyst technology for air pollution control [21]. However, there are no data available on the probability of  $N_2(\nu)$  quenching on its surface.

Figure 5.10 shows the evolution of the normalized value of  $(N_0 - \beta N_1)$  after a discharge pulse of 5 ms length at a current of  $I = 50$  mA in a  $N_2 + 0.3\%$   $CO_2$  gas mixture at a pressure of 133 Pa. One can note that with  $TiO_2$  relaxation is much faster than in the case of Pyrex and silica. As a consequence, the experimental data shown in figure 5.10 are more distorted by the noise due to a smaller number of data points over the relaxation time.

The characteristic relaxation time was found to be  $\tau = 5.5$  ms for no particle  $TiO_2$  film and  $\tau = 2.5$  ms for the film with impregnated particles. The best fit by the model was found as described in the previous sections with  $\gamma_I = 0.012$  and  $\gamma_I = 0.04$  for smooth and rough surfaces, respectively. Faster relaxation on the impregnated film may be caused by the increase in the surface area due to the presence of  $TiO_2$  particles. In addition to this geometric effect,  $TiO_2$  particles may possess an enhanced efficiency for quenching of  $N_2(\nu)$  due to the presence of different active sites compared with the sol-gel film.

By varying the amount of added  $CO_2$  the effect of  $CO_2$  concentration on the relaxation frequency was estimated. Extrapolation towards  $[CO_2] = 0$  gave  $\gamma_I = (9 \pm 2) \times 10^{-3}$  for  $TiO_2$

sol-gel film without particles. For varying concentrations of  $\text{CO}_2$  no measurable effect was observed with the impregnated surface. One should note that under our conditions the characteristic diffusion time is about 1 ms. Therefore, surface relaxation on the  $\text{TiO}_2$  film with particles is largely limited by the diffusion of vibrationally excited molecules towards the walls. In the diffusion-limited regime the relaxation frequency is almost independent on  $\gamma$  and hence the found  $\gamma = 0.04$  can be considered as the lower limit.



**Figure 5.10:**

*Time evolution of the normalized value of  $(N_0 - \beta N_1)$  after an  $I = 50 \text{ mA}$ ,  $\tau = 5 \text{ ms}$  pulse at  $P = 133 \text{ Pa}$  in a  $0.3\% \text{ CO}_2$  in  $\text{N}_2$  gas mixture. Experimental results are compared to the predictions of the model for a smooth  $\text{TiO}_2$  surface ( $-\triangle-$ ) and  $\text{TiO}_2$  film with impregnated P25 particles ( $-\square-$ ) [1].*

### 5.5.2 Kinetics of vibrational excitation of $\text{N}_2$ in pulsed DC discharge

As has been shown in the previous sections the depletion of the  $\text{CO}_2$  absorbance in the afterglow is determined by the vibrational excitation of  $\text{CO}_2$ . Modelling shows that only the  $\text{CO}_2(00^0v_3)$  mode has a significant non-equilibrium population. Thus, the amplitude of the measured depletion of the value of  $(N_0 - \beta N_1)$  can be related to the vibrational temperature of this mode:

$$T_v^{v_3} = \frac{E_1}{\ln\left(\frac{N_0}{N_1}\right)} \quad (5.9)$$

where  $E_1 = 3378 \text{ K}$  is the energy of  $\text{CO}_2(00^01)$ . In the case of non-Boltzmann  $v_3$  vibrational distribution,  $T_v$  defined by (5.9) is what is usually called the “effective vibrational temperature of the first level” of the mode. Assuming a Boltzmann distribution of  $\text{CO}_2(00^0v_3)$ , a normalized value of  $(N_0 - \beta N_1)$  can be rewritten as follows:

$$N_0 - \beta N_1 = (1 - \theta) - \beta(1 - \theta)\theta [\text{CO}_2] \quad (5.10)$$

where  $\theta = e^{-\frac{E_1}{T_v}}$  and  $[\text{CO}_2]$  is the total carbon dioxide concentration. One should note that the departure of the real vibrational distributions from the Boltzmann ones has only a minor influence on the determination of the effective vibrational temperature of the first level. The reason for this is a low population of the higher vibrational levels for which the difference with Boltzmann distribution is significant. The vibrational temperature of  $\text{CO}_2(00^0v_3)$ , which is related to the vibrational temperature of  $\text{N}_2$  by equation (5.7), can be calculated by solving (5.10) at any time point. The measurements are free from the distortion by the variation of the gas temperature starting from the  $\sim 3$  ms in the post discharge.

In figure 5.11 the evolution of the vibrational temperature of  $\text{N}_2$  calculated using (5.7), (5.9) and (5.10) in a mixture containing 0.2%  $\text{CO}_2$  in  $\text{N}_2$  at 133 Pa in a Pyrex discharge tube is shown. The discharge current was 50 mA, pulse durations were 1 ms and 5 ms. Good (within 10%) agreement between the model and the experiment proves the feasibility of the proposed method for vibrational temperature determination in  $\text{N}_2$ - $\text{CO}_2$  mixtures. The minimum measurable vibrational temperature is limited by the noise of the  $(N_0 - \beta N_1)$  signals when they reach the steady state. One can see that for the values of the vibrational temperature lower than 800 K the signals become buried in the noise.

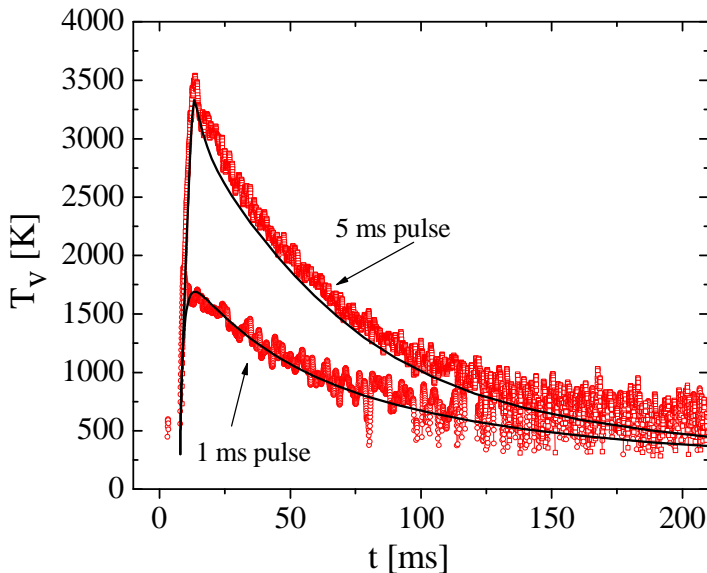


**Figure 5.11:**

*Evolution of the vibrational temperature of  $\text{N}_2$  in the afterglow of a discharge pulse with  $I = 50$  mA in a 0.2%  $\text{CO}_2$ - $\text{N}_2$  gas mixture at  $p = 133$  Pa. Pyrex discharge tube. Pulse durations were 1 ms ( $\text{---}\circ\text{---}$ ) and 5 ms ( $\text{---}\square\text{---}$ ). Simulation results are shown by solid lines [1].*

As was shown previously, the addition of  $\text{CO}_2$  increases the rate of  $\text{N}_2(v)$  relaxation in the post-discharge. However, according to the model calculations, it changes the value of  $T_1^{\text{N}_2}$  only slightly just after the end of the discharge pulse. Application of the described procedure to the experimental data from figure 5.4 resulted in similar values of  $T_1^{\text{N}_2}$  lying within 10%

scatter a few milliseconds after the discharge pulse. This proves that the value of  $T_1^{N_2}$  obtained using the titration technique with the  $\text{CO}_2$  admixture in the range 0.05–0.5% may be considered as a good approximation for the vibrational temperature in a pure  $\text{N}_2$  discharge.

One should note that both  $T_v$  and  $\gamma_{N_2}$  are determined in a single pulse experiment. This excludes uncontrollable drifts of the surface state due to long plasma exposure and allows measurements with specially pretreated surfaces.

## 5.6 Summary and conclusions

In this work investigation of vibrational kinetics in  $\text{CO}_2\text{-N}_2$  gas mixtures excited by pulsed DC discharge has been performed by means of time resolved QCLAS and numerical simulations. Due to a very efficient V-V' coupling between the  $\text{CO}_2(00^0v_3)$  and  $\text{N}_2(v)$ , carbon dioxide can be used as an IR active probe of vibrationally excited nitrogen. The effective relaxation frequency and the degree of vibrational excitation of  $\text{N}_2$  were determined from the time-resolved absorption measurements of  $\text{CO}_2$ . In the low-pressure conditions of this study, wall deactivation was the main loss mechanism of vibrationally excited  $\text{N}_2$ . The deactivation probability  $\gamma_{N_2}$  was found from the best agreement between the measured and simulated relaxation kinetics of  $\text{CO}_2$ . In the model it was assumed that  $\gamma_{N_2}$  for different vibrational levels of  $\text{N}_2$  is proportional to the vibrational quantum number  $\gamma_{N_2}(v) = \gamma_l - v$ . It was found that on Pyrex and fused silica surfaces  $\gamma_l = (1.1 \pm 0.15) \times 10^{-3}$ . The quenching probability on the  $\text{TiO}_2$  surface was measured to be  $\gamma_l = (9 \pm 2) \times 10^{-3}$  and  $\gamma_l \geq 4 \times 10^{-2}$  for smooth films and sol-gel films impregnated with  $\text{TiO}_2$  particles, respectively. It was found that in the 0.05 – 1%  $\text{CO}_2\text{-N}_2$  gas mixtures excited by a pulsed DC discharge, the surface deactivation probability of  $\text{N}_2(v)$  is proportional to the partial pressure of  $\text{CO}_2$ . This was interpreted as a proof of the vibrational energy transfer between the excited gas phase nitrogen molecules and adsorbed  $\text{CO}_2$  molecules. Carbon dioxide titration was found to be a feasible technique for  $\text{N}_2(v)$  vibrational temperature measurement in the afterglow of a pulsed DC discharge. An advantage of the proposed method is the possibility of  $\gamma_{N_2}$  determination on the surfaces being in direct contact with the plasma. The measurements are done in single plasma pulse experiments, which allow a better control of the state of the studied surface.



## 6 Influence of plasma treated catalytic surfaces on molecular oxidation

The reactivity of plasma treated and stimulated catalytic surfaces of  $\text{TiO}_2$  has been studied by analyzing the oxidation (i) of  $\text{C}_2\text{H}_2$  to CO and  $\text{CO}_2$  and (ii) of CO to  $\text{CO}_2$ . The inner surface of a Pyrex discharge tube was coated with  $\text{TiO}_2$  films impregnated with  $\text{TiO}_2$  nano-particles, which provides a surface area of about  $4 \text{ m}^2$ . In addition to the exposure of the  $\text{TiO}_2$  surface by low pressure RF plasmas using  $\text{O}_2$ , Ar or  $\text{N}_2$  ( $f = 13.56 \text{ MHz}$ ,  $p = 0.53 \text{ mbar}$ ,  $P = 17 \text{ W}$ ) the surfaces have been stimulated by heating and UV radiation treatment. The temporal development of the concentrations of the precursor gases  $\text{C}_2\text{H}_2$  or CO and of the reaction products has been monitored using quantum cascade laser absorption spectroscopy (QCLAS), which provides multi-component detection in the mid infrared spectral range. The  $\text{C}_2\text{H}_2$  concentration was found to be nearly constant over time after a pre-treatment with Ar or  $\text{N}_2$  discharges using an initial gas mixture of 1%  $\text{C}_2\text{H}_2$  in Ar. However, a strong decay of the concentration of  $\text{C}_2\text{H}_2$  is observed for pure  $\text{O}_2$  plasma pre-treatment. In general, the decay was found to be nearly exponential with time constant in the order of about 10 min. The reactive adsorption of  $\text{C}_2\text{H}_2$  molecules on the inner surface of the tube reactor showed a density of about  $7.5 \times 10^{12} \text{ C}_2\text{H}_2 \text{ molecules cm}^{-2}$ . This behavior demonstrates, that the reaction  $(\text{O}_{\text{ads}} + \text{C}_2\text{H}_2)_{\text{TiO}_2}$  produces some adsorbed intermediates, which can be thermally or photo-catalytically oxidized to  $\text{CO}_2$ . In contrast, when 1% CO in Ar has been used as initial gas mixture no adsorption processes on the  $\text{TiO}_2$  surface could be detected. An effective destruction of CO took part via photo-catalytic oxidation [48].

## 6.1 Introduction

An important contribution to environmental and health protection can be made by the development of technologies that can control the pollution to ensure improved indoor air quality. A lot of studies show that volatile organic compounds (VOCs) can dangerously influence human health through chronic exposure. Apart from traditional ways to remove harmful substances such as thermal and catalytic oxidation, scrubbers, and active charcoal, the use of electric discharges is a promising technique for toxic gas removal, especially when these gases are present at low concentrations [49-56]. For improved pollution destruction the approach of combining plasmas with catalysts has been a technical as well as a scientific challenge over the past decade. The plasma-catalyst synergy has been studied in air discharges with VOC admixtures using different types of catalysts at low and atmospheric pressure [21, 57-60]. One of the main issues of plasma-catalyst coupling is to understand the interaction of the plasma with the catalytic material, especially the processes involved in the destruction and production of molecules on the wall. This field is just at the beginning to become deeper analyzed due to the great complexity of physics and chemistry phenomena occurring at atmospheric pressure.

An alternative to understand plasma-catalytic surface interaction is to perform studies at lower pressure, where surface reactions are dominant over gas phase reactions; this gives an original way to perform time resolved diagnostics of the surface reactivity. Some aspects of the plasma activation of  $\text{SiO}_2$  and  $\text{TiO}_2$  have been in the focus of former studies [58, 59, 68]. The importance of surface reactions for the formation of molecules by recombination has been experimentally demonstrated in a  $\text{N}_2/\text{O}_2$  plasma [62, 63]. Recently a specially designed low pressure capacitively coupled radio-frequency (RF) plasma reactor has been used to investigate the reactivity of NO with a Pyrex surface pre-treated by oxygen, nitrogen or argon plasma [64]. In the case of an oxygen pre-treatment of the surface, oxygen atoms are chemisorbed leading to the oxidation of NO to  $\text{NO}_2$ . Based on these experimental data a simple kinetic model was developed and showed good agreement with the measured molecular gas phase concentrations. In the model a fraction of the surface is considered to be covered with chemisorption sites where atoms and molecules, in this case oxygen atoms, can be adsorbed, whereas they can be removed only by recombination [65]. The participation of adsorbed oxygen atoms on surfaces,  $\text{O}_{\text{ads}}$ , in the destruction of VOCs has been demonstrated also in low pressure DC plasmas, in atmospheric DBD and bed packed discharges [66, 67].

Similarly, using the same reactor type as in reference [64] the evidence of adsorption of oxygen atoms on the catalyst  $\text{TiO}_2$  under plasma exposure and the related surface reactivity of  $\text{C}_2\text{H}_2$  was studied in reference [68]. In this work the complex character of the interaction of catalytic material with plasmas has already been emphasized. In the case of using the  $\text{TiO}_2$  catalyst the reactive adsorption of  $\text{C}_2\text{H}_2$  molecules was found to be highly efficient on the walls, but only in the case the surface had been treated by an oxygen plasma, before acetylene was introduced into the discharge tube.

In contrast to the behavior of  $\text{O}_{\text{ads}}$  at a  $\text{TiO}_2$  surface no reactivity of  $\text{O}_{\text{ads}}$  on silica and Pyrex surfaces to  $\text{C}_2\text{H}_2$  was found [68, 69]. The hypothesis to explain this essential difference of the reactivity of  $\text{O}_{\text{ads}}$  to  $\text{C}_2\text{H}_2$  is based on the assumption of different binding energies on these materials. This approach has been supported by recent *ab-initio* studies of oxygen atom adsorption on rutile  $\text{TiO}_2$  [70] and on  $\beta$ -cristobalite  $\text{SiO}_2$  [71]. Calculations show, that the binding energy of oxygen atoms on  $\text{SiO}_2$  with a value of  $E_{\text{ads}} = 5.9$  eV is considerably higher than on  $\text{TiO}_2$  which has a value of  $E_{\text{ads}} = 1 - 1.5$  eV. Therefore, considering the results of these recent studies comparing between the reactivity of different surfaces, as  $\text{TiO}_2$ ,  $\text{SiO}_2$  and Pyrex, and different molecular reactants, as e.g. NO and  $\text{C}_2\text{H}_2$ , it could be concluded, that the reactivity of  $\text{O}_{\text{ads}}$  depends (i) on the nature of the surface and (ii) on the properties of the reacting molecule [68, 69]. However, in reference [68], the concentrations of CO,  $\text{CO}_2$  or of other by-products have not been monitored in the gas phase.

The aim of the present study is to analyze further the reactivity of plasma treated catalytic  $\text{TiO}_2$  surfaces using the examples (i) of the oxidation of  $\text{C}_2\text{H}_2$  to CO and  $\text{CO}_2$  and (ii) of CO to  $\text{CO}_2$ . In addition to the exposure of the  $\text{TiO}_2$  surface by low pressure RF plasmas using  $\text{O}_2$ , Ar or  $\text{N}_2$  as precursor gases the surfaces have been activated by heating and UV radiation treatment. The temporal development of the concentrations of the precursor gas and of the reaction products has been monitored using quantum cascade laser absorption spectroscopy (QCLAS), which provides multi-component detection in the mid infrared spectral range [22]. In addition mass spectrometry measurements have been performed to detect possible higher molecular reaction products. The analysis of the decay of the concentration of the precursors and of the production of carbon oxides has led to further insight into plasma surface interactions, molecular adsorption processes and surface chemistry phenomena.

## 6.2 Experimental

### 6.2.1 Discharge tube configuration

The experiments were performed in a cylindrical discharge tube with a length of  $l = 60$  cm and a diameter of  $d = 2$  cm, schematically shown on the figure 6.1. The tube was made of silica and additionally deposited with  $\text{TiO}_2$  on the inner surface using a sol-gel technique [73]. The coating was impregnated with Degussa P25  $\text{TiO}_2$  nanoparticles containing anatase and rutile phases in a ratio of about 3:1 [74]. Nano-particles can support the destruction of VOCs, as reported by Kim and co-workers [61]. The specific surface of this impregnated coating has a value of  $38 \text{ m}^2 \text{ g}^{-1}$ . The mass of the deposited catalyst was typically 0.1 g and hence the total surface area of  $\text{TiO}_2$  in the reactor was about  $4 \text{ m}^2$ . Considering that  $\text{TiO}_2$  with a combination of anatase and rutile phases has an enhanced photocatalytic activity compared to pure anatase phase  $\text{TiO}_2$  [72], the discharge tube was protected from ambient light sources to prevent uncontrolled photocatalytic degradation of added gases.

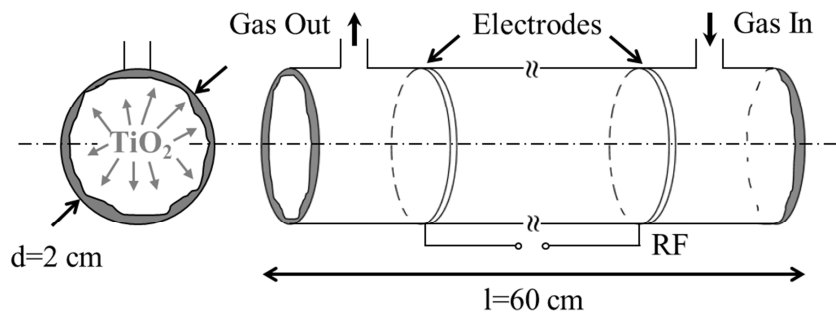


**Figure 6.1:** Scheme of the Pyrex tube coated with a  $\text{TiO}_2$  sol-gel film and  $\text{TiO}_2$  nanoparticles with two electrodes, placed around outside the tube [48].

In the tube a capacitively coupled discharge was generated by applying an RF voltage ( $f = 13.56$  MHz) to a pair of external metal electrodes. The injected discharge power was typically  $P = 17$  W. The external location of the electrodes has the advantage, that any contact between plasma and metal can be prevented. The discharge tube was pumped by a rotary pump and a base pressure of about  $p = 10^{-3}$  mbar could be achieved. In the experiments the pressure was varied between  $p = 0.26$  to 6.6 mbar. The discharge could be driven under flowing or static gas conditions. During the experiments at static conditions, i.e. using a closed tube, the pressure increase was lower than 0.1% over the time of the measurements, because a low leakage rate could be ensured. Further details of the experimental setup can be found in reference [64].

### 6.2.2. Time-resolved quantum cascade laser diagnostics

The QCLAS measurements for species concentration monitoring have been performed using a three quantum cascade laser measurement and control system (TRIPLE Q), a compact and transportable laser system based on infrared absorption spectroscopy [22]. In figure 6.2 the schematic diagram of the TRIPLE Q system connected to the RF discharge tube is given. The divergent radiation of three QCLs driven by electronic units (Q-MACS Basic, neoplas control) is collimated by a system of two Off-Axis Parabolic (OAP) mirrors and guided as single laser beam through the RF discharge tube to the detector (IRDM-600, neoplas control). The detector module contains a temperature controller, which is adjusted to the detector element (VIGO, PDI-2TE-10/12) and a pre-amplifier (bandwidth: 600 MHz, rise time: 2 ns).

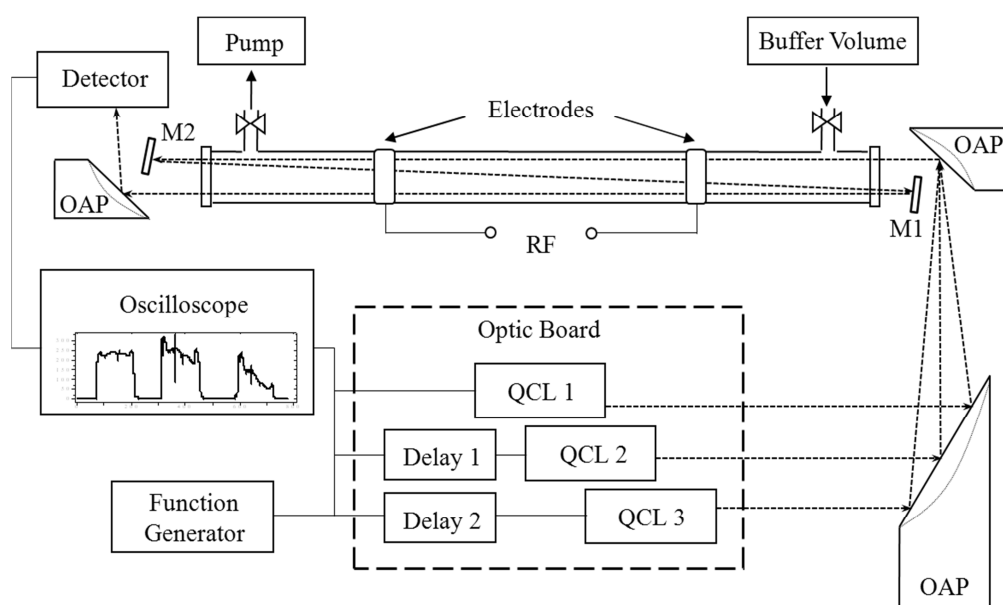


**Figure 6.2:** Scheme of the 3 channel QCLAS system TRIPLE Q combined with the RF discharge tube (OAP: off-axis paraboloid, M1, M2: mirrors) [48].

To increase the sensitivity of the *in-situ* QCLAS measurements three optical paths through the plasma volume were realized using a set of mirrors outside of the vacuum tube. The whole optical path from the lasers to the detector excluding the discharge tube was covered with plastic panels and purged with dry nitrogen to avoid absorptions caused by ambient air.

An oscilloscope (Waverunner Pro 760Zi, LeCroy, bandwidth: 6 GHz, sample rate: 40 GS/s) connected to the detector was used for data monitoring and recording. The spectral multiplexing was obtained by using a delay generator (DG535, Stanford Research Systems) and a function generator (33120A, Hewlett Packard) providing an appropriate trigger regime.

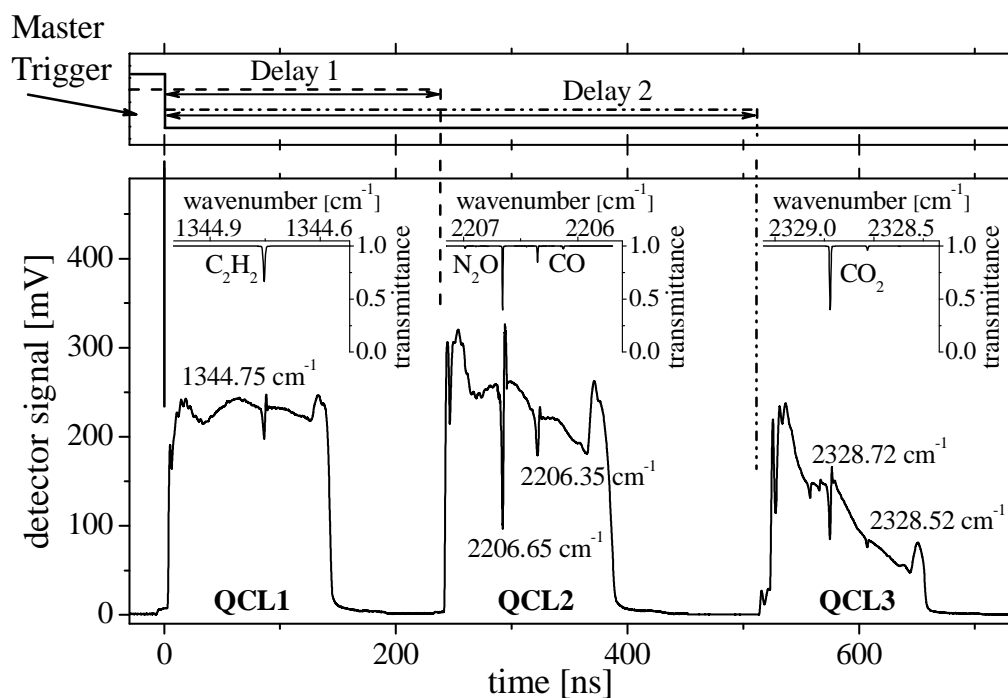


**Figure 6.3:** Example of absorption spectra of  $C_2H_2$ ,  $CO$ ,  $CO_2$  and  $N_2O$  measured in a multiplex regime with 3 QCLs working in the intra pulse mode at pulse duration of 150 ns. Simulated spectra for the specific emission range of the lasers are shown on the embedded diagrams [22, 29, 48].

A typical example of absorption spectra of  $C_2H_2$ ,  $CO$ ,  $CO_2$  and  $N_2O$  measured in a multiplex regime with the three 3 QCLs (Alpes Lasers) working in the intra pulse mode at pulse durations of about 150 ns recorded by the oscilloscope is shown in figure 6.3. Simulated spectra for the specific emission range of the QCLs around  $1344.75\text{ cm}^{-1}$ ,  $2206.35\text{ cm}^{-1}$  and  $2328.72\text{ cm}^{-1}$  are shown in the embedded diagrams [22, 29].

It should be mentioned that in the case of the QCL absorption measurements in the intra-pulse mode at low pressures, the absorption lines are strongly affected by non-linear phenomena called rapid passage effect [25]. This effect relates to the distortion of the absorption features due to intense rapidly swept radiation which passes over a molecular resonance on a timescale that is much shorter than the relaxation time [26]. This leads to reduced absorption signals and distorted line shapes and hence to underestimated molecular number densities. Therefore, the direct application of the Beer-Lambert law for concentration determination is not possible and a calibration function has to be determined [27, 28]. For this purpose a gas mixture of 1% of  $CO_2$  diluted in  $N_2$  and of 1%  $C_2H_2$  or 1%  $CO$  in Ar was filled at different pressures in the discharge tube. The calibration results also enable to determine the detection limits of the measured species. The detection limits of  $C_2H_2$ ,  $CO_2$  and  $CO$  were found to be in the range of  $10^{13}\text{ molecules cm}^{-3}$ .

### 6.2.3. Experimental procedure

Before every single measurement a clean inner surface of the tube was ensured by a procedure, which includes heating to 350°C, UV irradiation and O<sub>2</sub> plasma treatment. The duration of this preparation was about 50 min. In the series of the experiments this pre-treatment ensured that any memory effect of the tube surface could be avoided and a high level of reproducibility could be achieved.

The heating of the discharge tube at a temperature of 350°C for 30 min were performed by an Winkler Heating Jacket ( $P=360$  W,  $l=300$  mm) placed around the tube. After that the discharge tube was irradiate with two UV lamps (Philips PL-L 24W/10/4P,  $P=24$  W) for 20 min. The lamps, emitting UV-A radiation mainly between 300 and 400 nm, were located on both sides of the discharge tube in a distance of 10 cm. Simultaneously the inner surface of the tube was treated by a RF discharge in O<sub>2</sub> under flowing conditions at a pressure of  $p=0.53$  mbar. The discharge power was  $P=17$  W.

Based on XPS analysis Regonini and co-workers showed, that the treatment of TiO<sub>2</sub> samples at appropriate temperatures has a strong impact on the nitrogen, carbon and organic content of the catalyst. At annealed samples the density of these species was much lower compared with non-treated surfaces [75]. The photo catalytic oxidation can be improved by using heating and UV irradiation simultaneously. Via combining both treatments highly reactive electrons can be created, which support the destruction, for example, of hydrocarbons into CO<sub>2</sub> and H<sub>2</sub>O [76, 77].

**Table 6.1:** Experimental phases of the measurements.

Phase No.	1			2	3	4	
Phase Name	Pre-Treatment (Plasma Stimulation)			Evacuation	Filling and Adsorption	After-Treatment (Stimul. Oxidation)	
Sub-Phase Name						Heating 350°C	UV radiation
Precursor Gas	O <sub>2</sub>	N <sub>2</sub>	Ar		1 % C <sub>2</sub> H <sub>2</sub> or 1% CO in Ar	Ar Buffer	
Pressure [mbar]	1.25	0.75	0.26	Pumping	1.3 – 6.6	2.6	
Duration [min]	10-30	10-30	10-20	10	5 - 30	25	35
Flowing (FC) or Static (SC) Conditions	FC	FC	FC		SC	SC	

Following this general cleaning preparation the experiments have been structured in time in different phases, which characterize the change of important parameters, in particular, the general splitting in (i) a treatment of the inner surface of the tube and in kinetic studies (ii) of an adsorption of precursor molecules and (iii) of oxidation processes of adsorbed reaction intermediates or gas phase molecules.

The experimental details are given in table 6.1. The temporal evolution of experiments consists of four main phases: (1) pre-treatment, (2) evacuation, (3) filling and adsorption, and (4) after-treatment. Phase 1 is divided into three alternative sub-phases: (i) O<sub>2</sub>, (ii) N<sub>2</sub> or (iii) Ar plasma. While phase 4 is characterized by two alternative sub-phases: (i) heating 350°C and (ii) UV radiation.

The pre-treatment, phase 1, is used for the deposition of oxygen atoms, O<sub>ads</sub>, on the inner TiO<sub>2</sub> surface via sole O<sub>2</sub> plasma exposure for a duration of 10 – 30 min [68]. To verify the effect of the influence of the O<sub>2</sub> plasma for some specific experiments an Ar or N<sub>2</sub> plasma was used. After this pre-treatment phase, in phase 2 the tube was pumped for 10 min to evacuate all gaseous species and to allow a cooling of the tube down to room temperature. After the pre-treatment and the pumping, in phase 3 the tube was filled with the relevant probing gas containing either C<sub>2</sub>H<sub>2</sub> or CO. At that time the *in-situ* monitoring of the temporal evolutions of the concentrations of C<sub>2</sub>H<sub>2</sub>, CO and CO<sub>2</sub> using QCLAS was started under static conditions. In phase 4 an after-treatment was applied to activate the TiO<sub>2</sub> catalyst either by heating (350°C) or by UV radiation.

## 6.3 Results and discussion

### 6.3.1 Kinetics of C<sub>2</sub>H<sub>2</sub> destruction on a pre-treated TiO<sub>2</sub> surface

The time evolution of the C<sub>2</sub>H<sub>2</sub> concentration was studied depending on different types of plasma exposure of the TiO<sub>2</sub> surface in the pre-treatment phase 1. Figure 6.4 illustrates the reactive oxidation of C<sub>2</sub>H<sub>2</sub> after different pre-treatments of the surface and/or different initial concentrations of C<sub>2</sub>H<sub>2</sub>: i) Ar plasma pretreatment, ii) N<sub>2</sub> plasma pretreatment, iii) O<sub>2</sub> plasma pretreatment using two different initial concentration of C<sub>2</sub>H<sub>2</sub> and, iv) oxygen followed by argon plasma pre-treatment.

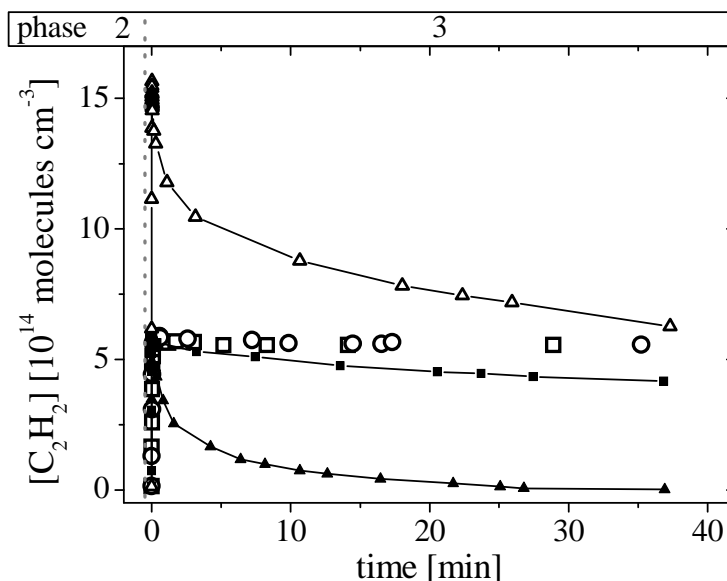


**Figure 6.4:** Time dependence of the  $C_2H_2$  concentration depending on different types of plasma treatment ( $t = 30$  min,  $P = 17$  W) of the  $TiO_2$  surface: □ – Ar ( $p = 0.26$  mbar,  $\phi = 14$  sccm), ○ –  $N_2$  ( $p = 0.75$  mbar,  $\phi = 40$  sccm), ▲ –  $O_2$  ( $p = 1.25$  mbar,  $\phi = 40$  sccm), ■ – 10 min of  $O_2$  plasma followed by 20 min of Ar plasma (same parameters as for Ar and  $O_2$  separately). The introduced mixture was 1%  $C_2H_2$  in Ar at  $p = 2.6$  mbar. The upper curve (Δ) represents the experiment, when the tube was filled with 6.6 mbar of 1%  $C_2H_2$  in Ar after  $O_2$  plasma exposure [48].

First of all, as already shown in reference [68], there is no reactive adsorption of  $C_2H_2$  onto  $TiO_2$  after a pre-treatment with Ar or  $N_2$  discharges, whereas there is reactive adsorption of  $C_2H_2$  after an oxygen plasma pre-treatment. In general, the decay was found to be nearly exponential with time constant in the order of about 10 min under the present experimental conditions.

These observed losses of  $C_2H_2$  can be explained by two mechanisms, (i) due to adsorption of  $C_2H_2$  on  $TiO_2$  nanoparticles and/or (ii) chemical reactions with species present on the pre-treated surface. As already discussed in reference [57] probably both mechanisms can take place. Moreover, when a discharge in pure Ar is operated for 20 min after the initial 10 min pre-treatment with oxygen plasma a significantly lower decrease of the concentration of  $C_2H_2$  is obtained compared to the decrease of the  $C_2H_2$  concentration after a sole  $O_2$  RF discharge treatment, see figure 6.4. This proves that  $C_2H_2$  is not effectively adsorbed on clean  $TiO_2$  and the removal of  $C_2H_2$  after  $O_2$  plasma pre-treatment is catalyzed by O atoms grafted to the surface [68]. These grafted O atoms can be partly removed by an Ar plasma treatment.

In order to estimate the maximum amount of  $C_2H_2$  that can be reactively adsorbed on the pre-treated catalyst, experiments with different pressures of injected acetylene were

performed. In figure 6.4 an example when the tube was filled with 1% of  $C_2H_2$  in Ar at  $p = 6.6$  mbar is shown, see the upper curve. A kind of saturation was found at the total number of about  $2 \times 10^{17}$  of  $C_2H_2$  molecules in the reactor. Taking into account the surface area of  $TiO_2$  of  $4\text{ m}^2$ , this corresponds to approximately  $7.5 \times 10^{12}$   $C_2H_2$  molecules  $\text{cm}^{-2}$ . It is interesting to note, that in a similar study using a discharge tube made of Pyrex, an essential higher value of the density of oxygen atoms of about  $2 \times 10^{14}$   $\text{cm}^{-2}$  after an  $O_2$  plasma treatment were found [64]. In order to check if some other products containing carbon are released upon the adsorption of  $C_2H_2$ , a mass spectrometric (MS) analysis (Pfeiffer PrismaPlus 0 – 100 a.m.u.) of the gas phase was performed additionally to the QCLAS measurements. Mass spectra of the initial mixture (1%  $C_2H_2$  in Ar) and of the gas mixture in the tube reactor 30 min after the introduction of the probe gas are shown in figure 6.5.

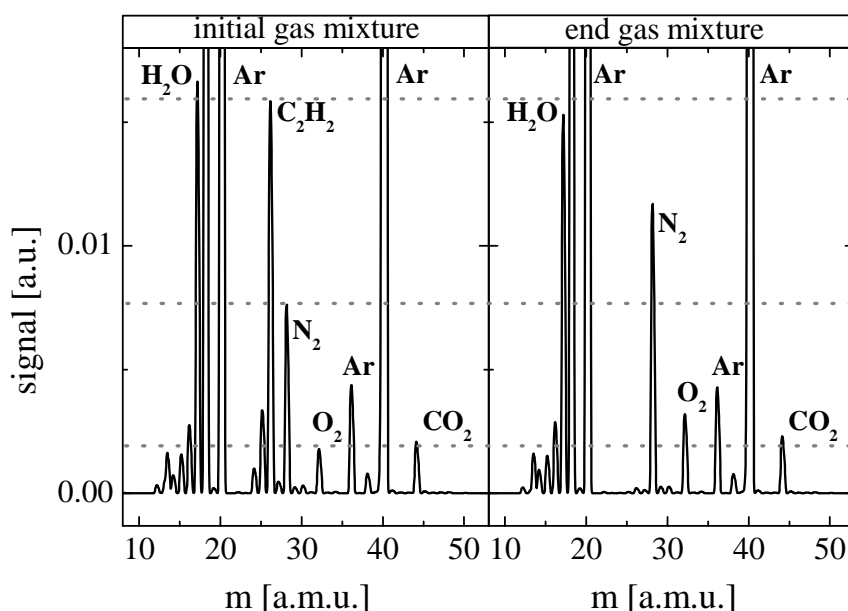


**Figure 6.5:** Mass spectra of the initial gas mixture (left panel), i.e. at the beginning of phase 3 and 30 min after the filling (right panel), i.e. at the end of phase 3. (1%  $C_2H_2$  in Ar;  $p = 2.6$  mbar; pre-treatment 2:  $O_2$  plasma) [48].

As a general result, no new mass spectroscopy signals could be detected in the range between 1 to 100 a.m.u. during the experiment. For clarity in figure 6.5 only a zoom on 10 – 50 a.m.u. is shown. Slight increases of the peak intensities related to  $m/z = 28$  and 32 a.m.u., corresponding to  $N_2$  and  $O_2$ , can be ascribed to a small leak in the vacuum system. Since during the  $C_2H_2$  adsorption on the  $TiO_2$  surface no new major gas phase products, except a small production of  $CO_2$ , see inset of figure 6.6, could be observed, it can be concluded that the major products of the reaction  $(O_{ads} + C_2H_2)_{TiO_2}$  stay adsorbed on the surface.

### 6.3.2 Oxidation of adsorbed reaction intermediates

For the experimental phases 3-4 figure 6.6 presents the results of concentration measurements of  $C_2H_2$  and  $CO_2$ . Already from the beginning of phase 3, after being fed into the tube ( $p = 2.6$  mbar), the initial concentration ( $\sim 6 \times 10^{14}$  molecules  $cm^{-3}$ ) of  $C_2H_2$  is fast decreasing due the adsorption process of the acetylene molecules on the wall of the tube reactor.

During the adsorption process of  $C_2H_2$  on the stimulated  $TiO_2$  surface a relatively small production of  $CO_2$  in the order of  $10^{13}$  molecules  $cm^{-3}$  could be observed, see inset of figure 6.6. The concentration of  $CO_2$  is slightly growing and after 20-25 min it reaches nearly a value of  $2-3 \times 10^{13}$  molecules  $cm^{-3}$ . This amount represents only about 2% of the carbon provided from the lost acetylene.

After the reduction of the  $C_2H_2$  concentration has stabilized the reactor contains mainly argon as buffer gas at a pressure of  $p = 2.6$  mbar. Therefore, to initiate oxidation reactions the catalyst was activated in two possible ways: (i) by heating to  $350^\circ C$  or (ii) by exposure to UV radiation, phase 4. It should be pointed out that no  $C_2H_2$  desorption has been seen, when the catalyst was heated. This fact confirms the reactive mechanism of the adsorption process. In the case acetylene would have been just molecularly adsorbed, a thermal initiated desorption of  $C_2H_2$  should be observable.

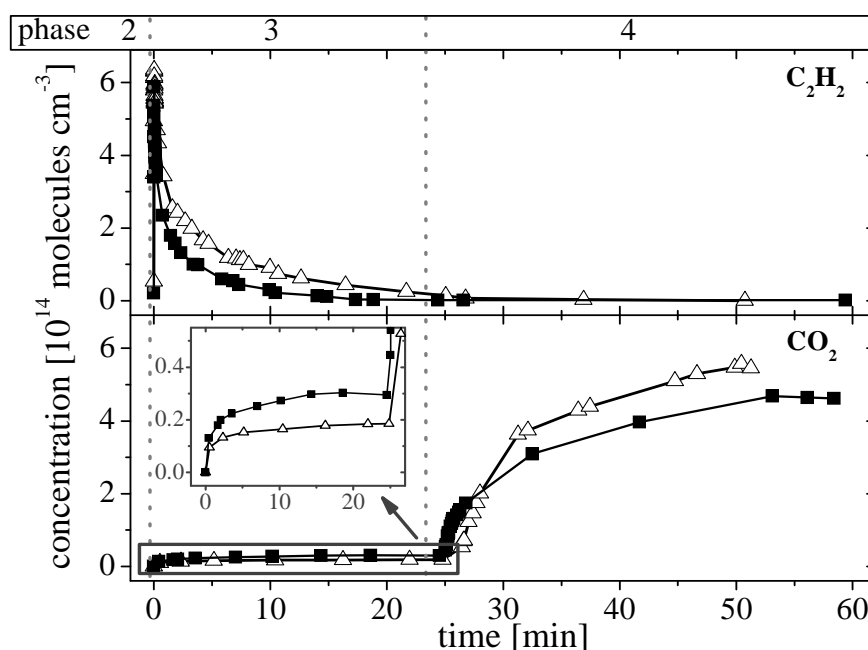
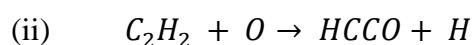
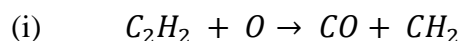


**Figure 6.6:** Time evolution of the concentrations of  $C_2H_2$  (upper panel) and of  $CO_2$  (lower panel) in phases 3 and 4 (initial gas mixture: 1%  $C_2H_2$  in Ar,  $p = 2.6$  mbar). After-treatment:  $\Delta$  - heating to  $350^\circ C$  and  $\blacksquare$  - UV radiation exposure [0].

As shown in figure 6.6, with time the process of formation of CO<sub>2</sub> stabilizes reaching the value of  $4.7 \times 10^{14}$  molecule cm<sup>-3</sup> for UV radiation and  $5.6 \times 10^{14}$  molecule cm<sup>-3</sup> for 350°C treatment. That means that in the most effective case by heating at 350°C the produced CO<sub>2</sub> represents only 50% of the carbon balance. Probably the stabilization of the CO<sub>2</sub> production can be explained by the absence of a sufficient number of O<sub>ads</sub> for the reaction. During the time of the measurements no production of CO could be observed within the detection limit, i.e. in the range of  $10^{13}$  molecules cm<sup>-3</sup>.

These experimental results demonstrate that the reaction (O<sub>ads</sub> + C<sub>2</sub>H<sub>2</sub>)<sub>TiO<sub>2</sub></sub> produces some adsorbed intermediates, which can be thermally or photo-catalytically oxidized to CO<sub>2</sub>.

It can be concluded that the oxidation of acetylene by O<sub>ads</sub> atoms is incomplete at room temperature and ensures only the first step of oxidation. Nevertheless, a hypothesis based on an analogy with the mechanisms of the gas phase reaction C<sub>2</sub>H<sub>2</sub> + O is possible to discuss briefly. In general, the oxidation of C<sub>2</sub>H<sub>2</sub> to CO<sub>2</sub> is a multistep process. In a first step two major reaction ways are relevant [69, 78]:



It is reasonable to suppose, that the oxidation of C<sub>2</sub>H<sub>2</sub> on the tube surface proceeds via similar bond breaking pathways. The reaction (i) may be less probable, since no CO could be detected in the gas phase. It should be also considered, that fragments of reactions may stay adsorbed on the surface. In order to get a better understanding into the mechanism of this process *in-situ* analysis of adsorbed species at the tube surface would be required.

### 6.3.3 Photo-catalytic oxidation of C<sub>2</sub>H<sub>2</sub> and CO

To achieve further insight into the photo-catalytic properties of the TiO<sub>2</sub> layer in the tube reactor the oxidation behavior of C<sub>2</sub>H<sub>2</sub> has been compared to that of CO. For this purpose in the experimental phase 1 the surface of the inner tube was pre-treated by a pure Ar plasma for 30 min. Then in phase 3 a gas mixture of 1% C<sub>2</sub>H<sub>2</sub> in Ar at a pressure of  $p = 1.3$  mbar was filled into the tube. After about 17 min the after-treatment phase 4 was started with the external exposure of UV radiation. Figure 6.7 shows the temporal evolution of the concentrations of the precursor C<sub>2</sub>H<sub>2</sub> and of the product molecules CO and CO<sub>2</sub> over the about 50 min of the experiment. Similarly to the data shown already in figure 6.3, no strong

decrease of the  $C_2H_2$  concentration could be observed in phase 3 after the Ar plasma treatment. In contrast, the following UV treatment led to strong decrease of the concentration of acetylene and to the production of CO and  $CO_2$ .

The temporal evolution of the concentration of  $C_2H_2$  is comparable to the adsorption experiment after  $O_2$  plasma stimulation, see figure 6.6. Both the concentrations of CO and of  $CO_2$  reached a value of about  $1 \times 10^{14}$  molecules  $cm^{-3}$ , which presents about 60% of the carbon balance provided by the  $C_2H_2$  removal from the gas phase. It becomes obvious, that in this experiment the photo catalytic destruction of  $C_2H_2$  is based on the lattice oxygen of the material.

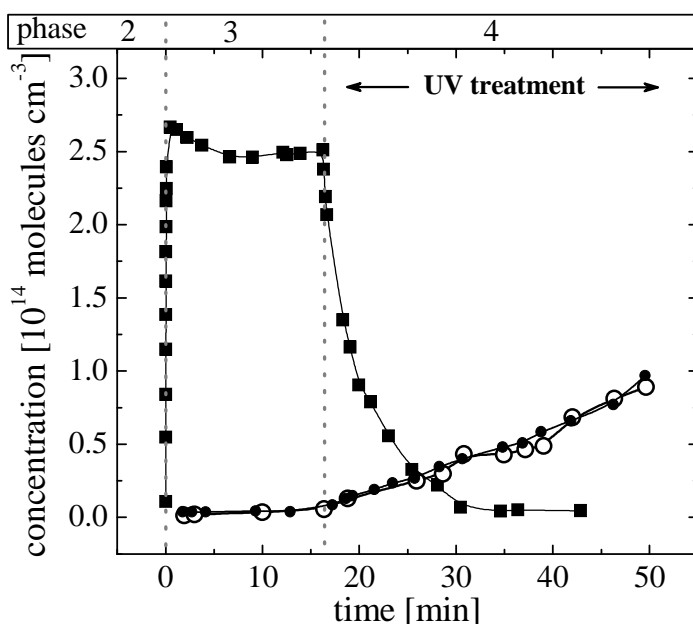


**Figure 6.7:**

*Photo-catalytic decomposition of  $C_2H_2$  (■), and formation of CO (●) and  $CO_2$  (○) in phases 3 and 4 after an Ar plasma pre-treatment in phase 1 ( $t = 30$  min,  $p = 0.26$  mbar,  $\phi = 14$  sccm, initial gas mixture: 1% of  $C_2H_2$  in Ar,  $p = 1.3$  mbar, UV light exposure in phase 4) [48].*

In case CO instead of  $C_2H_2$  is introduced into the tube volume following the same pre-treatment in phase 1, i.e. using an Ar plasma treatment of the inner surface, again no decrease of the CO concentration could be observed over time. Only if again the UV exposure is applied to the tube, the CO concentration is significantly reduced while the  $CO_2$  concentration increases. Within about 4 min 20% of the CO molecules are lost out of the tube volume. The CO concentration is reduced by about  $5 \times 10^{13}$  molecules  $cm^{-3}$ . The concentration of  $CO_2$  reaches a value of about  $2.5 \times 10^{13}$  molecules  $cm^{-3}$ , shown in figure 6.8.

In case the pre-treatment in phase 1 has been performed with an  $O_2$  plasma, the CO destruction in phase 4 via the UV exposure of the photo-catalytic  $TiO_2$  layer is much more effective. In figure 6.8 the evolution of both concentrations, CO and  $CO_2$ , for both cases of pre-treatment is given over time. In contrast to the  $C_2H_2$  case no reduction of the CO

concentration in phase 3 was observed. But in the case of an  $O_2$  plasmas pre-treatment with UV stimulation an effective CO oxidation and  $CO_2$  production takes place. Within only few minutes nearly all CO molecules have been oxidized (figure 6.8).

This experiment shows, that (i)  $O_{ads}$  are not reactive towards CO although they are reactive towards  $C_2H_2$ , i.e. the reactivity is dependent on the both the surface material and the target molecules, (ii) that O atoms of the  $TiO_2$  material are not very effective for photo catalytic oxidation of CO, and (iii)  $O_{ads}$  can be effectively used in photo catalytic oxidation [21].

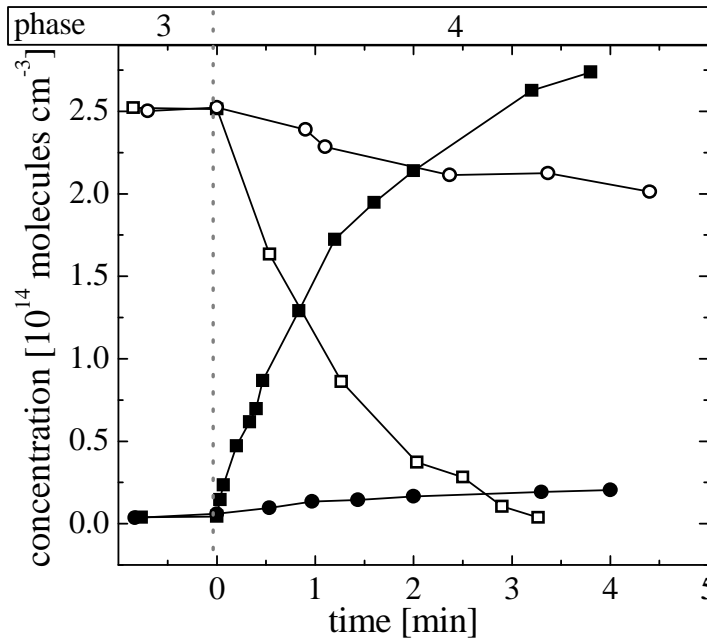


**Figure 6.8:** Photo-catalytic decomposition (i) of CO ( $\circ$ ), and formation of  $CO_2$  ( $\bullet$ ) in phases 3 and 4 after an Ar plasma pre-treatment in phase 1 and (ii) decomposition of CO ( $\square$ ) and formation of  $CO_2$  ( $\blacksquare$ ) after an  $O_2$  plasma pre-treatment in phase 1 (Ar RF plasma:  $p=0.26$  mbar,  $\phi=14$  sccm,  $t=40$  min,  $O_2$  RF plasma:  $p=0.53$  mbar,  $\phi=14$  sccm,  $t=30$  min, initial gas mixture: 1% CO in Ar,  $p=1.3$  mbar, UV light exposure in phase 4) [48].

## 6.4 Summary and conclusions

In this study it has been possible to further analyze the reactivity of plasma treated photo-catalytic TiO<sub>2</sub> surfaces at the examples of the oxidation of C<sub>2</sub>H<sub>2</sub> and CO. The temporal evolution of the concentrations of molecular species in the volume of the tube reactor was monitored based on QCLAS and MS techniques. Using a RF oxygen plasma in a pre-treatment phase, reactive oxygen species could be grafted on the surface of TiO<sub>2</sub>. It was found, that the reactivity of the adsorbed O atoms depends on the reacting molecule. For C<sub>2</sub>H<sub>2</sub> a high reactivity could be proven, characterized by a value of about  $7.5 \times 10^{12}$  C<sub>2</sub>H<sub>2</sub> molecules cm<sup>-2</sup> of the catalyst, which were removed from the tube volume. In the case CO was used as precursor gas no adsorption phenomena could be monitored on plasma pre-treated surfaces.

Studying the oxidation of C<sub>2</sub>H<sub>2</sub>, in the adsorption phase only about 2% of the carbon was detected as CO<sub>2</sub> in the gas phase of the reactor. In contrast, in an after-treatment phase stimulation by heating or UV radiation led to an effective oxidation of ca. 50% of the adsorbed acetylene to CO<sub>2</sub>. This behavior shows, that the reaction (O<sub>ads</sub> + C<sub>2</sub>H<sub>2</sub>)<sub>TiO2</sub> produces some adsorbed intermediates, which can be thermally or photo-catalytically oxidized to CO<sub>2</sub>.

In addition, both molecular precursors, C<sub>2</sub>H<sub>2</sub> and CO, can be also effectively oxidized by photo-catalytic processes only. It is interesting to note, that in the CO case again an oxygen plasma pre-treatment leading to grafted oxygen atoms on the TiO<sub>2</sub> surface, supports the oxidation to CO<sub>2</sub> considerably.

Although the present analysis of the C<sub>2</sub>H<sub>2</sub> and CO reduction and carbon oxide production in interaction with a TiO<sub>2</sub> catalyst provides information about plasma surface stimulation, molecular adsorption processes and surface chemistry phenomena, several detailed aspects, in particular, of molecular surface reaction are far from being fully understood. Future studies should include (i) other surface materials and molecular precursor gases and (ii) should be combined with direct *in-situ* techniques of surface analysis.

## Bibliography for Chapters 5 and 6

- [1] D. Marinov, D. Lopatik, O. Guaitella, M. Hübner, Y. Ionikh, J. Röpcke, A. Rousseau, *J. Phys. D: Appl. Phys.* **45**, 175201 (2012).
- [2] V. Guerra, J. Loureiro, *Plasma Sources Sci. Technol.* **6**, 361 (1997).
- [3] B. Gordiets, C.M. Ferreira, V. Guerra, J. Loureiro, J. Nahorny, D. Pagnon, M. Touzeau, M. Vialle, *IEEE Trans. Plasma Sci.* **23**, 750 (1995).
- [4] B.F. Gordiets, A.I. Osipov, L.A. Shelepin, *Kinetic Processes in Gases and Molecular Lasers* (Gordon and Breach: New York) (1988).
- [5] M. Capitelli, C.M. Ferreira, B.F. Gordiets, A.I. Osipov, *Plasma Kinetics in Atmospheric Gases* (Berlin: Springer) (2000).
- [6] A.K. Kurnosov, A.P. Napartovich, S.L. Shnyrev, M. Cacciatore, *J. Phys. Chem. A* **111**, 7057 (2007).
- [7] S.A. Smirnov, V.V. Rybkin, I.V. Kholodkov, V.A. Titov, *High Temperature* **40**, 323 (2002).
- [8] V. Guerra, J. Loureiro, *J. Phys. D: Appl. Phys* **28**, 1903 (1995).
- [9] L. Lefèvre, T. Belmonte, H. Michel, *J. Appl. Phys* **87**, 7497 (2000).
- [10] M. Lino da Silva, J. Loureiro, V. Guerra, *Plasma Sources Sci. Technol.* **18**, 034023 (2009).
- [11] S.M. Starikovskaia, *J. Phys. D: Appl. Phys.* **39**, R265 (2006).
- [12] C.K.N. Patel, *Phys. Rev.* **136**, A1187 (1964).
- [13] A.K. Kurnosov, A.P. Napartovich, S.L. Shnyrev, M. Cacciatore, *Plasma Sources Sci. Technol.* **19**, 045015 (2010).
- [14] M. Cacciatore, A.K. Kurnosov, A.P. Napartovich, *J. Chem. Phys.* **123**, 174315 (2005).
- [15] J.E. Morgan, H.I. Schiff, *Can. J. Chem* **41**, 903 (1963).
- [16] G. Black, H. Wise, S. Schechter, R. Sharpless, *J. Chem. Phys* **60** 3526 (1974).
- [17] J. Parish, P. Yaney, *Proc. 47th Annual Gaseous Electronics Conf. (Gaithersburg, MD)* *Bull. Am. Phys. Soc.* **39**, 1473 (1994).
- [18] J. Parish, P. Yaney, AFOSR AASERT Grant NoF49620-94-0370 Report (1999).

- [19] V.I. Egorov, Yu.M. Gershenzon, V.B. Rozenshtein, S.Ya. Umanskii, *Chem.Phys.Lett.* **20**, 77 (1973).
- [20] E.G. Thorsteinsson, J.T. Gudmundsson, *Plasma Sources Sci. Technol.* **18**, 045001 (2009).
- [21] O. Guaitella, F. Thevenet, E. Puzenat, C. Guillard, A. Rousseau, *Applied Catalysis B: Environmental* **80**, 296 (2008).
- [22] M. Hübner, S. Welzel, D. Marinov, O. Guaitella, S. Glitsch, A. Rousseau, J. Röpcke, *Rev. Sci. Instr.* **82**, 093102 (2011).
- [23] E. Normand, M. McCulloch, G. Duxbury, N. Langford, *Opt. Lett.* **28**, 16 (2003).
- [24] T. Beyer, M. Braun, A. Lambrecht, *J. Appl. Phys.* **93**, 3158 (2003).
- [25] S. Welzel, F. Hempel, M. Hübner, N. Lang, P.B. Davies, J. Röpcke, *Sensors* **10**, 6861 (2010).
- [26] E. Normand, G. Duxbury, N. Langford, *Opt. Commun.* **197**, 115 (2001).
- [27] S. Welzel, L. Gatilova, J. Röpcke, A. Rousseau, *Plasma Sources Sci. Technol.* **16**, 822 (2007).
- [28] J.H. Van Helden, S.J. Horrocks, G.A.D. Ritchie, *Appl. Phys. Lett.* **92**, 081506 (2008).
- [29] L.S. Rothman, D. Jacquemart, A. Barbe, D.C. Benner, M. Birk, L.R. Brown, M.R. Carleer, C. Chackerian, K. Chance, L.H. Coudert, V. Dana, V.M. Devi, J.M. Flaud, R.R. Gamache, A. Goldman, J.M. Hartmann, K.W. Jucks, A.G. Maki, J.Y. Mandin, S.T. Massie, J. Orphal, A. Perrin, C.P. Rinsland, M.A.H. Smith, J. Tennyson, R.N. Tolchenov, R.A. Toth, J.V. Auwera, P. Varanasi, G. Wagner, *J. Quant. Spectrosc. Radiat. Transfer.* **96**, 139 (2005).
- [30] D. Marinov, M. Hübner, O. Guaitella, J. Röpcke, A. Rousseau, *Proc. 63th Annual Gaseous Electronics Conf. (Paris, France) Bull. Am. Phys. Soc.* **55**, 7 (2010).
- [31] G. Cartry, X. Duten, A. Rousseau, *Plasma Sources Sci. Technol.* **15**, 479 (2006).
- [32] C.O. Laux, Radiation and Nonequilibrium Collisional-Radiative Models *Physico-Chemical Modeling of High Enthalpy and Plasma Flows (von Karman Institute Lecture Series 2002-07)* ed D. Fletcher et al, Rhode-Saint-Gense, Belgium, (2002).
- [33] W. Choi, M. Leu, *Geophys. Res. Lett.* **24**, 2957 (1997).

- [34] R. Rudolph, A. Harendt, P. Bisin, H. Gundel, *J. Phys. D: Appl. Phys.* **26**, 552 (1993).
- [35] M. Margottin-Maclou, L. Doyennette, L. Henry, *Applied Optics* **10**, 1768 (1971).
- [36] R.L. Taylor, S. Bitterman, *Rev.Mod.Phys.* **41**, 26 (1969).
- [37] J.A. Blauer, J.R. Nickerson, *AIAA* **P74**, 536 (1974).
- [38] V. Joly, A. Roblin, *Aerospace Science and Technology* **4**, 229 (1999).
- [39] V. Joly, C. Marmignon, P. Jacque, *Aerospace Science and Technology* **5**, 313 (1999).
- [40] V.V. Nevdakh, L.N. Orlov, N.S. Leshenyuk, *Journal of Applied Spectroscopy* **70**, 276 (2003).
- [41] F. Esposito, I. Armenise, M. Capitelli, *Chem. Phys.* **331**, 1 (2006).
- [42] N.A. Dyatko, I.V. Kochetov, A.P. Napartovich, A.G. Sukharev, EEDF: the software package for calculations of the electron energy distribution function in gas mixtures, <http://www.lxcat.laplace.univ-tlse.fr/software/EEDF>
- [43] D.I. Slovetski, *Mechanisms of Chemical Reactions in Nonequilibrium Plasma* (Nauka: Moscow) in Russian (1980).
- [44] C.D. Pintassilgo, O. Guaitella, A. Rousseau, *Plasma Sources Sci. Technol.* **18**, 025005 (2009).
- [45] Y.P. Raizer, *Gas Discharge Physics* (Berlin: Springer) (1991).
- [46] P. Macko, G. Cunge, N. Sadeghi, *J. Phys. D: Appl. Phys.* **34**, 1807 (2001).
- [47] M. Kovacs, R.D. Ramachandra, A. Javan, *J. Chem. Phys.* **48**, 3339 (1968).
- [48] D. Lopatik, D. Marinov, O. Guaitella, A. Rousseau, J. Röpcke, "On the reactivity of plasma treated photo-catalytic TiO<sub>2</sub> surfaces for oxidation of C<sub>2</sub>H<sub>2</sub> and CO", *submitted to J. Phys. D: Appl. Phys.*, (2013).
- [49] E.M. Van Veldhuizen, *Electrical Discharges for Environmental Purposes. Fundamentals and Applications* (NOVA Science Publishers), (2000).
- [50] B. Penetrante, *Non-Thermal Plasma Techniques for Pollution Control* ed S. Schultheis *NATO ASI Series G34* parts A and B, (1993).
- [51] T. Yamamoto, *J. Electrostatics* **42**, 227 (1997).
- [52] E. Filimonova, R. Amirov, H. Kim, I. Park, *J. Phys. D: Appl. Phys.* **33**, 1716 (2000).

- [53] J. Mc Adams, *J. Phys. D: Appl. Phys.* **34**, 2810 (2001).
- [54] E. Filimonova, Y-H. Kim, S. Hong, S-Y. Han, Y-H. Song, *Proc. 15th Int. Symp. Plasma Chem.* (Orléans) 3041 (2001).
- [55] F. Thevenet, O. Guaitella, E. Puzenat, C. Guillard, J-M. Herrmann, A. Rousseau, *Catal. Today* **122**, 186 (2007).
- [56] M. Kogoma, Y. Miki, K. Tanaka, K. Takahashi, *Plasma Process. Polym.* **3**, 727 (2006).
- [57] A. Rousseau, O. Guaitella, J. Röpkcke, L.V. Gatilova, Y.A. Tolmachev, *Appl. Phys. Lett.* **85**, 2199 (2004).
- [58] A. Rousseau, L.V. Gatilova, O. Guaitella, C. Guillard, F. Thevenet, J. Röpkcke, G. Stancu, *Appl. Phys. Lett.* **87**, 221501 (2005).
- [59] A. Rousseau, A.V. Meshchanov, J. Röpkcke, *Appl. Phys. Lett.* **88**, 021503 (2006).
- [60] O. Guaitella, F. Thevenet, C. Guillard, A. Rousseau, *J. Phys. D: Appl. Phys.* **39**, 2964 (2006).
- [61] H.H. Kim, J.H. Kim, A. Ogata, *J. Phys. D: Appl. Phys.* **42**, 135210 (2009).
- [62] R.A.B. Zijlmans, S. Welzel, O. Gabriel, G. Yagci, J.H. van Helden, J. Röpkcke, D.C. Schram, R. Engeln, *J. Phys. D: Appl. Phys.* **43**, 115204 (2010).
- [63] D. Marinov, O. Guaitella, A. Rousseau, Y. Ionikh, *J. Phys. D: Appl. Phys.* **43**, 115203 (2010).
- [64] O. Guaitella, M. Hübner, S. Welzel, D. Marinov, J. Röpkcke, A. Rousseau, *Plasma Sources Sci. Technol.* **19**, 045026 (2010).
- [65] O. Guaitella, M. Hübner, D. Marinov, V. Guerra, C.D. Pintassilgo, S. Welzel, J. Röpkcke, A. Rousseau, *Contrib. Plasma Phys.* **51**, 176 (2011).
- [66] F. Thevenet, O. Guaitella, C. Guillard, E. Puzenat, G. Stancu, J. Röpkcke, A. Rousseau, *Int. J. Plasma Environ. Sci. Techn.* **1**, 52 (2007),.
- [67] H.-H. Kim, A. Ogata, M. Schiorlin, E. Marotta, C. Paradisi, *Catal. Lett.*, **141**, 277 (2011).
- [68] O. Guaitella, C. Lazzaroni, D. Marinov, A. Rousseau, *Appl. Phys. Lett.*, **97**, 011502 (2010).
- [69] D. Marinov, PhD Thesis, Ecole Polytechnique Palaiseau, France, 2012.

- [70] Z. Qu ,G. Kroes, *J. Phys. Chem. B*, **110**, 23306 (2006).
- [71] M. Rutigliano, C. Zazza, N. Sanna, A. Pieretti, G. Mancini, V. Barone, M. Cacciatore, *J. Phys. Chem. A*, **113**, 15366 (2009).
- [72] D. Hurum, A. Agrios, K. Gray, T. Rajh, M. Thurnauer, *J. Phys. Chem. B* **107**, 4545 (2003).
- [73] S. Loganathan, F. Thevenet, P. Gravejat, and A. Rousseau, in *International Workshop on Plasma Spectroscopy*, Giens, France 2012, Conf. Proc.
- [74] T. Ohno, K. Sarukawa, K. Tokieda, M. Matsumura, *J. Catal.*, **203**, 82 (2001).
- [75] D. Regonini, A. Jaroenworarluck, R. Stevens, C.R. Bowen, *Surf. Interface Anal.* **42**, 139 (2010).
- [76] A.L. Linsebigler, L. Guangquan, J.T. Yates, *Chem. Rev.* **95** (3), 735 (1995).
- [77] S.S. Tan, L. Zou, E. Hu, *Catalysis Today* **115**, 269 (2006).
- [78] J. Peeters, W. Boullart, I. Langhans, *Int. J. Chem. Kin.*, **26**, 869 (1994).

## 7 Application potential of EC-QCLs for plasma diagnostics

Three continuous wave external cavity quantum cascade lasers (EC-QCLs) operating between  $1305$  and  $2260\text{ cm}^{-1}$  ( $4.42 - 7.66\text{ }\mu\text{m}$ ) have been tested as radiation sources for an absorption spectrometer focused on the analysis of physical and chemical phenomena in molecular plasmas. Based on the wide spectral tunability of EC-QCLs multiple species detection has become feasible and is demonstrated in a study of low pressure Ar/N<sub>2</sub> microwave plasmas containing methane as hydrocarbon precursor. Using the direct absorption technique, the evolution of the concentrations of CH<sub>4</sub>, C<sub>2</sub>H<sub>2</sub>, HCN and H<sub>2</sub>O has been monitored depending on the discharge conditions at a pressure of  $p=0.5\text{ mbar}$  and at a frequency of  $f=2.45\text{ GHz}$  in a planar microwave plasma reactor. The concentrations were found to be in the range of  $10^{11} - 10^{14}\text{ molecules cm}^{-3}$ . In addition, based on the analysis of the line profile of selected absorption lines, the gas temperature  $T_g$  has been calculated in dependence on the discharge power.  $T_g$  increased with the power values and was in the range between  $400$  and  $700\text{ K}$ . Further, in a pure He/Ar microwave plasma the wavelength modulation spectroscopy technique has been applied for the sensitive detection of transient plasma species with absorbencies down to  $10^{-5}$ . The typical spectral line width of an EC-QCL under the study was found to be in the range  $24$  or  $38\text{ MHz}$  depending (i) on the used chopping technique and (ii) on a single or averaged measurement approach. Further different methods for the modulation and tuning of the laser radiation have been tested. Varying the power values of an EC-QCL between  $0.1$  to  $154\text{ mW}$  for direct absorption measurements at low pressure conditions no saturation effects in determining the concentrations of methane, acetylene and carbon monoxide could be found under the used experimental conditions, i.e. for lines with line strengths between  $10^{-19}$  to  $10^{-22}\text{ cm molecule}^{-1}$  [1].

## 7.1 Introduction

Molecular plasmas are increasingly being used not only for basic research but also, due to their favorable properties, for materials processing technology. While offering a wide field of applications however for this type of plasmas a number of processes and properties are far from being fully understood. Therefore, the analysis of important plasma parameters, for example, the concentration measurement of molecular precursors, the monitoring of reaction products and the determination of the gas temperature can lead to a better understanding of plasma chemistry and reaction kinetics. In addition, the detection of low molecular weight transient species, as radicals and molecular ions, is of key importance, because they govern most of the chemical and kinetic processes in plasmas. Over the last two decades chemical sensing using mid infrared laser absorption spectroscopy (MIR-LAS) in the molecular fingerprint region from 3 to 20  $\mu\text{m}$  has been established as a powerful *in-situ* diagnostic tool for molecular plasmas [2-6]. The methods of MIR-LAS provide a means to measure molecular species concentrations in the ground state and the temperature of reactive species.

It is well known, that the application of high-resolved spectroscopic methods requires from the radiation source (i) wide spectral tunability, (ii) intrinsic narrow line width, and (iii) high output powers. Based on these attractive properties, EC-QCLs have a high potential to be applied for plasma diagnostic purposes, in particular for the monitoring of multiple species including larger plasma constituents characterized by broader spectral features.

In the present study three cw EC-QCLs operating between 1305 and 2260  $\text{cm}^{-1}$  (4.42 – 7.66  $\mu\text{m}$ ) have been tested as radiation sources for an absorption spectrometer focused on the analysis of physical and chemical phenomena in molecular plasmas. Multiple species detection has been feasible in low pressure Ar/N<sub>2</sub> microwave (MW) plasmas containing methane as hydrocarbon precursor. Using the direct absorption technique the evolution of the concentrations of CH<sub>4</sub>, C<sub>2</sub>H<sub>2</sub>, HCN and H<sub>2</sub>O have been monitored depending on the discharge conditions. In addition, based on the analysis of the line profile of selected absorption lines, the neutral gas temperature  $T_g$  has been calculated in dependence on the discharge power. Further, in a pure He/Ar microwave plasma the wavelength modulation spectroscopy technique (WMS) has been applied for the sensitive detection of transient plasma species. Different methods for the modulation, tuning and mechanical and acousto-optical chopping of the laser radiation have been tested. Another focus was the analysis of possible saturation effects caused by the high power values of the lasers in low pressure conditions.

## 7.2 Experimental

The EC-QCLs were purchased from Daylight Solutions. In table 6.1 the main parameters of the three lasers are given. The result of a first most simple experiment is shown in figure 6.1. The laser controller scans the laser No. 2 over the entire wavenumber range by turning the grating inside the laser head via a step motor. Such a wide scan takes in dependence on the tuning rate and the specific laser between 20 to 40 s. The transmitted intensity after a path length of 1 m in laboratory air shows strong absorption feature mainly due to water in the laboratory air, figure 6.1. The intensities and positions are in good general agreement with the data of the HITRAN spectral catalogue [7], see lower part of the figure. In addition to the detected absorption features a considerable fringe level of up to 10% of the entire laser intensity, an obvious inherent property of the used EC-QCLs, can be seen. The fringe level depends on the specific spectral position and might be influenced by the optical characteristics of internal antireflection coatings.

The applicability of EC-QCL for plasma diagnostics has been approved using two different experimental setups, (i) a flexible experimental configuration for the more detailed evaluation of the distinct laser properties (figure 6.2) and (ii) a 3 channel spectrometer in combination with a planar microwave (MW) plasma reactor (figure 6.4). The experimental setups consist of three main parts: the laser system, the investigated gas volume, and the detection and acquisition systems.

**Table 6.1:** *Parameters of the used cw EC-QCLs, given by the provider, and experimentally determined laser line width (MHF – mode hop free).*

Laser No.	Model	T [°C]	I [mA]	P <sub>max</sub> [mW]	Full Tuning Range [cm <sup>-1</sup> ]	MHF Tuning Range [cm <sup>-1</sup> ]	ν <sub>Instr.</sub> [MHz]
1	21074-MHF	15	650	150	1305-1445	1325-1415	38
2	21062-MHF	16	675	85	1594-1690	1628-1679	24
3	21045-MHF	17.8	675	300	2110-2260	2118-2165	35

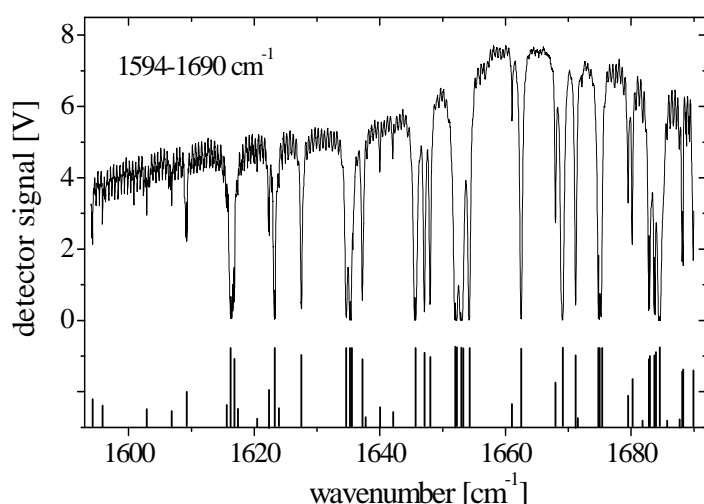
### 7.2.1 EC-QCL test setup

Figure 6.2 shows the principal arrangement of the EC-QCL test set-up. The laser is driven using a laser controller (Daylight Solutions, Model 1001-TLC) connected to a PC using the RS-232 interface. The alignment of the optical arrangement is performed by a He-Ne laser using a moveable mirror. The temperature of the laser chip is controlled by a thermoelectric cooling unit (TEC) integrated in the system. The cw operation mode requires

an additional external water cooler (Thermo Cube, Solid State Cooling System), not shown. In addition to the step motor control of the position of the internal EC grating with a minimum step width of  $0.01\text{ cm}^{-1}$ , finer wavelength tuning can be achieved using a piezoelectric transducer (PZT) attached to the EC grating in the range of  $1 - 2\text{ cm}^{-1}$  at frequencies of up to 100 Hz. In the present study the PZT was driven by an external driver (Thorlabs Single Channel Piezo Controller Model MDT694A). Further, the current of the QCL can be directly modulated in the frequency range between 10 kHz and 2 MHz by an external voltage source leading to a wavelengths modulation of up to  $0.1\text{ cm}^{-1}$ . This method has been used for wavelength modulation spectroscopy (WMS) focused on the sensitive detection of transient species, see sub-chapter 7.3.4. It should be noted, that both tuning methods can be used separately as well as simultaneously.

A stable operation of cw MHF EC-QCLs at short pulse lengths, e.g. in ms scale, is not feasible caused by the very narrow mode spacing [8]. A reliable concentration determination using the Beer-Lambert law requires measuring the relative radiation fluxes entering and leaving the absorbing gas or plasma column. This needs to monitor also the detector signal without any radiation, i.e. in an off-phase. Therefore, a periodical interruption of the laser radiation has to be provided. For this purpose three different methods of chopping the laser radiation have been tested, (i) a mechanical chopper (SR 540, Stanford Research), (ii) a mechanical shutter (FOS-1-Inline, Aventes) and (iii) an acousto-optical modulator (AOM) (GEM-40-4-10.6-BRAR (5-11), Brimrose).

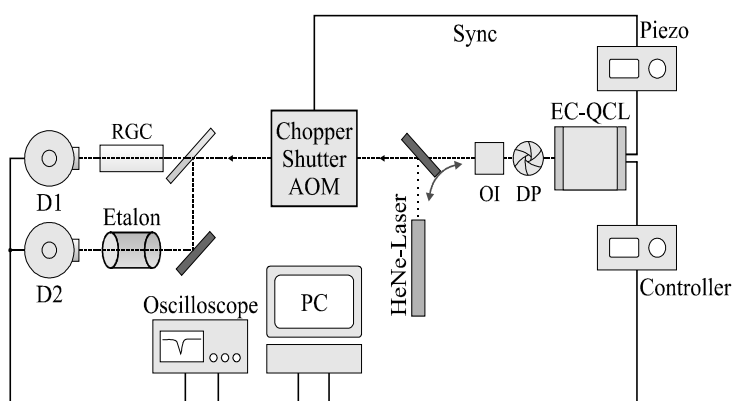
As shown in figure 6.2, the infrared laser beam from the EC-QCL with a diameter of about 0.5 cm passes a diaphragm and an optical isolator, consisting of a polarizer and a  $\lambda/4$  wave plate, before reaching the chopper, which can be replaced by the shutter or the AOM, and a ZnSe beam splitter. One beam is directed through the reference gas cell and the second one through one inch Ge etalon with a free spectral range (FSR) of about  $0.049\text{ cm}^{-1}$  for identification of the spectral position with high precision. A He-Ne laser combined with a moveable mirror can be used for alignment. The two HgCdTe infrared detectors (InfraRed Associates FTIR-16-1.0) are mounted in a liquid nitrogen dewar. The absorption signals of the detector are amplified and transferred to an oscilloscope and PC system. The data acquisition is provided by an AD converter card with a sampling rate of 2.5 MHz (National Instruments, NI PCI-6110).

**Figure 6.1:**

Transmitted intensity after a path length of 1 m in laboratory air showing a spectrum of water between 1594 and 1690  $\text{cm}^{-1}$  obtained by full tuning range scanning with the laser controller using laser No. 2 with step motor tuning. In the lower part line positions and relative intensities of water from the HITRAN data base are shown [1, 7].

**Figure 6.2:**

Principal arrangement of the EC-QCL test setup. (D1, D2: HgCdTe detectors, AOM: acousto-optical modulator, RGC: reference gas cell, DP: iris diaphragm, OI: optical isolator) [1].



The operation of the mechanical shutter and the AOM has been directly controlled and synchronized by the PC. The working frequency of the shutter was limited to 10 Hz, while the AOM could work at frequencies of up to 3.6 MHz. In the case the chopper was used, this element acted as trigger source for the PZT control with a maximal frequency of 100 Hz.

An example of a spectrum by using the AOM for chopping the laser radiation at a frequency of 5 kHz while tuning laser No. 3 over its entire wavenumber range is given in figure 6.3. The radiation passed a reference gas cell containing CO at a pressure of 0.05 mbar.

The relative intensities of the CO lines are given in the lower part of the figure. The inset shows a single line as part of the whole spectrum. Again as in case of laser No. 2, the high level of fringes should be noted here. In addition, in this configuration the usage of the optical isolator was very important to avoid back reflections of laser radiation into the EC-QCL from any optical element, because this would lead to serious instabilities, in particular to the appearance of mode hops.

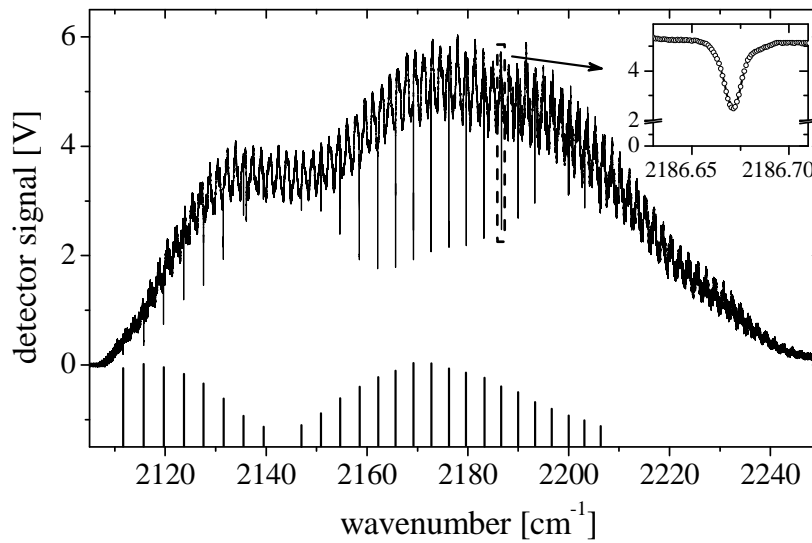


**Figure 6.3:** Spectrum of laser No. 3 using step motor tuning and an AOM for chopping the laser radiation at a frequency of 5 kHz. The radiation passed through a reference gas cell containing CO at a pressure of 0.05 mbar,  $l = 10$  cm. Line positions and relative intensities of CO are shown in the lower part of the diagram [7]. Inset: representative single CO line [1].

### 7.2.2 Three channel EC-QCL spectrometer and MW plasma reactor

The applicability of EC-QCLs for plasma diagnostics purposes has been tested by using a three channel absorption spectrometer combined with a planar microwave (MW) plasma source ( $f = 2.45$  GHz). Inside the MW plasma source an optical multi pass arrangement of White cell type (Gemini Scientific Instr.) has been installed providing absorption lengths of up to 30 m for high sensitivity detection [9]. As an advantage the discharge configurations in the planar MW plasma created in the reactor is well suited for spectroscopic observations, because plasma homogeneity can be achieved to a certain extent for these long plasmas. For more details see [10].

By ZnSe beam splitters the laser radiation is distributed into the 3 channels:

- (1) *Channel 1 (Measurement channel).* The beam enters the plasma chamber.
- (2) *Channel 2 (Reference channel).* The laser radiation passes a cell filled with a reference gas.
- (3) *Channel 3 (Etalon channel).* The laser radiation is guided through a 1 or 3 inch Ge etalon (FSR:  $0.049$  or  $0.016$   $\text{cm}^{-1}$ , respectively) or an air spaced etalon (FSR:  $0.01$   $\text{cm}^{-1}$ ).

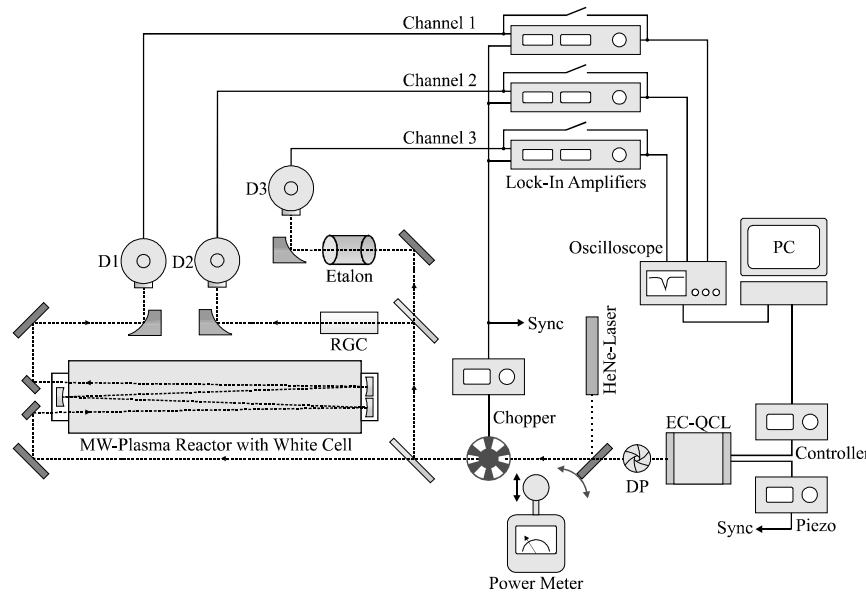


**Figure 6.4:** Schematic arrangement of the 3-channel EC-QCL spectrometer in combination with a planar microwave (MW) plasma reactor equipped with an optical multi pass configuration of the White cell type [10, 11]. (D1, D2, D3: HgCdTe detectors, RGC: reference gas cell, DP: iris diaphragm) [1].

The schematic setup of the 3-channel EC-QCL spectrometer is shown in figure 6.4. The infrared beam is guided using gold-coated mirrors. The output laser radiation is controlled using an iris placed in front of the laser head. The power of the laser radiation has been measured with a laser energy monitor (NOVA, Ophir Optonics Ltd.) behind the diaphragm. For chopping the laser radiation a mechanical chopper (SR 540, Stanford Research) has been used.

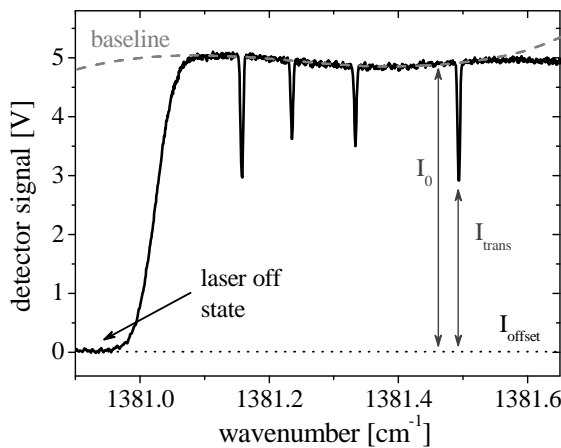


**Figure 6.5:** Transmission spectrum of CH<sub>4</sub> at a pressure value of  $p = 0.05$  mbar at an absorption length of  $l = 30$  m using laser No. 1 recorded with TDL Wintel [12] in the MW reactor. The detector offset signal  $I_{\text{offset}}$  (dotted line) was recorded in the off-phase. The calibration was performed using a 3 inch Ge etalon (FSR:  $0.016 \text{ cm}^{-1}$ ) [1].

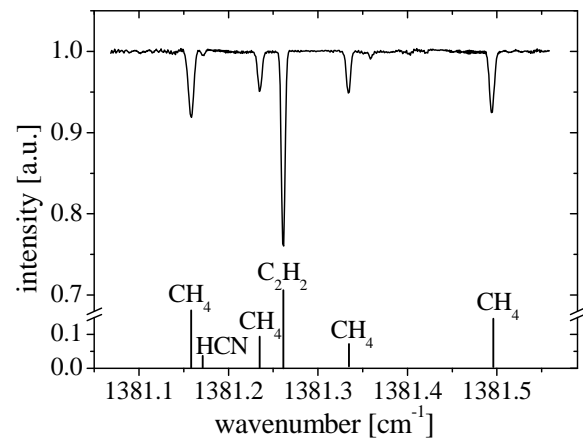


**Figure 6.6:** Example of an absorption spectrum in an Ar/N<sub>2</sub>/CH<sub>4</sub> MW plasma using laser No. 1 at  $p = 0.5$  mbar and  $P = 0.2$  kW showing absorption lines of CH<sub>4</sub>, C<sub>2</sub>H<sub>2</sub> and HCN at an absorption length of  $l = 30$  m in the MW reactor [1].

In the measurement channel the beam enters the plasma chamber via a KBr window and is focused into the White multi pass cell with 20 passes, corresponding to an optical path length of 30 m inside the reactor volume. Every channel is equipped with one AC coupled liquid-nitrogen-cooled HgCdTe detector unit combined with a pre-amplifier (InfraRed Associates FTIR-16-1.0). Because of the small sensitive detector area of about  $1 \text{ mm}^2$  the collimated laser radiation is focused using off-axis parabolic mirrors. Wedged beam combiners and windows are used to avoid unwanted etalon effects in the entire optical arrangement.

For direct spectroscopic studies the signal output from the detector is monitored using an oscilloscope (Tektronix TSX6005) in combination with an AD converter card with a sampling rate of 2.5 MHz (National Instruments, NI PCI-6110) and recorded at the PC employing the software TDL Wintel (Aerodyne Research Inc.) [13]. Recorded transmission spectra, an example using laser No. 1 is shown in figure 6.5, are transformed to absorbance spectra by extrapolating the base line  $I_0$  of each absorption line by a polynomial of appropriate order and calculating the absorbance by:

$$A = \ln \left( \frac{I_0 - I_{\text{offset}}}{I_{\text{trans}} - I_{\text{offset}}} \right) \quad (6.1)$$

In figure 6.6 an example of an absorption spectrum of an Ar/N<sub>2</sub>/CH<sub>4</sub> MW plasma at pressure of  $p = 0.5 \text{ mbar}$  and power of  $P = 0.2 \text{ kW}$  using laser No. 1 is presented showing absorption lines of the precursor CH<sub>4</sub> and the plasma chemical reaction products C<sub>2</sub>H<sub>2</sub> and HCN at an absorption length of  $l = 30 \text{ m}$  in the MW reactor.

The wavelength modulation spectroscopy technique (WMS) providing a phase sensitive detection with high signal to noise ratios has been focused on the detection of the HeAr<sup>+</sup> ion and for the exact determination of the spectral position of the detected absorption lines of this transient species. These measurements have been performed in pure He/Ar MW plasmas. Based on a study of Dahl, the MW discharge was ignited in a feed gas consisting of He (99.9999% purity) with 3% Ar admixture at a typical gas pressure of  $p = 0.266 \text{ mbar}$  and a power of  $P = 2.7 \text{ kW}$  [11].

The WMS was performed by slowly changing the emission wavelength of the EC-QCL using the PZT modulation at a frequency of 0.02 Hz while simultaneously modulating the injection current of the laser at a frequency of 50 kHz with an amplitude of 1 V, what caused a wavelength modulation of about  $10^{-3} \text{ cm}^{-1}$ . Using 3 parallel lock-in-amplifiers (Stanford

Research Systems SR830) the detected signals are demodulated at the second harmonic to the corresponding absorption spectra. The time constant of the lock-in amplifiers was set to 300 ms. Spectra are recorded synchronously with calibration gas lines of C<sub>2</sub>H<sub>4</sub>. A vacuum spaced etalon (FSR:  $\sim 0.01 \text{ cm}^{-1}$ ) was used for interpolating between absorption features of transient species and calibration lines. The estimated accuracy of the measurement of the line position was about  $0.0005 \text{ cm}^{-1}$ .

## 7.3 Results and discussions

### 7.3.1 Laser line width determination

The spectral line width, or instrumental profile, of the used EC-QCLs,  $\nu_{\text{Instr.}}$ , has been determined using a Doppler limited approach by passing the radiation through reference gas cells of appropriate molecular gas content. The pressure was chosen as low as possible to avoid pressure broadening effects. The detected absorption lines were fitted by Gaussian profiles. Subsequently the value of the full width half maximum (FWHM) of the fit,  $\nu_{\text{Fit}}$ , has been de-convoluted with the Doppler broadening of the probe gas,  $\nu_D$ , at room temperature:

$$\nu_{\text{Instr.}} = \sqrt{\nu_{\text{Fit}}^2 - \nu_D^2} \quad (6.2)$$

The Doppler broadening has been calculated by the formula:

$$\nu_D = \frac{2\nu_0}{c} \sqrt{2k_B N_A \ln 2 \frac{T}{M}} \quad (6.3)$$

where the Boltzmann constant  $k = 1.3806503 \times 10^{-23} \text{ J}\cdot\text{K}^{-1}$ , the Avogadro constant  $N_A = 6.02214129 \times 10^{23} \text{ mol}^{-1}$ ,  $T$  – temperature in K,  $M$  is the molar mass in  $\text{g mol}^{-1}$ ,  $\nu_D$  is the FWHM of the spectral line, and  $\nu_0$  is the wavenumber of the line center [14].

Figure 6.7 shows results of a study at the example of laser No. 2 at a spectral position of about  $1627 \text{ cm}^{-1}$ . The measurements were performed using a cell of 15 cm length filled with NO<sub>2</sub> at a pressure of  $p = 0.09 \text{ mbar}$ , while applying the three different chopping techniques. To improve the accuracy of the procedure four narrow spaced lines were analyzed.

In sub-diagram (a) of figure 6.7 the values of the instrumental profile,  $\nu_{\text{Instr.}}$ , for a single scan of the PZT over a spectral range of about  $0.1 \text{ cm}^{-1}$  are shown. For the interruption of the laser radiation, the AOM was driven at a frequency of 100 Hz and the shutter at 10 Hz, both

controlled by the PC. In contrast, the chopper acted as trigger source for the PZT at a frequency of 80 Hz. The single values of  $\nu_{\text{Instr.}}$  deviate within the errors of the measurement quite essentially, i.e. in the range of about 30 MHz, from each other. This is mainly caused by the high sensitivity of the fit procedure on optical fringes, which influence the baseline determination and could not be completely avoided in the measurement. The measurements at the spectral position of  $1627.118 \text{ cm}^{-1}$  showed relatively strong deviations and in the cases of AOM and shutter usage unrealistic low values of  $\nu_{\text{Instr.}}$ . The reasons for this behavior are not completely clear, but may be even partly caused by a sensitive overlap of optical fringes and single absorption features.

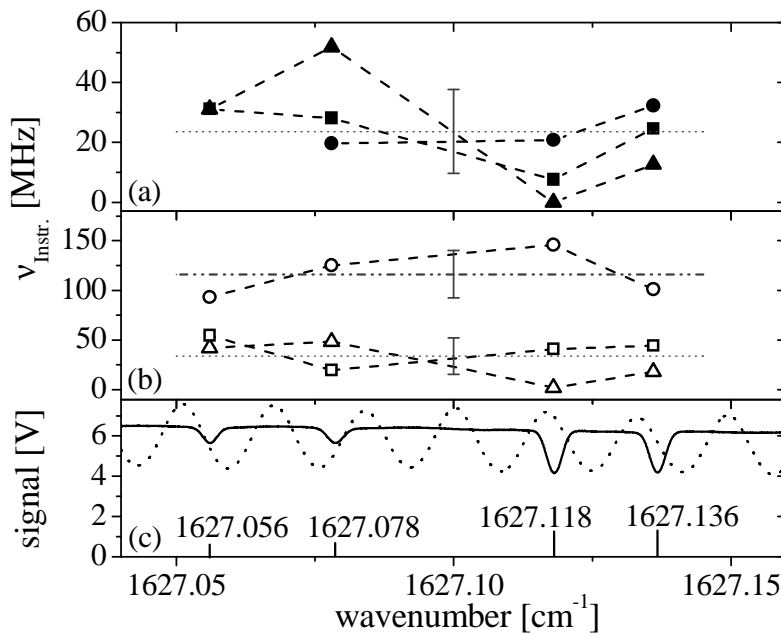


**Figure 6.7:** Determination of the laser line width of laser No. 2 from  $\text{NO}_2$  absorption lines using different chopping techniques. (a) Laser line width calculated from single measurements: ▲ – AOM, ■ – shutter, ● – chopper; (b) Laser line width calculated from 256 averaged measurements: Δ – AOM, □ – shutter, ○ – chopper; (c)  $\text{NO}_2$  absorption spectrum at  $1627 \text{ cm}^{-1}$  measured in a reference gas cell ( $l= 15 \text{ cm}$ ,  $p= 0.09 \text{ mbar}$ ) with etalon signal for calibration ( $\text{FSR: } 0.049 \text{ cm}^{-1}$ ) and the line positions from the HITRAN data base plotted as a stick spectrum in the lower part of the figure [1, 7].

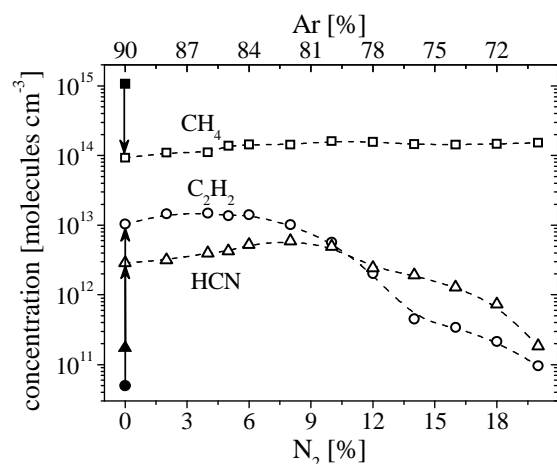
The averaged value for  $\nu_{\text{Instr.}}$  was found to be 24 MHz, what is in good coincidence with values from the literature [15, 16]. To achieve a better signal to noise ratio an averaging of several spectral scans seems to be worthwhile. In the case of the AOM and shutter usage, the values of the instrumental profiles are near to the single measurements, see sub-diagram (b) of

figure 6.7. The averaged value is found to be 33 MHz. Only if the spectral scans are performed using the chopper for radiation interruption the averaging has led to a much wider instrumental profile of about 118 MHz. This effect is caused by frequency fluctuations of the chopper blade rotation, which directly influences the frequency of the PZT control and therefore the scanned spectrum, see upper curve in sub-diagram (b).

### 7.3.2 *Evolution of molecular concentrations and of the gas temperature in Ar/N<sub>2</sub>/CH<sub>4</sub> MW plasmas*

The plasma chemical study of the methane fragmentation in the Ar/N<sub>2</sub> MW plasma has been performed (i) for a changed ratio of the Ar/N<sub>2</sub> mixture at a fixed value of CH<sub>4</sub> admixture at constant power and pressure and (ii) for changing the power at a fixed gas mixture at constant pressure. Laser No. 1 has been used. In figures 6.8 – 6.9 the experimental result of the evolution of molecular concentrations of the precursor molecule CH<sub>4</sub> and of selected reaction products, as HCN, C<sub>2</sub>H<sub>2</sub> and H<sub>2</sub>O are given. Some useful generalizations follow from these figures. The concentrations of the plasma chemical products, HCN, C<sub>2</sub>H<sub>2</sub> and H<sub>2</sub>O, were found to be in the range of about  $10^{11} - 10^{14}$  molecules cm<sup>-3</sup>. The concentration of the precursor molecule methane depends only slightly on the nitrogen content of the plasma, while strongly decreases with increasing power.

Figure 6.8 shows the variation of the concentration of CH<sub>4</sub> with increasing admixture of N<sub>2</sub> to the Ar/CH<sub>4</sub> plasma. It has been also possible to detect C<sub>2</sub>H<sub>2</sub> and HCN molecules but only at a relatively small admixture of N<sub>2</sub> of up to 20%. The concentration of these molecules decreased as more nitrogen was introduced. The detection limit was found at about  $5 \times 10^{10}$  molecules cm<sup>-3</sup> for C<sub>2</sub>H<sub>2</sub> and  $2 \times 10^{11}$  molecules cm<sup>-3</sup> for HCN. The initial measured concentration of CH<sub>4</sub> at the value of  $1.13 \times 10^{15}$  molecules cm<sup>-3</sup> was in a good agreement with calculated theoretical value of  $1.22 \times 10^{15}$  molecules cm<sup>-3</sup> corresponding to 10% methane admixture. The degree of dissociation of methane was found to be relatively constant near to 90 %. In contrast, increasing power values, varied between 0.2 and 1.0 kW, lead to an essentially increasing degree of dissociation of CH<sub>4</sub> of up to 97% at  $P = 1$  kW, shown in figure 6.9.



**Figure 6.8:** The variation of concentrations of the precursor gas  $\text{CH}_4$  (■, □) and reaction products  $\text{C}_2\text{H}_2$  (●, ○) and  $\text{HCN}$  (▲, Δ) simultaneously measured as a function of gas mixture at  $p = 0.5$  mbar and  $P = 0.2$  kW in the MW discharge. The arrows demonstrate the concentration values before igniting the discharge. Laser No. 1 has been used [1].

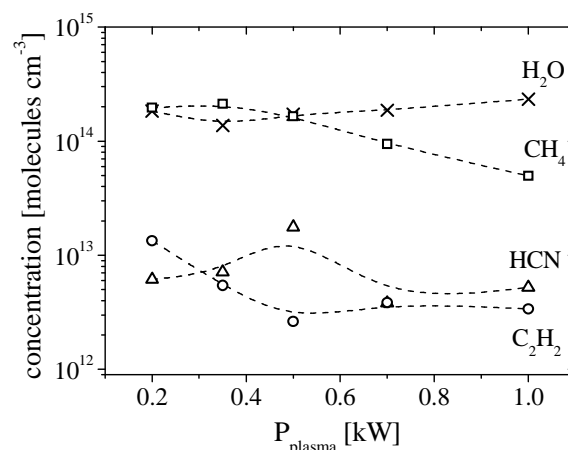


**Figure 6.9:** The concentration of 4 molecules  $\text{CH}_4$  (□),  $\text{C}_2\text{H}_2$  (○),  $\text{HCN}$  (Δ) and  $\text{H}_2\text{O}$  (x) simultaneously detected in a MW plasma depending on the applied plasma power for initial gas mixture of 5%  $\text{N}_2$  + 10%  $\text{CH}_4$  diluted in Ar at pressure of  $p = 0.5$  mbar. Laser No. 1 has been used [1].

In a plasma the knowledge of the gas temperature is a key to an improved understanding of volume and surface plasma chemistry since the rates of elementary processes depend exponentially on its value. For deriving the relative or absolute concentrations of molecules the temperature must be known as well.

In the present study the temperature of the plasma was deduced from the Doppler widths of four  $\text{CH}_4$  spectral lines detected in the area of  $1381 \text{ cm}^{-1}$  using the cw EC-QCL No. 1 as radiation source in the MW discharge. The line shapes were fitted and de-convoluted as described in sub-chapter 7.3.1. As a typical example, figure 6.10 shows experimental data of an absorption line of  $\text{CH}_4$  at  $1381.494 \text{ cm}^{-1}$  together with a Gaussian fit for the temperature determination. The line was recorded in a microwave discharge at  $P = 0.2$  kW in a gas mixture of 10%  $\text{N}_2$  + 10%  $\text{CH}_4$  diluted in Ar at  $p = 0.5$  mbar. Figure 6.11 depicts the increase of the gas temperature with the applied power from about 400 to 700 K in the MW discharge.

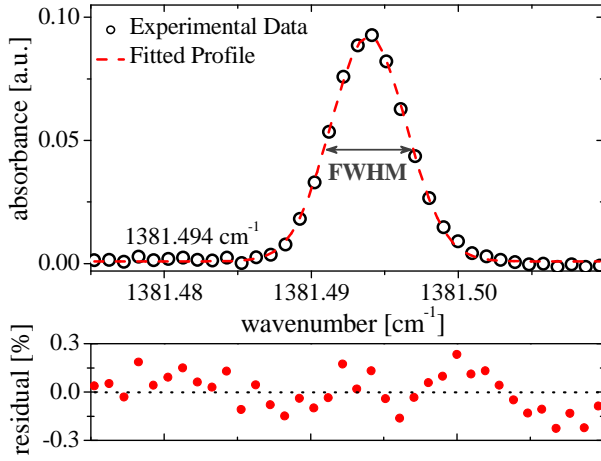


**Figure 6.10:** Experimental data of an absorption line of  $\text{CH}_4$  at  $1381.494 \text{ cm}^{-1}$  together with a Gaussian fit for temperature determination. The line was recorded in a microwave discharge at  $P = 0.2 \text{ kW}$  in a gas mixture of  $10\% \text{ N}_2 + 10\% \text{ CH}_4$  diluted in Ar at  $p = 0.5 \text{ mbar}$  [1].

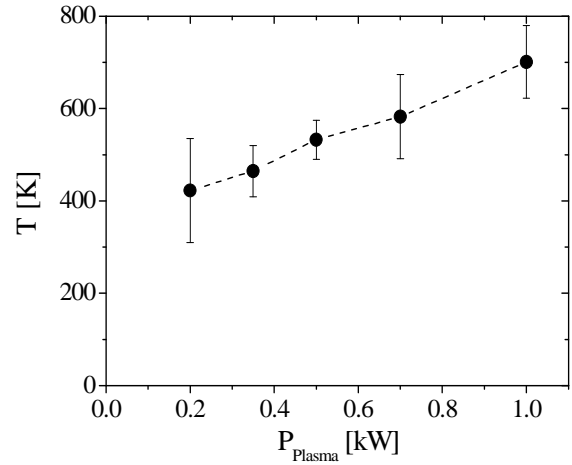


**Figure 6.11:** Gas temperatures as a function of plasma power calculated from line profiles. Measurements were performed in a gas mixture of  $10\% \text{ N}_2 + 10\% \text{ CH}_4$  diluted in Ar at  $p = 0.5 \text{ mbar}$ . The instrumental profile used for calculation was  $0.00127 \text{ cm}^{-1}$  ( $38.1 \text{ MHz}$ ) [1].

### 7.3.3 Laser power variation for validation of concentration measurements

Continuous wave EC-QCLs are characterized by high output power, which in dependence on the specific laser can reach values of up to  $300 \text{ mW}$ , see table 6.1. In particular under low pressure gas and plasma conditions reduced relaxation rates,  $\gamma$ , of rotational-vibrational molecular levels appear compared to conditions under atmospheric pressure. In case the laser intensity and therefore the electric field amplitude are sufficiently high power saturation effects may occur, which can lead to incorrect concentration measurements. This non-linear phenomenon is notable for the transfer of a substantial population between the lower and the upper energy level with the dipole moment  $\mu$ . It is described in [17] by:

$$\Sigma = \frac{\mu E_0}{h\gamma} \quad (6.4)$$

where  $\Sigma$  is the saturation parameter, describing the power saturation effect,  $E_0$  is the electric field amplitude and  $h$  is Planck's constant.

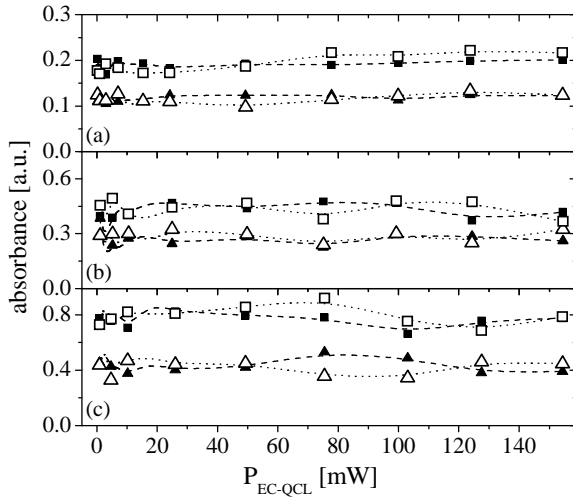


**Figure 6.12:** Absorption of 4 lines of  $\text{CH}_4$  (■, □ –  $1381.158$  and  $1381.494 \text{ cm}^{-1}$ , ▲, △ –  $1381.236$  and  $1381.333 \text{ cm}^{-1}$ ) measured as a function of the power of the laser radiation at different experimental conditions:  
 (a) – reference gas cell,  $l = 15 \text{ cm}$ ,  $p = 3 \text{ mbar}$ ;  
 (b) – MW reactor,  $l = 30 \text{ m}$ ,  $p = 0.5 \text{ mbar}$ ,  $5\% \text{ CH}_4$  admixture in Ar;  
 (c) – MW reactor,  $l = 30 \text{ m}$ ,  $p = 0.05 \text{ mbar}$ , Laser No. 1 has been used [1].

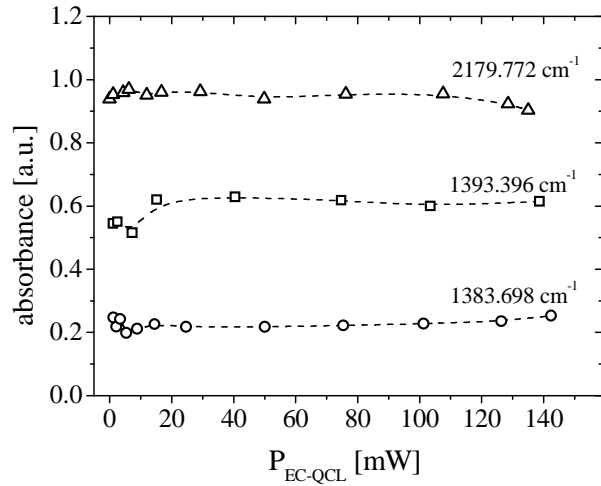


**Figure 6.13:** Absorbance of two lines of  $\text{C}_2\text{H}_2$  and one of CO measured as a function of the power of the laser radiation at different experimental conditions:  
 □ –  $1393.396 \text{ cm}^{-1}$ ,  $l = 15 \text{ cm}$ ,  $p = 5 \text{ mbar}$   $\text{C}_2\text{H}_2$ ,  
 ○ –  $1383.698 \text{ cm}^{-1}$ ,  $l = 24 \text{ m}$ ,  $p = 0.7 \text{ mbar}$   $1\% \text{ C}_2\text{H}_2$  in Ar, Laser No. 1 has been used.  
 △ –  $2179.772 \text{ cm}^{-1}$ ,  $l = 10 \text{ cm}$ ,  $p = 0.05 \text{ mbar}$  CO, Laser No. 3 has been used [1].

At low pressures the parameter  $\Sigma$  may exceed unity for strong absorption features, i.e. absorption lines with line strengths in the range of  $S \sim 10^{-20} \text{ cm molecule}^{-1}$ . According to pulsed QCLs this effect is rather known and has been described, e.g. see [18, 19] and references therein. In the present study lines with lines strength covering the range of  $10^{-19} - 10^{-22} \text{ cm molecule}^{-1}$  have been used.

For the validation of the correctness of concentration measurements the power of laser No. 1 has been varied, while detecting absorptions of  $\text{CH}_4$  and  $\text{C}_2\text{H}_2$  under low pressure conditions at pressure values of 0.05, 0.5 and 3 mbar at absorptions lengths of 15 cm in reference gas cells and of 30 m in the MW plasma reactor, respectively.

Figure 6.12 shows the absorbance values of four narrow  $\text{CH}_4$  lines at three different experimental conditions located in the spectral range of  $1381 \text{ cm}^{-1}$  using laser No. 1. The observed spectra were in good agreement with simulated spectra, generated using the HITRAN database [7]. In addition in the same spectral range two absorption lines of acetylene have been studied concerning possible saturation effects, shown in figure 6.13.

Although the power of the probing laser has been varied over more than two orders of magnitude no clear saturation effects have been detected so far in these experiments. To validate also the influence of pressure and absorption length, these parameters have been also changed in a wide scale without any notable influence. The line strengths of the used lines are in the range of  $10^{-21} - 10^{-22}$  cm molecule $^{-1}$ .

In addition to the relatively weak CH<sub>4</sub> and C<sub>2</sub>H<sub>2</sub> lines a CO absorption line at 2179.772 cm $^{-1}$ , line strength of  $4 \times 10^{-19}$  cm molecule $^{-1}$ , has been tested using laser No. 3 for possible saturation effects. Even at this strong absorbing line no saturation effect in dependence on the laser power could be observed, see figure 6.13.

### 7.3.4 Wavelength modulation spectroscopy in He/Ar plasmas

In figure 6.14 a typical example of WMS using laser No. 1 in a He MW discharge with 3% Ar admixture at a pressure of  $p = 0.265$  mbar and a power value of  $P = 2.7$  kW is shown.

The signals of the measurement, reference and etalon channels have been detected simultaneously. In sub-diagram (a) at the spectral position of 1410.639 cm $^{-1}$  a clear absorption feature of a transient species could be found. The sensitivity for detecting small absorptions can be estimated to be in the range of  $10^{-5}$ , what was proven by detecting lines of C<sub>2</sub>H<sub>4</sub> of very small absorptions (not shown).

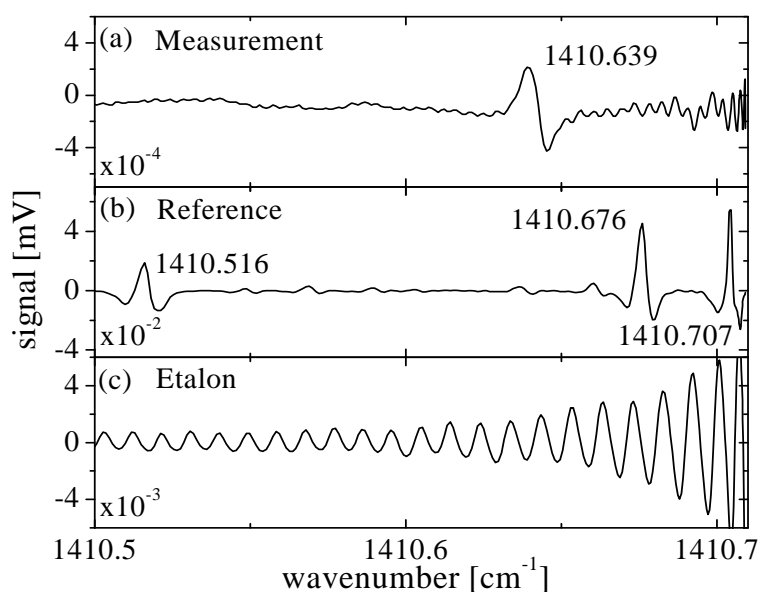


**Figure 6.14:** Example of WMS in a He MW discharge with 3% Ar admixture at  $p = 0.265$  mbar and  $P = 2.7$  kW, sub-diagram (a). The calibration of the wavenumber is based on absorption features of a C<sub>2</sub>H<sub>4</sub> reference gas cell, sub-diagram (b) and an air spaced etalon (FSR: 0.01 cm $^{-1}$ ), sub-diagram (c). Laser No. 1 has been used [1].

## 7.4 Summary and conclusions

In the present study cw EC-QCLs have been successfully tested as radiation sources for absorption spectrometer set-ups, which can be used as new tools for plasma diagnostics providing, based on its wide spectral tunability, an access to multiple species detection. The new aspects of this spectroscopic approach are demonstrated in low pressure Ar/N<sub>2</sub> microwave plasmas containing methane as hydrocarbon precursor. Using the direct absorption technique the evolution of the concentrations of the methane precursor and of three stable reaction products, C<sub>2</sub>H<sub>2</sub>, HCN and H<sub>2</sub>O, has been monitored. In addition, the line profiles of selected absorption lines have been analyzed to determine the neutral gas temperature  $T_g$  in dependence on the discharge power. As expected, the gas temperature was found to increase with power. Further, the feasibility of the wavelength modulation spectroscopy technique (WMS) using EC-QCLs has been demonstrated for the sensitive detection of transient plasma species. The typical spectral line width of an EC-QCL was found to be in good coincidence with values already reported in the literature. Unfortunately the cw EC-QCLs under the study cannot be driven in a pulsed mode. Therefore different methods for the modulation, tuning and chopping of the laser radiation have been tested. Common used chopping techniques based on mechanical elements are limited in frequency, while the usage of an AOM provides chopping frequencies up to the MHz region resulting in essentially improved signal to noise ratios. Varying the power values of an EC-QCL in a wide range at the used low pressure conditions no saturation effects could be found in the present study.

The used EC-QCLs are advantageously for multiple species detection, in case time resolution is not an issue. Tuning the laser just by the step motor over the entire spectral range the sensitivity suffers from relatively big fringes even in the mode hop free regions. Therefore the use of the PZT for tuning of small spectral windows, where the influence of these fringes is less disturbing, is one of the preferred working modes for plasma diagnostics. The high power values of up to several hundreds of mW simplifies on one hand several problems of former spectroscopic approaches of plasma diagnostics, but back reflection of light into the EC-QCL causes mode instabilities and must be avoided and possible non-linear effects should be considered. In general, for plasma diagnostics purposes EC-QCLs do not only provide multiple species detection useful for basic research. A further advantage is their compactness, which opens up a new potential for the development of spectrometers applicable for species monitoring and process control in industry.

## 8 Plasma chemistry in RF plasmas containing ATI

In Ar and Ar/N<sub>2</sub> RF plasmas with admixtures of aluminum tri-isopropoxide (ATI) the fragmentation of this metal-organic precursor has been studied by means of infrared absorption spectroscopy (IR-AS) using an external-cavity quantum cascade laser (EC-QCL) arrangement. The experiments were performed in an asymmetric capacitively coupled reactor at a frequency of  $f = 13.56$  MHz and a pressure of up to  $p = 10$  Pa. The discharge power was in the range of  $P = 40 - 100$  W. Using EC-QCLAS the evolution of the concentrations of six stable molecules, CH<sub>4</sub>, C<sub>2</sub>H<sub>2</sub>, C<sub>2</sub>H<sub>4</sub>, H<sub>2</sub>O, HCN and HNO<sub>3</sub>, has been monitored in the plasma. The concentrations of these plasma chemical products were found to be in the range of about  $7 \times 10^{12} - 2 \times 10^{14}$  molecules cm<sup>-3</sup> [20].

### 8.1 Introduction

Metal organic precursors are frequently used in plasma processes for the deposition of metal oxide layers. The advantage of these precursors is that they have a relatively low boiling point and, thus, they can easily be inserted into a plasma. Typical precursors for plasma-enhanced chemical vapor deposition (PECVD) include for example silane [21], hexamethyldisiloxane (HMDSO) [22, 23] and aluminum tri-isopropoxide (ATI). In contrast to silicon-based precursors, which have been widely studied in plasmas, only a few publications exist about the usage of aluminum-based precursors [24]. Already in the late 1960's Daasch *et al* made first investigations on ATI [25]. However, these investigations were not performed under plasma conditions. They used mass spectrometry to determine the components of hot ATI gas. One of their results was, that ATI consists of different types of

species with the formula  $(\text{Al}(\text{OC}_3\text{H}_7)_3)_x$ , where  $x$  ranges from 1 to 7. For illustration, in figure 8.1 the monomeric and tetrameric structure of ATI is shown. Solid ATI was studied by Folting *et al* in the 1990's [26] and by Turuva *et al* already in 1979 [27]. They carried out X-ray diffraction to determine crystal structure and bond lengths.

An important use of ATI is for the deposition of  $\text{Al}_x\text{O}_y$  layers in CVD processes [28]. For example, cutting tools are coated with  $\text{Al}_x\text{O}_y$  layers. These layers show high hardness, chemical resistance and low thermal conductivity, which is needed for high performance cutting applications [29]. Another example for alumina deposition is the use as diffusion barrier. These barriers are needed for the production of OLED devices to prevent permeation of  $\text{O}_2$  and  $\text{H}_2\text{O}$  through the flexible plastic substrates [30]. ATI also shows catalytic effects in chemical processes, for example for the co-polymerization of cyclohexene oxide with  $\text{CO}_2$  [31].

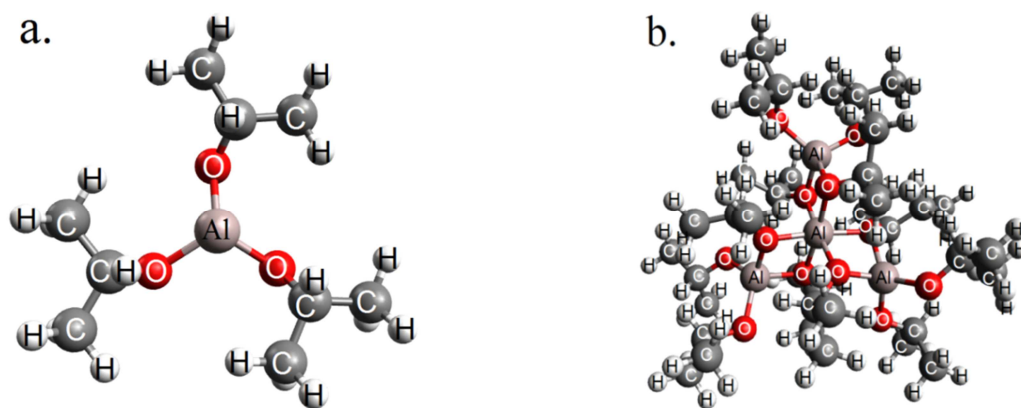


**Figure 8.1:** (a) Monomeric and (b) tetrameric ATI [20].

In the past properties of  $\text{Al}_x\text{O}_y$  layers have been studied using different methods. In the 1980's Saraie *et al* measured the deposition rate of  $\text{Al}_x\text{O}_y$  layers in CVD processes in dependence on the substrate temperature and on the source gas supply by multi-interference microscopy [32]. Huntz and co-workers made in situ investigations on growing layers using X-ray diffraction and scanning electron microscopy [33]. They also investigated the transformations occurring in  $\text{Al}_x\text{O}_y$  layers during heat-treatment. Long-term stability of the deposited alumina layers is an important issue. The investigations of Sovar *et al* showed that despite the ageing of ATI, it can be used principally for depositing stable  $\text{Al}_x\text{O}_y$  layers [34]. For high temperature applications also mixed structures were used. For example,  $\text{Al}_x\text{O}_y$  and  $\text{SiO}_x$  layers were deposited on polyimide composites for thermo-oxidative protection. These coatings improved the stability of polyimide composites at elevated temperatures [35].

Although ATI containing plasmas are used for deposition in PECVD processes [36] the chemical reactions are far from being completely understood in these plasmas. In discharges containing ATI for an analysis of chemical phenomena information about the absolute ground state concentration of molecular precursors, fragments and products including transient species like radicals in relation to the discharge parameters as e.g. gas mixture and power would be very helpful.

Tunable diode laser absorption spectroscopy (TDLAS) in the mid-infrared spectral range using lead salt lasers as radiation sources has been proven to be a versatile diagnostic technique of molecular gases and plasmas. In particular TDLAS is well suited for the measurement of absolute ground state concentrations of a wide variety of molecular species including radicals and molecular ions thereby providing a link with chemical modelling of the plasma (see [5] and references therein). Until now, the main applications of TDLAS have been for investigating molecules and radicals in fluorocarbon etching plasmas [37] and in plasma containing hydrocarbons [5]. For the simultaneous monitoring of multiple molecular plasma species TDLAS systems, which make use of several lead salt lasers, have been developed in the past [12, 13]. In contrast to ATI the plasma based fragmentation of other precursors, as silane and HMDSO, has been already investigated in several TDLAS studies, e.g [38, 39].

The recent development and commercial availability of pulsed and continuous wave quantum cascade lasers (QCLs) for wavelengths longer than  $3.4\ \mu\text{m}$  and inter-band cascade lasers (ICLs) for shorter wavelength offer an attractive new option for mid-infrared laser absorption spectroscopy (MIR-LAS) for plasma diagnostic purposes. Distributed feedback (DFB) QCLs provide continuous mode-hop free wavelength tuning. Their total emission range is typically limited to less than  $7\ \text{cm}^{-1}$ . Therefore, a multi-component detection to study infrared active compounds in reactive plasmas requires, as in the TDLAS case, the combination of several QCLs in a spectrometer [40]. Meanwhile the variety of QCLs and ICLs operating at room temperature are considered as substitutes for cryogenic cooled lead salt lasers, which has led to a rapid development of MIR-LAS from a niche position to a standard diagnostic technique [18], even for the study of metal-organic precursor fragmentation, as silane and HMDSO, and also of fluorocarbons in plasmas [41-43].

Recently, tunability over much broader spectral ranges than with a typical lead salt lasers or DFB-QCL has been achieved using external cavity (EC) configurations. Nowadays, EC-QCLs, which are available in pulsed or continuous (cw) wave working mode, can be

tuned over more than  $100\text{ cm}^{-1}$ . Modern cw EC-QCL provide mode-hop free tuning ranges in the order of up to  $80\text{ cm}^{-1}$ , at small line width of typically 20 to 60 MHz ( $6 - 18 \times 10^{-4}\text{ cm}^{-1}$ ) at power values of up to 150 mW [44]. At present EC-QCLs are used for an increasing number of applications including high resolution isotope analysis, trace gas monitoring and explosive detection [45-47]. Recently, cw EC-QCLs have been tested as radiation sources for MIR-LAS studies of molecular plasmas [1].

In the presented investigation chemical phenomena of Ar and Ar/N<sub>2</sub> RF discharges containing ATI as metal-organic precursor have been in the focus of interest. Using MIR-LAS based on a cw EC-QCL arrangement the evolution of the concentrations of six stable molecules, CH<sub>4</sub>, C<sub>2</sub>H<sub>2</sub>, C<sub>2</sub>H<sub>4</sub>, H<sub>2</sub>O, HCN and HNO<sub>3</sub>, has been monitored in the plasma. One of the objectives was to determine main fragmentation pathways of the ATI precursor molecule and to receive information about the influence of added rare and molecular gases, as e.g. Ar and Ar/N<sub>2</sub>.

## 8.2 Experimental

The investigations have been performed in an asymmetric capacitively coupled RF discharge at a frequency of  $f = 13.56\text{ MHz}$ . The vacuum chamber with a volume of about  $50\text{ dm}^3$  is cylindrical with a plain electrode and several ports for diagnostics approaches. The used RF generator was a CESAR™ 133 from Advanced Energy Industries. The vacuum chamber was evacuated by a turbo pump (Varian Turbo-V 301) and a roughing pump (Varian IDP3 scroll pump). The pressure was measured by a pirani and a baratron vacuum meter. As shown in the scheme of the experimental setup in figure 8.2, on the top of the chamber the gas inlet for carrier and reactive gas is located. As carrier gas argon (99.999%) and nitrogen (99.999%) and as metal-organic precursor ATI were used. The measurements were performed at pressure values of up to  $p = 10\text{ Pa}$  and at discharge power values in the range of  $P = 40 - 100\text{ W}$ . To keep the total pressure constant, the Ar and N<sub>2</sub> gas flows were adjusted manually by a needle valve and the ATI gas flow by a viscometer. The ATI vapor was provided by a special designed heating system. The turbo-molecular pump has a throughput of  $1\text{ mbar s}^{-1}$  at the operating pressure, leading to a residence time of about 1 s for the incoming gas flow.

By variation of one of the parameters, (i) discharge power, (ii) total pressure or (iii) gas mixture, molecular concentrations of generated stable molecular species, CH<sub>4</sub>, C<sub>2</sub>H<sub>2</sub>, C<sub>2</sub>H<sub>4</sub>,

$\text{H}_2\text{O}$ ,  $\text{HCN}$  and  $\text{HNO}_3$ , were measured by an EC-QCL absorption spectrometer. The scheme of the spectrometer is given in figure 8.3. The set-up consists (i) of the radiation source, an EC-QCL, Daylight Solution, with a full tuning possibility in the range of  $1305$  to  $1445\text{ cm}^{-1}$ , providing a mode hop free range between  $1345$  and  $1400\text{ cm}^{-1}$  at a maximum power of about  $150\text{ mW}$ , (ii) a chopper, (iii) two standard HgCdTe detectors for measuring and reference path and (iv) opto-mechanical elements for beam guiding. Further details can be found in reference [1]. The infrared laser beam from the EC-QCL system has a diameter of about  $1\text{ cm}$  and is transferred using gold-coated mirrors via KBr-windows to an optical long path cell (White cell type [9], 20 passes, absorption length:  $15.8\text{ m}$ ), which is mounted to the plasma chamber for improved sensitivity (figure 8.2). The diode laser beam leaving the cell was focused on a standard HgCdTe infrared detector by an off-axis parabolic mirror. The identification of lines and the determination of their absolute positions were carried out using well-documented reference gas spectra and an etalon of known free spectral range for interpolation. Spectral positions and absorption line strengths of molecular ground state absorption lines used for the measurements are listed in table 8.1.

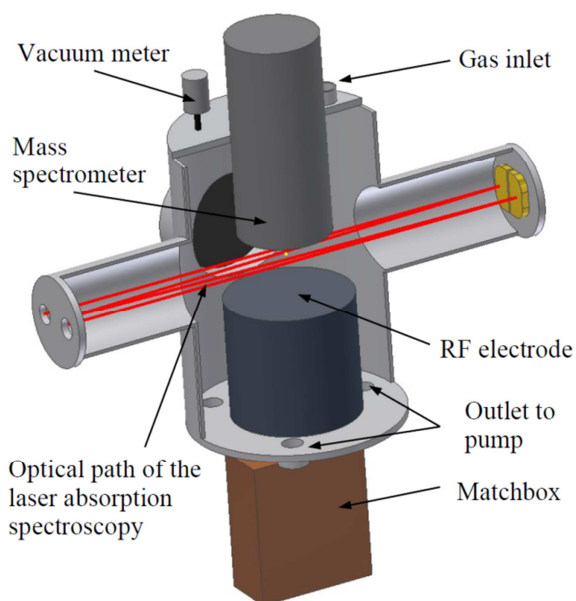


**Figure 8.2:** Experimental arrangement of the RF plasma reactor [20].

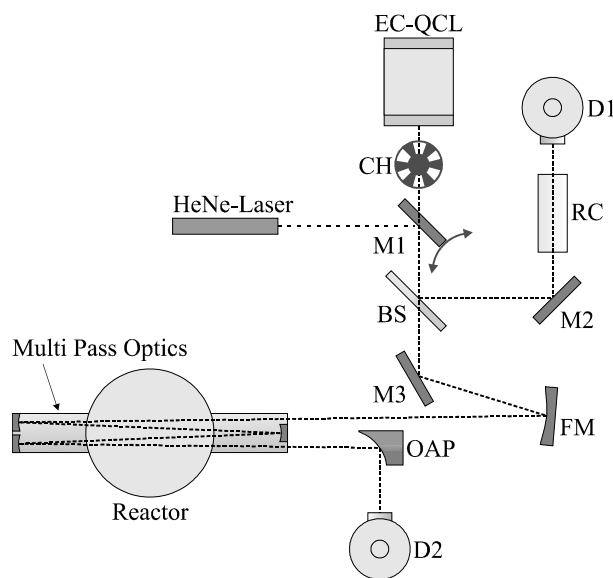


**Figure 8.3:** Scheme of the EC-QCLAS spectrometer in combination with the RF plasma reactor. (CH: chopper, M1-M3: mirrors, BS: beam splitter, RC: reference gas cell, D1, D2: HgCdTe detectors, FM: focal mirror, OAP: out of axis paraboloid) [20].

**Table 8.1:** Species, spectral positions and line strengths used for the EC-QCLAS measurements [7].

Species	Spectral position [cm <sup>-1</sup> ]	Absorption line strength [cm <sup>-1</sup> /( molecule cm <sup>-2</sup> )]
CH <sub>4</sub>	1332.731	9.557E-20
C <sub>2</sub> H <sub>2</sub>	1332.803	4.583E-20
C <sub>2</sub> H <sub>4</sub>	1413.212	5.645E-21
H <sub>2</sub> O	1375.086	1.490E-20
HCN	1382.514	4.408E-20
HNO <sub>3</sub>	1332.891	1.530E-20

The used data acquisition method is an advanced form of sweep integration which is carried out based on the software package TDLWintel [13].

Absolute species concentrations are returned from the nonlinear least-squares fits of the measured absorption features so that external calibration is not required. For the calculations of the concentrations a gas temperature of 300 K was used since this is a good average for the gas temperature over the line of sight, comprising the active zone over the discharge electrode and the afterglow surrounding them, and over the course of the measurement.

Figure 8.4 shows an exemplary spectrum of CH<sub>4</sub>, C<sub>2</sub>H<sub>2</sub> and HNO<sub>3</sub> absorption lines in an Ar/N<sub>2</sub>/ATI plasma.

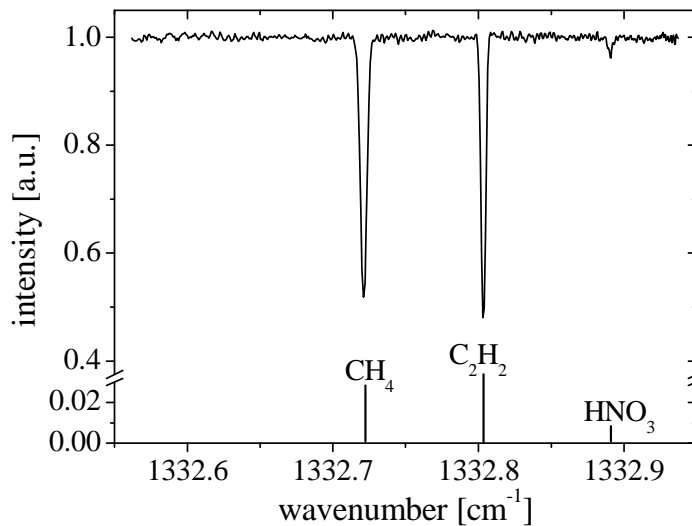


**Figure 8.4:** Exemplary spectrum of of CH<sub>4</sub>, C<sub>2</sub>H<sub>2</sub> and HNO<sub>3</sub> absorption lines in an Ar/N<sub>2</sub>/ATI plasma [20].

### 8.3 Results and discussion

The plasma chemical study of the ATI fragmentation in the RF plasma has been performed for two different conditions of the gas mixture, i.e. case 1: within a pure ATI-Ar mixture and case 2: using an ATI-N<sub>2</sub>-Ar feed gas. In figures 8.5 - 8.7 the experimental results for the ATI-Ar case are given.

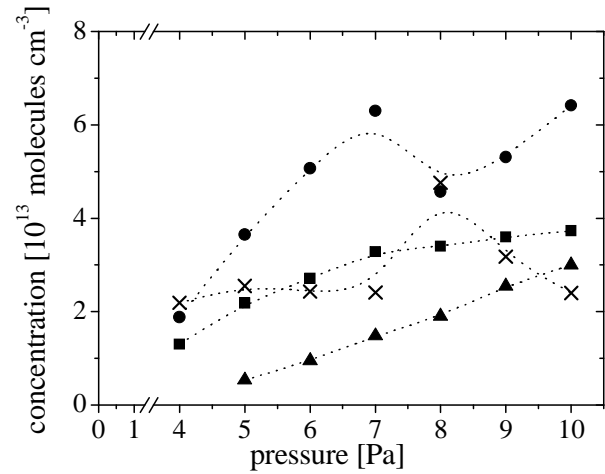
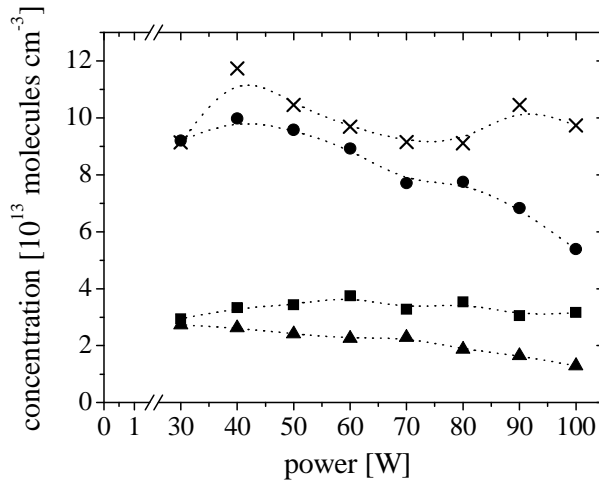


**Figure 8.5:** Concentration of CH<sub>4</sub> - ■, C<sub>2</sub>H<sub>2</sub> - ●, C<sub>2</sub>H<sub>4</sub> - ▲ and H<sub>2</sub>O - × in dependence on the discharge power in an Ar/ATI plasma,  $p = 6$  Pa, ratio Ar/ATI=2/1 [20]. **Figure 8.6:** Concentration of CH<sub>4</sub> - ■, C<sub>2</sub>H<sub>2</sub> - ●, C<sub>2</sub>H<sub>4</sub> - ▲ and H<sub>2</sub>O - × in dependence on the pressure in an Ar/ATI plasma  $P = 80$  W, ratio Ar/ATI=2/1 [20].

Some useful generalizations follow from these figures. The concentrations of the plasma chemical products, CH<sub>4</sub>, C<sub>2</sub>H<sub>2</sub>, C<sub>2</sub>H<sub>4</sub> and H<sub>2</sub>O, were found to be in the range of about  $7 \times 10^{12} - 2 \times 10^{14}$  molecules cm<sup>-3</sup>. Plasma dissociation of the ATI precursor molecules leads not only to AlO<sub>x</sub> fragments but also to a relatively high density of methyl (CH<sub>3</sub>) groups and hydrogen [48].

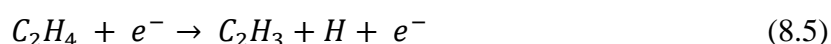
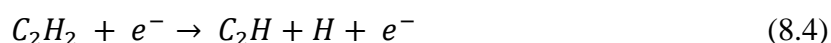
The methyl radicals can directly react with hydrogen to methane (CH<sub>4</sub>):



In a plasma environment also acetylene as well as ethylene are formed by two methyl groups, see formula (8.2) and (8.3) [49, 50].



The largest of the hydrocarbon product molecules,  $C_2H_4$ , shows the lowest concentration, while acetylene is appearing with the highest density. For methane intermediate values could be monitored. It is interesting to note, that the concentrations of  $C_2H_2$  and  $C_2H_4$  decrease with power, while the methane concentration remains nearly constant, see figure 8.5. This behaviour may be caused by the increasing degree of dissociation with power not only of the ATI precursor molecule, but also of the higher hydrocarbon products. Hydrogen can be dissociated from  $C_2H_2$  or  $C_2H_4$  by electron collisions [51, 52]:



The enhanced dissociation is caused by an increased collision rate of electrons and molecules due to higher electron density with increasing RF power [48].

As expected the concentration of all four molecular species increases with increasing pressure, see figure 8.6. A comparable behaviour is observed, in case the total pressure remained constant and only the ATI partial pressure has been varied as shown in figure 8.7. This observation indicates that the increasing ATI pressure results in a higher concentration of fragmentation products.

In all of these three experiments the water concentration was found to be on a comparable high value, reaching a maximal value of  $2 \times 10^{14}$  molecules  $cm^{-3}$  at high ATI admixture (figure 8.7). In general the detected water can originate from two different sources, (i) from the plasma chemical conversion of ATI and (ii) from residual water inside the reactor, in particular, adsorbed at the reactor walls. From the present experimental results, it is difficult to distinguish between these two sources. However, one could speculate that the main source is the ATI precursor itself, because the amount of water is nearly constant for a constant ATI admixture (figures 8.5 and 8.6) but it is increasing at higher ATI admixture (figure 8.7).

For the second experimental situation, case 2, nitrogen was used additionally as feed gas component. In the available spectral range of the used EC-QCL two other additional molecular species could be identified, HCN and  $HNO_3$ . These molecules are certainly generated by reactions of ATI fragmentation products with nitrogen. The results of the plasma chemical QCLAS study are shown in figures 8.8 and 8.9.

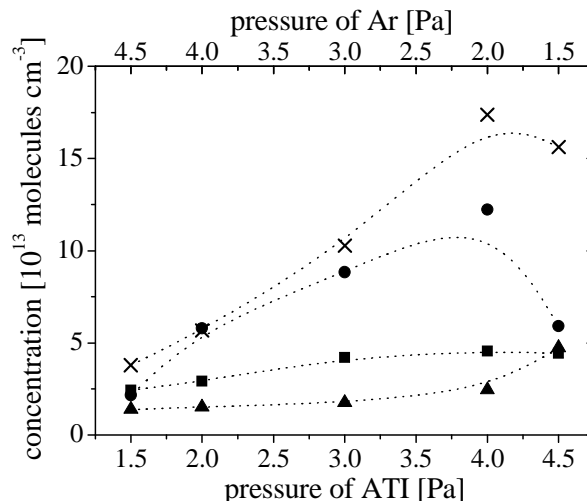


**Figure 8.7:** Concentration of  $\text{CH}_4$  - ■,  $\text{C}_2\text{H}_2$  - ●,  $\text{C}_2\text{H}_4$  - ▲ and  $\text{H}_2\text{O}$  - × in dependence on the mixing ratio of Ar to ATI, given in pressure values, in an Ar/ATI plasma,  $p = 6 \text{ Pa}$ ,  $P = 80 \text{ W}$  [20].

In figure 8.8 the concentration of six observable product molecules,  $\text{CH}_4$ ,  $\text{C}_2\text{H}_2$ ,  $\text{C}_2\text{H}_4$ ,  $\text{H}_2\text{O}$ ,  $\text{HCN}$  and  $\text{HNO}_3$ , in dependence on the discharge power in an Ar/ $\text{N}_2$ /ATI plasma with a mixing ratio of 1/1/1 at a total pressure of  $p = 6 \text{ Pa}$  are given. It is interesting to note, that the concentrations of all molecules, except water, show a maximum at medium power values between 50 and 90 W. The decrease of concentration above 90 W may be explained by more effective collisions of electrons with nitrogen molecules, finally leading to a limited fragmentation of ATI. The maximum concentration was found for  $\text{C}_2\text{H}_2$  to be about  $5 \times 10^{13} \text{ molecules cm}^{-3}$ , followed by  $\text{HCN}$ ,  $\text{H}_2\text{O}$  and  $\text{CH}_4$ . A second group of molecular species is formed by  $\text{C}_2\text{H}_4$  and  $\text{HNO}_3$  with concentrations of about one order of magnitude lower than the species of the former group.

With increasing admixture of ATI compared to the nitrogen partial pressure again most of the molecules show increasing concentrations except  $\text{HCN}$  (figure 8.9). For the concentration of  $\text{HCN}$  a slight maximum was found at an ATI admixture of about 1 Pa. The concentration of  $\text{HNO}_3$  was again in the range of  $10^{12} \text{ molecules cm}^{-3}$ . The coupled process of decreasing nitrogen pressure and increasing ATI concentration makes it difficult to give an explanation about the formation of  $\text{HCN}$  and  $\text{HNO}_3$  regarding the fragmentation process and the chemical reactions of the products with nitrogen. But it seems to be obvious that the different electron collision cross sections for ATI and  $\text{N}_2$  dissociation are the reason for this behavior, e.g. the importance of different reaction channels in dependence on the plasma process conditions causes the observed changes. Even the Ar- $\text{N}_2$  mixing ratio can have a

considerable influence on the dissociation behavior of the molecular feed gases, as described by Saloum and co-workers [53].

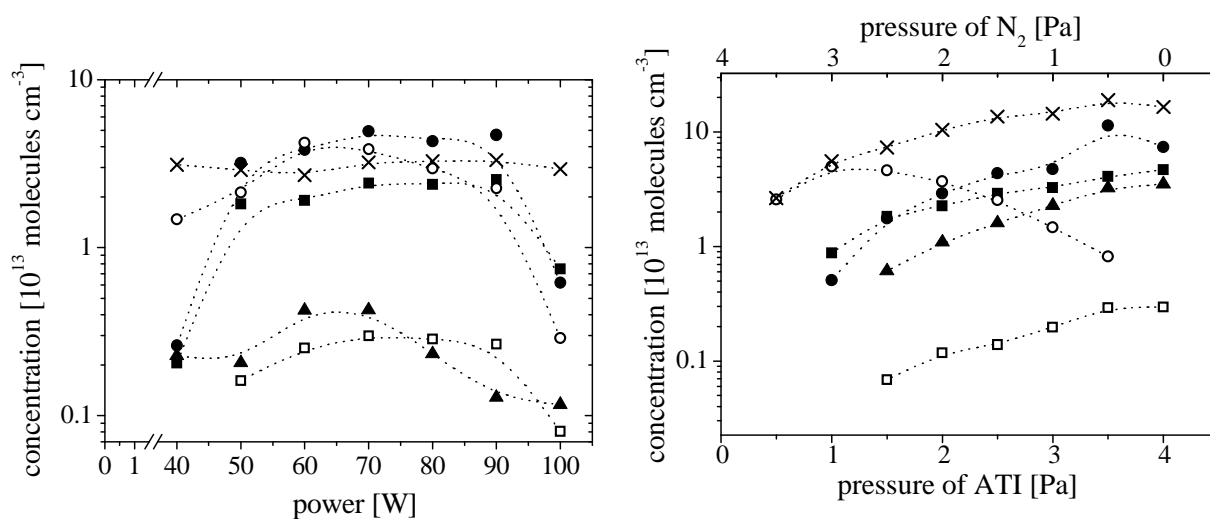


**Figure 8.8:** Concentration of CH<sub>4</sub> - ■, C<sub>2</sub>H<sub>2</sub> - ●, C<sub>2</sub>H<sub>4</sub> - ▲, H<sub>2</sub>O - ×, HCN - ○ and HNO<sub>3</sub> - □ in dependence on the discharge power in an Ar/N<sub>2</sub>/ATI plasma,  $p = 6$  Pa, ratio Ar/N<sub>2</sub>/ATI=1/1/1 [20].

**Figure 8.9:** Concentrations of CH<sub>4</sub> - ■, C<sub>2</sub>H<sub>2</sub> - ●, C<sub>2</sub>H<sub>4</sub> - ▲, H<sub>2</sub>O - ×, HCN - ○ and HNO<sub>3</sub> - □ in dependence on the mixing ratio of N<sub>2</sub> to ATI, given in pressure values, in an Ar/N<sub>2</sub>/ATI plasma,  $p = 6$  Pa,  $p_{Ar} = 2$  Pa,  $P = 80$  W [20].

## 8.4 Summary and conclusions

In the present study the absolute ground state concentrations of six stable species under a wide range of experimental conditions have been determined by infrared laser absorption spectroscopy providing a link with the fragmentation behaviour of ATI in a capacitively coupled RF discharge. The final objective to get a better understanding of chemical processes occurring in plasmas containing metal-organic precursors for metal oxide PECVD deposition can be achieved by applying this method. Although several molecular species concentrations have been monitored in absolute scale, the mass balance of the whole ATI fragmentation process is far to be comprehensively analysed. Future studies should include (i) the ATI precursor molecule itself, (ii) further stable, in particular higher hydrocarbon molecules as well as other important intermediates, but also (iii) a quantitative analysis of the molecular production rates in the discharge. Especially, other radicals, as for example CH<sub>3</sub>, C<sub>2</sub>H, CH<sub>2</sub>, CH and metal-organic species should be monitored. Further, the combination of infrared absorption with mass-spectrometric techniques, see reference [48] where the complex fragmentation of the ATI molecule were studied recently, could lead to an optimization of deposition processes

and to an improved modelling potential for ATI containing plasmas based on kinetic data as e.g. reliable reaction rates.

It has been shown, that based on the attractive properties of EC-QCLs, as in particular (i) wide spectral tunability, (ii) intrinsic narrow line width, and (iii) high output powers, this radiation source for absorption spectroscopy has a high potential to be applied for other plasma diagnostic purposes. In particular EC-QCLAS is well suited for the monitoring of multiple species including larger plasma components characterized by broader spectral features and also to be used under atmospheric pressure conditions, where pressure broadening effects have to be considered [54]. Further interesting fields like the kinetics of oxygen containing electronegative plasmas and also phenomena of plasma surface interaction should be accessible using these new MIR radiation sources.

## Bibliography for Chapters 7 and 8

- [1] D. Lopatik, N. Lang, U. Macherius, H. Zimmermann, J. Röpcke, *Meas. Sci. Technol.* **23**, 115501 (2012).
- [2] E. Hirota, K. Kawaguchi, *Ann. Rev. Phys. Chem.* **36**, 53 (1985).
- [3] P.B. Davies, *Spectrochim. Acta* **55**, 1987 (1999).
- [4] R.F. Curl, F.K. Tittel, *Ann. Rep. Prog. Chem., Sect. C. Phys. Chem.* **98**, 219 (2002).
- [5] J. Röpcke, G. Lombardi, A. Rousseau, P.B. Davies, *Plasma Sources Sci. Technol.* **5**, S148 (2006).
- [6] M. Lackner, *Rev. Chem. Eng.* **23**, 65 (2007).
- [7] L.S. Rothman, D. Jacquemart, A. Barbe, D.C. Benner, M. Birk, L.R. Brown, M.R. Carleer, C. Chackerian, K. Chance, L.H. Coudert, V. Dana, V.M. Devi, J.M. Flaud, R.R. Gamache, A. Goldman, J.M. Hartmann, K.W. Jucks, A.G. Maki, J.Y. Mandin, S.T. Massie, J. Orphal, A. Perrin, C.P. Rinsland, M.A.H. Smith, J. Tennyson, R.N. Tolchenov, R.A. Toth, J. Vander Auwera, P. Varanasi, G. Wagner, *J. Quant. Spectrosc. Radiat.* **96**, 139 (2005).
- [8] Daylight Solutions, *User Manual*, Rev. A 2009.02.
- [9] J.U. White, *J. Optical Soc. America* **32**, 285 (1942).
- [10] F. Hempel, P.B. Davies, D. Loffhagen, L. Mechold, J. Röpcke, *Plasma Sources Sci. Technol.* **12**, S98 (2003).
- [11] D. Dahl, *Master Thesis*, University of Greifswald, 2009.
- [12] J.B. McManus, D. Nelson, M. Zahniser, L. Mechold, M. Osiac, J. Röpcke, A. Rousseau, *Rev. Sci. Instr.* **74**, 2709 (2003).
- [13] J. Röpcke, L. Mechold, M. Känig, J. Anders, F.G. Wienhold, D. Nelson, M. Zahniser, *Rev. Sci. Instr.* **71**, 3706 (2000).
- [14] H.R. Griem, *Plasma Spectroscopy*, McGraw-Hill Book Company, New York, 1964.
- [15] C.W. Van Neste, L.R. Senesac, T. Thundat, *Appl. Phys. Lett.* **92**, 234102 (2008).
- [16] X. Liu, Y. Xu, Z. Zu, W.S. Tam, I. Leonov, *Appl. Phys. B: Lasers and Optics* **102**, 629 (2011).

- [17] G. Duxbury, *Infrared Vibrational-Rotation Spectroscopy: from Free Radicals to the Infrared Sky*; Wiley: Chichester, UK, 2000.
- [18] S. Welzel, F. Hempel, M. Hübner, N. Lang, P.B. Davies, J. Röpcke, *Sensors* **10**, 6861 (2010).
- [19] S. Welzel, J. Röpcke, *Appl Phys B* **102**, 303 (2011).
- [20] D. Lopatik, S. Niemietz, M. Fröhlich, J. Röpcke, H. Kersten, *Contrib. Plasma Phys.* **1**, 201200044 (2012).
- [21] K. Bhattacharya, D. Das, *Nanotechnology* **18**, 415704 (2007).
- [22] M. Hähnel, V. Brüser, H. Kersten, *Plasma Process. Polym.* **6**, 629 (2007).
- [23] S. Bornholdt, M. Wolter, H. Kersten, *Eur. Phys. J. D* **60**, 653 (2010).
- [24] H. Kersten, G. Thieme, M. Fröhlich, D. Bojic, D.H. Tung, M. Quaas, H. Wulff, R. Hippler, *Pure Appl. Chem.* **77**, 415 (2005).
- [25] L. Daasch, H. Fales, *Organic Mass Spectr.* **2**, 1043 (1969).
- [26] K. Folting, K.E. Streib, K.G. Caulton, O. Poncelet, L.G. Hubert-Pfalzgraf, *Polyhedron* **10**, 1639 (1991).
- [27] N.Y. Turova, V.A. Kozunov, A.I. Yanovskii, N.G. Bokii, Y.T. Struchkov, B.L. Tarnopolskii, *J. Inorg. Nuclear Chem.* **41**, 5 (1979).
- [28] S. Blittersdorf, N. Bahlawane, K. Kohse-Höinghaus, B. Atakan, J. Müller, *Chemical Vapor Dep.* **9**, 194 (2003).
- [29] M. Kathrein, W. Schintlmeister, W. Wallgram, U. Schleinkofer, *Surf. Coat. Technol.* **163**, 181 (2003).
- [30] M.D. Groner, S.M. George, R.S. McLean, P.F. Garcia, *Appl. Phys. Lett.* **88**, 051907 (2006).
- [31] T.A. Zevaco, A. Janssen, J., Sypien, E. Dinjus, *Green Chem.* **7**, 659 (2005).
- [32] I. Saraie, J. Kwon, Y. Yodogawa, *J. Electrochem. Soc.* **132**, 890 (1985).
- [33] A.M. Huntz, M. Andrieux, C. Vahlas, M.M. Sovar, D. Samelor, A.N. Gleizes, *J. Electrochem. Soc.* **154**, 63 (2007).
- [34] M.M. Sovar, D. Samelor, A. Gleizes, C. Vahlas, *Surf. Coat. Technol.* **201**, 9159 (2007).

- [35] L.M. Miller, D.A. Gulino, *Surf. Coat. Technol.* **68**, 76 (1994).
- [36] H. Kersten, R. Wiese, G. Thieme, M. Fröhlich, A. Kopitov, D. Bojic, F. Scholze, H. Neumann, M. Quaas, H. Wulff, R. Hippler, *New J. Phys.* **5**, 93.1 (2003).
- [37] S. Stepanov, J. Meichsner, *Plasma Sources Sci. Technol.* **21**, 024008 (2012).
- [38] C. Yamada, E. Hirota, *Phys. Rev. Lett.* **56**, 923 (1986).
- [39] J. Röpcke, G. Revalde, M. Osiac, K. Li, J. Meichsner, *Plasma Chem. Plasma Process.* **22**, 139 (2002).
- [40] M. Hübner, S. Welzel, D. Marinov, O. Guaitella, S. Glitsch, A. Rousseau, J. Röpcke, *Rev. Sci. Instr.* **82**, 093102 (2011).
- [41] R. Bartlome, A. Feltrin, C. Ballif, *Appl. Phys. Lett.* **94**, 201501 (2009).
- [42] M. Wolter, M. Hundt, H. Kersten, *Vacuum* **85**, 482 (2010).
- [43] S. Welzel, S. Stepanov, J. Meichsner, J. Röpcke, *J. Phys. D: Appl. Phys.* **43**, 124014 (2010).
- [44] R.F. Curl, F. Capasso, C. Gmachl, A.A. Kostorev, B. McManus, R. Lewicki, M. Pusharsky, G. Wysocki, F.K. Tittel, *Chem. Phys. Lett.* **487**, 1 (2010).
- [45] R.J. Walker, R.J. Van Helden, G.A.D. Ritchie, *Chem. Phys. Lett.* **501**, 20 (2010).
- [46] A. Karpf, G.N. Rao, *Appl. Optics* **49**, 1406 (2010).
- [47] R. Furstenberg, C.A. Kendziora, J. Stepnowski, S.V. Stepnowski, M. Rake, M.R. Papantonakis, V. Nguyen, G.K. Hubler, R.A. McGill, *Appl. Phys. Lett.* **93**, 224103 (2008).
- [48] S. Niemietz, M. Fröhlich, H. Kersten, *Plasma Process. Polym.* DOI: 10.1002/ppap.201200012. (2012).
- [49] M. Masi, C. Cavallotti, S. Carra, *Chemical Engineering Sci.* **53**, 3875 (1998).
- [50] K. Bleecker, A. Bogaerts, W. Goedheer, R. Gijbels, *IEEE Trans. Plasma Sci.* **32**, 691 (2004).
- [51] M. Hundt, P. Sadler, I. Levchenko, M. Wolter, H. Kersten, K. Ostrikov, *J. Appl. Phys.* **109**, 123305 (2011).
- [52] E. Kovacevic, I. Stefanovic, J. Berndt, J. Winter, *J. Appl. Phys.* **93**, 2924 (2003).

- [53] S. Saloum, M. Naddaf, B. Alkhaled, *J. Phys. D: Appl. Phys.* **41**, 045205 (2008).
- [54] S. Reuter, J. Winter, S. Iseni, S. Peters, A. Schmidt-Bleker, M. Dünnbier, J. Schäfer, R. Foest, K.-D. Weltmann, *Plasma Sources Sci. Technol.* **21**, 034015 (2012).



## 9 Conclusions and outlook

Methods of infrared laser absorption spectroscopy (IR-LAS) employing several types of semiconductor lasers have been applied to get better view inside processes occurring in non-equilibrium plasmas. Additionally to the phenomena of plasma-surface interaction, the knowledge of the kinetics of the surrounding gas phase as well as reactive plasma chemistry were under the focus of this study.

The most important results obtained in the presented work and suggestions for further research are summarized as follows:

### 1. *Active screen plasma nitriding processes*

- ✓ Two spectroscopic techniques TDLAS and QMS have been applied for monitoring of the reactions in the  $\text{H}_2\text{-N}_2$  pulsed DC plasma in industrial-scale reactor.
- ✓ Strong evidence for the dependence of the  $\text{NH}_3$  concentration on the  $\text{N}_2\text{-H}_2$  mixture ratio for different values of the bias power was observed. An increase of the bias power as well as the admixture of bigger amounts of  $\text{H}_2$  up to 50% leads to increasing concentration of  $\text{NH}_3$ , which was found to be in the range of  $5 \times 10^{13} - 2 \times 10^{14} \text{ molecules cm}^{-3}$ .
- ✓ A clear coincidence of TDLAS and QMS measurements has been seen.
- ✓ Several probe nitriding tests has been proven that, the generation rate of the  $\text{NH}_x$ -species depends on the ASPN process conditions and is related to the activity of the active nitrogen. A 1:1 gas mixture of the  $\text{N}_2\text{-H}_2$  process gases was found to be most effective to get thick compound layers.
- The results of performed measurements will definitely find further practical application, whereas the determination of  $\text{N}_2(v)$  relaxation probability on different surfaces ( $\gamma_{\text{N}_2}$ ) using the method proposed in chapter 5 as well as better control of

concentration and the energetic state of N<sub>2</sub>-species during the ASPN process are the future diagnostic challenges.

## 2. *Dust producing RF plasmas*

- ✓ The temporal evolution of the concentrations of the methyl radical and of four stable molecules, C<sub>2</sub>H<sub>2</sub>, CH<sub>4</sub>, C<sub>2</sub>H<sub>4</sub> and CO, has been studied in dust producing Ar and He RF-cc plasmas with admixtures of C<sub>2</sub>H<sub>2</sub> and CH<sub>4</sub> simultaneously to dust particle formation processes.
- ✓ The degree of dissociation of acetylene was found to be nearly constant in the range of 96% under stabilized conditions for both the Ar and He plasmas, whereas the degree of dissociation of the methane varied between 45% and 90% depending on the appearance of dust particles in the reactor volume and on the Ar or He plasma conditions.
- ✓ Strong correlation of the concentrations of all hydrocarbon species with the dynamic of the dust formation has been observed.
- ✓ A different reactivity of the He plasma compared with the Ar plasma has been shown by analyzing the temporal concentration for phase when CH<sub>4</sub> has been used as hydrocarbon precursor instead of C<sub>2</sub>H<sub>2</sub>. In Ar containing plasma the C<sub>2</sub>H<sub>2</sub> density reached the value of 10<sup>12</sup> molecules cm<sup>-3</sup> in less than 60 s. In contrast, in case He as buffer gas was used, the C<sub>2</sub>H<sub>2</sub> concentration stabilized first in 7 min, but reaching a one order of magnitude higher in the range of 10<sup>13</sup> molecules cm<sup>-3</sup>.
- ✓ The observed dynamics of CH<sub>3</sub> concentration is in a good agreement with a start of the nucleation process of the dust production.
- ✓ Detected CO molecules probably come from the interaction of plasma with the previously deposited layers on the reactor walls.
- ✓ In additional, absolute fragmentation efficiencies of C<sub>2</sub>H<sub>2</sub> and CH<sub>4</sub> and conversion efficiencies of the observed CH<sub>4</sub>, C<sub>2</sub>H<sub>2</sub>, C<sub>2</sub>H<sub>4</sub> and CH<sub>3</sub> have been estimated (see sub-chapter 4.3.3 or table 4.3)
- *In-situ* analysis (for example transmission FTIR) of further stable, in particular higher hydrocarbon molecules as well as other free radicals (C<sub>2</sub>H, CH<sub>2</sub> and CH) is required in order to get a deeper insight into the mechanism of dust producing RF discharges. The further development of plasma-chemical models is a good potential to get an improved knowledge about kinetic data on elementary reactions.

### 3. Surface vibrational relaxation of $N_2$

- ✓ Based on a nearly resonant fast vibrational transfer between of  $N_2(v)$  and titration molecule a new experimental technique for the study of the vibrational relaxation probability of  $N_2$  molecules ( $\gamma_{N_2}$ ) on different surfaces exposed to low-pressure plasmas has been proposed.
- ✓ The vibrational relaxation of titration molecule ( $CO_2$ ) was monitored using an *in-situ* QCL diagnostics (TRIPLE Q) after a few ms long discharge pulse.
- ✓ A good agreement between measurements and modelling has allowed determination of the value of the  $N_2(v=1)$  relaxation probability found to be  $\gamma = 1.1 \times 10^{-3}$  for Pyrex and silica,  $\gamma = 9 \times 10^{-3}$  for smooth  $TiO_2$  surfaces and  $\gamma = 4 \times 10^{-2}$  for sol-gel films impregnated with  $TiO_2$  particles. These results are well correlated with literature values.
- ✓ It has been estimated, that the surface deactivation probability of  $N_2(v)$  is proportional to the varying initial mixture composition. This effect was explained by vibrational energy transfer between the excited gas phase nitrogen molecules and adsorbed  $CO_2$  molecules.
- ✓ Furthermore,  $CO_2$  titration was found to be a feasible technique for  $N_2(v)$  vibrational temperature measurement in the afterglow of a pulsed dc discharge.
- Forthcoming measurements may include the study of  $N_2$  relaxation probability on the example of titration with other molecules, e.g. CO and  $N_2O$ . The investigation of  $\gamma_{N_2}$  by the infrared titration technique in combination with QCLAS on a variety of oxide surfaces can be an interesting challenge.

### 4. Atomic oxidation on $TiO_2$ surfaces

- ✓ The reactivity of catalytic surface exposed to low pressure RF discharge on the example of the oxidation of  $C_2H_2$  and CO on the  $TiO_2$  has been investigated by time-resolved QCLAS using TRIPLE Q spectrometer.
- ✓ It has been found, that under RF oxygen plasma exposure, reactive oxygen species could be grafted on the  $TiO_2$  and they reactivity depend on the reacting molecule. Moreover, reactivity of  $O_{ads}$  towards  $C_2H_2$  has been proven.
- ✓ A value of about  $7.5 \times 10^{12}$   $C_2H_2$  molecules  $cm^{-2}$  has been calculated as a value of the maximum number of  $C_2H_2$  lost on the  $TiO_2$  exposed to oxygen plasma.
- ✓ In the adsorption phase the oxidation of  $C_2H_2$  into  $CO_2$  has been detected to be only

about 2% of the introduced carbon molecules. Further effective oxidation of ca. 50% of the adsorbed acetylene to  $\text{CO}_2$  has been achieved owing to stimulation by heating or UV radiation. It has been proven the fact, that the reaction  $(\text{O}_{\text{ads}} + \text{C}_2\text{H}_2)_{\text{TiO}_2}$  produces some adsorbed intermediates.

- ✓ Additional, the influence of photo-catalytic oxidation on effective destruction of CO has been demonstrated.
- However, the application at industrial conditions requires atmospheric pressure discharges and adsorption of oxygen atoms at changed conditions on the surface must be considered. In order to answer this question, the interaction between catalyst surface and atmospheric pressure discharge has to be investigated. Moreover, further studies are necessary for a deeper understanding of reaction mechanisms on different catalytic surfaces pretreated by the plasma exposure, for example *in-situ* analysis of adsorbed species by transmission FTIR.

#### 5. Multi-component EC-QCL spectroscopic measurements of MW plasmas

- ✓ Several EC-QCLs operating between  $1305$  and  $2260\text{ cm}^{-1}$  ( $4.42 - 7.66\text{ }\mu\text{m}$ ) have been successfully tested as a broad spectral radiation source for direct spectroscopy measurements for investigation of Ar/ $\text{N}_2$ / $\text{CH}_4$  MW plasma.
- ✓ The evolution of molecular concentrations of the precursor molecule  $\text{CH}_4$  and of selected reaction products, as HCN,  $\text{C}_2\text{H}_2$  and  $\text{H}_2\text{O}$  has been monitored for changing  $\text{CH}_4$  admixture or the power at constant pressure. The number density of observed molecular species has been found to be in the range of about  $10^{11} - 10^{15}\text{ molecules cm}^{-3}$ . It has been also established, that the  $\text{CH}_4$  concentration depends only slightly on the nitrogen content of the plasma, while strongly decreases with increasing power.
- ✓ From the Doppler widths of several selected spectral lines the neutral gas temperature  $T_g$  in dependence on the discharge power has been determined.
- ✓ Further, on the example of He/Ar MW discharge, the application of EC-QCL for the sensitive detection of transient plasma has been demonstrated. Using WMS technique, the detection absorption limit was estimated to be in the range of  $10^{-5}$ .
- ✓ By the way, influence of other parameters on the measurements results has been checked. It has been shown, that choosing of methods for the modulation, tuning and chopping as well as rational power values should be carefully performed.
- It is to be concluded, that the tested on MW plasmas EC-QCLs is a useful

spectroscopic radiation source Using these new mid infrared radiation sources, further fields like the kinetics of oxygen containing electronegative plasmas and also phenomena of plasma surface interaction should be accessible.

#### 6. *Metal-organic precursor in RF plasmas*

- ✓ The investigation of chemical processes occurring in plasmas containing metal-organic precursors for metal oxide PECVD deposition has been performed using methods of IRLAS based on the attractive properties of EC-QCLs.
- ✓ The absolute ground state concentrations of six stable species ( $\text{CH}_4$ ,  $\text{C}_2\text{H}_2$ ,  $\text{C}_2\text{H}_4$ ,  $\text{H}_2\text{O}$ ,  $\text{HCN}$  and  $\text{HNO}_3$ ) have been determined under a wide range of experimental conditions in Ar and Ar/ $\text{N}_2$  RF plasmas with admixtures of aluminum tri-isopropoxide (ATI). These values were found to be in the range of about  $7 \times 10^{12} - 2 \times 10^{14}$  molecules  $\text{cm}^{-3}$ .
- ✓ The appearance of  $\text{HCN}$  and  $\text{HNO}_3$  molecules in discharge was explained as a generation by reactions of ATI fragmentation products with introduced nitrogen.
- Better understanding of occurring processes and sensitive species control can support optimization of deposition processes and an improved modelling potential for ATI containing plasmas based on kinetic data. Therefore, future studies should collect information about the ATI precursor molecule itself and about further stable important intermediates, with a focus on radicals as for example  $\text{CH}_3$ ,  $\text{C}_2\text{H}$ ,  $\text{CH}_2$ , and  $\text{CH}$ . A following quantitative analysis of the molecular production rates in the discharge is also needed to get deeper insight.



# 10 Appendix

## 10.1 Abbreviations

AC	Alternating Current
AD	Analog-to-Digital
AOM	Acousto-Optical Modulator
AS	Active Screen
ASPN	Active Screen Plasma Nitriding
ATI	Aluminum Tri-Isopropoxide
CARS	Coherent Anti-Stokes Raman Scattering
CCP	Capacitively Coupled Plasma
CEA	Cavity Enhanced Absorption
CL	Compound Layer
CRDS	Cavity Ring-Down Spectroscopy
CVD	Chemical Vapor Deposition
CW	Continuous Wave
DBD	Dielectric Barrier Discharge
DBR	Distributed Bragg Reflector
DC	Direct Current
DFB	Distributed FeedBack
EC	External Cavity
EC-QCL	External Cavity Quantum Cascade Laser

---

EEDF	Electron Energy Distribution Function
FSR	Free Spectral Range
FTIR	Fourier Transform InfraRed (Spectroscopy)
FWHM	Full Width Half Maximum
GC	Gas Chromatography
GDOES	Glow Discharge Optical Emission Spectrometry
GEISA	Gestion et Étude des Information Spectroscopiques Atmosphérique
HITRAN	High Resolution Transmission
HMDSO	HexaMethylDiSilOxane
HTP	High-Temperature Plasma
HWHM	Half Width Half Maximum
ICL	Inter-band Cascade Laser
ICP	Inductively Coupled Plasma
IR	InfraRed
IR-LAS	InfraRed Laser Absorption Spectroscopy
IRMA	Infrared Multi-component Acquisition System
LIF	Laser Induced Fluorescence
LTP	Low-Temperature Plasma
MCT	Mercury Cadmium Telluride
MFC	Mass Flow Controller
MHF	Mode-Hop Free
MIR	Mid InfraRed
MIR-LAS	Mid InfraRed Laser Absorption Spectroscopy
MPA	Multiple Pass Absorption
MS	Mass Spectrometry
MW	MicroWave
OAP	Off-Axis Parabolic (Mirror)
OAS	Optical Absorption Spectroscopy
OES	Optical Emission Spectroscopy
OLED	Organic Light-Emitting Diode
PECVD	Plasma-Enhanced Chemical Vapor Deposition

---

PZT	PieZoelectric Transducer
QCL	Quantum Cascade Laser
QCLAS	Quantum Cascade Laser Absorption Spectroscopy
Q-MACS	Quantum cascade laser Measuring And Control System
QMS	Quadruple Mass Spectrometry
RF	Radio Frequency
SNR	Signal-to-Noise Ratio
TDL	Tunable Diode Laser
TDLAS	Tunable Diode Laser Absorption Spectroscopy
TRIPLE Q	3-channel QCLAS spectrometer
VDF	Vibrational Distribution Function
VOC	Volatile Organic Compound
VUV	Vacuum UltraViolet
WMS	Wavelength Modulation Spectroscopy
XUV	Extreme Ultraviolet

## 10.2 List of symbols

$A$	absorption coefficient
$\alpha$	amplitude of the modulated frequency
$B_{ik}$	Einstein coefficient
$c$	light velocity
$d$	diameter of the discharge tube
$D$	diffusion coefficient / percentage degree of dissociation
$\Delta E$	energy loss of the excited system
$E_0$	electric field amplitude
$E_i (E_k)$	rotational energy of the lower or upper level
$f$	frequency ( $\neq$ angular frequency)
$\Phi, \Phi_P, \Phi_{total}$	gas flow rate (volume/time interval)
$g_i (g_k)$	statistical weight of the lower or upper level
$\gamma$	surface de-excitation probability
$h$	Planck constant $h = 6.6261 \times 10^{-27} \text{ cm}^2 \text{ g s}^{-1}$
$\hbar$	Planck's constant reduced by $2\pi$ , $\hbar = 1.0546 \times 10^{-27} \text{ cm}^2 \text{ g s}^{-1}$
$I$	current
$I_0$	intensity of incident beam without absorption
$I_{abs}$	absorbed intensity, $I_{abs} = I_0 - I_{trans}$
$I_{offset}$	detector offset
$I_{trans}, I(l)$	transmitted intensity
$j(\nu)$	emission coefficient
$k$	Boltzmann constant $k = 1.3806503 \times 10^{-23} \text{ J} \cdot \text{K}^{-1}$
$k(\nu)$	absorption coefficient
$K$	calibration factor accounting for the line distortion
$l, L$	thickness of absorbing layer (medium)
$\Lambda$	characteristic diffusion length
$m/z$	mass number

$M$	gram molecular weight in $\text{g mol}^{-1}$
$\mu$	dipole moment
$n, n_{\text{molecule}}$	molecular concentration in molecules $\text{cm}^{-3}$
$n_i (n_k)$	population of the lower or upper level
$N_0$	number of molecules per $\text{cm}^3$ at STP ( $2.69 \times 10^{19}$ molecules $\text{cm}^{-3}$ )
$\nu$	vibrational quantum number
$\nu_0$	wavenumber of the line center
$\nu_D$	inhomogeneous (Doppler) line width
$\nu_{ik}$	frequency of the observed transition
$\nu_{Instr.}$	spectral line width (instrumental profile)
$\nu_L$	Lorentz line width
$\nu_m$	modulation frequency
$\nu_{\text{obs}}, \nu_{\text{Fit}}$	width of the observed line profile
$\nu_p$	line width due to the pressure broadening
$N_A$	Avogadro constant $N_A = 6.02214129 \times 10^{23} \text{ mol}^{-1}$
$p$	pressure
$P$	injected power
$Q_{rot}$	rotational partition function
$r$	tube radius
$R_C$	conversion efficiencies
$R_F$	fragmentation efficiencies
$S$	line strength
$\sigma(\nu)$	absorption cross section
$\Sigma$	saturation parameter
$T, T_g, T_e, T_v$	temperature gas, electron, vibrational
$\tau$	pulse duration / relaxation time
$\tau_l$	time constant of the energy loss
$U_{HV}$	voltage
$v_{th}$	average thermal velocity of the molecules



# Acknowledgement

At this point I would like to thank everyone who has contributed to this dissertation.

First of all I would like to thank sincerely my supervisor Prof. Dr. Jürgen Röpcke for giving me the opportunity to work at the INP Greifswald on this challenging research project. Jürgen, I thank you very much for introducing me to the field of laser diagnostic of plasmas, for your many valuable suggestions and willingness to discuss everything, whatever it was. I sincerely appreciate your enthusiasm, your patience, and your constructive criticism. Your farsightedness has opened for me new horizons. I benefited a lot from your external cooperation, since many of the results presented in this thesis have been obtained in the framework of collaborative research. Moreover, I really enjoyed travelling abroad, taking part in many international conferences and workshops. I was glad to represent INP and its progress as well as to find more about other companies and institutions and their contributions to plasma science.

I gratefully acknowledge Prof. Dr. Antoine Rousseau from École Polytechnique, Palaiseau, France for proposing a very exciting research topic and for co-supervising me. Antoine, I always enjoyed staying there and working in your team. It was a great experience in any respect. I would like to thank Dr. Olivier Guaitella und Dr. Daniil Marinov for the excellent team-work, intensive knowledge exchange and fruitful social life organization. I would always remember your endless output: our sitting before the running setup and playing guitar late on Fridays evening.

Many thanks go to Prof. Jörg Winter (University Bochum), Prof. Heinz-Joachim Spies (TU Bergakademie Freiberg) and Prof. Holger Kersten (University Kiel) for making intense experimental campaigns possible. I wish to thank their group members, especially Brankica Sikimic, Dr. Ilija Stefanovic, Dr. Igor Burlacov, Stefan Niemietz and Dr. Maik Fröhlich for spending long time in the lab and sharing their wide expert knowledge with me.

I kindly appreciate the help of my colleagues, namely Uwe Macherius, Sven Glitsch, Frank Weichbrodt, Dr. Andrei Pipa, Dr. Frank Hempel, Dr. Marko Hübner, Stephan Saß, Henrik Zimmermann, Dr. Norbert Lang, and many others. Thank you for many brainstorming discussions and helpful suggestions, your availability and hospitality. I have always felt your support.

I cannot but mention Dr. Natalie Savastenko, who was the first to introduce me to the world of plasma physics and has helped me to apply for this Ph.D. position at the INP.

I am very grateful to all my friends, who accompanied me on my way to the present.

I feel sincere gratitude to Prof. Tatiana Lopatik and Prof. Larisa Hlazyrina, my mother and grandmother respectively, for their standing support, efficient motivation as well as for their endless love and prayers. Thank you for your constant presence in my life despite of the hundred kilometers distance. I warmly thank my both brothers for their faith and their interest in what I do. And last but not least Olga Ermakova for being very special to me.

Sincerely yours,  
Dmitry Lopatik

# Curriculum vitae

## Personal information

Name	Dmitry Lopatik
Date of birth	23/11/1986
Place of birth	Minsk, Republic of Belarus
Citizenship	Belarusian

## Education

2004 – 2009	Student at the Belarusian State University, Faculty of Physics (Laser Physics and Spectroscopy), Minsk Qualification: Dipl. Physicist. Manager.
2008 – 2009	DAAD scholarship at the University of Leipzig, Leipzig
2009 – 2013	Ph.D. study at the Ernst-Moritz-Arndt University, Greifswald

## Experience

2006 – 2008	Participant of the training program for lieutenants in reserve
2007 – 2009	Researcher at the National Academy of Sciences of Belarus, B.I. Stepanov Institute of Physics, Minsk
2009 – 2013	Researcher at the INP Greifswald Collaborative Research Centre (SFB-TRR 24)
2009 – 2011	Student of the International Max-Planck Research School on Bounded Plasmas (IMPRS)
2011 – 2013	Student of the International Helmholtz Graduate School for Plasma Physics (HEPP)
2010 – 2013	Continuous collaborative program with Ecole Polytechnique, Palaiseau, France (11 weeks external measurement campaigns)

## External measurement campaigns ( $\geq 1$ week)

01/2010	Ruhr University Bochum
10/2010	TU Bergakademie Freiberg
10/2011	Christian-Albrechts University of Kiel



# Scholarly contributions

## Refereed Journal Publications

- [1] A. Nevar, N. Savastenko, V. Brüser, **D. Lopatik**, F. May, A. Butsen, N. Tarasenko, V. Burakov, “*Plasma synthesis and treatment of nanosized chalcopyrite particles*”, J. Appl. Spectrosc. **77**, 126 (2010).
- [2] I. Burlacov, K. Börner, H.-J. Spies, H. Biermann, **D. Lopatik**, H. Zimmermann, J. Röpcke, “*In-situ monitoring of plasma enhanced nitriding processes using infrared absorption and mass spectroscopy*”, Surface & Coatings Technology **206**, 3955 (2012).
- [3] D. Marinov, **D. Lopatik**, O. Guaitella, M. Hübner, Y. Ionikh, J. Röpcke, A. Rousseau, “*Surface vibrational relaxation of N<sub>2</sub> studied by CO<sub>2</sub> titration with time-resolved quantum cascade laser absorption spectroscopy*”, J. Phys. D: Appl. Phys. **45**, 175201 (2012).
- [4] F. Hempel, **D. Lopatik**, B. Sikimić, I. Stefanović, J. Winter, J. Röpcke, “*Monitoring of hydrocarbon concentrations in dust-producing RF plasmas*”, Plasma Sources Sci. Technol. **21**, 055001 (2012).
- [5] **D. Lopatik**, S. Niemietz, M. Fröhlich, J. Röpcke, H. Kersten, “*Plasma chemical study of a RF discharge containing aluminum tri-isopropoxide using MIR absorption spectroscopy based on external-cavity quantum cascade lasers*”, Contrib. Plasma Phys. **1**, 201200044 (2012).
- [6] **D. Lopatik**, N. Lang, H. Zimmermann, U. Macherius, J. Röpcke, “*On the application of external cavity quantum cascade infrared lasers for plasma diagnostics*”, Meas. Sci. Technol. **23**, 115501 (2012).
- [7] **D. Lopatik**, M. Hübner, D. Marinov, O. Guaitella, A. Rousseau, J. Röpcke, “*On the reactivity of plasma treated photo-catalytic TiO<sub>2</sub> surfaces for oxidation of C<sub>2</sub>H<sub>2</sub> and CO*”, J. Phys. D: Appl. Phys. **46**, 255203 (2013).
- [8] D. Marinov, **D. Lopatik**, O. Guaitella, Y. Ionikh, J. Röpcke, A. Rousseau, “*On vibrational relaxation of N<sub>2</sub> on different surfaces studied by titration combined with quantum cascade laser absorption spectroscopy*”, to be submitted, (2013).

## Conference Proceedings

### *Oral and Poster Presentations*

- [1] **D. Lopatik\***, A. Nevar, E. Bykova, “*Morphological features and optical properties of zinc oxide nanostructures prepared via submerged discharge in liquid*”, Conference of young scientists and specialist "Modern problems in physics", 10-12.06.2008, Minsk, Belarus, 144-148.
- [2] **D. Lopatik\***, F. Hempel, J. Röpcke, N. Sadeghi, B. Sikimić, I. Stefanović, B. Niermann, M. Böke, J. Winter, “*Plasma chemistry and reaction kinetics in dust producing rf plasmas*”, 4th International Workshop on Infrared Plasma Spectroscopy (IPS), 25-27.08.2010, Rolduc, The Netherlands, P16.
- [3] **D. Lopatik\***, M. Hübner, D. Marinov, O. Guaitella, A. Rousseau, J. Röpcke, “*On the reactivity of plasma stimulated catalytic surfaces*”, DPG-Spring Meeting, 28-31.03.2011, Kiel, Germany P 3.5.
- [4] **D. Lopatik\***, D. Marinov, O. Guaitella, M. Hübner, A. Rousseau, J. Röpcke, “*On plasma- and UV-induced VOC oxidation on TiO<sub>2</sub> surface pre-treated by plasma exposure monitored by QCLAS*”, IX Workshop on Frontiers in Low Temperature Plasma Diagnostics (FLTPD), 09-12.05.2011, Greifswald/Zinnowitz, Germany, P50.
- [5] **D. Lopatik**, M. Hübner, N. Lang, S. Glitsch, S. Welzel, D. Marinov, O. Guaitella, A. Rousseau, P.B. Davies, J. Röpcke, “*Reaction Kinetics of Molecular Plasmas - From Low-Pressure to Atmospheric Discharges*”, The HEPP Kick-off Colloquium, 26-28.10.2011, Garching near Munich, Germany.
- [6] **D. Lopatik\***, D. Marinov, O. Guaitella, M. Hübner, Y. Ionikh, J. Röpcke, A. Rousseau, “*Surface vibrational relaxation of N<sub>2</sub> studied by CO<sub>2</sub> titration with time resolved quantum cascade laser absorption spectroscopy*”, DPG-Spring Meeting, 12-16.03.2012, Stuttgart, Germany, P26.6.
- [7] **D. Lopatik**, H. Zimmermann, J. Röpcke, “*On the plasma chemistry of low-pressure Ar/N<sub>2</sub>/CH<sub>4</sub> microwave discharges using an external cavity quantum cascade laser*”, DPG-Spring Meeting, 12-16.03.2012, Stuttgart, Germany, P20.7.
- [8] **D. Lopatik**, N. Lang, H. Zimmermann, U. Macherius, J. Röpcke, “*On application of cw external-cavity quantum cascade infrared lasers for plasma diagnostics*”, 5th International Workshop on Plasma Spectroscopy (IPS), 13-16.05.2012, Presqu'île de Giens, France, P31.
- [9] **D. Lopatik**, F. Hempel, B. Sikimić, I. Stefanović, J. Winter, J. Röpcke, “*On the hydrocarbon kinetics in dust producing symmetrically driven rf plasmas*”, 21th ESCAMPIG, 10-14.07.2012, Viana do Castelo, Portugal, P2.7.4.

---

\* - oral presentation

[10] **D. Lopatik\***, D. Marinov, O. Guaitella, M. Hübner, Y. Ionikh, J. Röpcke, A. Rousseau, “*Surface vibrational relaxation of N<sub>2</sub> studied by CO<sub>2</sub> titration with time resolved quantum cascade laser absorption spectroscopy*”, International Helmholtz Graduate School for Plasma Physics HEPP-Colloquium 2012, 26-28.09.2012, Greifswald, Germany.

### *Other Contributions*

- [1] F. May, N. Savastenko, V. Brüser, **D. Lopatik**, A. Nevar, A. Butsen, N. Tarasenko, V. Burakov, “*Ar:O<sub>2</sub> Plasma Treatment of CuFeS<sub>2</sub> Nanoparticles*”, Proc. 6th International Conference on Plasma Physics and Plasma Technology, 1 (2009), p. 382-385.
- [2] N. Tarasenko, A. Nevar, M. Nedelko, **D. Lopatik**, “*Properties of zinc oxide nanoparticles synthesized by electrical discharge technique in liquids*”, E-MRS 2009 Fall meeting (Symp. C), 7-11.09.2009, Warsaw, Poland, P71.
- [3] N. Lang, F. Hempel, M. Hübner, **D. Lopatik**, J. Röpcke, “*On the status and the potential of MIR absorption spectroscopy for diagnostics of microplasmas*”, International Workshop on diagnostics of microplasmas, 21-23.03.2010 Bochum, Germany.
- [4] **D. Lopatik**, B. Sikimić, F. Hempel, M. Böke, I. Stefanović, N. Sadeghi, J. Winter, J. Röpcke, “*On the hydrocarbon chemistry in dust producing rf plasmas*”, 20th ESCAMPIG, 13-17.07.2010, Novi Sad, Serbia, P3.07.
- [5] J. Röpcke, P.B. Davies, R. Engeln, S. Glitsch, F. Hempel, M. Hübner, N. Lang, **D. Lopatik**, M. Nägele, A. Rousseau, S. Wege, S. Welzel, “*On recent progress using MIR absorption techniques for plasma diagnostics - from basic research to industrial applications*”, 4th International Workshop on Infrared Plasma Spectroscopy (IPS), 25-27.08.2010, Rolduc, The Netherlands, P22.
- [6] **D. Lopatik**, B. Sikimić, F. Hempel, M. Böke, I. Stefanović, N. Sadeghi, J. Winter, J. Röpcke, “*On the hydrocarbon kinetics in dust producing symmetrically driven rf plasmas*”, 63rd Annual Gaseous Electronics Conference and 7th International Conference on Reactive Plasmas, 04-08.10.2010, Paris, France, 55, Number 7, CTP.00043.
- [7] D. Marinov, O. Guaitella, M. Hübner, **D. Lopatik**, V. Guerra, C.D. Pintassilgo, J. Röpcke, A. Rousseau, “*Reactivity of atoms adsorbed on catalytic surfaces under plasma exposure*”, Astrochemistry 2011: annual meeting, 5-7.01.2011, Eindhoven, Netherlands, C9.

- [8] I. Burlacov, H.-J. Spies, **D. Lopatik**, H. Zimmermann, J. Röpcke, “*In-situ monitoring of plasma enhanced nitriding processes using infrared absorption-, optical emission- and mass spectroscopy*”, Plasma Technology 15, 28.02-02.03.2011, Stuttgart, Germany.
- [9] J. Röpcke, P.B. Davies, S. Glitsch, F. Hempel, M. Hübner, N. Lang, **D. Lopatik**, A. Rousseau, S. Welzel, “*Applications of MIR-Laser Absorption Techniques for Plasma Diagnostics in Basic Research and Industry*”, 4th Int. Conference Plasma-Nano Technology & Science (IC-PLANTS), 10-12.03.2011, Takayama, Japan, I-4.
- [10] D. Marinov, **D. Lopatik**, O. Guaitella, M. Hübner, Y. Ionikh, J. Röpcke, A. Rousseau, “*Vibrational relaxation of  $N_2$  studied by IR titration with time-resolved Quantum Cascade Laser diagnostics*”, IX Workshop on Frontiers in Low Temperature Plasma Diagnostics (FLTPD), 09-12.05.2011, Greifswald/Zinnowitz, Germany, P98.
- [11] D. Marinov, **D. Lopatik**, M. Hübner, O. Guaitella, C. Corbella, A. von Keudell, T. de los Arcos, J. Röpcke, A. Rousseau, “*Reactivity of atoms adsorbed on catalytic surfaces under plasma exposure*”, 20th International Symposium on Plasma Chemistry (ISPC), 24-29.07.2011, Philadelphia, USA, (4pp).
- [12] D. Marinov, **D. Lopatik**, M. Hübner, O. Guaitella, J. Röpcke, A. Rousseau, “ *$C_2H_2$  oxidation by oxygen atoms adsorbed on plasma pretreated  $TiO_2$* ”, 30th International Conference on Phenomena in Ionized Gases (ICPIG), 28.08-02.09.2011, Belfast, Northern Ireland, UK, A3-360.
- [13] D. Marinov, **D. Lopatik**, M. Hübner, O. Guaitella, J. Röpcke, A. Rousseau, “*Surface vibrational relaxation of  $N_2$  studied by  $CO_2$  titration with time resolved Quantum Cascade Laser diagnostics*”, 30th International Conference on Phenomena in Ionized Gases (ICPIG), 28.08-02.09.2011, Belfast, Northern Ireland, UK, B6-355.
- [14] F. Hempel, **D. Lopatik**, B. Sikimic, I. Stefanovic, J. Winter, J. Röpcke, “*On investigations of the reaction kinetics in dust producing rf discharges in gas-mixtures of Argon or Helium and hydrocarbons*”, 5th International Workshop on Plasma Spectroscopy (IPS), 13-16.05.2012, Presqu’île de Giens, France, P29.
- [15] D. Marinov, **D. Lopatik**, O. Guaitella, M. Hübner, Y. Ionikh, J. Röpcke, A. Rousseau, “*Surface vibrational relaxation of  $N_2$  studied by infrared titration with time resolved Quantum Cascade Laser diagnostics*”, 5th International Workshop on Plasma Spectroscopy (IPS), 13-16.05.2012, Presqu’île de Giens, France, P6.
- [16] D. Marinov, **D. Lopatik**, O. Guaitella, M. Hübner, Y. Ionikh, J. Röpcke, A. Rousseau, “*Surface vibrational relaxation of  $N_2$  studied by infrared titration with time resolved Quantum Cascade Laser diagnostics*”, 21th ESCAMPIG, 10-14.07.2012, Viana do Castelo, Portugal, P2.4.11.
- [17] **D. Lopatik**, N. Lang, U. Macherius, H. Zimmermann, J. Röpcke, „*On application of cw external-cavity quantum cascade infrared lasers for plasma diagnostics*”, International Quantum Cascade Lasers School and Workshop, 2-6.09.2012, Baden near Vienna, Austria, P76.

- [18] D. Marinov, **D. Lopatik**, O. Guaitella, M. Hübner, Y. Ionikh, J. Röpcke, A. Rousseau, “*Surface vibrational relaxation of  $N_2$  studied by infrared titration with time resolved Quantum Cascade Laser diagnostics*”, 65th Annual Gaseous Electronics Conference (GEC), 22–26.10.2012, Austin, Texas, USA, 57, Number 7, UF3.00003.
- [19] **D. Lopatik**, N. Lang, H. Zimmermann, U. Macherius, J. Röpcke, “*On multiple component detection in molecular plasmas using cw external-cavity quantum cascade infrared lasers*”, 65th Annual Gaseous Electronics Conference (GEC), 22–26.10.2012, Austin, Texas, USA, 57, Number 7, DT1.00009.
- [20] J. Röpcke, S. Hamann, M. Hübner, N. Lang, **D. Lopatik**, J. H. van Helden, “*On recent progress in studying plasma chemical phenomena using infrared absorption techniques*”, 5th CESPC, 25-29 August 2013, Balatonalmádi, Hungary.



# **Declaration/**

# **Selbständigkeitserklärung**

Hiermit erkläre ich, dass diese Arbeit bisher von mir weder an der Mathematisch-Naturwissenschaftlichen Fakultät der Ernst-Moritz-Arndt-Universität Greifswald noch einer anderen wissenschaftlichen Einrichtung zum Zwecke der Promotion eingereicht wurde.

Ferner erkläre ich, dass ich diese Arbeit selbständig verfasst und keine anderen als die darin angegebenen Hilfsmittel und Hilfen benutzt und keine Textabschnitte eines Dritten ohne Kennzeichnung übernommen habe.

.....

